第56回 フラーレン・ナノチューブ・グラフェン 総合シンポジウム講演要旨集

平成31年3月2日～5日

FNTG Research Society

第 56 回
フラーレン・ナノチューブ・グラフェン
総合シンポジウム

The 56th Fullerenes-Nanotubes-Graphene General Symposium

講演要旨集
Abstracts

2019 年 3 月 2 日（土） ～ 5 日（火）
東京大学　伊藤国際学術研究センター
The University of Tokyo, ITO INTERNATIONAL RESEARCH CENTER

主催　フラーレン・ナノチューブ・グラフェン学会
The Fullerenes, Nanotubes and Graphene Research Society

共催 ・ 後援
日本化学会　The Chemical Society of Japan
東京大学大学院工学系研究科　School of Engineering, The University of Tokyo
東京大学 CIAiS　Consortium for Innovation of Advanced Integrated Science (UTokyo)
東京大学 GMSI　Graduate Program for Mechanical Systems Innovation (UTokyo)

協賛
日本物理学会　The Physical Society of Japan
応用物理学会　The Japan Society of Applied Physics
高分子学会　The Society of Polymer Science, Japan
電気化学会　The Electrochemical Society of Japan

研究から量産まで

グラフェン、カーボンナノチューブ & 2Dマテリアル用 先端成長技術

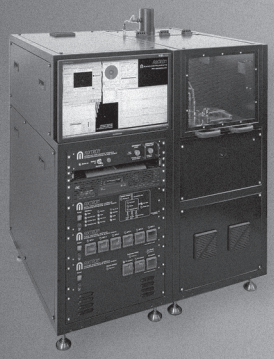

BM Pro

Your deposition workhorse
for wafer scale

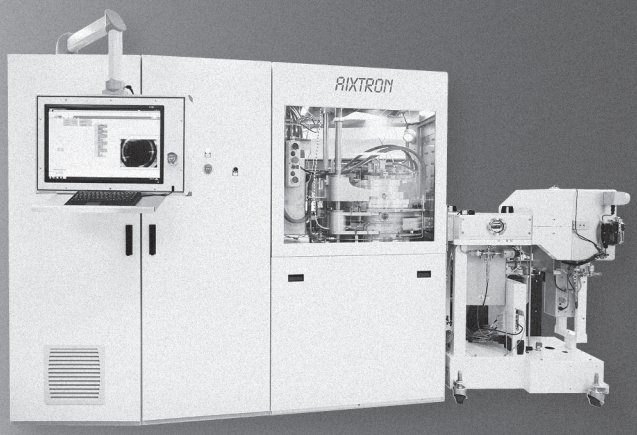

BM 300T

For your production needs
at wafer scale

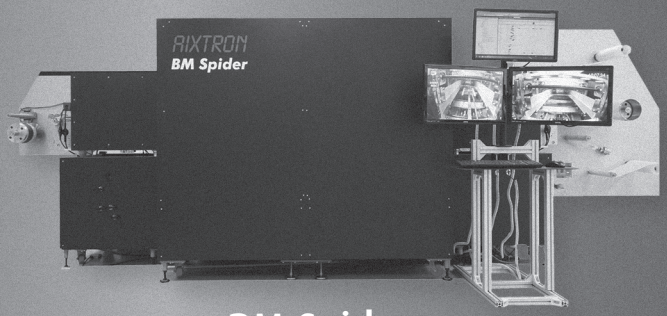

BM Spider

Your roll-to-roll solution

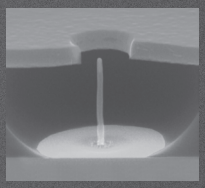
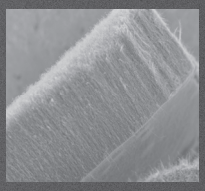
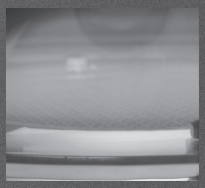
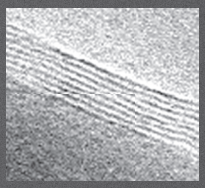
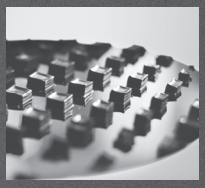
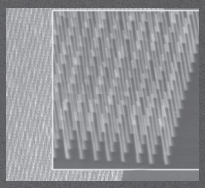
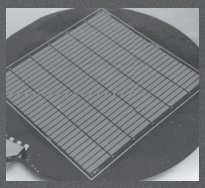
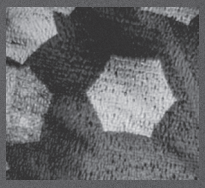

	BM Pro	BM 300T	BM spider
プロセス	CVD/PECVD Batch	CVD/PECVD Batch	CVD / Roll-to-roll
材料	CNTs, graphene & other 2D	CNTs & graphene	CNTs & graphene
基板サイズ	Up to 8″	8″ & 12″	300 mm web width
基板タイプ	wafer & foil	wafer	foil
最高温度	1,050° C (*up to 1,700° C)	1,050° C	1,050° C
シャワーヘッド方式 ガス供給	Yes	Yes	Yes
プラズマ	Yes	Yes	No
ハンドラー/インライン インテグレーション	No	Yes	Yes
両面コーティング	No	No	Yes

アイクストロン株式会社 · www.aixtron.com
〒140-0001 東京都品川区北品川1-8-11 Daiwa品川Northビル 9F
E-mail: japaninfo@aixtron.com · Phone: 03-5781-0931 · Fax: 03-5781-0940

AIXTRON
Our technology. Your future.

Abstract of
The 56th Fullerenes-Nanotubes-Graphene General Symposium

Sponsored by : The Fullerenes, Nanotubes and Graphene Research Society

Co-Sponsored by : The Chemical Society of Japan
School of Engineering, The University of Tokyo
Consortium for Innovation of Advanced Integrated Science (UTokyo)
Graduate Program for Mechanical Systems Innovation (UTokyo)

Supported by : The Physical Society of Japan
The Japan Society of Applied Physics
The Society of Polymer Science, Japan
The Electrochemical Society of Japan

Date : March 2nd(Sat.) – March 5th(Tue.), 2019

Place : The University of Tokyo, ITO INTERNATIONAL RESEARCH CENTER
7-3-1 Hongo, Bunkyo-ku, Tokyo 113-8656

Presentation Time : Special Lecture (25 min presentation + 5min discussion)
Invited Lecture (10 min presentation + 5min discussion)
General Lecture (10 min presentation + 5min discussion)
Poster Preview (1 min presentation without discussion)

第 56 回フラーレン・ナノチューブ・グラフェン総合シンポジウム
講演要旨集

主催 : フラーレン・ナノチューブ・グラフェン学会

共催・後援 : 日本化学会
東京大学大学院工学系研究科
東京大学 CIAiS
東京大学 GMSI

協賛 : 日本物理学会、応用物理学会、高分子学会、電気化学会

日時 : 平成 31 年 3 月 2 日(土)～3 月 5 日(火)

場所 : 東京大学　伊藤国際学術研究センター　伊藤謝恩ホール
〒113-8656　東京都文京区本郷 7-3-1

発表時間 : 特別講演　　(発表　25 分 + 質疑応答　5 分)
招待講演　　(発表　10 分 + 質疑応答　5 分)
一般講演　　(発表　10 分 + 質疑応答　5 分)
ポスタープレビュー (発表 1 分・質疑応答　なし)

展示団体御芳名 （五十音順、 敬称略）

（株）島津製作所

（株）セントラル科学貿易

ナカライテスク（株）

日本シノプシス（同）

（株）日本レーザー

（株）日本ローパー

（株）堀場製作所

（株）名城ナノカーボン

広告掲載団体御芳名 （五十音順、 敬称略）

アイクストロン（株）

（株）コロナ社

（株）セントラル科学貿易

ソーラボジャパン（株）

日本電子（株）

（株）日本レーザー

（株）日本ローパー

Contents

目次

プログラム早見表

3月2日 （土）

	受付開始 8:30～ 講演開始 9:30～
9:30	招待講演（Yan Li）9:30–9:45
9:45	一般講演 2件 （内包ナノチューブ）9:45–10:15
10:15	休憩 10:15–10:30
10:30	特別講演 （北浦 良） 10:30–11:00
11:00	一般講演 2件 （原子層） 11:00–11:30
11:30	ポスタープレビュー （ 1P–1 ～ 1P–38 ） 11:30–12:15
12:15	昼食 （幹事会） 12:15–13:30
13:30	ポスターセッション 【 多目的スペース 】 13:30–15:15 13:30–14:00 若手奨励賞候補審査優先時間
15:15	招待講演（河野 淳一郎）15:15–15:30
15:30	一般講演 3件 （ナノチューブの物性・ナノチューブの生成と精製） 15:30–16:15
16:15	休憩 16:15–16:30
16:30	特別講演 （若林 克法） 16:30–17:00
17:00	一般講演 3件 （グラフェンの応用・グラフェンの物性） 17:00–17:45
17:45	休憩 17:45–18:00
18:00	チュートリアル 講師：（小久保 研） AIST 【 伊藤謝恩ホール 】 18:00–19:30
19:30	

3月5日 （火）

第12回ﾅﾉｶｰﾎﾞﾝ実用化推進研究会
【 伊藤謝恩ホール 】
10:00–17:00

3月3日 （日）

	受付開始 8:30～ 講演開始 9:00～
9:00	招待講演（Esko I. Kauppinen）9:00–9:15
9:15	一般講演 3件 （ナノチューブの物性・ナノチューブの応用） 9:15–10:00
10:00	休憩 10:00–10:15
10:15	特別講演 （竹延 大志） 10:15–10:45
10:45	一般講演 3件 （原子層） 10:45–11:30
11:30	ポスタープレビュー （ 2P–1 ～ 2P–38 ） 11:30–12:15
12:15	昼食 12:15–13:30
13:30	ポスターセッション 【 多目的スペース 】 13:30–15:15 13:30–14:00 若手奨励賞候補審査優先時間
15:15	授賞式 15:15–16:00
16:00	特別講演 （本間 芳和） 16:00–16:30
16:30	一般講演 3件 （ナノチューブの物性） 16:30–17:15
17:15	休憩 17:15–17:30
17:30	招待講演（井関 隆之）17:30–17:45
17:45	一般講演 3件 （ナノチューブの応用・ナノ炭素粒子・その他） 17:45–18:30
18:30	休憩 18:30–18:45
18:45	懇親会 【 多目的スペース 】 18:45–20:30
20:30	

3月4日 （月）

	受付開始 8:30～ 講演開始 9:00～
9:00	特別講演 （Fei Wei） 9:00–9:30
9:30	一般講演 3件 （ナノチューブの生成と精製・グラフェンの応用）9:30–10:15
10:15	休憩 10:15–10:30
10:30	特別講演 （斎藤 毅） 10:30–11:00
11:00	一般講演 2件 （ナノチューブの応用）11:00–11:30
11:30	ポスタープレビュー （ 3P–1 ～ 3P–37 ） 11:30–12:15
12:15	昼食 12:15–13:30
13:30	ポスターセッション 【 多目的スペース 】 13:30–15:15 13:30–14:00 若手奨励賞候補審査優先時間
15:15	特別講演 （Alberto Bianco） 15:15–15:45
15:45	一般講演 4件 （金属内包フラーレン・フラーレンの化学・フラーレン） 15:45–16:45
16:45	招待講演（Erik Einarsson）16:45–17:00
17:00	一般講演 2件 （グラフェンの応用）17:00–17:30
17:30	

講演会場 伊藤謝恩ホール
特別講演 発表25分・質疑5分
招待講演 発表10分・質疑5分
一般講演 発表10分・質疑5分
ﾎﾟｽﾀｰﾌﾟﾚﾋﾞｭｰ 発表1分・質疑なし

Time table

March 2 (Sat.)

	Registration begins at 8:30 Lectures begin at 9:30
9:30	Invited Lecture (Yan Li) 9:30–9:45
9:45	General Lectures [2] (Endohedral nanotubes) 9:45–10:15
10:15	Coffee Break 10:15–10:30
10:30	Special Lecture (Ryo Kitaura) 10:30–11:00
11:00	General Lectures [2] (Atomic Layers) 11:00–11:30
11:30	Poster Preview (1P-1 through 1P-38) 11:30–12:15
12:15	Lunch (Administrative meeting) 12:15–13:30
13:30	Poster Session 【 Event Space 】 13:30–15:15 During 13:30–14:00, please give priority to selection of candidates for Young Scientist Poster Award
15:15	Invited Lecture (Junichiro Kono) 15:15–15:30
15:30	General Lectures [3] (Properties of nanotubes・Formation and purification of nanotubesgraphene) 15:30–16:15
16:15	Coffee Break 16:15–16:30
16:30	Special Lecture (Katsunori Wakabayashi) 16:30–17:00
17:00	General Lectures [3] (Applications of graphene・Properties of graphene) 17:00–17:45
17:45	Coffee Break 17:45–18:00
18:00	Tutorial Lecturer : (Ken Kokubo) AIST 【 Ito Hall 】 18:00–19:30
19:30	

March 3 (Sun.)

	Registration begins at 8:30 Lectures begin at 9:00
9:00	Invited Lecture (Esko I. Kauppinen) 9:00–9:15
9:15	General Lectures [3] (Properties of nanotubes・Applications of nanotubes) 9:15–10:00
10:00	Coffee Break 10:00–10:15
10:15	Special Lecture (Taishi Takenobu) 10:15–10:45
10:45	General Lectures [3] (Atomic Layers) 10:45–11:30
11:30	Poster Preview (2P-1 through 2P-38) 11:30–12:15
12:15	Lunch 12:15–13:30
13:30	Poster Session 【 Event Space 】 13:30–15:15 During 13:30–14:00, please give priority to selection of candidates for Young Scientist Poster Award
15:15	Award Ceremony 15:15–16:00
16:00	Special Lecture (Yoshikazu Homma) 16:00–16:30
16:30	General Lectures [3] (Properties of nanotubes) 16:30–17:15
17:15	Coffee Break 17:15–17:30
17:30	Invited Lecture (Takayuki Iseki) 17:30–17:45
17:45	General Lectures [3] (Applications of nanotubes・Carbon nanoparticles・Other topics) 17:45–18:30
18:30	Coffee Break 18:30–18:45
18:45	Banquet 【 Event Space 】 18:45–20:30
20:30	

March 4 (Mon.)

	Registration begins at 8:30 Lectures begin at 9:00
9:00	Special Lecture (Fei Wei) 9:00–9:30
9:30	General Lectures [3] (Formation and purification of nanotubes・Applications of graphene) 9:30–10:15
10:15	Coffee Break 10:15–10:30
10:30	Special Lecture (Takeshi Saito) 10:30–11:00
11:00	General Lectures [2] (Applications of nanotubes) 11:00–11:30
11:30	Poster Preview (3P-1 through 3P-37) 11:30–12:15
12:15	Lunch 12:15–13:30
13:30	Poster Session 【 Event Space 】 13:30–15:15 During 13:30–14:00, please give priority to selection of candidates for Young Scientist Poster Award
15:15	Special Lecture (Alberto Bianco) 15:15–15:45
15:45	General Lectures [4] (Endohedral metallofullerenes・Chemistry of fullerenes・Fullerenes) 15:45–16:45
16:45	Invited Lecture (Erik Einarsson) 16:45–17:00
17:00	General Lectures [2] (Applications of graphene) 17:00–17:30
17:30	

March 5 (Tue.)

The 12th NanoCarbon Application Forum
【 Ito Hall 】
10:00–17:00

Place : Ito Hall
Special Lecture : 25 min (Presentation) + 5 min (Discussion)
Invited Lecture : 10 min (Presentation) + 5 min (Discussion)
General Lecture : 10 min (Presentation) + 5 min (Discussion)

座長一覧 (Chairpersons)

3月2日（土） （敬称略）

セッション	時　　間	座　　長
招待講演(Yan Li)	9:30 ～9:45	丸山 茂夫
一般講演	9:45 ～10:15	
特別講演(北浦 良)	10:30 ～ 11:00	竹延 大志
一般講演	11:00～ 11:30	
ポスタープレビュー	11:30 ～ 12:15	井ノ上 泰輝 / 中西 勇介
招待講演(河野 淳一郎)	15:15 ～ 15:30	加藤 雄一郎
一般講演	15:30 ～ 16:15	
特別講演(若林 克法)	16:30 ～ 17:00	長汐 晃輔
一般講演	17:00 ～ 17:45	
チュートリアル(小久保 研)	18:00 ～ 19:30	丸山 茂夫

3月3日（日）

セッション	時　　間	座　　長
招待講演(Esko I. Kauppinen)	9:00 ～ 9:15	北浦 良
一般講演	9:15 ～10:00	
特別講演(竹延 大志)	10:15 ～10:45	高井 和之
一般講演	10:45 ～ 11:30	
ポスタープレビュー	11:30 ～ 12:15	大町 遼 / 杉目 恒志
特別講演(本間 芳和)	16:00 ～ 16:30	山本 貴博
一般講演	16:30～ 17:15	
招待講演(井関 隆之)	17:30 ～ 17:45	齋藤 理一郎
一般講演	17:45 ～ 18:30	

3月4日（月）

セッション	時　　間	座　　長
特別講演(Fei Wei)	9:00 ～ 9:30	項 榮
一般講演	9:30 ～ 10:15	
特別講演(斎藤 毅)	10:30 ～ 11:00	野田 優
一般講演	11:00～ 11:30	
ポスタープレビュー	11:30 ～ 12:15	廣谷 潤 / 辻 享志
特別講演(Alberto Bianco)	15:15 ～ 15:45	湯田坂 雅子
一般講演	15:45 ～ 16:45	
招待講演(Erik Einarsson)	16:45 ～ 17:00	千足 昇平
一般講演	17:00 ～ 17:30	

3月 2日（土）

特別講演　　発表 25分 ・ 質疑応答 5分
招待講演　　発表 10分 ・ 質疑応答 5分
一般講演　　発表 10分 ・ 質疑応答 5分
ポスタープレビュー　　発表 1分 ・ 質疑応答 なし

招待講演（ 9:30–9:45 ）

一般講演（ 9:45–10:15 ）

内包ナノチューブ

>>>>>>> 休憩（ 10:15–10:30 ）<<<<<<<

特別講演（ 10:30–11:00 ）

一般講演（ 11:00–11:30 ）

原子層

ポスタープレビュー（ 11:30–12:15 ）　（☆） 若手奨励賞候補

若手奨励賞候補

3月 2日（土）

フラーレンの化学

金属内包フラーレン

フラーレン

ナノ環境と安全評価

ナノチューブの物性

3月 2日（土）

3月 2日（土）

原子層

ナノ炭素粒子

その他

＞＞＞＞＞＞＞ 昼食（ 12:15-13:30 ）＜＜＜＜＜＜＜

ポスターセッション（ 13:30-15:15 ）
13:30-14:00 若手奨励賞候補審査優先時間

招待講演（ 15:15-15:30 ）

一般講演（ 15:30-16:15 ）
ナノチューブの物性 ・ ナノチューブの生成と精製

3月 2日（土）

＞＞＞＞＞＞＞ 休憩（ 16:15-16:30 ）＜＜＜＜＜＜＜

特別講演（ 16:30-17:00 ）

一般講演（ 17:00-17:45 ）
グラフェンの応用 ・ グラフェンの物性

＞＞＞＞＞＞＞ 休憩（ 17:45-18:00 ）＜＜＜＜＜＜＜

チュートリアル（ 18:00-19:30 ）

ナノ炭素材料の実用化研究発展のための産官学連携
＊小久保 研

3月 3日（日）

特別講演　　発表 25分 ・ 質疑応答 5分
招待講演　　発表 10分 ・ 質疑応答 5分
一般講演　　発表 10分 ・ 質疑応答 5分
ポスタープレビュー　　発表 1分 ・ 質疑応答 なし

招待講演（ 9:00–9:15 ）

一般講演（ 9:15–10:00 ）
ナノチューブの物性 ・ ナノチューブの応用

＞＞＞＞＞＞＞ 休憩（ 10:00–10:15 ）＜＜＜＜＜＜＜

特別講演（ 10:15–10:45 ）

一般講演（ 10:45–11:30 ）
原子層

ポスタープレビュー（ 11:30–12:15 ）　（☆） 若手奨励賞候補
若手奨励賞候補

フラーレンの応用

金属内包フラーレン

ナノチューブの物性

3月 3日（日）

グラフェンの物性

原子層

ナノ炭素粒子

バイオ

>>>>>>> 昼食（ 12:15-13:30 ）<<<<<<<

3月 3日（日）

ポスターセッション（ 13:30-15:15 ）
13:30-14:00 若手奨励賞候補審査優先時間

大澤賞・飯島賞・若手奨励賞の授賞式（ 15:15-16:00 ）

特別講演（ 16:00-16:30 ）

一般講演（ 16:30-17:15 ）
ナノチューブの物性

>>>>>>> 休憩（ 17:15-17:30 ）<<<<<<<

招待講演（ 17:30-17:45 ）

一般講演（ 17:45-18:30 ）
ナノチューブの応用 ・ ナノ炭素粒子 ・ その他

>>>>>>> 休憩（ 18:30-18:45 ）<<<<<<<

懇親会（ 18:45-20:30 ）

3月 4日（月）

特別講演　　発表 25分 ・ 質疑応答 5分
招待講演　　発表 10分 ・ 質疑応答 5分
一般講演　　発表 10分 ・ 質疑応答 5分
ポスタープレビュー　　発表 1分 ・ 質疑応答 なし

特別講演（ 9:00–9:30 ）

一般講演（ 9:30–10:15 ）
ナノチューブの生成と精製 ・ グラフェンの応用

＞＞＞＞＞＞＞ 休憩（ 10:15–10:30 ）＜＜＜＜＜＜＜

特別講演（ 10:30–11:00 ）

一般講演（ 11:00–11:30 ）
ナノチューブの応用

ポスタープレビュー（ 11:30–12:15 ）　（☆） 若手奨励賞候補
若手奨励賞候補

金属内包フラーレン

ナノチューブの物性

ナノチューブの応用

ナノチューブの生成と精製

内包ナノチューブ

グラフェン生成

グラフェンの応用

3月 4日（月）

グラフェンの物性

原子層

その他

>>>>>>> 昼食（ 12:15-13:30 ）<<<<<<<

ポスターセッション（ 13:30-15:15 ）
13:30-14:00 若手奨励賞候補審査優先時間

特別講演（ 15:15-15:45 ）

3月 4日（月）

一般講演（ 15:45-16:45 ）
金属内包フラーレン ・ フラーレンの化学 ・ フラーレン

招待講演（ 16:45-17:00 ）

一般講演（ 17:00-17:30 ）
グラフェンの応用

March 2nd, Sat.

Special Lecture: 25min (Presentation) + 5min (Discussion)
Invited Lecture: 10min (Presentation) + 5min (Discussion)
General Lecture: 10min (Presentation) + 5min (Discussion)
Poster Preview: 1min (Presentation)

March 2nd, Sat.

Carbon nanoparticles

Other topics

>>>>>>> Lunch Time (12:15-13:30) <<<<<<<

Poster Session (13:30-15:15)

During 13:30-14:00, please give priority to selection of candidates for Young Scientist Poster Award

Invited Lecture (15:15-15:30)

General Lecture (15:30-16:15)

Properties of nanotubes ・ Formation and purification of nanotubes

>>>>>>> Coffee Break (16:15-16:30) <<<<<<<

March 2nd, Sat.

Special Lecture （ 16:30-17:00 ）

General Lecture （ 17:00-17:45 ）

Applications of graphene ・ Properties of graphene

>>>>>>> Coffee Break （ 17:45-18:00 ）<<<<<<<

Tutorial （ 18:00-19:30 ）

March 3rd, Sun.

Special Lecture: 25min (Presentation) + 5min (Discussion)
Invited Lecture: 10min (Presentation) + 5min (Discussion)
General Lecture: 10min (Presentation) + 5min (Discussion)
Poster Preview: 1min (Presentation)

Invited Lecture （ 9:00–9:15 ）

General Lecture （ 9:15–10:00 ）

Properties of nanotubes ・ Applications of nanotubes

>>>>>> Coffee Break （ 10:00–10:15 ）<<<<<<

Special Lecture （ 10:15–10:45 ）

General Lecture （ 10:45–11:30 ）

Atomic Layers

>>>>>>> Lunch Time （ 12:15-13:30 ）<<<<<<<

Poster Session （ 13:30-15:15 ）

During 13:30-14:00, please give priority to selection of candidates for Young Scientist Poster Award

Awards Ceremony （ 15:15-16:00 ）

Special Lecture （ 16:00-16:30 ）

March 3rd, Sun.

General Lecture （ 16:30–17:15 ）

Properties of nanotubes

>>>>>>> Coffee Break （ 17:15–17:30 ）<<<<<<<

Invited Lecture （ 17:30–17:45 ）

General Lecture （ 17:45–18:30 ）

Applications of nanotubes ・ Carbon nanoparticles ・ Other topics

>>>>>>> Coffee Break （ 18:30–18:45 ）<<<<<<<

Banquet （ 18:45–20:30 ）

March 4th, Mon.

Special Lecture: 25min (Presentation) + 5min (Discussion)
Invited Lecture: 10min (Presentation) + 5min (Discussion)
General Lecture: 10min (Presentation) + 5min (Discussion)
Poster Preview: 1min (Presentation)

Poster Preview (11:30–12:15) (☆)Candidates for the Young Scientist Poster Award

Candidates for the Young Scientist Poster Award

Endohedral metallofullerenes

Other topics

>>>>>>> Lunch Time （ 12:15-13:30 ）<<<<<<<

Poster Session （ 13:30-15:15 ）

During 13:30-14:00, please give priority to selection of candidates for Young Scientist Poster Award

Special Lecture （ 15:15-15:45 ）

General Lecture （ 15:45-16:45 ）

Endohedral metallofullerenes ・ Chemistry of fullerenes ・ Fullerenes

Invited Lecture （ 16:45-17:00 ）

General Lecture （ 17:00-17:30 ）

Applications of graphene

特別講演
Special Lecture

1 S – 1 ～ 1 S – 2
2 S – 3 ～ 2 S – 4
3 S – 5 ～ 3 S – 7

Transition metal dichalcogenide atomic layers and their heterostructures

Ryo Kitaura

Department of Chemistry, Nagoya University, Nagoya 464-8602, Japan

The significant interests on graphene research have led to searching for other two-dimensional systems, and hexagonal boron nitrides (hBN) and transition metal dichalcogenides (TMDs) were isolated in its monolayer form. The wide variety of two-dimensional systems, in particular TMDs (MoS_2, WS_2, NbS_2, $MoSe_2$, etc.), and recent advancement on experimental technique of fabrication of heterostructures provide us an excellent platform to explore novel phenomena in two-dimensions. Although further development of fabrication method is still needed to achieve multiple heterostructures with fully-controlled stacking or junction sequences, heterostructures suggest the exciting possibility to realize designer 2D systems with desired electronic band structure and physical properties. We are working on fabrication of TMD-based heterostructures in a controlled way by the exfoliation-based dry-transfer method and direct growth including molecular beam epitaxy and chemical vapor deposition[1-4]. In this presentation, I will talk about our recent results on fabrication and characterization of TMD heterostructure, including hBN/$MoSe_2$/hBN, hBN/MoS_2/hBN, and hBN/MoS_2/WS_2/hBN, etc.

References:
[1] M. Okada, et. al., ACS Nano, 8, 8273-7277 (2014)
[2] T. Hotta, et. al., Appl. Phys. Lett., 109, 133101 (2016).
[3] M. Okada, et. al., Sci. Rep., 7, 322 (2017)
[4] Y. Hoshi, et. al., Phys. Rev. B., 95, 241403 (2017).
[5] M. Okada, et. al., ACS Nano., 12, 2498-2505 (2018).

Corresponding Author: R. Kitaura
Tel: +81-52-789-2482, Fax: +81-52-747-6442,
E-mail: r.kitaura@nagoya-u.jp

Fig.1 Structure representations of structure of (a) hexagonal boron nitride and (b) transition metal dichalcogenides.

Topological Properties of Graphene and Related 2D Materials

○Katsunori Wakabayashi

Department of Nanotechnology for Sustainable Energy, School of Science and Technology, Kwansei Gakuin University, Sanda 669-1337, Hyogo, Jpana

In atomically-thin materials such as graphene and transition metal dichalcogenide nanosheet, the electronic properties crucially depend on the size, edge structures and topological properties of the system. It is well-known that graphene zigzag edges possess edge states at Fermi energy. The presence of edge states in graphene provides peculiar magnetic properties and perfectly conducting channel for electron conduction [1].

The origin of edge states can be understood from the topological properties of bulk wavefunctions. There are two fundamental topological quantities i.e. Berry curvature and Berry connection, which are understood as magnetic field and vector potential in momentum space, respectively. The origin of graphene edge states is attributed to the existence of nonzero Zak's phase (integration of Berry connection) of bulk wavefunction. This is distinct difference from conventional topological insulators where the existence of topological edge states is guaranteed by the nonzero Berry curvature owing to the presence of spin-orbit interactions.

In my talk, I will briefly give overview of edge and nanoscale effects on electronic transport properties of graphene nanostructures [1]. After that, we shall discuss a two-dimensional lattice model which exhibits a nontrivial topological phase in the absence of the Berry curvature on the basis of two-dimensional Su- Schrieffer–Heeger (SSH) model [2]. Since this system possesses both time-reversal and inversion symmetries, Berry curvature is zero but finite Berry connection. In spite of the absence of Berry curvature, the system leads to the robust edge states. Also, we discuss possible candidates of topological 2D materials, e.g. A3B biatomic sheet on the basis of first-principles calculations [3], and 2D photonic crystals [2]. Our approach will serve to design the topological 1D and 2D materials in absence of spin-orbit interactions.

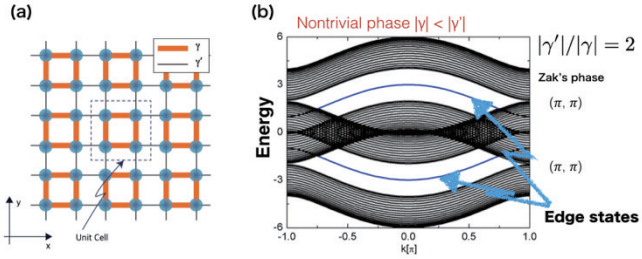

Fig.1 (a) 2D SSH model and (b) corresponding energy dispersion for ribbon structure in nontrivial phase.

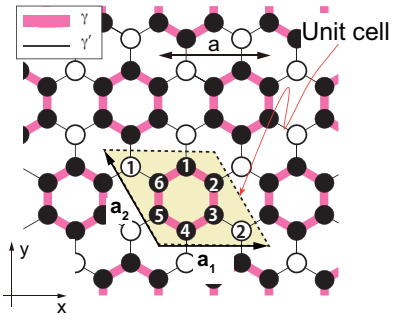

Fig.2 Lattice structure of A3B biatomic sheet

[1] K. Wakabayashi, et.al., Sci. Technol. Adv. Mat. **11,** 054504 (2010), Sold Stat. Comm. **152**, 1420 (2012).

[2] F. Liu, and K. Wakabayashi, PRL **118**, 076803 (2017), Phys. Rev. B**97**, 035442 (2018), J. Phys. Soc. Jpn. 123707 (2017).

[3] T. Kameda, F. Liu, S. Dutta, K. Wakabayashi, Phys. Rev. B (under review)

Corresponding Author: K. Wakabayashi

Tel: +81-79-565-9751, Fax: +81-79-565-9729,

E-mail: waka@kwansei.ac.jp URL: http://www.kg-nanotech.jp/tmd/

Electroluminescence from transition metal dichalcogenide monolayers

Taishi Takenobu

Department of Applied Physics, Nagoya University, Nagoya 464-8603, Japan

Transition metal dichalcogenide (TMDC) monolayers, such as molybdenum disulfide (MoS_2) and tungsten diselenide (WSe_2), have attracted strong attention as novel graphene-like materials due to their large bandgap (1−2 eV) and excellent transport properties. Moreover, the thickness of monolayer TMDCs is less than 1 nm, which is one of the thinnest materials, and it leads to strong confinement effects, resulting in large binding energy of exciton (> 100 meV) and formation of charged excitons. Particularly, due to their layered structure, there are no dangling-bond states on the surface of TMDC monolayers and it could be an ideal quantum well, providing potential as novel optoelectronic functionalities and devices [1,2].

One of the interesting functionalities of TMDCs is circularly polarized light emission (CPE), due to a non-centrosymmetric two-dimensional crystal, strong spin-orbit interaction, non-zero Berry curvature and resulting spin-valley coupling [3-5]. Although there have been many reports on CPE confirmed by photoluminescence spectra, the demonstrations of circularly polarized electroluminescence are still limited. This is because the technical difficulty in the fabrication of TMDC light-emitting device, which requires the intentional doping techniques for formation of p-n junctions [2].

Recently, we developed the electrochemical method to dope holes and electrons [6-10], and demonstrated light-emitting device of MoS_2, $MoSe_2$, WS_2 and WSe_2 monolayers [11-13]. Firstly, we fabricated ion-gel (a mixture of ionic liquid and triblock co-polymer) gated EDLTs (Electric Double Layer Transistors) using large-area TMDC monolayers, grown by chemical vapor deposition [6-10]. The Fermi level of TMDCs can be continuously controlled by gate voltages. The hole mobility of WSe_2 can be 90 cm^2/Vs at high carrier density of 10^{14} cm^{-2}, whereas the MoS_2 showed electron mobility of 60 cm^2/Vs. By the combination of p-type WSe_2 and n-type MoS_2, we also demonstrated CMOS inverters [10].

Finally, we use this technique for photo-detection and light-emitting devices based on various forms of TMDCs, such as monolayer polycrystalline films, single crystalline flakes, and lateral heterojunctions [11-13]. Particularly, using single crystal samples, we observed robust circularly polarized EL emission and, very recently, we are challenging the demonstration of circularly polarized EL emission at room temperature.

[1] X. Xu *et al.* Nat. Phys. **10**, 343 (2014).
[2] J. Pu and T. Takenobu, Adv. Mater. **30**, 1707627 (2018).
[3] D. Xiao *et al.* Phys. Rev. Lett. **108**, 196802 (2012).
[4] K. F. Mak *et al*. Nat. Nanotechnol. **7**, 494 (2012).
[5] Y. J. Zhang *et al*. Science **344**, 725 (2014).
[6] J. Pu, T. Takenobu *et al.* Nano Lett. **12**, 4013 (2012).
[7] J. Pu, T. Takenobu *et al*. Appl. Phys. Lett. **103**, 23505 (2013).
[8] J.-K. Huang, T. Takenobu *et al*. ACS Nano. **8**, 923 (2014).
[9] Y.-H. Chang, T. Takenobu *et al*., ACS Nano. **8**, 8582 (2014).
[10] J. Pu, T. Takenobu *et al*. Adv. Mater. **28**, 4111 (2016).
[11] D. Kozawa, T. Takenobu *et al*. Appl. Phys. Lett. **109**, 201107 (2016).
[12] J. Pu, T. Takenobu *et al*. Adv. Mater. **29**, 1606918 (2017).
[13] M.-Y. Li, J. Pu, T. Takenobu *et al*. Adv. Funct. Mater. **28**, 1706860 (2018).

Corresponding Author: T. Takenobu
Tel: +81-52-789-5173, Fax: +81-52-789-3712, E-mail: takenobu@nagoya-u.jp

Single SWCNT spectroscopy

○Yoshikazu Homma[1], Shohei Chiashi[2]

[1]*Department of Physics, Tokyo University of Science, Tokyo 163-8601, Japan*
[2]*Department of Mechanical Engineering, The University of Tokyo, Tokyo 113-8656, Japan*

A single-walled carbon nanotube (SWCNT) has several remarkable features: in shape, it is an inert cylinder with a nanometer diameter, serving as an excellent vessel for molecular confinement; its quasi-one dimensionality causes the singular electronic states, which make SWCNTs attractive objects in physics and electronics; the covalent carbon bonds make an SWCNT an extremely tough wire, which is stable in ambient air. Combining those features, we can use SWCNTs for measurements of adsorbed or encapsulated molecules as well as SWCNTs' intrinsic properties.

SWCNTs grown by chemical vapor deposition form a power-line like structure between micropillars in a self-assembling fashion [1,2]. With a careful preparation, we can grow singly suspended SWCNTs, as long as tens of micrometers, which are free from the substrate and other SWCNTs and have both the outer surface and inner space for molecular adsorption. Because an SWCNT is a monolayered material, it receives dielectric interaction from adsorbates. Furthermore, the quasi 1D electronic structure allows resonant optical transitions, which are sensitively influenced by the dielectric environment. A suspended SWCNT is thus an ideal material for examining the behaviors of molecules on the surface or in the nano-space by means of optical spectroscopy.

We used isolated SWCNTs to investigate molecular adsorption/encapsulation (ethanol [3], water [4-6], and DNA [7]), and intrinsic phonon/thermal properties of SWCNTs by photoluminescence and Raman spectroscopy. The nanotube wall provides special restriction to adsorbed/encapsulated molecules via van der Waals potential. Molecules condensed in the nano-space of SWCNT can be regarded as a pure lD system, while those on the outer surface form a 2D system. The investigations of phase transition of those structures offer test beds for low dimensional thermodynamics. For intrinsic phonon/thermal properties, radial-breathing mode frequencies free from environmental effects [8], phonon symmetry of G-bands [9], as well as thermal conductivity of SWCNTs [10] were elucidated using individual SWCNTs. The single SWCNT spectroscopy provides fruitful information on nano-scale physics and chemistry.

[1] Y. Homma *et al.* Appl. Phys. Lett. **81**, 2261 (2002).
[2] Y. Homma, S. Chiashi, Y. Kobayashi, Rep. Prog. Phys. **72**, 066502 (2009).
[3] S. Chiashi *et al.* Nano Lett. **8**, 3097 (2008).
[4] Y. Homma, S. Chiashi *et al.* Phys. Rev. Lett. **110**, 157402 (2013).
[5] S. Chiashi *et al.* J. Phys. Chem. Lett. **5**, 408 (2014).
[6] S. Chiashi *et al.* ACS Nano in press.
[7] M. Ito *et al*. J. Phys. Chem. C. **119**, 21141 (2015).
[8] S. Chiashi *et al.* Phys. Rev. B **91**, 155415 (2015).
[9] Y. Tanaka *et al.* in preparation.
[10] K. Yoshino *et al.* ACS Omega **3**, 4352 (2018).

Corresponding Author: Y. Homma
Tel: +81-3-2558-8244, Fax: +81-3-2558-47388,
E-mail: homma@rs.tus.ac.jp

Structure control, Mass Production and Applications of Well Aligned Carbon Nanotubes

Fei Wei

Beijing Key Lab of Green Reaction Engineering & Technology, Tsinghua University, China

As one of the nanomaterial representatives, one-dimensional carbon nanotubes (CNTs) possess extraordinary mechanical, electrical, thermal, optical properties, as well as controllable reactivity. This renders their broad applications in the fields of energy storage and transition, composites, heterogeneous catalysis, environmental protection, and drug delivery. This talk presents the chemical and engineering principles of CNTs mass production. The detailed strategies for mass production of multi-walled CNTs, single-walled CNTs, double-walled CNTs, CNT arrays, super-aligned CNTs, super-long CNTs, doped CNTs, coiled CNTs, CNT junctions, as well as CNT/graphene hybrids were all presented. Meanwhile, the key engineering considerations in standardization, environment, health, and safety were analyzed, and their commercialization process was evaluated. During recent decades, CNT production capacity has reached more than thousands of tons per year, greatly decreasing the price of CNTs. The bulk applications for Li-ion battery, conductive nanocomposites, automotive, sporting goods have been achieved. Although the unique physiochemical properties of an individual CNT are stated repeatedly, manifestation of such unique properties in a macroscopic material, e.g., realization of high-strength CNT fibers, remains a great challenge. If such challenges are solved, many critical applications will be enabled. However, more efforts should be devoted on the chemical route for mass production and engineering route for commercialization of high performance CNTs, in order for versatile properties and applications. The basic research for CNTs production and application will flourish the nanotechnology industry for sustainable society.

Biography

Fei Wei Cheungkong scholar Professor,
Director of Beijing key lab of green chemical reaction engineering and technology, Fei Wei obtained his PhD in chemical engineering from China University of Petroleum in 1990. After a postdoctoral fellowship at Tsinghua University (China), he was appointed an associate professor in 1992 and professor of chemical engineering of Tsinghua University (China) in 1996. His scientific interests are technological applications of chemical reaction engineering, multiphase flow, carbon nano materials, and sustainable energy. He has designed and successfully running over 30 industrial fluidized bed reactors, and authored three books and over 600 refereed publications with more than 37000 citations with H index 87

Environment effects on the charge states of metallic and semiconducting SWCNTs during ELF separation

Yuki Kuwahara [1], ○Takeshi Saito[1]

[1] *National Institute of Advanced Industrial Science and Technology, Tsukuba 305-8565, Japan*

Since the as-produced SWCNTs are generally a mixture of those with metallic (m-) and semiconducting (s-) electrical properties, their separation is desirable, especially for the semiconducting applications because these are extremely sensitive to impurities. To separate the m- and s-SWCNTs, we have recently developed the electric-field-induced layer formation (ELF) method.[1] In the ELF method, a DC electric field is applied in the longitudinal direction to a SWCNT dispersion containing the nonionic surfactant of polyoxyethylene (100) stearyl ether (Brij S100) as a surfactant. Interaction with the electric field leads to the accumulation of m- and s-SWCNTs into the upper and lower parts of the dispersion, respectively, forming divided layers. The s-SWCNT dispersion obtained from ELF separation is promising as an ink in printed electronics. We have fabricated s-SWCNT thin film transistors by using the ELF-separated s-SWCNT dispersion as a semiconductor ink, and demonstrated that these devices possess high performance, small hysteresis, and low variability in their characteristics.[2,3]

Because of the similarity between ELF separation and electrophoresis, the charge states of SWCNTs in the dispersion are expected to play an important role in the ELF separation. We had firstly explained the ELF separation mechanism by difference in the charge states between micelles containing s- and m-SWCNTs.[1] However, in our previous study, the m- and s-SWCNTs separated by ELF showed no difference in their electrophoretic behavior, which obviously contradicted the proposed mechanism. Thus far, the detailed mechanism of ELF separation remained an open question.

In this study, the environment effects, namely the pH and Brij-S100 concentration in the SWCNT dispersion during ELF separation were investigated. The zeta potentials, as an important property for evaluating the charge state and the influence in electric field, were measured for the m- and s-SWCNTs after the separation.

Time course analysis showed that the pH and surfactant concentration in the cell become inhomogeneous during the ELF separation process. The zeta potential measurements revealed that the s-SWCNTs are much more negatively charged than m-SWCNTs in the specific pH range. The mechanism of ELF separation of m- and s-SWCNTs is attributed to the dynamic changing/balancing of the electrophoretic and electroosmotic forces acting on the different SWCNTs.

[1] K. Ihara, H. Endoh, T. Saito, F. Nihey, J. Phys. Chem. C **115**, 22827 (2011).
[2] H. Numata, K. Ihara, T. Saito, H. Endo, F. Nihey, Appl. Phys. Express **5** 055102 (2012).
[3] S. Ohmori, K. Ihara, F. Nihey, Y. Kuwahara, T. Saito, RSC Adv. **2** 12408 (2012).

Corresponding Author: T. Saito
Tel: +81-29-861-4863, Fax: +81-29-861-4413,
E-mail: takeshi-saito@aist.go.jp

Multifunctional carbon nanomaterials for biomedical applications

Alberto Bianco

University of Strasbourg, CNRS, Immunology, immunopathology and therapeutic chemistry, UPR 3572, 67000 Strasbourg, France

Carbon-based nanomaterials are considered unique systems for many applications in different fields including biomedicine. All these carbon forms are offering the possibility of original chemical functionalization and design of complex multifunctional systems that allow further their exploitation in therapy, imaging and diagnosis [1, 2].

In this presentation, I will describe the chemical strategies to functionalize different carbon nanomaterials with appropriate functional groups and therapeutic molecules in view of their biomedical applications. I will also present few example of their use in therapy (i.e. cancer) [3, 4] and imaging (i.e. ultrasonography and MRI) [5].

In addition, the intense research activity on applications of carbon materials imperatively needs a strong association with the assessment of their safety profile [6]. We have evidenced a correlation between the structure and the chemical nature of the different materials and their potential toxicity. In this context, I will describe how it is possible to enhance the biodegradability and tune the toxic effects of these different materials [7-11].

[1] K. Kostarelos, A. Bianco, M. Prato, Nat. Nanotech. **4**, 627 (2009).

[2] G. Reina, G.; J. M. González-Domínguez, A. Criado, E. Vázquez, A. Bianco, M. Prato, Chem. Soc. Rev. **6**, 4400 (2017).

[3] I. Marangon, C. Ménard-Moyon, A. K. A. Silva, A. Bianco, N. Luciani, F. Gazeau, Carbon **97**, 110 (2016).

[4] J. Russier *et al.* Angew. Chem. Int. Ed. **56**, 3014 (2017).

[5] L. Delogu *et al.* Proc. Natl. Acad. Sci., USA **109**, 16612 (2012).

[6] A. Bianco, Angew. Chem. Int. Ed. **52**, 4986 (2013).

[7] H. Ali-Boucetta et al. Angew. Chem. Int. Ed. **52**, 2274 (2013).

[8] R. Kurapati *et al.* Small **11**, 3985 (2015).

[9] A. R. Sureshbabu *et al.* Biomaterials **72**, 20 (2015).

[10] R. Kurapati *et al.* 2D Materials **5**, 015020 (2018).

[11] R. Kurapati *et al.* Angew. Chem. Int. Ed. **57**, 11722 (2018).

Corresponding Author: A. Bianco
Tel: +81-75-753-6833, Fax: +81-75-753-6833,
E-mail: a.bianco@ibmc-cnrs.unistra.fr

招待講演
Invited Lecture

1 I – 1 ～ 1 I – 2
2 I – 3 ～ 2 I – 4
3 I – 5

Atomic Scale Stability of Nano-Sized Tungsten-Cobalt Intermetallic Compounds in Reactive Environment at High Temperature

Feng Yang and Yan Li
College of Chemistry and Molecular Engineering, Peking University, Beijing 100871, China

Revealing the catalyst structure and chemistry in the reactive environment at the atomic scale is imperative for the rational design of catalysts as well as the investigation of reaction mechanism for the synthesis of single-walled carbon nanotubes, while in situ characterization at the atomic scale in high temperature (>700 ºC) is still a great challenge. Here, tracking intermetallic Co_7W_6 nanoparticles with a defined structure and a high melting point by in situ environmental transmission electron microscope in combination with synchrotron X-ray absorption spectroscopy, we directly present the structural and chemical stability of the Co_7W_6 nanocrystals in methane, carbon monoxide, and hydrogen at the temperature of 700–1100 ºC. The evidences are in situ and real time. They are of both atomic scaled resolution and collective information. This research offers an example of systematic investigation at atomic scale on catalysts under reactive condition.

Corresponding Author: Yan. Li
Tel & Fax: +86-10-6275-6773
E-mail: yanli@pku.edu.cn

New Developments in the Science and Applications of Wafer-Scale Crystalline Carbon Nanotube Films

Weilu Gao,[1] Natsumi Komatsu,[1] Fumiya Katsutani,[1] Kazuhiro Yanagi,[4] and Junichiro Kono[1-3]

[1]*Department of Electrical and Computer Engineering,* [2]*Department of Physics and Astronomy, and* [3]*Department of Materials Science and NanoEngineering, Rice University, Houston, Texas 77005, U.S.A.*
[4]*Department of Physics, Faculty of Science and Engineering, Tokyo Metropolitan University, Hachioji, Tokyo 192-0397, Japan*

Recently, we have developed a controlled vacuum filtration method for the preparation of wafer-scale films of crystalline chirality-enriched single-wall carbon nanotubes, and such films have enabled new fundamental studies and applications [1]. In this talk, we will first discuss the controlled vacuum filtration technique [2,3], and then summarize recent discoveries in optical spectroscopy studies and optoelectronic device applications using films prepared by this technique. These include the observation of intersubband plasmons [4], microcavity exciton polaritons with polarization-dependent ultrastrong coupling [5], isotropic Seebeck coefficient with anisotropic electrical conductivity [6], and the direct observation of cross-polarized excitons [7].

1. W. Gao and J. Kono, "Science and Applications of Wafer-Scale Crystalline Carbon Nanotube Films Prepared through Controlled Vacuum Filtration," arXiv:1810.02928.
2. X. He, W. Gao, L. Xie, B. Li, Q. Zhang, S. Lei, J. M. Robinson, E. H. Hároz, S. K. Doorn, R. Vajtai, P. M. Ajayan, W. W. Adams, R. H. Hauge, and J. Kono, "Wafer-Scale Monodomain Films of Spontaneously Aligned Single-Walled Carbon Nanotubes," *Nature Nanotechnology* **11**, 633 (2016).
3. N. Komatsu, W. Gao, P. Chen, C. Guo, A. Babakhani, and J. Kono, "Modulation-Doped Multiple Quantum Wells of Aligned Single-Wall Carbon Nanotubes," *Advanced Functional Materials* **27**, 1606022 (2017).
4. K. Yanagi, R. Okada, Y. Ichinose, Y. Yomogida, F. Katsutani, W. Gao, and J. Kono, "Intersubband Plasmons in the Quantum Limit in Gated and Aligned Carbon Nanotubes," *Nature Communications* **9**, 1121 (2018).
5. W. Gao, X. Li, M. Bamba, and J. Kono, "Continuous Transition between Weak and Ultrastrong Coupling through Exceptional Points in Carbon Nanotube Microcavity Exciton–Polaritons," *Nature Photonics* **12**, 362 (2018).
6. K. Fukuhara, Y. Ichinose, H. Nishidome, Y. Yomogida, F. Katsutani, N. Komatsu, W. Gao, J. Kono, and K. Yanagi, "Isotropic Seebeck Coefficient of Aligned Single-Wall Carbon Films," *Applied Physics Letters* **113**, 243105 (2018).
7. F. Katsutani, W. Gao, X. Li, Y. Ichinose, Y. Yomogida, K. Yanagi, and J. Kono, "Direct Observation of Cross-Polarized Excitons in Aligned Single-Chirality Single-Wall Carbon Nanotubes," *Physical Review B* **99**, 035426 (2019).

Corresponding Author: J. Kono
Tel: +1-713-348-2209
E-mail: kono@rice.edu

FC-CVD of SWNTs with Pre-made Bimetallic catalysts and the Effect of Sulphur

○ Saeed Ahmed, Yongping Liao, Aqeel Hussain, Qiang Zhang, Er-Xiong Ding, Hua Jiang and Esko I. Kauppinen

Department of Applied Physics, Aalto University School of Science, Puumiehenkuja 2, 00076 Aalto, Finland

We studied systematically effect of catalyst composition on yield, morphology, conductivity and helicity of SWNTs grown with the floating catalyst chemical vapor deposition (FC-CVD). To the best of our knowledge, this is the first report on single-step synthesis of SWNTs with well characterized, both monometallic(Fe, Co, Ni) as well as bimetallic (Co-Ni, Co-Fe) catalyst particles with 3 nm mean diameter made via physical vapor condensation i.e. the spark discharge method. Ethylene was used as the carbon source and nitrogen with 20 vol. % of hydrogen as the carrier gas at the 1050 ºC synthesis temperature. Optical characterizations revealed that as-grown SWNTs have high quality and their mean diameter is around 1 nm. Moreover, SWCNTs synthesized by bimetallic Co-Ni catalyst have very unique optical properties compared to others. Furthermore, from unambiguous electron diffraction (ED) technique, we observed that Co-Ni can produce comparatively narrower chirality and diameter distribution. In addition, we studied the effect of adding sulphur via introducing H_2S into the reactor.

Corresponding Author: E. Kauppinen
Tel: +358-40-509-8064, Fax: +358-9-2451-3517,
E-mail: esko.kauppinen@aalto.fi

[1], [2][3][4][5][6]

[1] D. Sun *et al.*, “Flexible high-performance carbon nanotube integrated circuits,” *Nat. Nanotechnol.*, vol. 6, no. 3, pp. 156–161, Mar. 2011.
[2] D.-M. Sun *et al.*, “Mouldable all-carbon integrated circuits,” *Nat. Commun.*, vol. 4, pp. 1–8, 2013.
[3] A. E. Islam, J. A. Rogers, and M. A. Alam, “Recent Progress in Obtaining Semiconducting Single- Walled Carbon Nanotubes for Transistor Applications,” *Adv. Mater.*, vol. 27, pp. 7908–7937, 2015.
[4] Q. Cao, S. Han, G. S. Tulevski, A. D. Franklin, and W. Haensch, “Evaluation of Field-Effect Mobility and Contact Resistance of Transistors That Use Solution-Processed Single-Walled Carbon Nanotubes,” *ACS Nano*, vol. 6, no. 7, pp. 6471–6477, 2012.
[5] E. A. Laird *et al.*, “Quantum transport in carbon nanotubes,” *Rev. Mod. Phys.*, vol. 87, no. 3, pp. 703–764, 2015.
[6] P. Stokes and S. I. Khondaker, “High quality solution processed carbon nanotube transistors assembled by dielectrophoresis,” *Appl. Phys. Lett.*, vol. 96, p. 83110, 2010.

[1] D. Sun *et al. Nat. Nanotechnol.* 6, 156 (2011).
[2] D.-M. Sun *et al. Nat. Commun.* 4,2302 (2013).
[3] A. E. Islam, J. A. Rogers, and M. A. Alam *Adv. Mater.* 27, 7908 (2015).
[4] Q. Cao, S. Han, G. S. Tulevski, A. D. Franklin, and W. Haensch *ACS Nano* 6, 6471 (2012).
[5] E. A. Laird *et al. Rev. Mod. Phys.* 87, 703 (2015).
[6] P. Stokes and S. I. Khondaker *Appl. Phys. Lett.*96, 83110 (2010).

NEDO-TSC's future efforts in 2-D materials R&D

○Takayuki Iseki

Technology Strategy Center (TSC), New Energy and Industrial Technology Development Organization (NEDO), Kanagawa 224-8550, Japan

Since the discovery of carbon nanotube (CNT) by Dr. Iijima in 1991 [1], NEDO has been supporting R&D of nanocarbon materials and their applications. Particularly since 2014, graphene research has been included in NEDO's nanocarbon practical utilization project [2]. Through this project, large-area Roll-to-Roll graphene plasma growth method [3] and multilayered graphene X-ray beam sensor for large-scale particle accelerators have been developed and the latter has been commercialized [4]. This project was completed in 2016 and some of the application research activities are now being conducted in another project [5].

Today, not only graphene but also another two-dimensional (2-D) materials such as transition metal dichalcogenides (TMD), black phosphorene and h-BNs are widely studied. 2-D materials are expected to offer higher potential for technology innovation because of their unique electrical characteristics.

In Japan, the SATL (Science of Atomic Layers) research project was conducted by JSPS (Japan Society for the Promotion of Science) from 2013 to 2017, and since 2014, 2-D materials project has been conducted by JST-CREST. The Japanese government considers TRL (Technology readiness level) transition with three project steps the most ideal R&D scheme. TRL includes JSPS, JST and NEDO projects (Fig.1). NEDO-TSC is responsible for producing R&D strategies of national project by backcasting of the possible socioeconomic status and forecasting from the current technology trend. Attainment of excellent 2-D materials research results are anticipated in order to realize the NEDO/TSC strategy.

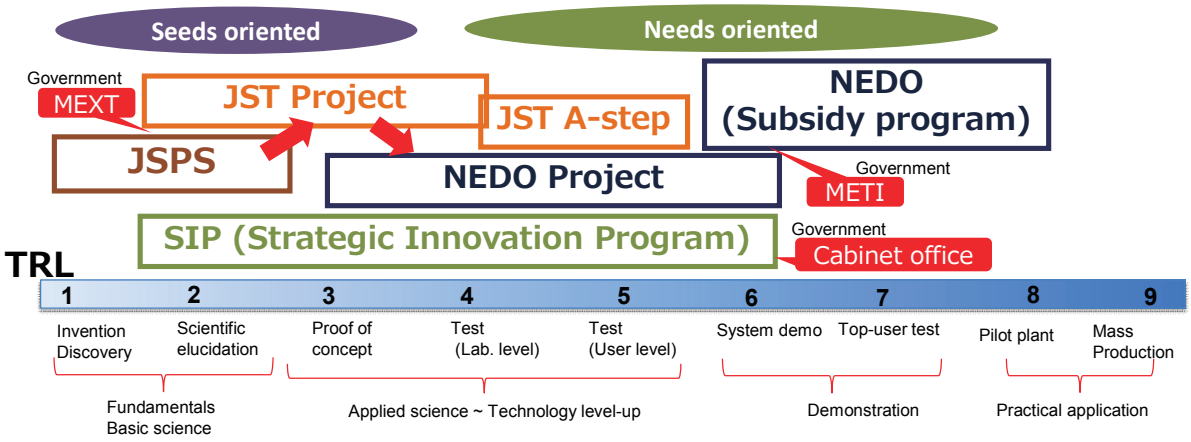

Fig.1 Japanese national projects stages and TRL. (Source : NEDO-TSC)

[1] S. Iijima, Nature, 354 (1991), page 56–58
[2] https://www.nedo.go.jp/activities/ZZJP_100020.html (In Japanese)
[3] T. Yamada *et al*, Thin Solid Films, Volume 532(2013), Pages 89-93
[4] A. Tatami *et al*, AIP Conference Proceedings 1962, 030005 (2018);
[5] https://www.nedo.go.jp/activities/ZZJP_100119.html (In Japanese)

Corresponding Author: Takayuki Iseki
Tel: +81-44-520-5150, Fax: +81-44-520-5204,
E-mail: isekitky@nedo.go.jp

Graphene-based reflectarrays for wireless terahertz communications

Arka Karmakar[1], Farah Vandrevala[1], Arjun Singh[1], Josep M. Jornet[1] and Erik Einarsson[1,2]

[1]Department of Electrical Engineering, University at Buffalo, Buffalo, NY USA
[2]Department of Materials Design and Innovation, University at Buffalo, Buffalo, NY USA

Edholm's law of bandwidth describes the observation that wireless data rates have doubled approximately every 18 months. If this trend continues, we should cross the terabit-per-second threshold very soon, but conventional technologies are not capable of such speeds. Graphene may enable this next generation of wireless technology [1] due to its unique ability to support surface plasmon polaritons at terahertz frequencies [2].

In pursuit of this idea, we design, model, fabricate, and characterize all-graphene and metal–graphene antenna designs [3,4]. Using time-domain THz spectroscopy, we extract graphene's complex optical properties as well as the response of the antenna arrays [5].

A metal–graphene hybrid reflectarray and the corresponding simulated response are shown in the upper part of Fig. 1. The lower part of the same figure shows the graphene quality was unaffected by the fabrication process. The design was for 1.5 THz, and spectroscopic characterization shown in Fig. 2 reveals a clear reflection enhancement at 3λ/2. Graphene affects this response, suggesting the reflected power should be tunable by modifying graphene's electrical conductivity.

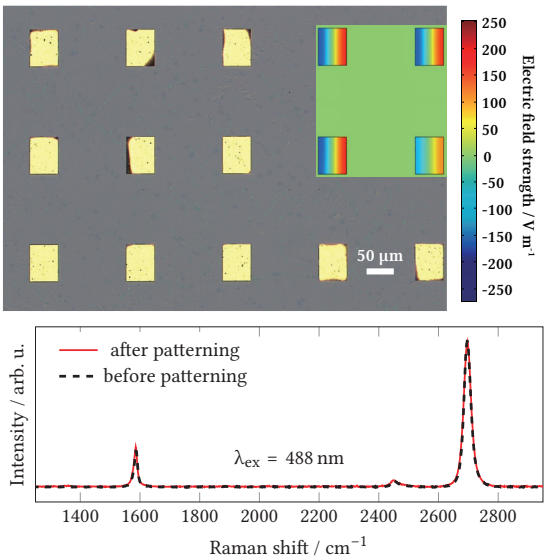

Fig. 1 (Top) Optical micrograph showing an array of gold antennas fabricated atop continuous graphene. Inset shows a numerical simulation of the electric field response. Scale bar applies to both images. (Bottom) Normalized Raman spectra obtained before and after graphene patterning.

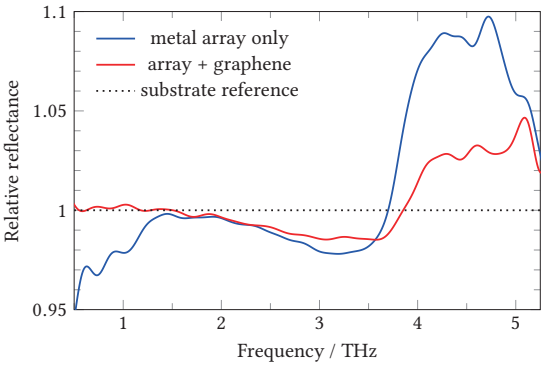

Fig. 2 THz reflectance measured relative to the underlying Si substrate. Increased reflectance is apparent at 4.5 THz, and is weakened by the presence of underlying graphene.

[1] A. F. Akyildiz and J. M. Jornet, *IEEE Wireless Comm. Mag.* **17** (2010) 58.

[2] A. H. Castro Neto et al., *Rev. Mod. Phys.* **81** (2009) 109.

[3] L. Zakrajsek et al., *IEEE Ant. Wireless Prop. Lett.* **15** (2015) 1553.

[4] A. Karmakar et al., in *NANOCOM '18: Proceedings of the 5th ACM International Conference on Nanoscale Computing and Communication,* Reykjavík (2018).

[5] F. Vandrevala et al., in *NANOCOM '18: Proceedings of the 5th ACM International Conference on Nanoscale Computing and Communication,* Reykjavík (2018).

Corresponding Author: E. Einarsson
Tel: +1-716-645-5089, E-mail: erikeina@buffalo.edu

一般講演
General Lecture

1 – 1 ～ 1 – 10
2 – 1 ～ 2 – 12
3 – 1 ～ 3 – 11

Carbyne@CNT on a film scale formed after field emission: Characterization by Raman and TEM

Satoshi Toma[1], Koji Asaka[1], Satoshi Kashiwaya[1], Tomonari Wakabayashi[2] and ○Yahachi Saito[3]

[1] *Department of Applied Physics, Nagoya University, Nagoya 464-8603, Japan*
[2] *Department of Chemistry, Kindai University, Higashi-Osaka 577-8502, Japan*
[3] *Toyota Physical and Chemical Research Institute, Nagakute 480-1192, Japan*

Carbyne, an infinite carbon chain, has attracted much interest and induced significant controversy for many decades. Recently, long linear carbon chains (LCCs) confined stably inside carbon nanotubes (CNTs), which were produced by arc-discharge [1] and high-temperature annealing [2], have been reported. We accidentally discovered a novel method to produce long LCCs encapsulated inside single-wall CNTs (SWCNTs) on a film scale after field emission (FE) experiments of SWCNT films, as reported in Ref. 3. In the present report, additional findings obtained especially by Raman spectroscopy are presented.

After a thick film of eDIPS SWCNT (Meijo Nano Carbon) underwent a severe FE experiment, long LCCs encapsulated inside SWCNTs (Fig. 1) as well as double-wall and triple-wall CNTs were found in the film. Long LCCs inside CNTs are longer than 30 nm (i.e., more than 230 carbon atoms). Beside transmission electron microscopy (TEM), Raman scattering spectroscopy of SWCNT films containing carbyne@CNT was carried out using several excitation laser wavelengths (355, 532, 671 and 785nm) at room temperature. At 532 nm laser excitation, a prominent LCC peak at around 1860 cm^{-1} originating from longitudinal optical phonons of carbyne (long polyyne) as shown in Fig. 2, where 2nd and 3rd harmonics of the LCC peak are clearly observed. FWHM of the fundamental LCC band at 532 nm excitation is relatively wide ca. 200 cm^{-1}, suggesting it is composed of several components. At 671 nm excitation, split LCC peaks ranging from 1790 to 1850 cm^{-1}, being red-shifted, were observed. On the other hand, at 355 and 785 nm excitations, no LCC peak was observed. These observations indicate strong resonant Raman scatterings at excitation photons (1.85 - 2.33 eV) which match with energy gaps of the present long LCCs.

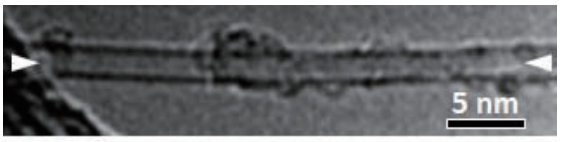

Fig. 1 TEM picture of a long LCC inside SWCNT.

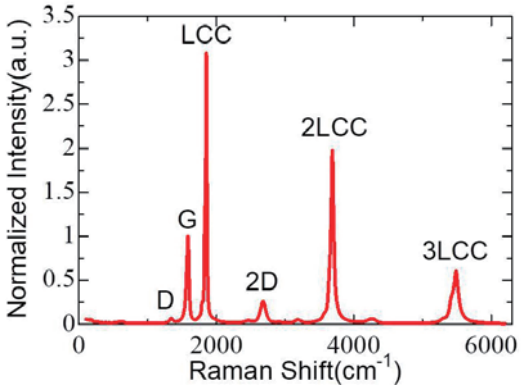

Fig. 2 Raman spectrum from a SWCNT film containing LCC@CNT.

Raman measurement at 671 nm excitation was conducted by Nanophoton Corp.

[1] X. Zhao et al, Phys. Rev. Lett. **90** (2003) 187401.
[2] L. Shi et al, Nature Mater. **15** (2016) 634.
[3] S. Toma, K. Asaka, M. Irita, and Y. Saito, Surf. Interface Anal. **51** (2019) 131.

Corresponding Author: Y. Saito
Tel: +81-561-57-9516, Fax: +81-561-63-6302, E-mail: ysaito@toyotariken.jp

Isolation of Single-wired Transition Metal Monochalcogenides by Carbon Nanotubes

○Yusuke Nakanishi[1, 2], Masataka Nagata[2], Shivani Shukla[3], Zheng Liu[4, 5], Yung-Chang Lin[5], Takuma Shiga[6], Yuto Nakamura[7], Takeshi Koyama[7], Hideo Kishida[7], Kazu Suenaga[5], and Hisanori Shinohara[1]

[1] *Department of Physics, Tokyo Metropolitan University, Hachioji 192-0397, Japan.*
[2] *Department of Chemistry, Nagoya University, Nagoya 464-8602, Japan.*
[3] *Department of Materials Science & Engineering, Carnegie Mellon University, PA, USA.*
[4] *National Institute of Advanced Industrial Science & Technology, Nagoya 463-8560, Japan.*
[5] *National Institute of Advanced Industrial Science & Technology, Tsukuba 464-8602, Japan.*
[6] *Department of Mechanical Engineering, The University of Tokyo, Tokyo 113-8656, Japan.*
[7] *Department of Applied Physics, Nagoya University, Nagoya 464-8603, Japan.*

The successful isolation of single-layers from 2D van der Waals (vdW)-layered materials has opened new frontiers in materials science. Their discovery and unique properties laid the foundation for exploring 1D counterparts. However, the isolation of 1D vdW-wired materials has thus far remained a challenge due to inefficient techniques. In theory, single-wires of some vdW-wired materials could possess electronic properties distinct from their bulk counterparts [1, 2], although this has never been fully verified by experiments.

Here we report the facile isolation of transition metal monochalcogenide MoTe nanowires (MoTeNWs) by using carbon nanotubes (CNTs) as templates. Individual MoTeNWs are perfectly separated by CNTs with a minimal interaction, allowing easy handling and detailed characterization of MoTeNWs. Atomic-resolution transmission electron microscopy revealed unusual torsional motions absent in their bundles (Figure 1). Our findings indicate their potential for building blocks of electromechanical switching devices.

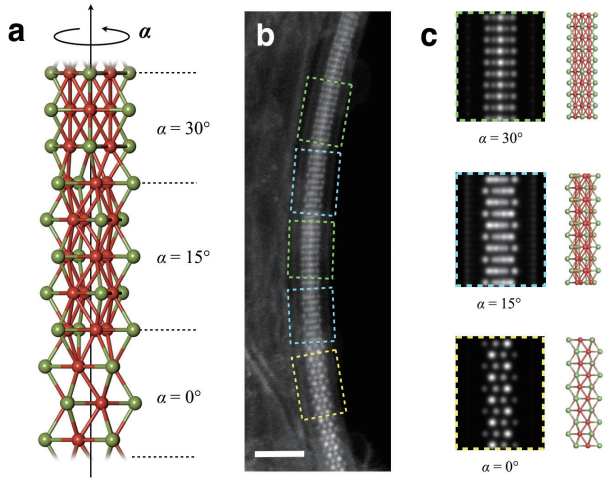

Fig. 1 (a) Schematic of dynamic movements of MoTeNWs. (b) Experimental and (c) Simulated STEM image of a twisted MoTe confined in a single CNT. Scale bar, 1 nm.

[1] I. Popov *et al*. *Nano Lett.* **8**, 4093 (2008).
[2] Y. Yu *et al*. *Nano Lett.* **18**, 675 (2018); H. Zhu *et al*. *Adv. Mater.* **29**, 1606264 (2017).

Corresponding Author: Y. Nakanishi
Tel: +81-42-677-2449 (3324)
E-mail: naka24ysk@tmu.ac.jp

Enhancement of Excitonic Valley Polarization by Carrier Doping in Monolayer WSe_2

○Keisuke Shinokita[1], Xiaofan Wang[1], Yuhei Miyauchi[1], Kenji Watanabe[2], Takashi Taniguchi[2], Kazunari Matsuda[1]

[1]*Institute of Advanced Energy, Kyoto University, Uji 611-0011, Japan*

[2]*Advanced Materials Laboratory, National Institute for Materials Science, Tsukuba 305-0044, Japan*

Atomically thin transition metal dichalcogenides (TMDs) is ideal two-dimensional system and possesses valley degrees of freedom inherently, making monolayer (1L) TMDs an excellent platform to explore new physics and applications [1]. The exploits of the valley degrees of freedom require high valley polarization by overcoming the ultrafast valley relaxation processes. Here we report that intentional carrier doping could suppress the valley relaxation process by fine-tuning of Coulomb screening.

We investigated the effect of carrier doping on valley depolarization process using photoluminescence (PL) measurement on 1L-WSe_2. Figure 1(a) shows colormap of the PL spectra of 1L-WSe_2 on Si/SiO_2 substrate as a function of applied gate voltage using field-effect-transistor structure at 70 K. The gate voltage controlled doped carrier density, which is clearly observed in appearance of charged exciton (T^+, T^-) in addition to neutral exciton (X). Figure 1(b) shows the PL spectra with gate voltages of −12 V (circles). Figure 1(c) shows polarization-resolved PL spectra with various gate voltages, under σ_+ excitation corresponding to K valley excitation. The σ_+ component of the PL spectra of the neutral exciton (closed circles) has a higher intensity than the σ_- component of the PL spectra (open circles) under gate voltage of −4 V. The photoexcited excitons are more populated in the pumped K valley, which corresponds to the valley-polarized state of the excitons (valley polarization). By increasing the hole density by decreasing the gate voltage from -4 V to -12 V and -20 V, the difference between the σ_+ and σ_- component increased, showing the valley polarization of the neutral exciton was enhanced. The results indicate the intentional carrier doping suppressed valley relaxation between the K and −K valleys by screening the momentum-dependent long-range e–h exchange interactions [2, 3].

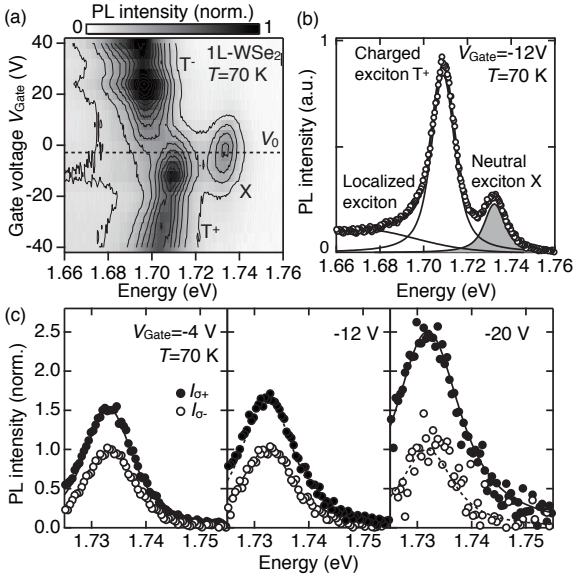

Fig.1: (a) Contour plot of PL spectra of 1L-WSe_2 as a function of applied gate voltage at 70 K. (b) PL spectra at the gate voltage of −12 V (circles), and a spectral fitting using Voigt functions (curves). The shaded peak shows the exciton PL (X). (c) Polarization-resolved PL spectra under σ_+ excitation at various gate voltages. The red and blue circles show the σ_+ and σ_- PL intensities, respectively. The spectra were normalized with the σ_- intensity of the neutral exciton.

[1] X. Xu *et al*., Nat. Phys. **10**, 343 (2014).
[2] Y. Miyauchi *et al*., Nat. Commun. 9, 2598 (2018).
[3] K. Shinokita *et al*., submitted for publication.

Corresponding Author: K. Shinokita
Tel: +81-774-38-3465, FAX: +81-774-38-4567,
E-mail: shinokita.keisuke.4r@kyoto-u.ac.jp

STM images of graphene/C-doped h-BN heterostructures from first-principles electronic-structure calculations

○Taishi Haga [1], Yoshitaka Fujimoto [1], Susumu Saito [1,2,3]

[1] Department of Physics, Tokyo Institute of Technology, Tokyo 152-8551, Japan
[2] Advanced Research Center for Quantum Physics and Nanoscience, Tokyo Institute of Technology, Tokyo 152-8551, Japan
[3] Materials Research Center for Element Strategy, Tokyo Institute of Technology, Kanagawa 226-8503, Japan

Hexagonal boron nitride (h-BN) is a wide-gap semiconductor in contrast to graphene while h-BN has a honeycomb lattice structure in each layer similar to graphene. Therefore, h-BN attracts much attention not only as substrate for graphene and other 2D materials but also itself as future nanoelectronics materials. Defects in semiconductor often play an important role to determine and modulate the electronic properties of the system. Actually, it has been suggested that defects in h-BN substrate affects transport properties of graphene [1,2]. Therefore, it is important to investigate how a impurity in h-BN substrate affects the electronic properties of graphene. In the present work, we study the effect of impurity state induced by carbon atom doped at the B site and that at the N site in h-BN substrate layers on the electronic structure of the graphene/h-BN heterostructures using first-principles calculations within the framework of the density functional theory (DFT) [3]. Furthermore, we simulate scanning tunneling microscopy (STM) images of the C-doped heterostructues. It is found that substitutional doping of the C atom at the B site and that at the N site in underlying h-BN lead to asymmetric charge carrier concentrations in the graphene layer. It is also found that the C impurity at the N site affects electronic states of the system up to surface graphene layer, and it can be visualized even in the case of the doping in the third h-BN layer [Fig.1], while the C impurity at the B site does not change the STM image of the graphene layer on the pristine h-BN.

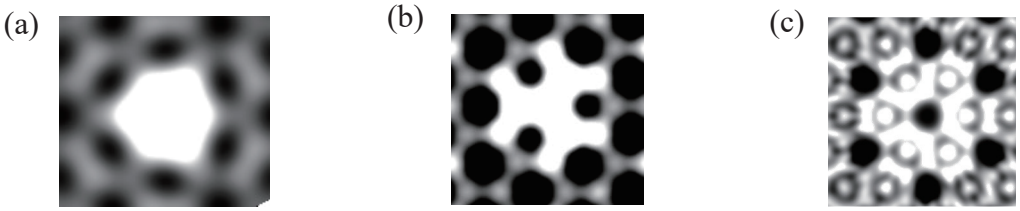

Figure 1 Simulated STM images of graphene on C-doped h-BN substrate model. The doped C atom is at N site in the (a) first layer, (b) second layer, (c) third layer of h-BN.

[1] D. Wong *et al.*, Nat. Nanotechnol. **10**, 949 (2015).
[2] T. Kaneko, M. Koshino, and R. Saito, Phys. Rev. B **95**, 125421 (2017).
[3] T. Haga, Y. Fujimoto, and S. Saito, to be published.

Corresponding Author: T. Haga
E-mail: haga.t@stat.phys.titech.ac.jp

Sedimentation particle size analysis of carbon nanotube aggregates

○Yuichi Kato, Takahiro Morimoto, Kazufumi Kobashi, Takeo Yamada, Toshiya Okazaki, Kenji Hata

CNT-Application Research Center, National Institute of Advanced Industrial Science and Technology (AIST), Central 5, 1-1-1 Higashi, Tsukuba 305-8565, Japan

Measuring particle size distribution of carbon nanotube (CNT) aggregates in liquids is important for evaluating debundling, size reduction, dispersion stability, and film formation properties from their dispersions. Here we propose a method to determine "universal" sedimentation particle diameter with a disk centrifuge.

We found a phenomenon that the Stokes diameter (D_{stokes}) of CNT aggregates decreases as the rotation speed (ω) increases (Fig. 1, dashed lines). This indicates that particle sedimentation can not be interpreted by the common Stokes equation (1),

$$u = \frac{\Delta\rho {D_{\mathrm{stokes}}}^2 R\omega^2}{18\eta} \tag{1}$$

where u is the sedimentation velocity, $\Delta\rho$ is the difference of density between particle and fluid, R is the disk radius, and η is the viscosity. The D_{stokes} is not suitable for representing particle size distribution for CNT aggregates. As a result of investigating several hypotheses explaining this Stokes diameter dependence of the rotation speed, it is found that the Stokes diameter change can be explained by the buoyancy caused by the density difference between the inner fluid of the particle and the outer fluid (Fig. 1, inset illustration). This buoyancy slows the particle sedimentation. The density difference between inner and outer fluids increases when the particle sediments in the density gradient solution. The density difference then decreases due to the diffusion of sucrose into the inner fluid.

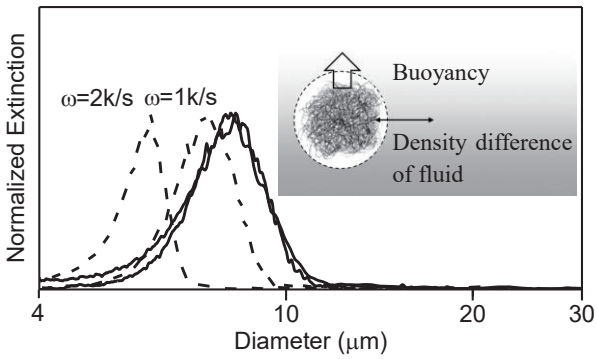

Fig. 1 Sedimentation particle diameter distribution of CNT aggregate measured with a disk centrifuge. (dashed lines): D_{stokes}, (solid lines): $D_{\mathrm{corrected}}$.

The corrected sedimentation particle diameter ($D_{\mathrm{corrected}}$) can be obtained by using the relation between the sedimentation velocities and the rotation speeds based on the simple equation (2),

$$u = \frac{\Delta\rho {D_{\mathrm{corrected}}}^2 R\omega^2}{18\eta + \tau\frac{d\rho_{f,e}}{dR}\phi {D_{\mathrm{corrected}}}^2 R\omega^2} \tag{2}$$

where τ is the time constant of diffusion of sucrose, $\frac{d\rho_{f,e}}{dR}$ is the density gradient, and ϕ is the porosity of the particle.

Corresponding Author: Toshiya Okazaki
Tel: +81-29-861-4173, Fax: +81-029-861-4851
E-mail: toshi.okazaki@aist.go.jp

One-dimensional van der Waals heterostructure nanotubes: synthesis and characterization

○Rong Xiang,[1]* Yongjia Zheng,[1] Taiki Inoue,[1] Shohei Chiashi,[1] Shigeo Maruyama[1,2]*

[1] *Department of Mechanical Engineering, The University of Tokyo, Tokyo 113-8656, Japan*
[2] *Energy NanoEngineering Lab., National Institute of Advanced Industrial Science and Technology (AIST), Tsukuba. 305-8564, Japan*

Recently, we proposed a conceptually new structure, in which single- or few-walled hexagonal boron nitride nanotube (BNNT) and/or MoS_2 nanotube seamlessly wrap around a single-walled carbon nanotube (SWCNT), and result in an atomically smooth coaxial nanotube consisting different materials. As different shells are stacked by van der Waals (vdW) force and in one-dimensional (1D) geometry, we name it "1D vdW heterostructure".[1] Electron energy loss spectroscopy mappings reveal the composition of co-axial structure (Figure 1) and TEM/STEM direct imaging together with electron diffractions confirm each layer is single-crystal nanotube.

However, the current synthesis technique is still in its early stage, and locating the heterostructure relies mostly on TEM. In this presentation, we will further demonstrate our efforts on the controlled synthesis and characterizations of this new structure. 1D vdW heterostructure nanotubes can now be synthesized on longer, and mostly isolated SWCNTs suspended on micro-pillars or TEM micro-grids, which allows us to take optical characterizations on this structure at single-nanotube level. Furthermore, we present a direct comparison between TEM and SEM contrast for the same nanotube, suggesting that SEM may be employed as a quick assessment for such 1D vdW heterostructure nanotubes.

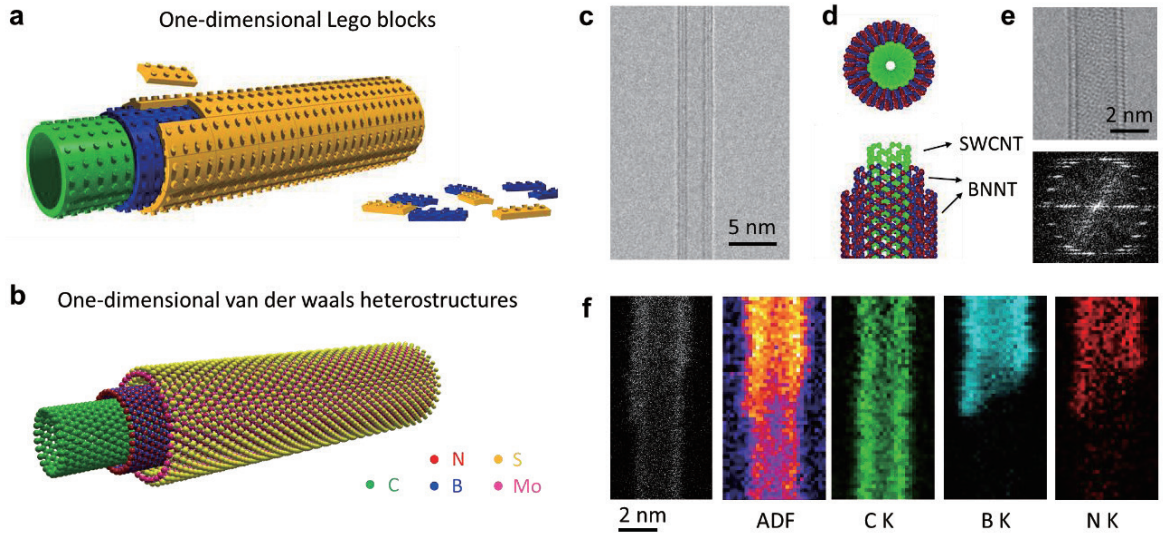

Figure 1 Overview of 1D vdW heterostructures. (a) A one dimensional Lego block showing the concept of this work; (b) the atomic model of one material built in this study: metal-insulator-semiconductor (M+I+S) 1D vdW heterostructures; (c-f) TEM image and EELS mapping of a SWCNT-BNNT 1D vdW heterostructure.

[1] R. Xiang et al., arXiv:1807.06154

Email: xiangrong@photon.t.u-tokyo.ac.jp (RX); maruyama@photon.t.u-tokyo.ac.jp (SM).

Diameter-Dependent Superconductivity in Individual WS_2 Nanotubes

○Feng Qin[1], Toshiya Ideue[1], Wu Shi[1, 2], Xiao-xiao Zhang[3], Masaro Yoshida[4], Alla Zak[5], Reshef Tenne[6], Tomoka Kikitsu[4], Daishi Inoue[4], Daisuke Hashizume[4], Yoshihiro Iwasa[1, 4]

[1] *Quantum Phase Electronics Center (QPEC) and Department of Applied Physics, The University of Tokyo, Tokyo, Japan.*

[2] *Materials Science Division, Lawrence Berkeley National Laboratory, Berkeley, USA.*

[3] *Quantum Matter Institute, University of British Columbia, Vancouver, Canada.*

[4] *RIKEN Center for Emergent Matter Science (CEMS), Wako, Saitama, Japan.*

[5] *Department of Materials and Interfaces, Weizmann Institute of Science, Rehovot, Israel.*

[6] *Faculty of Sciences, Holon Institute of Technology, Holon, Israel.*

Superconductivity in low dimensional Transition Metal Dichalcogenides (TMD) materials has been attracting significant attention in recent years. Among them, the TMD nanotube is a fascinating platform for researching superconductivity because of its unique dimensionalities and geometries. Here we report the first observation of superconductivity in an individual multi-walled tungsten disulfide (WS_2) nanotube [1], realized by electrochemical doping via the liquid gating technique as shown in Fig. 1. Remarkably, for the first time, the chirality of the nanotube has been confirmed in the superconducting state, and the chiral signal displays an unprecedented quantum oscillation in conjunction with the periodic oscillating magnetoresistance, known as the Little-Parks effect. In addition, the critical temperature of superconductivity displays an unexpected linear behaviour as a function of the inverse diameter, that is, the curvature of the nanotube [2]. The present results are an important step in understanding the microscopic mechanism of superconductivity in a nanotube, opening up a new way of superconductivity in crystalline nanostructures.

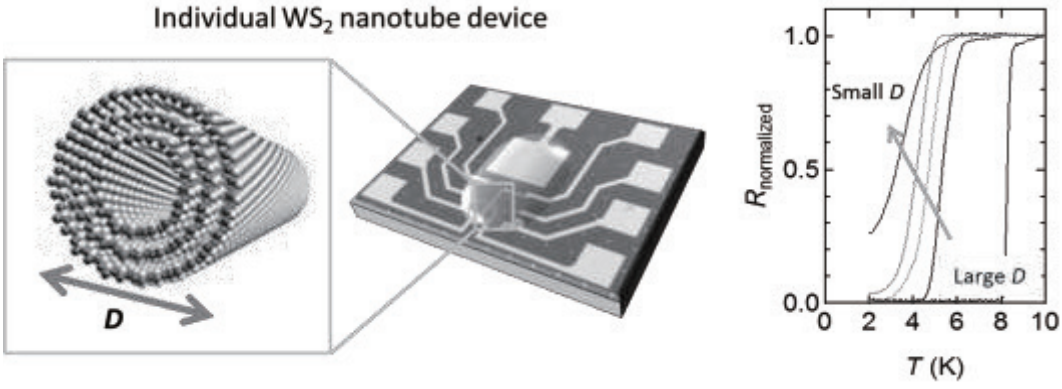

Fig. 1. Schematic figure of liquid gating device and the diameter-dependent superconducting properties in individual WS_2 nanotubes.

[1] F. Qin *et al.*, *Nature Communications* **8**, 14465 (2017).

[2] F. Qin *et al.*, *Nano Letters*, **18**, 6789-6794 (2018).

Corresponding Author: F. Qin

Tel: 03-5841-6822(26822), Fax: 03-5841-6822(26822),

E-mail: qinfeng@mp.t.u-tokyo.ac.jp

Synthesis of Heteroatom-doped Graphene as Active Catalysts for Hydroquinones Oxidation Reaction

○Masanori Hara, Prerna Joshi, Hsin-Hui Huang, Masamichi Yoshimura

Toyota Technological Institute, Nagoya 468-8511, Japan

1. Introduction

Recently, to overcome environmental and energy issues such as global warming and depletion of fossil fuels, combining renewable energies with energy storage and supply system has attracted attention to utilize renewable energies effectively. Direct-type fuel cell (DFC), where hydrogen carrier molecules [1,2] formed by surplus renewable energies are used as fuel, is one of the candidates of efficient energy supply systems. DFC has similar constitution of polymer electrolyte fuel cell and requires specific catalysts for hydrogen carrier molecule oxidation as anode. Improvement of the catalytic activity of the anode is important topic for practical applications. In the present study, we have synthesized heteroatom, nitrogen and boron, doped graphene as catalysts for electro-oxidation reaction of hydroquinones. We characterized the novel catalysts and evaluated its catalytic activity.

2. Experimental

Graphene oxide (GO) was prepared by Hummers' method. The nitrogen and boron-doped reduced graphene oxide, N-rGO and B-rGO, were synthesized by thermal annealing synthesis. Briefly, mixture of GO and urea or B_2O_3 were heated at 800 or 1000 °C for 1 h, respectively. Reduced graphene oxide (rGO) was prepared by thermal annealing at 150 °C for 2 h under 3% H_2 + Ar atmosphere. The rGO, N-rGO, and B-rGO were characterized by SEM-EDX, XPS, and electrochemical methods, LSV and RDE, in 0.1 M H_2SO_4 + 1 mM hydroquinones.

3. Results and discussion

The composition of the catalysts, 2.9 wt% of boron for B-rGO and 10.4 wt% of nitrogen for N-rGO, were estimated by SEM-EDX and XPS characterization. Figure 1 shows LSV curves of oxidation reaction of methyl-hydroquinone (Me-HQ) on rGO, N-rGO and B-rGO measured in 0.1 M H_2SO_4 + 1 mM Me-HQ. On rGO, oxidation current of Me-HQ was observed from 0.56 V and reached to mass transport limiting current around 0.82 V. On the other hand, potential of mass transport limiting region of the Me-HQ oxidation reaction shifted to 0.77 and 0.70 V on N-rGO and B-rGO, respectively. The LSV curves show that heteroatom doped graphene catalysts have high activity for hydroquinone oxidation. The present results suggest that the heteroatom modified graphene is a promising candidate of anode for DFC.

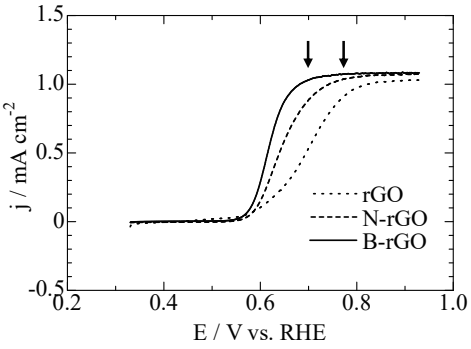

Fig. 1 Linear sweep voltammogram of rGO, N-rGO, and B-rGO in 0.1 M H_2SO_4 + 1 mM methyl hydroquinone solution. Scan rate: 5 mV s^{-1}, Rotation rate: 1000 rpm.

[1] D. Sopchak, B. Miller, Y. Avyigal, R. Kalish, J Electroanal. Chem. 538 (2002) 39.

[2] B. Rausch, M. D. Symes, L. Cronin, J. Am. Chem. Soc. 135 (2013) 13656.

Corresponding Author: M. Hara

Tel: +81-52-809-1850, Fax: +81-52-809-1851,

E-mail: haram@toyota-ti.ac.jp

Electrostatic properties of bilayer graphene nanoribbons under an external electric field

○Yanlin Gao, Susumu Okada

Graduate School of Pure and Applied Sciences, University of Tsukuba, Tsukuba, 305-8571, Japan

Graphene has been attracting a great deal of attention in the fields of nanoscience and nanotechnology due to its peculiar physical property and extensive application prospects. The atom thickness, high electrical conductivity, and remarkable chemical stability allow graphene to be a promising material for field emission devices. In such devices, graphene exhibits rich variation in its morphologies, such as the functionalized edges, edge shape variations, surface wrinkles, and step structures, depending on the fabricating conditions. Our previous works have clarified that the field emission properties of graphene depends on its edge shape [1] and functionalization [2,3]. On the other hand, the knowledge about the electrostatic properties of graphene with surface wrinkles and step edges is insufficient to date. Therefore, in this work, to understand the morphological effects arising from the multi-layered structures on field emission property of graphene, we investigated electrostatic properties of bilayer graphene nanoribbons (GNRs) with different edge morphologies and interlayer stacking, using the density functional theory combined with the effective screening medium method.

Our calculations show that field emission property for the bilayer GNR depends on the edge shape and the terrace width. Armchair bilayer GNRs have higher field emission current than zigzag ones due to their lower potential barriers. Moreover, the potential barrier for bilayer GNRs decreases with increasing the terrace width irrespective of the edge shape, so that the field emission current from bilayer GNRs increases with increasing the terrace width for both armchair and zigzag edges [Fig.1]. In addition, for the edge morphology, we consider the folded zigzag and armchair GNRs, and found that the field emission property is sensitive to the chirality of the folded moiety. Folded zigzag GNRs have lower potential barrier, producing higher field emission current compared with folded armchair GNRs due to the absences of the dangling bond and edge states.

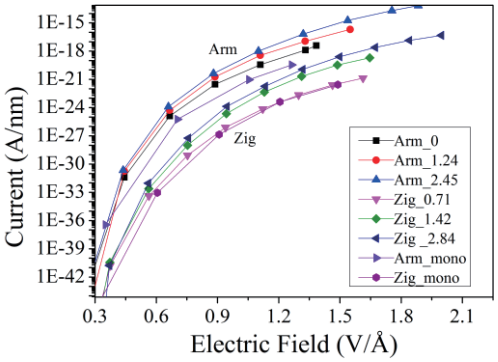

Fig.1 Field emission current for bilayer GNRs with different terrace width.

Reference

[1] Y. Gao and S. Okada, *Appl. Phys. Lett.* **112**, 163105 (2018)
[2] Y. Gao and S. Okada, *Appl. Phys. Express* **10,** 055104 (2017)
[3] Y. Gao and S. Okada, *Carbon* **142**, 190-195, (2019)

Corresponding Author: Y. Gao
TEL: +81-29-853-5921, FAX: +81-29-853-5924
E-mail: ylgao@comas.frsc.tsukuba.ac.jp

Geometric and electronic structures of three-dimensional polymerized triptycene

Y. Fujii[1], M. Maruyama[1], and S. Okada[1]

[1]*Graduate School of Pure and Applied Science, University of Tsukuba, 1-1-1 Tennodai, Tsukuba, Ibaraki305-8571, Japan*

Triptycene is the Y-shaped hydrocarbon molecule composed of sp^2 and sp^3 C atoms, in which three benzene rings are adjoined to two sp^3 C atoms with D_{3h} symmetry. Because the molecule possesses a threefold symmetry axis, it is able to form two-dimensional covalent framework in which the molecules are hexagonally arranged. Several polymeric forms of triptycene have been indeed synthesized experimentally and they are energetically stable with peculiar electronic band structures [1,2]. In addition, by stacking the two-dimensionally polymerized layers of triptycene and connecting them each other via sp or sp2 C atoms, we can get three-dimensional covalent networks, being expected to exhibit further interesting variation in their electronic structure. Therefore, in the present work, each two-dimensional covalent layer is connected via sp^3 C atom with C2 chain (Fig. 1). Because of the negligible π electron between the layers, the electronic structure of the three-dimensional networks reflect that of the two-dimensional network: The three-dimensional networks still have peculiar electronic band structure in its valence and conduction states consisting of the combination of the Dirac cone and a flat dispersion band (Fig. 2). Total energy of the polymer is 128meV per atom higher than that of benzene, indicating that the networks are energetically stable.

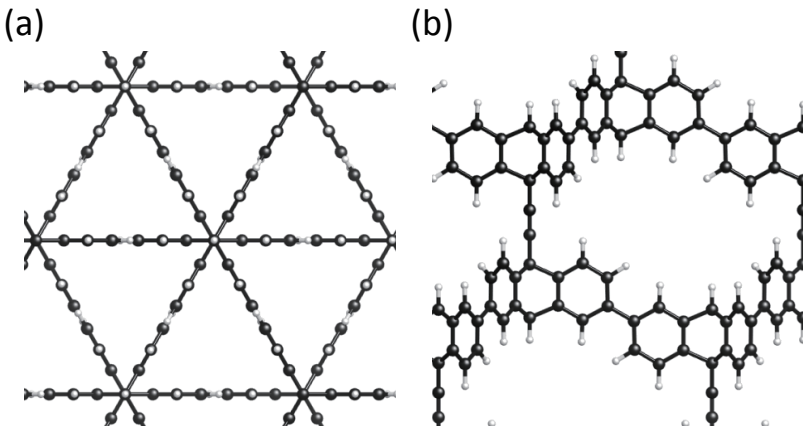

Fig. 1 (a) Top and (b) side views of an optimized structure of three-dimensional triptycene polymer.

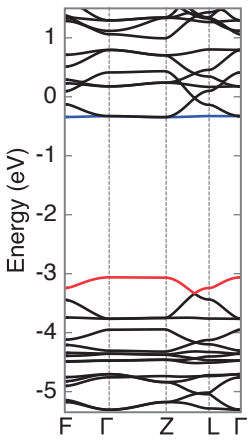

Fig. 2 Electronic structure of three-dimensional triptycene polymer

[1] Y. Fujii, M. Maruyama, K. Wakabayashi, K. Nakada, and S. Okada, J. Phys. Soc. Jpn. **87**, 034704 (2018).

[2] Y. Fujii, M. Maruyama and S. Okada, Jpn. J. Appl. Phys. **57**, 125203 (2018).

Corresponding author: Y. Fujii (yfujii@comas.frsc.tsukuba.ac.jp)

Chirality engineering and metal-to-semiconductor transition of individual CNTs by in situ TEM

○ Dai-Ming Tang [1], Chang Liu [2], Yoshio Bando [1], Hui-Ming Cheng [2], Dmitri Golberg [1]

[1] *World Premier International Center for Materials Nanoarchitectonics, National Institute for Materials Science, Namiki 1-1, Tsukuba, Ibaraki 305-0044, Japan*
[2] *Shenyang National Laboratory for Materials Science, Institute of Metal Research, Chinese Academy of Sciences, 72 Wenhua Road, Shenyang 110016, China*

Chirality is a unique intrinsic structure for the carbon nanotubes (CNTs), determining the electronic, physical and chemical properties. Controlling the chirality is one of the ultimate goals for nanotube science. In recent years, progresses have been made by designing the catalyst seeds for growing CNTs and chirality-specific growth has been realized by using the symmetry matched stable solid catalysts.[1-3]

In the current work, we propose to use a new strategy to control the chirality of CNTs. Instead of controlling the chirality of the whole nanotube, we are aiming at engineering the chirality of the nanotube segment. For example, by changing one segment of the metallic nanotube into semiconducting, the whole nanotube will behave as a semiconductor.

As shown in Fig. 1a, we use a special in situ TEM-STM holder, on which two STM probes are available, so that electrical pulses could be applied and electrical properties of transistors could be measured.[4-8] The structure changes including the chirality could be monitored in real-time (Fig. 1b-c). An interesting pattern of the chirality transitions has been unveiled that the chirality favors changing by continuous (1, 0) dislocations. Importantly, metal-to-semiconductor transition has been realized (Fig. 1d), and an intramolecular Schottky junction is fabricated. Our work not only provides insights to the fundamental chirality dynamics but also offers implications for the CNT based molecular electronic devices. [9]

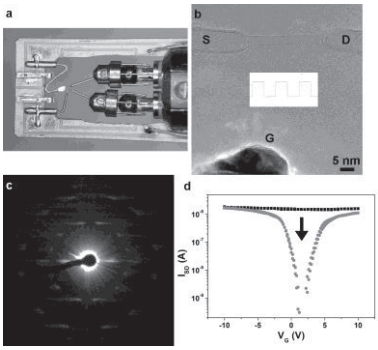

Fig.1 Chirality engineering of individual CNT by in situ TEM probing. (a) Twin-probe TEM-STM holder. (b) TEM image of an engineered SWCNT transistor. (c) Electron diffraction of individual CNT. (d) Transfer curve of a CNT transistor demonstrating metal-to-semiconductor transition

[1] J. R. Sanchez-Valencia et al., Nature 512, 61 (2014).
[2] F. Yang et al., Nature 510, 522 (2014).
[3] S. Zhang et al., Nature 543, 234 (2017).
[4] D.-M. Tang et al., Proc. Natl. Acad. Sci. USA 107, 9055 (2010).
[5] D. Golberg et al., Adv. Mater. 24, 177 (2012).
[6] D.-M. Tang et al., Nat. Commun. 5, 3631 (2014).
[7] D.-M. Tang et al., Nano Lett. 15, 4922 (2015).
[8] J. Han et al., Nat. Commun. 9, 402 (2018).
[9] D.-M. Tang et al., Ultramicroscopy 194, 108-116 (2018).

Corresponding Author: D.-M. Tang
Tel: +81-29-860-4949,
E-mail: Tang.Daiming@nims.go.jp

Derivation of breaking temperature of multi-walled carbon nanotube by using in-situ TEM observations and I-V measurements

○Hitoshi Nakahara[1], Kentaro Yamauchi[1], Koji Asaka[1], Yahachi Saito[2], Satoshi Kashiwaya[1]

[1] *Department of Applied Physics, Nagoya University, Nagoya 464-8603, Japan*
[2] *Toyota Riken, Yokomichi 41-1, Nagakute 480-1192, Japan*

It is well known that a multi-walled carbon nanotube (MWNT) breaks in sequence from its outer layer by direct current heating, but it is extremely difficult to experimentally measure the temperature of the break point at the breaking moment. So that, there is no report on breaking temperature at present. In this research, we focused on the electric resistance change during breaking of a MWNT, and propose a new method to derive the temperature at the breaking moment.

Fig. 1 shows a electric resistance change versus retreat distance during retraction of a broken outer layer of MWNT as shown in inset TEM images. As you can see, the resistance value increases almost linearly with the retreat distance. Fig. 2 is another experiment in which successive breaking of outer layer from 13 layers to 5 layers occurred. In this case, it is impossible to observe outer layer moving directly as shown in Fig. 1, because of the limitation in time resolution of our apparatus (20 ms). However, comparing the resistance change in Figs. 1 and 2 with calculated results of MWNT resistance, it is possible to determine the retraction speed at the moment of breaking of the outer layer. Since the retraction of the outer layer is considered to be associated with the evaporation of carbon atoms at the end of the layer, the temperature can be derived from the retraction speed and the vapor pressure of carbon atoms. By using this method, the result of estimating the temperature at the breaking moment of each layer in Fig. 2 was 3130±40 K, and no significant layer number dependence was observed. Details of derivation method and calculation model will be explained in the presentation.

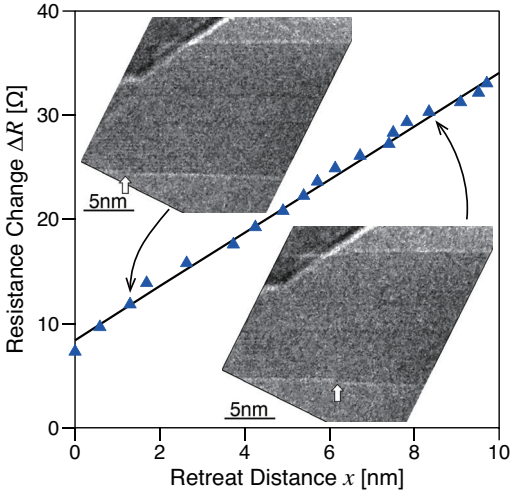

Fig:1 Resistance change versus outer layer retreat distance. Inset figures are TEM images at distances indicated by corresponding arrows. White up-arrows in TEM images indicate outer layer edge positions.

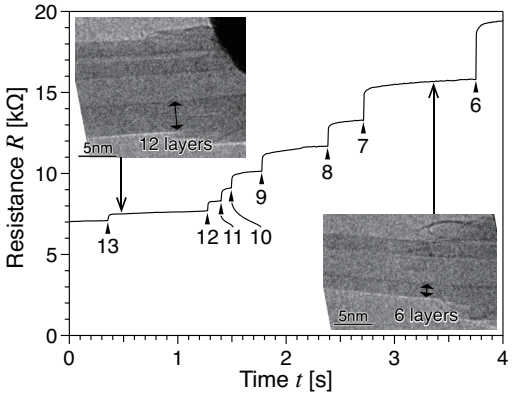

Fig:2 Resistance change during successive breaking of MWNT outer layer by direct current heating. Numbers (n) with arrow heads indicate breaking time of n-th layer. Inset figures are TEM images at time points indicated by corresponding arrows.

Corresponding Author: H. Nakahara
Tel: +81-52-789-4659
E-mail: nakahara@nagoya-u.jp

Semiconducting Carbon Nanotubes as Crystal Growth Templates and Grain Bridges in Perovskite Solar Cells

○Il Jeon[1], Seungju Seo[1], Rong Xiang,[1] Yang Yang[2], Hiromichi Kataura[3], Yutaka Matsuo[1,4], Shigeo Maruyama[1,3]

[1] Department of Mechanical Engineering, The University of Tokyo, Tokyo 113-8656, Japan
[2] Department of Materials Science and Engineering, University of California, Los Angeles, CA 90095, USA
[3] National Institute of Advanced Industrial Science and Technology (AIST), 305-8564, Japan
[4] Hefei National Laboratory for Physical Sciences at the Microscale, University of Science and Technology of China, Anhui 230026, China

Perovskite solar cells (PSCs) have drawn a great deal of attention as an alternative energy source owing to the high absorption coefficient, long-range diffusion length and high defect tolerance of the lead-halide perovskite photoactive layer. Although PSCs are considered to be promising next-generation solar devices, further breakthroughs in terms of power conversion efficiency (PCE) is necessary to supersede conventional silicon solar cells. In this regard, the perovskite grain size control and the passivation of grain boundaries are the key to obtaining high PCE. In particular, inducing homogeneous nucleation while retarding the crystal growth is important for the grain size control. In addition, the passivation of grain surface has a favorable effect as structural disorders at the interface of the grains induce shallow trap states, which lead to non-radiative recombination of localized charge carriers. Therefore, technologies aiming at controlling the grain size as well as passivating the grain interfaces need to be developed.

Over the last two decades, carbon nanotubes have generated a lot of excitement among researchers for their device applicability thanks to their exceptional charge carrier property with outstanding chemical and mechanical stability. In particular, semiconducting single-walled carbon nanotubes (s-SWNTs) possess a direct bandgap of up to 2 eV and high conductivity along the tube axis, qualifying for charge-transporting media in PSCs.

Herein, we demonstrate s-SWNTs dispersed in water functioning as both perovskite crystal growth templates and charge transporters inside a perovskite layer, increasing the PCE of PSCs from 18.1% to 19.5%. Chiral-selective sodium deoxycholate (DOC) surfactants not only allowed the dispersion of s-SWNTs in water but also induced homogeneous and slow crystal growth of the perovskite crystals. s-SWNTs on the surface of the perovskite grains functioned as charge transporters at the grain interface as well.

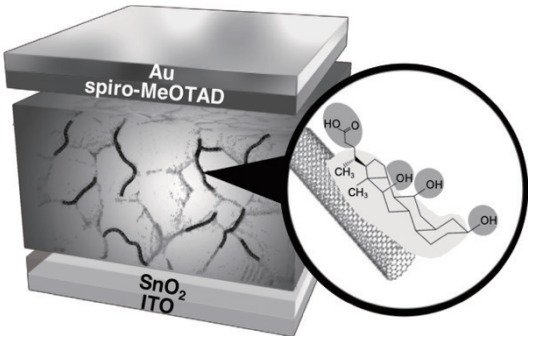

Corresponding Author: Prof. S. Maruyama, Tel: +81-3-5841-6408, E-mail: maruyama@photon.t.u-tokyo.ac.jp

Carrier accumulation in $MoS_2/MoSe_2$-FET by an external electric field

○Mina Maruyama, Susumu Okada

Graduate School of Pure and Applied Sciences, University of Tsukuba, Tsukuba 305-8571, Japan

Transition metal dichalcogenides (TMDCs) are representative semiconducting two-dimensional materials which consist of transition metal atomic layer sandwiched by chalcogen atomic layers in prismatic manner. Thus, they are attracting much attention as for the staring materials for designing van der Waals (vdW) heterostructures with TMDCs or other two dimensional materials, such as graphene and h-BN, by layer-by-layer stacking. Because of the substantial wavefunction overlap between layers, the vdW heterostructures of TMDCs exhibit versatile electronic structure, depending on the constituent layers, their stacking sequence, and mutual stacking arrangements [1]. In our previous work, carrier accumulations in MoS_2/WS_2 heterostructure is sensitive to mutual arrangements of the constituent TMDC layer with respect to the gate electrode. Furthermore, the biaxial strain further modulates the carrier distribution in the heterstructures. In this work, we investigate carrier accumulation in vdW heterostuctures of MoS_2 and $MoSe_2$ under an external electric field for providing a theoretical insight into carrier distribution with respect to the chalcogen species, using the density functional theory combined with the effective screening medium methods.

Our calculations show that carrier accumulation in $MoS_2/MoSe_2$ heterostructure is insensitive to the interlayer arrangement of TMDCs relative to the electrode. Furthermore, we find that the carrier distribution also insensitive to the biaxial compressive/tensile strain, in sharp contrast to the MoS_2/WS_2 heterosheet in the field-effect transistor (FET) structure where the carrier distribution is sensitive to the biaxial strain and to the stacking arrangements. This fact indicates that the transition metal species is the important factor to control the field effect carrier accumulation in FET consisting of TMDC heterostructures.

[1] A. K. Geim and I. V. Grigorieva, Nature **499**, 419 (2013).

Corresponding Author: M. Maruyama
Tel: +81-29-853-5921, Fax: +81-29-853-5924,
E-mail: mmaruyama@comas.frsc.tsukuba.ac.jp

Formation process of long range ordered structure in 1*T*-$TiSe_2$ by electron beam irradiation

○Keita Kobayashi[1], Hidehiro Yasuda [1, 2]

[1] *Research Center for Ultra-High Voltage Electron Microscopy, Osaka University, 7-1, Mihogaoka, Ibaraki, Osaka 567-0047, Japan*
[2] *Division of Materials and Manufacturing Science, Graduate School of Engineering, Osaka University, 2-1, Yamadaoka, Suita, Osaka 565-0871, Japan*

1*T*-$TiSe_2$ is a typical transition metal dichalcogenide with a CdI_2-type structure. Previously, we reported that a multilayer 1*T*-$TiSe_2$ flake with thickness of about 100 nm is induced formation of 2*a* × 2*a* (where *a* is the original lattice constant) long range ordered (LRO) structure by electron beam irradiation with an acceleration voltage of 125 kV [1]. Based on transmission electron microscope (TEM) observations, we also considered that the LRO structure originates from periodic distortion of Ti atomic position [1]. However, it remains unclear that detailed formation process of the LRO structure in 1*T*-$TiSe_2$.

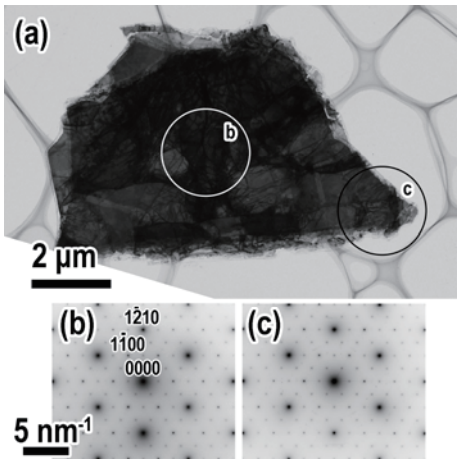

Fig.1 (a) TEM image of a 1*T*-$TiSe_2$ flake. (b and c) Selected area electron diffraction (SAED) patterns obtained from areas "b" and "c" shown in the TEM image. To form the LRO structure in the 1*T*-$TiSe_2$, only area "a" was irradiated by condensed electron beam. Although area "b" had not be irradiated by condensed electron beam, both SAED patterns show ordered reflection attributed to formation of the LRO structure.

Based on this background, we attempted to clarify formation process of the LRO structure in 1*T*-$TiSe_2$ induced due to electron beam irradiation by TEM observation. Consequently, we clarified that the formation process is not contributed by knock-on process and specimen heating due to inelastic electron scattering. We, therefore, consider that the formation process is induced by electronic excitation of 1*T*-$TiSe_2$ due to electron beam irradiation. Moreover, we found that the LRO structure is not only formed in the area irradiated by condensed electron beam but also enlarged to the adjacent unirradiated area (Fig. 1). Since specimen heating due to electron beam irradiation does not contribute to formation of the LRO structure and electron beam broadening through the 1*T*-$TiSe_2$ flake due to electron scattering can be considered to be negligible, we consider that the enlargement of the LRO structure may be proceeded due to chain chemical reaction.

[1] K. Kobayashi, H. Yasuda, Mater. Res. Express **5**, 085006 (2018).

Corresponding Author: K. Kobayashi
Tel: +81-6-6879-7941, Fax: +81-6-6879-7942,
E-mail: kobayashi-z@uhvem.osaka-u.ac.jp

Energetics and electronic structures of in-plane heterostructures of MoS_2 and WS_2

○Hisaki Sawahata[1], Mina Maruyama[1], Susumu Okada [1]

[1] *Graduate School of Pure and Applied Sciences, University of Tsukuba, Tsukuba 305-8571, Japan*

Two-dimensional materials have been attracting much attention in the field of nanosciences and nanotechnologies because of their geometries and electronic properties. They can easily form the three-dimensional van der Waals heterostructures by stacking each other, which possess the unusual electronic and optical properties, depending on the constituent two-dimensional materials and their stacking arrangements. Besides the van der Waals heterostructures, two-dimensional materials could be constituent units for in-plane heterostructures in which the constituent materials form the one-dimensional border, when the materials have similar lattice parameters each other. Indeed, graphene and h-BN form such heterostructure with zigzag borders consisting of BC bonds. Furthermore, appropriate combinations of transition metal dichalcogenides (TMDCs), such as MoS_2/$MoSe_2$ and MoS_2/WS_2, lead to in-plane heterostrcutures. For the heterostructure consisting of graphene and h-BN, our theoretical calculation demonstrated that the energetics and electronic structure of the border strongly depend on its shape [1]. Thus, we can also expect that the physical properties of the heterostructures consisting of TMDCs strongly depend on their border shapes, as the case of the graphene/ h-BN. Therefore, in this work, we aim to elucidate the energetics and electronic structures of heteronanoribbons consisting of MoS_2 and WS_2 strips in terms of their border shapes, using the density functional theory with the generalized gradient approximation and the effective screening medium method.

Figure 1 shows the optimized structure of nanoribbons consisting of MoS_2 and WS_2 with armchair, chiral, and zigzag borders. Among these borders, the armchair border is the most stable, while the zigzag border is the least stable, with the border energies of -1.38, -1.60 and -1.73 eV/Å for zigzag, armchair and chiral borders, respectively. We also found that the electronic structure also depends on the border shape.

[1] H. Sawahata *et al*. Appl. Phys. Express **11**, 065201 (2018).

Corresponding Author:
H. Sawahata
Tel: +81-29-8535921
E-mail:
hsawahata@comas.frsc.tsukuba.ac.jp

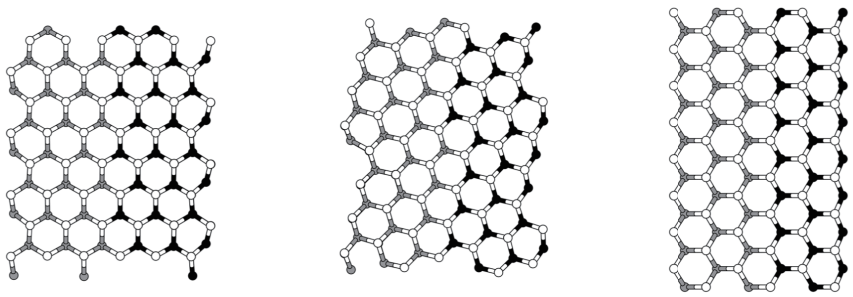

Fig.1 Optimized structures of the ribbons consisting of MoS_2 and WS_2 with armchair, chiral, and zigzag borders. Black, gray and white circles donate W, Mo and S atom, respectively.

Chirality dependence of plasmon peaks in carbon nanotubes

Riichiro Saito○, Daria Sacco, Ahmad R. T. Nugraha, M. Shoufie Ukhtary

Department of Physics, Tohoku University, Sendai

When Kazaoui doped single carbon nanotube, he observed that interband optical absorption which is denoted by *Eii* is suppressed from the lower energy side, that is *E11, E22, E33* by occupying (unoppcupying) electrons (holes) in the conduction (valence) energy band by n (p) doping [1]. When the Fermi energy is located in the conduction (or valence) band of a semiconducting or a metallic nanotube, we expect intraband, optical conductivity which makes a strong optical absorption that is known as plasmon absorption peak. Sasaki has pointed out that the plasmon absorption occurs by the linear polarization of the light perpendicular to the nanotube axis [2]. Yanagi has observed the plasmon peak using the aligned nanotube sample by changing the polarization of light. [3] Senga has observed the plasmon peak of an isolated nanotube in electron energy loss spectroscopy. [4] Thus it is important to investigate the chirality dependence the plasmon frequency and the intensity of the plasmon peaks as a function of *(n,m)* of nanotube and the Fermi energy.

In this presentation, we will show "Plasmon Kataura Plot as a function of the Fermi energy" theoretically for characterizing nanotubes by plasmon peaks. [5] In particular, we discuss (1) the most contributed cutting lines (one-dimensional Brillouin zone) for observing the each plasmon peak and (2) scaling the plasmon peak as a function of the diameter.

References

[1] S. Kazaui et al., *Appl. Phys. Lett.* 78.22, 3433 (2001).

[2] K. Sasaki and Y. Tokura, *Phys. Rev. Appl.* **9**, 034018 (2018).

[3] K. Yanagi et al., *Nature Commn.*, 9,. 1121 (2018)

[4] R. Senga et al., *Nano Letters* 16, 3661 (2016).

[5] D. Sacco et al., unpublished.

Corresponding Author: Riichiro Saito

e-mail : rsaito@flex.phys.tohoku.ac.jp

Web: http://flex.phys.tohoku.ac.jp

Decay dynamics and diffusion lengths of bright and dark excitons in air-suspended carbon nanotubes

○Akihiro Ishii[1,2], Hidenori Machiya [1,3], Yuichiro K. Kato [1,2]

[1] *Nanoscale Quantum Photonics Laboratory, RIKEN Cluster for Pioneering Research, Saitama 351-0198, Japan*
[2] *Quantum Optoelectronics Research Team, RIKEN Center for Advanced Photonics, Saitama 351-0198, Japan*
[3] *Department of Electrical Engineering, The University of Tokyo, Tokyo 113-8656, Japan*

As excitonic states play an important role in optical phenomena [1] in carbon nanotubes, their fundamental properties such as emission lifetime and diffusion length have been studied by various optical techniques [2]. In the lowest lying states of excitons, however, there exist other "dark" states, whose properties are not well understood yet because they are not optically accessible. Here we separately investigate exciton dynamics of parity-odd bright state and parity-even dark state by performing time-resolved photoluminescence measurements on defect-free as-grown carbon nanotubes. The emission decay curves exhibit bi-exponential behavior, where the fast and slow decay components arise from the dynamics of bright and dark excitons, respectively. We analyze such exciton dynamics using a three-level model including the effects of end quenching by measuring chirality-identified nanotubes with different suspended lengths [Fig. 1]. We find that bright excitons have lifetimes of ~70 ps and diffusion lengths of several hundred nanometers, consistent with the known values. In comparison, dark excitons have much longer lifetimes in the order of nanoseconds and diffusion lengths longer than 3 μm. We also observe a tendency that nanotubes with larger diameter have higher bright-dark transition rate, which is likely due to the diameter dependence of the splitting energy between bright and dark states.

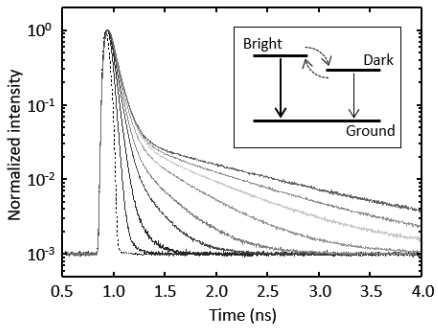

Fig.1 Emission decay curves obtained from (9,8) nanotubes with various lengths ranging from 0.5 μm (bottom) to 4.2 μm (top). The broken line indicates the instrument response function. (inset) Schematic of the three-level model for exciton decay dynamics.

Work supported by JSPS (KAKENHI JP16K13613 and JP17H07359), MEXT (Nanotechnology Platform), and RIKEN (Incentive Research Project). H.M. acknowledges support by RIKEN Junior Research Associate Program. We acknowledge the Advanced Manufacturing Support Team at RIKEN for technical assistance.

[1] A. Ishii, T. Uda, Y. K. Kato, *Phys. Rev. Appl.* **8**, 054039 (2017).
[2] A. Ishii, M. Yoshida, Y. K. Kato, *Phys. Rev. B* **91**, 125427 (2015).

Corresponding Author: Yuichiro K. Kato
Tel: +81-48-462-1111 (ext. 3432)
E-mail: yuichiro.kato@riken.jp

Surface-Enhanced Raman Spectroscopy of Individual Single-Walled Carbon Nanotubes

Juan Yang*, Chenmaya Xia, Daqi Zhang, Henan Li, Sheng Li,
Haoming Liu, Ruoming Li, Yan Li*

College of Chemistry and Molecular Engineering, Peking University, Beijing 100871, China

The resonant Raman spectroscopy can only detect on-resonance single-walled carbon nanotubes (SWNTs). In principle, surface-enhanced Raman scattering (SERS) spectroscopy can enhance the weak signal and expand the resonance window [1]. However, detection of off-resonance SWNTs by SERS remains challenging due to the difficulties in locating the SWNTs exactly at the hot spots with enormous SERS enhancements. Here, we report a facile design of a ultrasonic spray pyrolysis method to *in-situ* form a unique nanocomposite structure with closely spaced polyhedral gold nanocrystals (AuNCs) deposited on suspended SWNTs. The fact that the edges of the AuNCs attach to the SWNTs ensures the location of SWNTs at the hot spots. Consequently, we achieve enormous enhancements of the Raman signal of the SWNTs that are two orders of magnitude higher than any previous values. The enormous enhancements enable the detection of many off-resonance SWNTs and allow the detection of several Raman bands of the SWNTs that have not been reported previously [2].

Moreover, We show that single molecules (SM) encapsulated inside the SWNT and located at the SERS hot spot can be unambiguously detected. We then monitor those SERS fingerprints as the single molecules undergo a chemical reaction inside the SWNTs. The encapsulation of the single molecules inside the SWNT reduces the vast complexities caused by the SM signal fluctuations (including temporal blinking, intensity variation, and spectral wandering) that exist otherwise [3], and may help to achieve a fundamental understanding of the SM behavior and SM reactivity. This approach not only offers a robust and reliable method for SM detection but also opens new possibilities towards SM science by providing an excellent system facilitating the studies of chemistry and physics at the SM level [4].

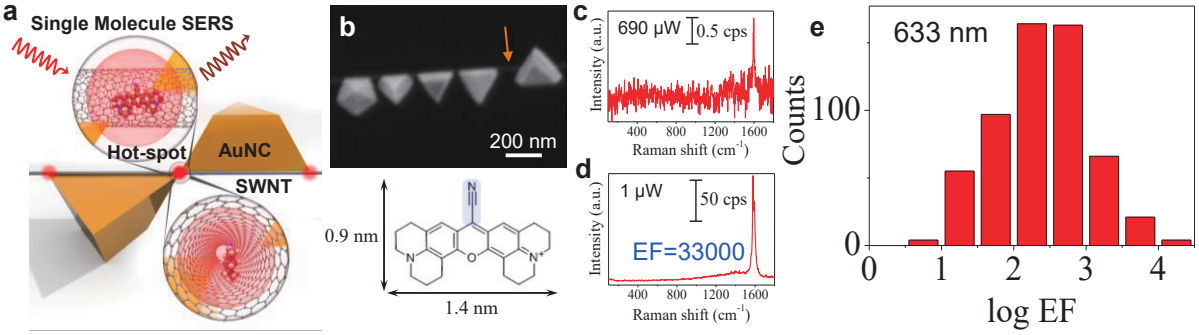

Fig.1 Schematics (a) and SEM image (b) of the AuNCs-SWNT nanocomposite with a single rhodamine 800 molecule encapsulated inside the SWNT and located at the hot spot. The Raman enhancements (c-e) of the AuNCs-SWNT.

[1] H. Chu, J. Wang, L. Ding, *et al.* J. Am. Chem. Soc. **131**, 14310 (2009).

[2] J. Yang, D. Zhang, C. Xia, *et al.* in preparation.

[2] A. B. Zrimsek, N. Chiang, M. Mattei, *et al.* Chem. Rev. **117**, 7583 (2017).

[3] J. Yang, C. Xia, H. Li, *et al.*submitted.

Corresponding Author: J. Yang

Tel: +86-10-62755357

E-mail: yang_juan@pku.edu.cn

Design and Synthesis of a New Ir-catalyst Deposited on Ti Nanotubes for Efficient Water Splitting

Junfang Cheng, Jun Yang, Sho Kitano, Miho Yamauchi, ○Naotoshi Nakashima

International Institute for Carbon-Neutral Energy Research (WPI-I2CNER), Kyushu University, 744 Moto-oka, Nishi-ku Fukuoka, 819-0395, Japan

Development of reliable renewable energy technologies is always the prevailing strategy to balance the mismatch between energy supply and demand[1]. Water electrolysis is a potentially effective method to address the issues of environmental emissions and energy sustainability, while it is severely limited by the sluggish oxygen evolution reaction (OER). IrO_x-based materials are regarded as the most promising candidates in acidic media, but still limited due to the high cost of the Ir metal. To solve this problem, it is crucial to design and fabricate a novel catalyst having a very high OER performance with a reduced Ir amount.

Here, we report a novel Iridium (Ir) catalyst, deposited on Ti nanotubes, with a high concentration of active OH species on its surface. We have discovered that the obtained catalyst shows an excellent OER activity (1.43 V vs. RHE at 10 mA cm^{-2}), which is, to the best of our knowledge, the best performance in acidic media. Moreover, no apparent potential increase was observed even after a chronopotentiometry test at 10 mA cm^{-2} for 100 h and cyclic voltammetry for 700 cycles.

[1] N. Nakashima (Editor), Nanocarbons for Energy Conversion-Supramolecular Approach, *Springer*. pp. 1-564 (2018).

Corresponding Author: N. Nakashima
Tel: +81-92-802-6745, Fax: +81-92-802-6745
E-mail: nakashima.naotoshi.614@m.kyushu-u.ac.jp

Self-Assembly of Nanodiamonds from their Solutions

○Toshihiko Tanaka[1,3], Yasuhiro F. Miura[2], Tetsuya Aoyama[3],
Kazunori Miyamoto[4], Masanobu Uchiyama[3,4], Eiji Osawa[5]

[1]*Department of Chemistry and Biochemistry, National Institute of Technology, Fukushima College, 30 Aza-nagao, Tairakamiarakawa, Iwaki, Fukushima, 970-8034, Japan*
[2]*Hamamatsu University School of Medicine, 1-20-1 Handayama, Higashi-ku, Hamamatsu city, Shizuoka, 431-3192, Japan*
[3]*Elements Chemistry Laboratory, RIKEN Cluster for Pioneering Research, 2-1 Hirosawa, Wako, Saitama, 351-0198, Japan*
[4]*Graduate School of Pharmaceutical Sciences, the University of Tokyo, 7-3-1 Hongo, Bunkyo-ku, Tokyo 113-0033, Japan*
[5]*Nano Carbon Research Institute Ltd., Asama Research Extension Center, Shinshu University, 3-15-1 Tokida, Ueda, Nagano, 386-8567 Japan*

We demonstrate herein further results on the self-assembly of detonation nanodiamonds (DND) from their aqueous colloidal solutions. We already reported two kinds of anisotropic precipitates of DND: one is a fine whisker[1-3] and the other is a nanosheet[3,4]. They are significant with respect to their research and applications because it has suggested the existence of elementary particles of DND, which is a possible novel nanocarbon species containing sp^3 carbons.

The nanosheets were crystallized from a diluted DND solution to the adsorbed DND particles on a Langmuir monolayer of arachidic acid (Ar). We postulate that the monolayer induces the crystallization under the PTFE bars of a Langmuir trough and that the precipitates of ultrathin rectangular nanosheets (~26 nm thick) are squeezed out from the undersurface of the bars to the water surface.(**Fig.1**) Such a process should result in a low content of Ar in the nanosheets. In fact Raman spectra showed that the sheets contain a negligible amount of Ar and that the adsorbed monolayer contains a comparable amount of Ar to that of DND in turn.

Recent procedures provided a small ring (ϕ ~7 mm) of a curved whisker on the wall of a test tube. If a DND solution of over 4 wt.% dries out in the tube, whiskers can be removed easily after drying, thus becoming a ring (**Fig,2**). Although the rings were generally brittle, they were slightly elastic, being able to deform a little without breaking. We will discuss the origin of the self-assembly in these two cases.

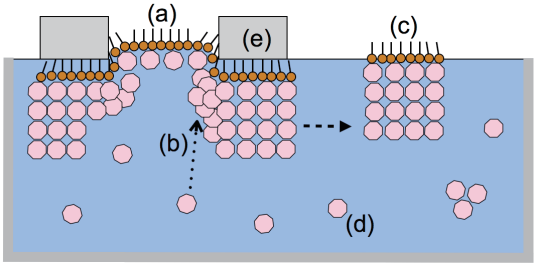

Fig.1 The model of the crystallization under the bar: a) Langmuir monolayer; b) crystallization; c) nanosheet; d) elementary particles of DND; e) PTFE bar.

Fig.2 A ring of a curved DND whisker.

[1] E. Osawa; *Diamond & Related Materials.* 16, 2018–2022(2007). [2] H. Huang, L. Dai, D. H. Wang, L-S. Tanc, E. Osawa; *J. Mater. Chem.*, 18, 1347–1352 (2008,). [3] T.Tanaka, Y.F. Miura, T. Aoyama, M. Takahashi, T. Sato,E. Osawa; *Abstract of the 54th FNTG Symposium*, 28(2018). [4] T.Tanaka, Y.F. Miura, T. Sato, E. Osawa; *Abstract of the 53th FNTG Symposium*, 66(2017)./Tel:+81-268-75-8381/E-mail: osawa@nano-carbon.jp

A Case Study for Nanoparticles on Nanodiamond: Facile Preparation of Nanodiamond-iron oxide Nanohybrid

Ahmad Tayyebi[1], Takuya Hayashi[2], Fumi Yoshino[3], Naoki Komatsu[1]

[1] Graduate School of Human and Environmental Studies, Kyoto University
[2] Institute of Engineering, Water Environment and Civil Engineering, Shinshu University
[3] Department of Obstetrics and Gynecology, Shiga University of Medical Science

Nanodiamonds (NDs) have excellent mechanical and optical properties, large surface areas and tunable surface structures. They were found to be relatively less toxic among nanoparticles, making them well suited to biomedical applications [1]. In order to enhance the intrinsic properties and append new properties, hybridization of NDs with other nanoparticles seems promising technique. However, most of the related work towards such fundamental hybridization is limited to top-down lithography which is typically a very complicated and time-consuming process and is difficult to be scaled up. Here, we develop a facile bottom-up synthetic approach to prepare ND-superparamagnetic iron oxide nanoparticle (SPION) nanohybrid using solvothermal method and investigate its magnetic resonance imaging (MRI) contrast ability and heat generation property in alternating magnetic field.

To prepare ND-SPION particles, first, ND with 50 nm and 100 nm sizes (ND50 and ND100, respectively) were covalently functionalized with hyperbranched polyglycerol (PG) according to the procedure we reported previously [2]. Then, appropriate amount of ND-PG (5.0 mg of NDs) mixed with iron acetylacetone ($Fe(acac)_3$, 13.5 or 31.5 mg) in triethylene glycol (30 mL) to prepare ND: SPION (70:30) or ND: SPION (50:50), respectively. Finally, the mixture was heated up to 230 °C in a 60 mL autoclave for 30 min and kept at the temperature for 30 min.

Figure 1 shows a transmission electron microscopy (TEM) image of ND50-SPION in which SPION are hybridized on the surface of ND50. Inset in Figure 1 shows a high resolution TEM image of SPION in which crystal lattice of SPION was observed. Furthermore, the both X-ray diffraction (XRD) peaks of SPION and ND were confirmed in NDs-SPION nanohybrid. Dynamic light scattering measurements in water indicated that hydrodynamic size of ND50-PG and ND100-PG increased from 78 and 120 nm to 135 and 170 nm for ND50-SPION (50:50) and ND100-SPION (50:50), respectively. As for the physical properties, their MRI contrast ability is found to improve from 210 $mM^{-1}s^{-1}$ for pure SPION to 330 $mM^{-1}s^{-1}$ for ND50-SPION (50:50) at r_2 relaxivity. ND100-SPION (50:50) raised temperature of aqueous dispersion twice faster compared to pure SPION in alternating magnetic field. We believe that our button-up synthetic strategy can be applied to hybridize various kinds of nanoparticles on the ND surface.

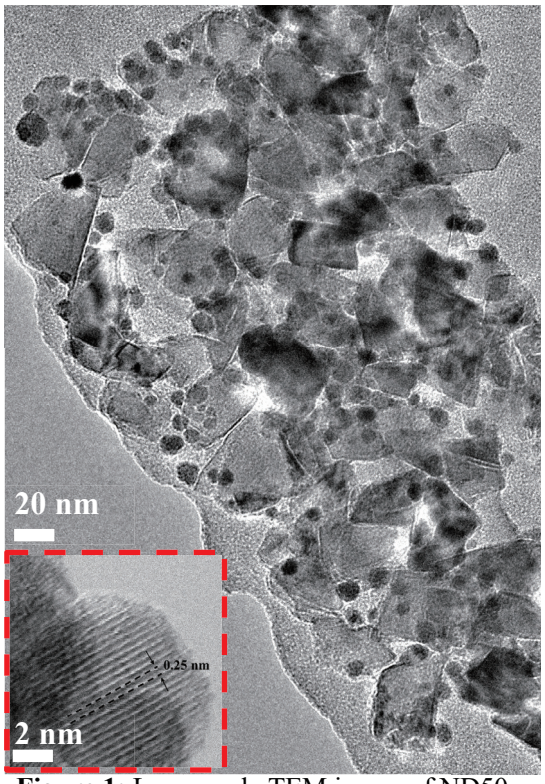

Figure 1: Large scale TEM image of ND50-SPION, inset Figure shows high resolution image of SPION.

[1] Choy, J. T. et al. Nat. Photonics 5, 738 (2011).
[2] N. Komatsu, et al. Adv. Funct. Mat. 24, 5348 (2014).

Corresponding Author: A. Tayyebi Tel, Fax: +81-75-753-7871, E-mail: atayebi162@gmail.com

Growth mechanism of multi-millimeter-tall single-wall carbon nanotube forests using Fe/Gd/Al catalysts

○Hisashi Sugime[1*], Rei Nakagawa[2], Toshihiro Sato[2], Cinzia Cepek[3], Suguru Noda[2]

[1]*Waseda Institute for Advanced Study, Waseda University*
[2]*Department of Applied Chemistry, Waseda University*
[3]*Istituto Officina dei Materiali-CNR, Laboratorio TASC*

Growth of vertically-aligned single-wall carbon nanotube (VA-SWCNT) forests by the catalytic chemical vapor deposition (CVD) is an attractive method for making applications. However, the growth termination of the CNT forests is an obstacle, and the deactivation of the catalyst nanoparticles due to the structure change of the catalyst nanoparticles is thought to be one reason for the termination. In general, maintaining smaller catalyst nanoparticles which are necessary for the SWCNT growth is more difficult because the smaller nanoparticles are less stable. As for the growth temperature, higher temperature is preferred for the high growth rate, but the structure change of the catalyst nanoparticles by migration, sintering, or Ostwald ripening is accelerated resulting in the shorter growth lifetime. To realize the longer growth lifetime, engineering catalysts is crucially important. So far, Fe-Gd catalyst on Al_2O_3 layer was reported to realize the growth lifetime of 13h and 22-mm-tall multi-walled CNT (MWCNT) forest at the growth temperature of 780 °C [1]. However, the growth rate is relatively low as ~0.5 μm s^{-1}, and the possibility of using Gd for SWCNT growth was not discussed in detail.

In this work, we applied the Fe/Gd/Al catalyst to the growth of SWCNT forests, and systematically studied the mechanism behind the enhanced growth (Fig. 1a). By optimizing the catalyst condition, we achieved a high initial growth rate of ~2 μm s^{-1} and long catalyst lifetime of ~50 min at 800 °C. Correspondingly, the areal mass continued increasing up to ~8 mg cm^{-2} in 60 min (Fig. 1b). It was found that Gd layer with the thickness of less than 1 nm is effective when it is deposited between Fe and Al layers. The Raman spectra showed the radial breathing mode (RBM) peaks from the top to the bottom of the CNT forests, which suggests the continuous growth of SWCNTs.

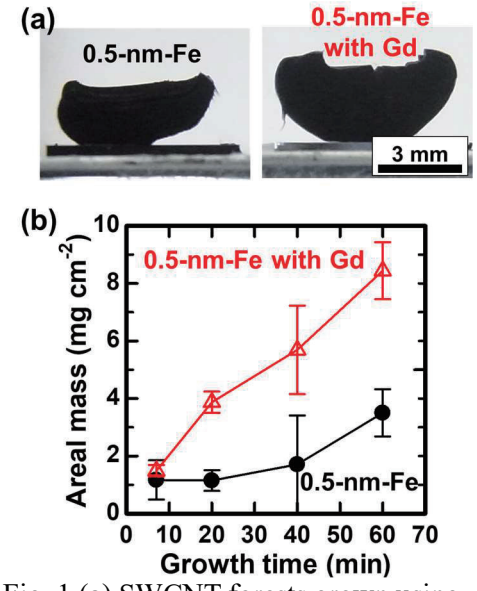

Fig. 1 (a) SWCNT forests grown using Fe/Al or Fe/Gd/Al catalysts. (b) Areal mass of the SWCNT forests with two different catalysts.

[1] W. Cho et al., *Carbon* **72**, 264 (2014).

Corresponding Author: H. Sugime, E-mail: sugime@aoni.waseda.jp

Single-walled carbon nanotube growth onto graphene crystals

○ Kamal P Sharma[1,2], Takuya Okada[1], Aliza K Sharma[1], Takahiro Maruyama[1,2]

[1] *Department of Applied Chemistry, Meijo University, Nagoya 468-8502, Japan*
[2] *Nanomaterials Research Center, Meijo University, Nagoya 468-8502, Japan*

Graphene and single-walled carbon nanotubes (SWCNT), sp^2 hybridized honeycomb structures of carbon, are realized as the promising materials for the wide ranges of applications due to their high carrier mobilities, high electrical and thermal conductivities, and large surface areas [1, 2]. A high quality 3D hybrid structures of graphene and SWCNT is highly desirable to further enhance their properties so as to use in various applications [3,4]. Here we attempt to address this issue by growing small-diameter SWCNTs onto graphene crystals.

Graphene crystals were synthesized on Cu by chemical vapor deposition (CVD) technique and transferred onto SiO_2/Si as reported elsewhere [5]. Then, Ir nanoparticles were deposited onto them, which were utilized as growth substrates. SWCNT growth was carried out at an optimized condition using ethanol gas as carbon source in ultra-high vacuum CVD (UHV-CVD) system [6]. Optical microscope (OM), Raman spectrometer, FESEM, and XPS were employed for the characterization.

Dark contrast circular regions in Fig. 1(a) corresponding to graphene crystals were confirmed prior to SWCNT growth. After SWCNT growth, radial breathing mode (RBM) peaks were observed in typical Raman spectra taken from both graphene and SiO_2/Si area (Fig. 1(b)). In reference to Kataura plot, SWCNTs with diameters of 0.8 to 1.2 nm were successfully grown onto graphene crystals.

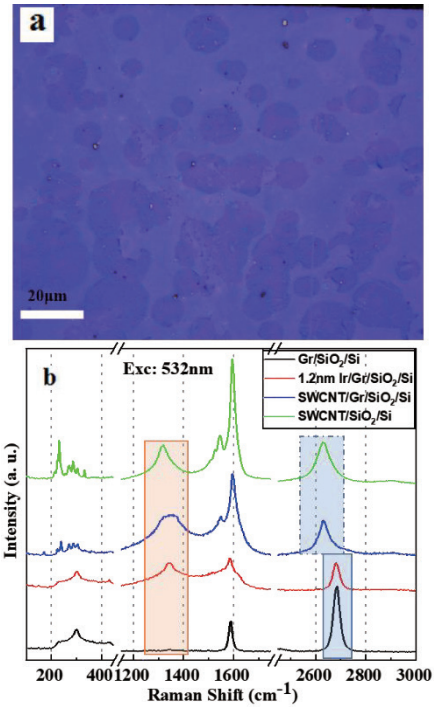

Fig. 1. (a) OM images of graphene crystals after SWCNT growth. Circular structures with dark contracts represent graphene crystals. (b) Raman spectra highlighted in different colors represent as listed in the inset.

This work was supported in part by Private University Research Branding Project from the Ministry of Education, Culture, Sports, Science and Technology (MEXT), Japan.

[1] C. Wang et al., Chem. Soc. Rev. **42**, 2592 (2013)
[2] A. C. Ferrari et al., Nanoscale **7**, 4598 (2015).
[3] D. H. Lee et al., Adv. Mater. **22**, 1447 (2010).
[4] L. Xu et al., J. Mater. Chem. **22**, 1435 (2011).
[5] K. P. Sharma et al., J. Mater Sci. **51**, 7220 (2016).
[6] T. Maruyama et al., Mater. Express, **1**, 267 (2011).

Corresponding Author: Takahiro Maruyama
E-mail: takamaru@meijo-u.ac.jp

Enhanced gas-phase production of single-wall carbon nanotubes by overheating of catalyst source

Katsuya Namiki[1], Hisashi Sugime[2], Toshio Osawa[1], ○Suguru Noda[1,3,*]

[1] *Department of Applied Chemistry, Waseda University, Tokyo 169-8555, Japan*
[2] *Waseda Institute for Advanced Study, Waseda University, Tokyo 169-8050, Japan*
[3] *Research Institute for Science and Engineering, Waseda University, Tokyo 169-8555, Japan*

Floating catalyst chemical vapor deposition (FCCVD) has enabled production of high quality single-wall carbon nanotubes (SWCNTs) [1–3]. It has realized mass production of vapor grown carbon fibers (VGCFs) at hundreds ton annually, however mass production of SWCNTs is still underway. A SWCNT (d~1–2 nm) has a mass 1/10000 of a VGCF (~150 nm) of the same length. Increasing the catalyst density is the key for mass production, however the floating catalyst quickly aggregates in the gas-phase. We have developed the flame-assisted CVD method, in which catalyst source vapors are decomposed in <1 ms at >2000 °C using a premixed flame, and then *cooled* to ~1000 °C in ~1 ms by gas-mixing to nucleate Fe particles and grow SWCNTs [4]. This method yields SWCNTs with d = 1 nm, but the process optimization is complicated due to the large content of H_2O in the flaming gas.

We here report the FCCVD method with overheating of catalyst source. We used catalyst preheater instead of the premixed flame. Compared with the normal FCCVD (w/o preheating), both quality and quantity improved with preheating, and even more with overheating (Fig. 1).

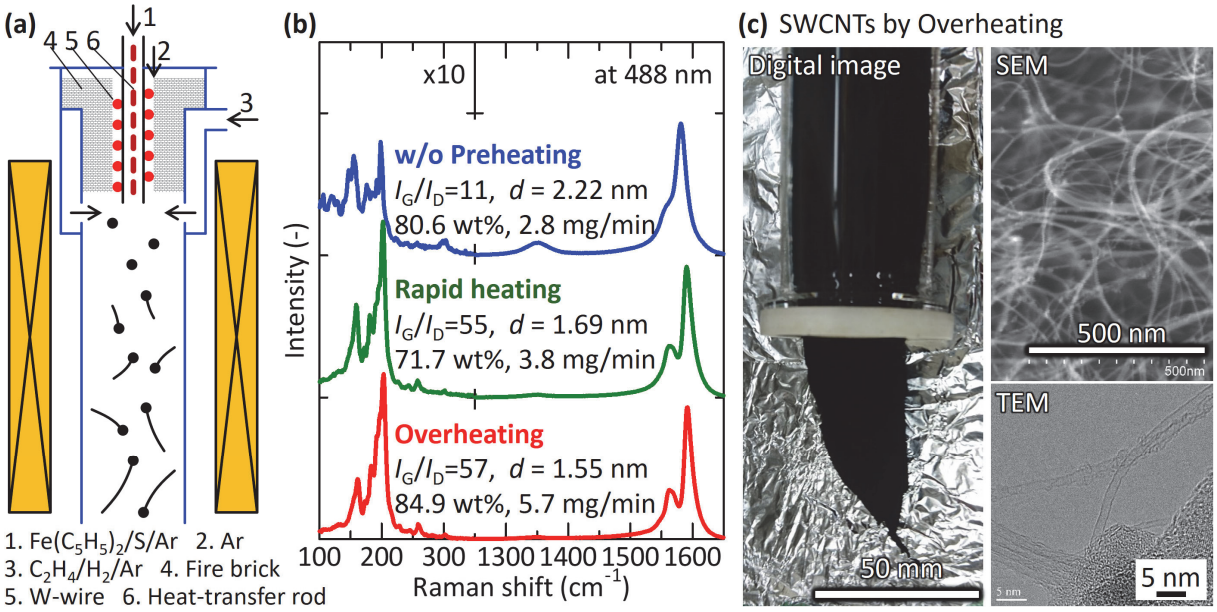

Fig. 1. Production of SWCNTs by FCCVD with preheating of catalyst source. (a) Apparatus. (b) Raman spectra with product properties. (c) Digital image, SEM and TEM of the SWCNTs produced by overheating of the catalyst source.

[1] H.M. Cheng, et al., Appl. Phys. Lett. 72, 3282 (1998).
[2] A.G. Nasibulin, et al., Chem. Phys. Lett. 313, 91 (2005).
[3] T. Saito, et al., J. Phys. Chem. B 110, 5849 (2006).
[4] S. Okada, et al., Carbon 138, 1 (2018).

*Corresponding Author: S. Noda Tel&Fax: +81-3-5286-2769, E-mail: noda@waseda.jp

All solution-processed heterogeneously integrated junction diode

○Kuniharu Takei[1,2], Daisuke Yamamoto[1], Mao Shiomi[1], Takayuki Arie[1], Seiji Akita[1]

[1] *Dep. of Physics and Electronics, Osaka Prefecture University, Osaka 599-8531, Japan*
[2] *JST PRESTO, Saitama 332-0012, Japan*

Macroscale electronics enable to monitor a variety of information especially for future human interactive application and "Internet of Things" (IoT) concepts. To build ideal platform for these concepts, low-cost, multi-functional devices are required to integrate on versatile macroscale substrates. One of the possible methods to cover all requirements is a solution-based printing technique to form all electrical components. In this study, we report one of the approaches to fabricate a diode using InZnO (IZO) thin film as n-type semiconductor and carbon nanotube (CNT) network film as p-type semiconductor using only solution process [1].

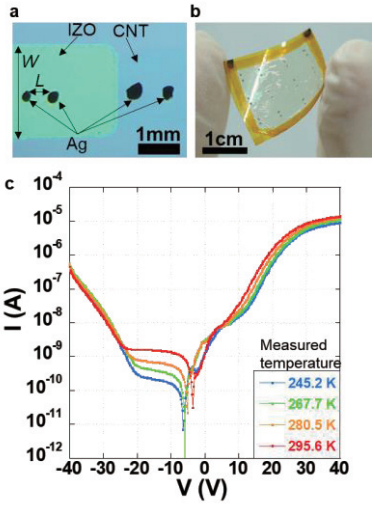

Fig. 1 Photos of (a) CNT-IZO junction diode and (b) flexible diode. (c) Rectifying diode characteristics as a function of temperature.

First, fabrication process is briefly explained. IZO precursor (Nissan Chemical) was spin-coated on SiO_2/Si or polyimide surfaces, followed by annealing at 300 °C. After patterning of the IZO film, semiconductor-enriched CNT solution was drop-casted over the pre-determined chemically treated surface to form IZO-CNT junction and rinsed by DI water. Ag electrodes for the contacts were painted on IZO and CNT films. Finally, annealing at 200 °C in air and 150 °C in N_2 gas ambient was conducted to improve the electrical properties. Fig. 1a-b shows the device photos. p-type CNT (n-type IZO) transistors have mobility of 3.9±2.3 cm^2/Vs (1.87±0.3 cm^2/Vs), threshold voltage of 2.7±9.8 V (11.7±4.9 V), and log (I_{ON}/I_{OFF}) of 3.73±0.3 (5.71±0.3). It should be noted that the dimensions of the transistors (width *W* and length *L*) shown in Fig. 1a were used to extract the mobility, resulting in that the value reported is underestimate because Ag electrode width is much smaller than *W*. Uniformity for especially CNT film needs to be improved to optimize the surface and deposition conditions in the future.

After confirming each semiconductor layer, rectifying electrical characteristics were measured. To analyze the band height between CNT and IZO film, temperature dependence study was also conducted as shown in Fig. 1c. Importantly, using CNT/IZO junction, rectifying diode characteristics is successfully realized by using only solution-based processes on both rigid and flexible substrates. By analyzing off-current between -10 and -20 V shown in Fig. 1c using thermionic emission theory, barrier height of the junction was extracted to be ~150 meV. Based on the band gap and work function of these films, the band alignment is type II junction, which means that the rectifying behavior is mostly based on Schottky-like contacts between IZO and CNT. Although improvements of the device performance are required for the practical application, this all solution-based heterogeneously integrated diode is an important step to move forward to realizing the macro-scale low-cost electronics.

Acknowledgements: This work was supported by KAKENHI JP17H04926, JST PRESTO JPMJPR17J5, and Nissan Chemical Corporation.

Reference: [1] D. Yamamoto *et al*. ACS Appl. Mater. Interfaces **11**, 1021 (2019).

Corresponding Author: K. Takei, Tel: +81-72-254-9497, E-mail: takei@pe.osakafu-u.ac.jp

3-5

Low-voltage operable complementary carbon nanotube thin-film transistors with threshold tuning by controlled doping on plastic substrate

○Fu-Wen Tan[1], Jun Hirotani[1], Shigeru Kishimoto[1], and Yutaka Ohno[1,2]

[1]*Department of Electronics, Nagoya University, Nagoya 464-8603, Japan*
[2]*Institute of Material and Systems for Sustainability, Nagoya University, Nagoya 464-8601, Japan*

Carbon nanotube thin-film transistors (CNT TFTs) exhibit excellent electrical and mechanical properties, coupled with complementary metal-oxide semiconductor (CMOS)-based circuits, would enable high-performance and low-power flexible electronics. Although complementary CNT TFTs have been achieved by featuring n-type TFTs by doping, its counterpart p-type devices are usually left as-fabricated without addressing issues such as switching voltage threshold and its variability, which may lead to unreliable CMOS circuit operation [1-2]. In this work, we demonstrate more than 100 complementary CNT CMOS inverters with low operation voltage of 0.5 V by intentional doping of both p- and n-type TFTs to tune the switching threshold.

Bottom-gated complementary TFTs connected in inverter configuration were fabricated on a flexible poly(ethylene naphthalate) (PEN) substrate as illustrated in Fig. 1. Semiconductor -enriched CNTs were utilized as the channel material. We confirmed that all 129 devices showed p-type behavior with on/off ratio ~10^4 and uniform characteristic prior to doping. Then, potassium hydroxide/benzo-18-crown-6-ether (KOH/CE) was spin-coated only on selective devices to achieve n-type doping. An Al_2O_3 passivation layer was formed by atomic layer deposition on the n-type devices. Next, a similar process was repeated by spin coating silver-bis(trifluoromethane)imide (AgTFSI) on the p-type devices intended for threshold tuning. Then, a polymethyl methacrylate (PMMA) and Al_2O_3 passivation layer was formed on top of the p-type devices.

Figure 2 shows the transfer characteristics of 126 devices after (a) KOH/CE and (b) AgTFSI doping with a yield 95.4 %. The p- and n-doped devices were successfully characterized without significant degradation of on-current and mobility at the end of the fabrication process. We confirmed the operation of CMOS inverters with supply voltage of 0.5 V, as shown in Fig. 2(c) with a small hysteresis width of 0.02 V on average.

[1] Y. Zhao *et al*., ACS Nano **10**, 2193 (2016)
[2] J. Tang *et al*., Nat. Nanotechnol. **1**, 191 (2018).
Corresponding Author: Y. Ohno
Phone & Fax: +81-52-789-5387,
E-mail: yohno@nagoya-u.jp

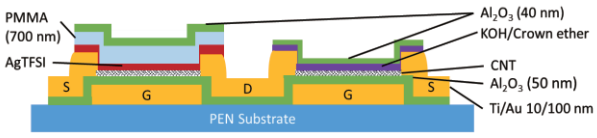

Fig.1 Schematic structure of a complementary CNT TFT device in inverter configuration.

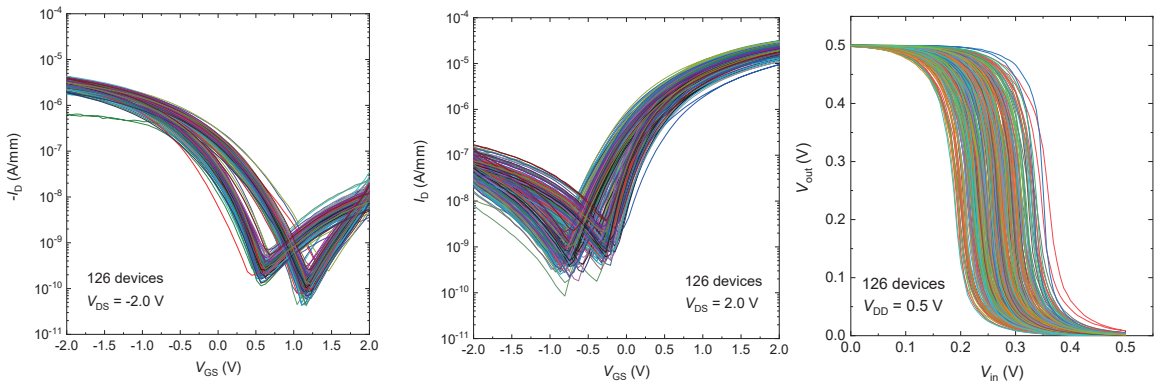

Fig. 2 I_D-V_{GS} characteristics at V_{DS} = | 2.0 V | of 129 CNT TFTs with channel length L_{ch} = 50 μm after (a) AgTFSI and (b) KOH/CE doping. (c) Output characteristics of 126 CNT CMOS inverters at V_{DD} = 0.5 V.

What controls whether $[M_2@C_n]^-$ (n=78, 80) is stably formed or not?

○Kazuhiro Kobayashi, Koichi Kikuchi, Yohji Achiba, Takeshi Kodama

Department of Chemistry, Tokyo Metropolitan University, Tokyo 192-0397, Japan

Recently, $M_2@C_n$(M=Y[1], Gd[2]; n=78, 80) were isolated as an anion form by using the method combining the ion-pair chromatography with the mixed solvent extraction. Because they are unstable in a neutral form, they could not be extracted from the soot by the usual extraction method, so they have been known as so-called missing metallofullerenes. Then, the possibility of production and isolation for such missing metallofullerenes was suggested. Therefore, we have been trying to produce $[M_2@C_n]^-$ containing other rare earth metals[3-7]. As a result, $[M_2@C_n]^-$ could be obtained for Nd, Dy, Er, and Tm, but could not for Eu and Yb.

In this work, to explain the difference between the two types of metals that give $[M_2@C_n]^-$ or not, we considered the ionization potentials of metals and the electrostatic potential between metals and fullerene cage. As shown in Fig. 1, the border seems to be where the sum is about -32 eV but there are some exceptions. More details will be discussed in the presentation.

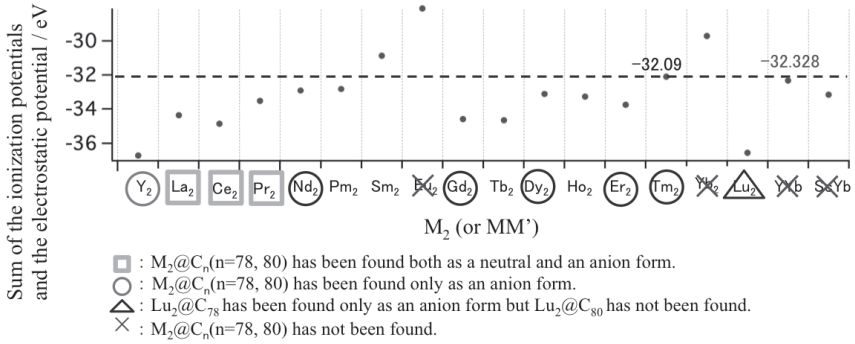

Fig. 1 Sum of the ionization potentials and the electrostatic potential

[1] N. Nakatori, et al. *The 49th Fullerenes-Nanotubes-Graphene General Symposium* 46 (2015).
[2] T. Mitani, et al. *The 50th Fullerenes-Nanotubes-Graphene General Symposium* 95 (2016).
[3] S. Nishimoto, et al. *The 54th Fullerenes-Nanotubes-Graphene General Symposium* 47 (2018).
[4] R. Takai, et al. *The 55th Fullerenes-Nanotubes-Graphene General Symposium* 127 (2018).
[5] K. Kobayashi, et al. *The 54th Fullerenes-Nanotubes-Graphene General Symposium* 48 (2018).
[6] K. Kobayashi, et al. *The 52nd Fullerenes-Nanotubes-Graphene General Symposium* 128 (2017).
[7] K. Kobayashi, et al. *The 11th Annual meeting of Japan Society for Molecular Science* 2P055 (2017).

Corresponding Author: Takeshi Kodama
Tel: +81-42-677-2530, Fax: +81-42-677-2525
E-mail: kodama-takeshi@tmu.ac.jp

Fullerene-Cation-Mediated Synthesis of Cyclo[60]fullerenes with 5-Membered-Rings and their Application to Perovskite Solar Cells

○Hao-Sheng Lin [1], Il Jeon [1], Shigeo Maruyama [1], Yutaka Matsuo [1]

[1] *Department of Mechanical Engineering,The University of Tokyo, Tokyo 113-8656, Japan*

Cyclo[60]fullerenes have attracted intensive attentions due to their excellent performance in photovoltaics, such as organic solar cells (OSCs) and perovskite solar cells (PSCs). Accordingly, great endeavors has been devoted into the efficient synthesis of cyclo[60]fullerenes, including phenyl-C_{61}-butyric acid methyl ester ($PC_{61}BM$), indene-C_{60} bisadduct (ICBA), and methylene indene fullerene (MIF). It is worth noting that decreasing the π-system of C_{60} ($60\,\pi$) by derivatization can effectively increase the LUMO level of derivatives, which benefits the V_{OC} in OSCs as the $V_{oc} = LUMO_{acceptor} - HOMO_{donor}$. However, in terms of PSCs, fullerene derivatives with multi-addend gave a much poor performance than pristine C_{60} as they are being as electron transporting layer. The molecular volume can be enlarged by multiple addends, which negatively influence the efficiency of the electron transporting ability. Consequently, conventional molecular design in OSCs is far-fetched to be conceived in PSCs.

Among cyclo[60]fullerenes, especially derivatives with full carbon ring present much excellent performance such as three-membered ring (PCBM) and six-membered ring (ICBA, MIF). Nevertheless, five-membered ring has not been efficiently produced, which hinders the investigation of their property and performance in photovoltaics. To the best of our knowledge, although fullerenyl anion and radical mediated reaction elegantly pave the road for the efficient synthesis of cyclo[60]fullerenes, they confess feeble when faced with five-membered ring unit. Fullerene cation mediated reaction, a recently boosted methodology, showed its superiors in fullerene synthetic chemistry especially for unique molecules.[1] Here in, we presented a fullerene-cation-mediated synthesis of cyclo[60]fullerenes and comprehensively evaluated the performance of five-membered ring fullerenes in PSCs, which gave a impressive high PCE up to 20.7%.

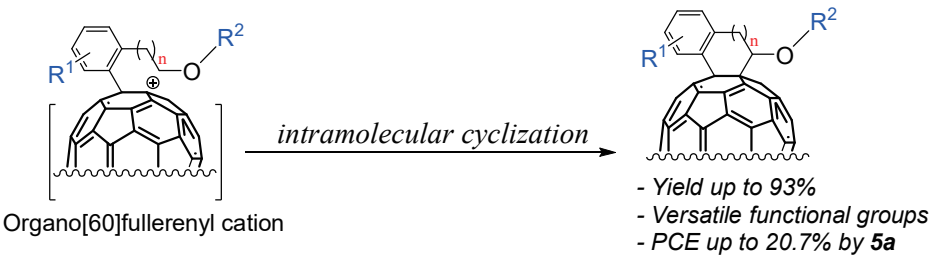

Organo[60]fullerenyl cation

[1] H.-S. Lin, Y. Matsuo Chem. Comm. **54**, 11244 (2018).

Corresponding Author: Y. Matsuo
Tel: +81-3-5841-0978
E-mail: matsuo@photon.t.u-tokyo.ac.jp

Transformation kinetics from Li^+@[5,6]-PCBM to Li^+@[6,6]-PCBM: Reaction rate enhancement by the encapsulated Li^+

○Yue Ma [1], Hiroshi Ueno [2,3], Hiroshi Okada [3,4] , Yutaka Matsuo [1,3,4]

[1] *Hefei National Laboratory for Physical Sciences at Microscale, University of Science and Technology of China, 96 Jin-zhai Road, Hefei, Anhui 230026, China*
[2] *School of Chemistry, Northeast Normal University, Changchun, Jilin 130024, China*
[3] *Center for Fundamental and Applied Research of Novel Nanocarbon Derivatives, Center for Key Interdisciplinary Research, Tohoku University*
[4] *Department of Mechanical Engineering, School of Engineering, The University of Tokyo, Bunkyo-ku, Tokyo 113-8656, Japan*

Apart from general endohedral metallofullerenes, $Li^+@C_{60}$ is regarded as cationic fullerene consisting of encapsulated lithium ion (Li^+) and neutral C_{60} cage. It is emphasized that the internal Li^+ is trapped by C_{60} cage, and thus $Li^+@C_{60}$ can be considered as "perfect" Li^+-C_{60} complex. Previously we have reported greatly enhanced Diels-Alder reaction of $Li^+@C_{60}$ as a first example of the catalytic effect of Lewis acid for heteroatomless substrate. However, no other detailed kinetics for the specific Li^+-C_{60} complex have been studied so far. In this work, we report the transformation kinetics from [5,6]-fulleroid to [6,6]-methanofullerene by comparing the reaction rate of Li^+@PCBM and its empty analogue.

The Li^+@[5,6]-PCBM was prepared based on reported procedure. The kinetic parameters including the rate constant, activation energy, activation enthalpy, activation entropy and activation Gibbs free energy were estimated experimentally. Compared with the reaction of empty one, Li^+@[5,6]-PCBM converted 1000-fold faster at 400 K, corresponded to lowering the activation energy by ca. 100 kJ mol^{-1} (Figure 1). We also performed the reaction for empty PCBM with adding "external" lithium salt such as LiTFSI, however, almost no reaction acceleration was observed. The details will be shown on the presentation.

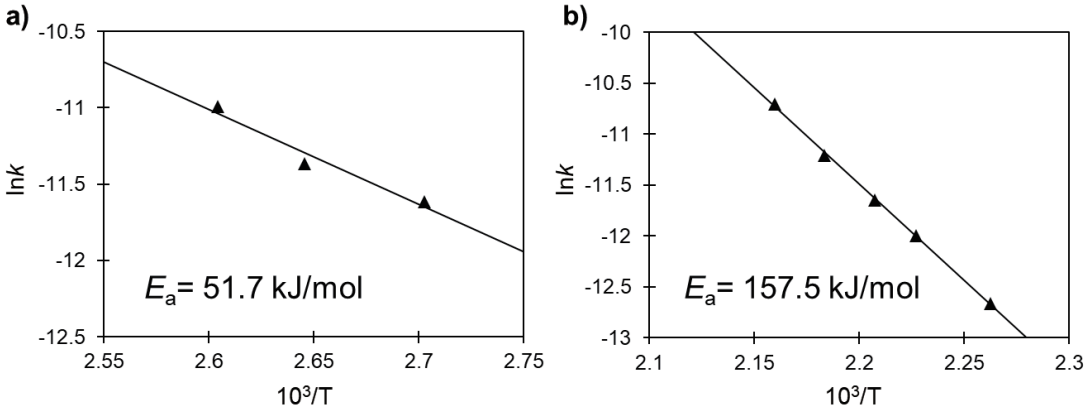

Figure 1. Arrhenius plots in the conversion reaction of (a) Li^+@PCBM and (b) empty PCBM.

.

[1] Ueno, H. *et al*. *J. Am. Chem. Soc.* **2014**, 136, 11162−11167
[2] Matsuo, Y. *et al. Org. Lett.* **2012**, 14, 3784-3787

Corresponding Author: Y. Matsuo
Tel: +81-3-5841-0978, E-mail: matsuo@photon.t.u-tokyo.ac.jp

Vibrational Finger Prints in the Spectra of C_{60}

○Tomonari Wakabayashi[1], Takamasa Momose[2], Mario E. Fajardo[3]

[1] Department of Chemistry, Kindai University, Higashi-Osaka 577-8502, Japan
[2] Department of Chemistry, University of British Columbia, Vancouver V6T 1Z1, Canada
[3] Munitions Directorate, US Air Force Research Laboratory, Eglin AFB, FL 32542-5910, USA

Infrared spectroscopy was one of the major tools upon the discovery of macroscopic amount of synthesis for fullerene C_{60} [1]. Recently, infrared emission features were identified for the discovery of C_{60} in young planetary nebula [2]. The relatively small number of infrared-active vibrational modes enables one to identify such a large molecule of C_{60}, i.e. only four T_{1u} modes are IR-active among the 46 vibrational modes in the total 174 vibrational degrees of freedom. Turning our eyes to the presence of isotopologues, namely $^{13}C_x{}^{12}C_{60-x}$ ($x \geqq 1$), we realize that our terrestrial sample of C_{60} is a mixture of distinguishable molecules containing natural isotopic abundance of 1.1% ^{13}C. Indeed, Raman signal of the totally symmetric A_g mode of C_{60} at 1470 cm^{-1} is reported to split into a few peaks under the dilute condition in a solid CS_2 matrix at 30 K [3]. Very recently, rovibrational quantum states of C_{60} were resolved in the gas-phase frequency-comb spectroscopy [4]. Here high-resolution IR absorption spectra of matrix-isolated C_{60} is revisited to understand the symmetry breaking of icosahedral $^{12}C_{60}$ by substitutions of ^{12}C nuclei by ^{13}C isotopes.

High-resolution IR absorption spectra of C_{60} were reported previously by our research group using solid para-H_2 matrices at 2 K, where the spectral features in each of the four IR-active vibrational mode spectra were attempted to be understood by molecular rotational structures taking missing levels due to Boson-exchange symmetry restrictions into account [5]. In the present work, we reanalyzed these spectra by another idea of isotopologues present in the C_{60} sample, which contains calculated abundance of 51% $^{12}C_{60}$, 34% $^{13}C^{12}C_{59}$, 11% $^{13}C_2{}^{12}C_{58}$, and 2.5% $^{13}C_3{}^{12}C_{57}$ for the natural isotopic abundance. New spectroscopic data were also obtained for the isotope-reduced and -enriched samples of C_{60}. Molecular orbital calculations for vibrational spectra of these isotopologues led to a better agreement to the experimental data [6].

[1] W. Krätschmer *et al*. Chem. Phys. Lett. **170**, 167 (1990).
[2] J. Cami *et al*. Science **329**, 1180 (2010).
[3] S. Guha *et al*. Phys. Rev. Lett. **72**, 3359 (1994).
[4] P. B. Changala *et al*. Science **363**, 49 (2019).
[4] N. Sogoshi *et al*. J. Phys. Chem. A **104**, 3733 (2000).
[5] T. Wakabayashi *et al*. in preparation.

Corresponding Author: T. Wakabayashi
Tel: +81-6-4307-3408, Fax: +81-6-6723-2721,
E-mail: wakaba@chem.kindai.ac.jp

Density functional theory-based study of O_2 adsorption on S- and P-doped graphitic carbon nitride/graphene layer

○Wilbert James C. Futalan[1], Koichi Kusakabe [2], Allan Abraham B. Padama [3], Joey D. Ocon [1]

[1] *Department of Chemical Engineering, University of the Philippines, Diliman, Quezon City, 1101, Philippines*
[2] *Graduate School of Engineering Science, Osaka University, 1-3 Machikaneyama-chou, Toyonaka, Osaka, 560-8531, Japan*
[3] *Institute of Mathematical Sciences and Physics, University of the Philippines, Los Banos, Laguna, 4031, Philippines*

Graphitic carbon nitride, whose activity is due to the electronegativity difference between the carbon and nitrogen atoms, has gained popularity among metal-free catalysts. Experiments with graphitic carbon nitride have shown that addition of a conductive carbon support to GCN improves its activity towards oxygen reduction reaction (ORR)[1, 2]. Following previous studies on doped GCN, substitution of nitrogen or carbon with heteroatoms such as sulfur and phosphorus can further enhance GCN's ORR activity[3, 4]. In this work, we investigate through a density functional theory-based calculation the effect of substitutionally doping sulfur and phosphorus on the graphitic carbon nitride/graphene layer in terms of adsorption energies and charge transfer extent upon oxygen adsorption. The results of the calculations suggest that sulfur doping provides higher adsorption energy compared to phosphorus doping. In terms of doping location, the calculations reveal that doping along the edge sites gives the most energetically favorable structure for oxygen adsorption. Moreover, this work considers the possible relationship between the oxygen-GCN/graphene separation distance and the oxygen bond length as an indicator of the interaction of molecular oxygen as it adsorbs onto the GCN/graphene surface.

[1] S. Lyth *et al*. J. Phys. Chem. C **113**, 47, 20148-20151 (2009).
[2] S. Yang *et al.* Angew. Chem. Int. Ed **50**, 23, 5339-5343 (2011)
[3] Y. Zheng *et al.* J. Am. Chem. Soc. **133** 50, 20116-20119 (2011)
[4] Q. Han *et al.* J. Mater. Horiz **4**, 832-850 (2017)

Corresponding Author: J. Ocon
Tel: +63-981-8500 loc. 3213
E-mail: jdocon@up.edu.ph

High yield fabrication of quantum device made of graphene nanoribbon using Plateau-Rayleigh instability

○Wakana Okita[1], Hiroo Suzuki[1], Toshiro Kaneko[1], Toshiaki Kato[1,2]
[1] *Graduate School of Engineering, Tohoku University, Sendai 980-8579, Japan*
[2] *JST-PRESTO*

Graphene is one of the topical nanomaterials attracting attentions as next generation electronic materials due to its superior electrical conductivity, mechanically flexible structure and high optical transparency. While graphene has 2-dimensional sheet structure and shows metallic like behaviour, it has been discovered that graphene nanoribbon (GNR) has finite bandgap, which can be obtained by making graphene into 1-dimensional structure. This discovery made GNR conspicuous material in semiconductor device field around the world.

One of our significant achievements so far is that we succeeded in integrated synthesis of suspended GNR for the first time [1-3] by unique plasma CVD process [4] combining with a creative idea, using nanobar structure as a catalyst. Heading towards implementation of practical application of suspended GNR grown by our method, it is essential to comprehend its detailed electrical property. For this purpose, we prepare a narrow (~20 nm) GNR and carried out transport measurement at low temperature (~15 K). As a result, almost perfectly periodic Coulomb diamonds property was observed (Fig.1 (a)), which can be caused by quantum confinement effect. However, in previous research the probability of Coulomb diamonds observation was exceptionally low, which makes it difficult to realize integrated quantum devices with GNRs. Therefore, it is very valuable subject to tackle how to improve fabrication yield for quantum device made of suspended GNR grown by plasma CVD.

In this research, it is aimed to increase fabrication yield for quantum device by optimization of original nanobar structures. In our GNR growth method, liquid Ni dewetting is caused by Plateau-Rayleigh (P-R) instability during CVD and GNR can be obtained after CVD (Fig.1 (b)). It has been revealed that our GNRs have local fine-structure by P-R instability which behaves as a quantum dot. Based on this fact, fabrication yield for quantum device turned out to be increased up to 50 % by using nanobar with similar length as wave length of P-R instability. This research possesses very useful results to realize future integrated-quantum devices with GNRs.

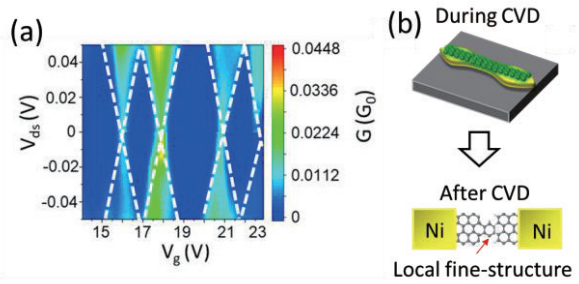

Fig. 1: (a) Overview of 2D color map of conductance (G) normalized by e^2/h (G_0) against drain-source bias (V_{ds}) and gate bias (V_g) voltage. (b) Illustration of Ni nanobar during CVD and after CVD.

[1] T. Kato and R. Hatakeyama: Nature Nanotechnology **7** (2012) 651.
[2] H. Suzuki, T. Kaneko, Y. Shibuta, M. Ohno, Y. Maekawa and T. Kato: Nature Communications **7** (2016) 11797.
[3] H. Suzuki, N. Ogura, T. Kaneko, and T. Kato, Scientific Reports **8** (2018) 11819.
[4] T. Kato and R. Hatakeyama: ACS Nano **6** (2012) 8508.

Corresponding Author: W. Okita
Tel:+81-22-795-7046,
E-mail:wakana.okita.r5@dc.tohoku.ac.jp

ポスター発表
Poster Preview

1 P – 1 ～ 1 P – 38
2 P – 1 ～ 2 P – 38
3 P – 1 ～ 3 P – 37

Synthesis and characterization of fullerene-based molecular torsion balance for investigating noncovalent fullerene–arene interaction

○Haruna Narita[1], Yutaka Maeda[1], Michio Yamada [1]

[1] *Department of Chemistry, Tokyo Gakugei University, Koganei, Tokyo 184-8501, Japan*

Fullerenes are expected to be utilized for a variety of applications in the fields of materials chemistry and medicinal chemistry [1]. Understanding noncovalent fullerene–arene interactions is therefore a demanding task to understand fullerene-based molecular assembled systems and molecular recognition events. Recent advances in supramolecular chemistry of fullerenes have shown that structurally well-defined molecular receptors provide strong noncovalent interactions with fullerenes to form stable complexes [2]. Nevertheless, little has explored in the quantitative analysis of noncovalent fullerene–arene interactions, because of its difficulty in observation of such weak interactions. In this context, Wilcox and co-workers developed a model system, called a molecular torsion balance, to evaluate noncovalent arene–arene interactions in the 1990s [3]. That success motivated us to apply the molecular torsion balance system for investigation of non-covalent fullerene–arene interaction. In this study, we designed, synthesized, and characterized the fullerene-based molecular torsion balances to perform quantitative analysis for noncovalent fullerene–arene interaction for the first time. As shown in Scheme 1, the proposed model system features, in its folded conformation, an interaction between the fullerene surface and an arene moiety, while the interaction is absent in its unfolded conformation. When the rotation around the biphenyl C–C bond is slow on the ^{1}H NMR timescale, the population of the two conformers can be determined by integration of the methyl signals (the corresponding methyl group is denoted by 'Me' in Scheme 1) at different temperatures. In this presentation, we show the synthesis and characterization of the molecular torsion balances possessing substituted arene moieties. In addition, the thermodynamic parameters obtained from variable-temperature (VT)-^{1}H NMR measurements will be discussed.

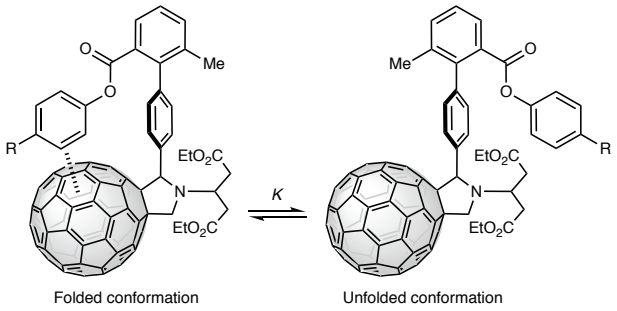

Scheme 1. Two conformers of the fullerene-based torsion balance.

[1] (a) *Chemistry of Nanocarbons*, T. Akasaka, F. Wudl, S. Nagase, Eds.; John Wiley & Sons: Chichester, 2010. (b) *Organic Nanomaterial*s, T. Torres, G. Bottari, Eds.; John Wiley & Sons: Hoboken, 2013.

[2] *Supramolecular Chemistry of Fullerenes and Carbon Nanotubes*, N. Martín, J.-F. Nierengarten, Eds.; Wiley-VCH:Weinheim, 2012.

[3] (a) S. Paliwal et al. J. Am. Chem. Soc. **116**, 4497 (1994). (b) E.-i. Kim et al. J. Am. Chem. Soc. **120**, 11192 (1998).

Corresponding Author: M. Yamada

Tel: +81-42-329-7493, Fax: +81-42-329-7493

E-mail: myamada@u-gakugei.ac.jp

Controlling Thermal Conductivity of Carbon Nanotubes by Side-Wall Functionalization to Improve the Figure of Merit

○Angana Borah [1] and Tsuyohiko Fujigaya [1, 2, 3, 4]

[1]*Kyushu University, Fukuoka 819-0395, Japan,* [2]*WPI-I²CNER, Fukuoka 819-0395, Japan,* [3]*CMS, Fukuoka 819-0395, Japan,* [4] *JST-PRESTO, Saitama 332-0012, Japan*

Introduction: SWNTs have gathered ample attention as thermoelectric (TE) materials due to their extremely high electrical conductivity (σ), Seebeck coefficient (S), light weight, mechanical toughness and flexibility [1]. However, high thermal conductivity (κ), which is a property of SWNT, is undesirable as it cannot maintain a temperature gradient necessary to generate electricity using the TE principle [2]. Previously, it was reported that introduction of defects on SWNT decreased thermal conductivity [3]. However, the effect of these defects on the figure of merit (ZT) is not known. Thus, in this study, we functionalized SWNT sheets with different concentrations of 3,5-di-tert-butylbenzenediazonium tetrafluoroborate (3,5-DTBBD) (Fig. 1) to investigate the dependence of *ZT*.

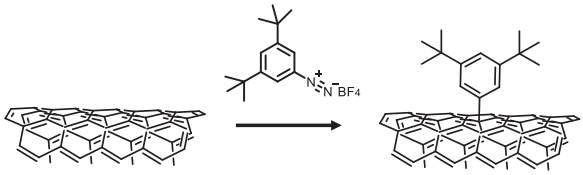

Fig. 1 Scheme of the functionalization using 3,5-DTBBD

Experiment: SWNTs (eDips 1.5 nm in diameter) were dispersed in an aqueous SDBS solution and vacuum filtrated, oven dried and heat treated to obtain a free standing sheet. The sheet was dipped in 3,5-DTBBD solution at different concentrations for functionalization.

Results and discussion: Fig. 2 summarizes the in plane κ (♦) and ZT (□) of the sheet depending on the concentration of 3,5-DTBBD solution used for the functionalization. The κ decreased from around 32 $Wm^{-1}K^{-1}$ to around 15 $Wm^{-1}K^{-1}$, that is, decreased by around 50%. This is because with increasing concentration more defect sites are produced and decreases κ. On the other hand, the ZT value was almost constant. This was due to the decrease in S which cancelled the decrease in κ and increase in σ.

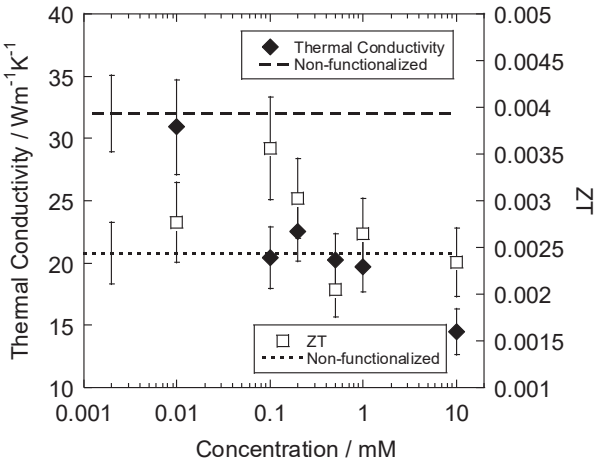

Fig. 2 Dependence of thermal conductivity and ZT on concentration of 3,5-DTBBD

[1] M. Ohnishi *et al*. Phys. Rev. B. **95**, 155405 (2017).
[2] F. Lian *et al.* Appl. Phys. Lett. **108**, 103101 (2016).
[3] J. Blackburn *et al.* Adv. Mater. **30**, 11 (2018).

Corresponding Author: T. Fujigaya
Tel: +81-92-802-2842, Fax: +81-92-802-2842,
E-mail:
fujigaya.tsuyohiko.948@m.kyushu-u.ac.jp

Soft Aerogels Supported by ~1 mass% Carbon Nanotubes for Thermal Interface Materials

○Satoru Kawakami[1], Hisashi Sugime[2], Junichiro Shiomi[3], Suguru Noda[1,4]

[1] *Department of Advanced Science and Engineering, Waseda University, Tokyo 169-8555, Japan*
[2] *Waseda Institute for Advanced Study, Waseda University, Tokyo 169-8050, Japan*
[3] *Department of Mechanical Engineering, The University of Tokyo, Tokyo 113-8656, Japan*
[4] *Department of Applied Chemistry, Waseda University, Tokyo 169-8555, Japan*

Thermal interface materials (TIMs) are used for enhancing heat transfer between solid surfaces by creating thermal paths. Their important characteristics are high thermal conductivity and softness for filling the air gaps. However, many conventional TIMs consist of thermal conductive fillers dispersed in polymer matrix, which has disadvantages of low thermal conductivity and poor thermal stability.

Here we propose aerogel TIM replacing polymer matrix with air matrix. Air matrix is released upon pressing and conductive fillers can directly contact each other. Soft, sponge-like self-supporting films can be fabricated using carbon nanotubes (CNTs), and this structure is able to support fillers 100 times larger in mass compared with their own mass [1]. Moreover, the CNTs are thermally stable (500 °C in air) and do not disturb thermal conduction between the fillers because of their high thermal conductivity.

We selected Ag and h-BN particles as thermal conductive fillers. The aerogel TIMs were fabricated by hybridizing Ag or h-BN particles with CNTs by simple dispersion-filtration process (Fig. 1a, b). The TIMs were self-supporting even when the filler content was >100 times as large as that of CNTs. Furthermore, insulating aerogel TIMs were fabricated by replacing CNTs with boron nitride nanotubes (BNNTs) and hybridizing them with h-BN particles (Fig. 1c). The thermal resistances were evaluated by the steady-state method by setting the TIMs between two Cu rods under 0.8 MPa (Fig. 1d) and were 40 mm^2 K/W for the electrically conducting TIM (99.5 mass% Ag with 0.5 mass% CNT) and 165 mm^2 K/W for the insulating TIM (97 mass% BN with 3 mass% BNNT). Optimization of the structure is now underway, and the latest results will be reported.

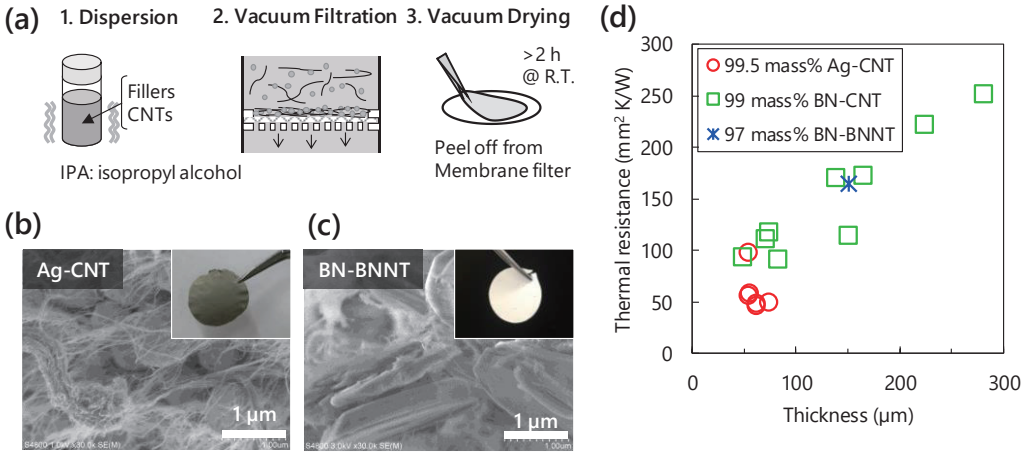

Figure 1: The aerogel TIMs. (a) Fabrication process. (b) Digital and SEM images of Ag-CNT. (c) Digital and SEM images of h-BN-BNNT. (d) Thermal resistances of the TIMs.

[1] K. Hasegawa and S. Noda, J. Power Sources 321, 155 (2016).

Corresponding Author: S. Noda, Tel: +81-3-5286-2769, Fax: +81-3-5286-2769, E-mail: noda@waseda.jp

1P-4

Preparation of SWNTs on porous glass (PG) sheet

○Tokinaru Matsuoka[1], Hiroshi Nagasawa[2], Shinzo Suzuki[1],

[1]Department of Physics, Kyoto Sangyo University, Kyoto 603-8555, Japan
[2]Kankyo Resilience Co. Ltd., Yokohama 240-8501, Japan

In 2005, Aoki et al., reported about the formation of SWNTs on porous glass (PG) material by using ACCVD technique [1], where metal particles (e.g. Co particles) were deposited on PG material before ethanol was introduced as carbon source for making SWNTs on PG material. The advantage of using PG material is that, it is very easy to make any kind of shape (rod, sheet.., etc.) made of PG, which implies that the as-grown SWNT-PG complex itself is expected to be used as an optical or other kind of device [2]. Since ACCVD technique has been widely used, because that the ambient temperature suitable for the formation of SWNTs is relatively lower (typically, less than 800°C), and the purity of SWNTs in as-grown material is better than those obtained by other technique, e.g. arc-burning procedure.

In this presentation, this ACCVD technique was further applied to PG sheet as well as PG particles, and the most appropriate experimental condition for the preparation of SNWTs on PG sheet was examined. In addition to Co particles as catalyst, Fe/Co alloy particles were also used for comparison. Based on the thermal gravimetric (TG) analysis combined with Raman spectroscopy [3], heat treatment was found to be able to purify as-grown SWNTs on PG sheet. Further experimental findings are presented and discussed [4].

References:

[1] Y. Aoki et al., *Chem. Lett.*, **34**, 562(2005).
[2] K. Nagao et al., *Proceeding of the 46th fullerenes-nanotubes-graphene general symposium*, **3P-15**(2014).
[3] T. Matsuoka, et al., *Proceeding of the 54th fullerenes-nanotubes-graphene general symposium*, **2P-12**(2018).
[4] T. Matsuoka, *A Master's Thesis*, Kyoto Sangyo University (2019).

Corresponding Author: Shinzo Suzuki
Tel: +81-75-705-1631, Fax: +81-75-705-1820,
E-mail: suzukish@cc.kyoto-su.ac.jp

Characterization of Atomically Precise MoS_2 Nanoribbons Confined Inside Boron Nitride Nanotubes

○Motoki Aizaki,[1] Yusuke Nakanishi,[*1, 2] Zheng Liu,[3] GogoiPranjal Kumar,[3] Jinhua Hong,[3] Ryosuke Senga,[3] Kazu Suenaga,[3] and Hisanori Shinohara[1]

[1] *Department of Chemistry, Nagoya University, Nagoya 464-8602, Japan.*
[2] *Department of Physics, Tokyo Metropolitan University, Hachioji 192-0397, Japan.*
[3] *National Institute of Advanced Industrial Science and Technology, Tsukuba 305-8565, Japan.*

Materials with reduced dimensionality could show exotic properties absent in their bulk counterparts. In recent years, this has been significantly demonstrated in transition-metal dichalcogenides (TMDs). For instance, monolayer MoS_2 exhibits a direct bandgap that changes from indirect in bulk, allowing various applications in optoelectronics. Furthermore, 1D MoS_2 nanoribbons (MoS_2NRs) are predicted to exhibit electronic and magnetic properties distinct from 2D monolayers [1]. Quantum confinement and edge effects should alter the electronic structures. However, exploring the potential of MoS_2NRs is hampered by their limited availability: although they have been fabricated using chemical [2] and lithographic [3] methods as well as through carbon nanotube-template reaction [4], their characterization still remains a significant challenge.

Here we report bottom-up synthesis of atomically precise MoS_2NRs by using boron nitride nanotubes (BNNTs) as molds. A self-assembly process causes the selective formation of zigzag edges (Figure 1a). More importantly, insulating BNNTs has a large bandgap of ~6 eV, allowing for a spectroscopic studies of inner MoS_2NRs. We successfully examined the electronic structures of MoS_2NRs by means of electron energy loss spectroscopy (Figure 1b). Our results will offer the opportunities to explore the potential of TMDNRs as well as a new direction in the research of 1D materials.

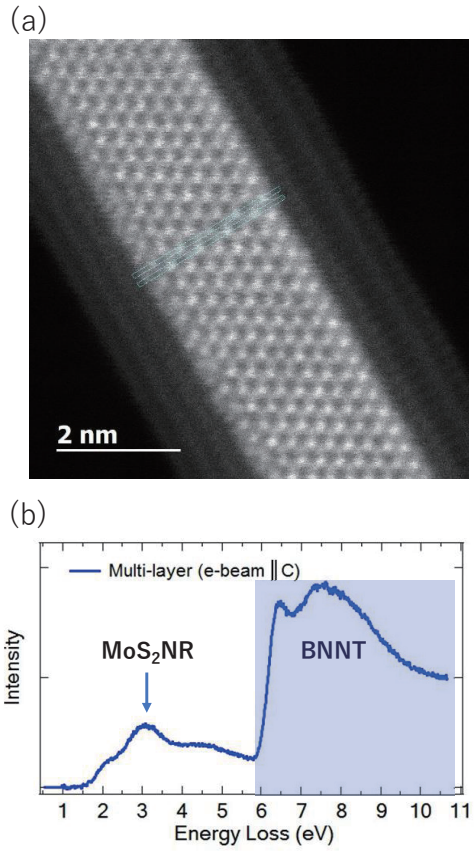

Fig. 1 (a) HAADF-STEM Z-contrast image and (b) Atomic-resolution EEL spectrum of an individual MoS_2NR encapsulated inside a BNNT.

[1] Y. Li *et al., J. Am. Chem. Soc.*, **130**, 16739 (2008); P. Cui *et al., Nano Lett.*, **17**, 1097 (2017). [2] Y. H. Hung *et al.*, *Appl. Mater.,* **8**, 20993 (2016). [3] H. Liu *et al.*, *IEEE Electron Device Letters*, **33**, 1273 (2012). [4] Z. Wang *et al.*, *J. Am. Chem. Soc.,* **132**, 13840 (2010); A. Botos *et al.*, *J. Am. Chem. Soc.*, **138**, 8175 (2016)

Corresponding Author: Y. Nakanishi
Tel: +81-52-789-3660, Fax: +81-52-747-6442, E-mail: naka24ysk@tmu.ac.jp

Precise carrier density control of SWCNTs by chemical doping with binary molecules

○Guowei Wang, Takeshi Tanaka, Atsushi Hirano, and Hiromichi Kataura*

Nanomaterials Research Institute, National Institute of Advanced Industrial Science and Technology (AIST), Tsukuba, Ibaraki 305-8565, Japan

Electric power can be generated by moving an electrolyte droplet on an ultra-thin single-wall carbon nanotube (SWCNT) films. To achieve high efficiency, the carrier density of the SWCNT film should be controlled precisely. In this study, we plan to fulfill this purpose by encapsulating organic dopant molecules [1] and controlling the number of them inside SWCNTs. To do this, we selected 2,4-bis[4-(*N,N*-diphenylamino)-2,6-dihydroxyphenyl] squaraine (DPSQ) as a hole dopant molecule and coronene as a dummy molecule. SWCNTs (EC1.5, Meijo Nano Carbon, unsorted) were refluxed in 1,4-dioxane for 3 h with pre-dissolved dopant and dummy molecules. We have prepared several SWCNTs with different DPSQ molecule density (Fig. 1) by simply adjusting the concentration ratio of DPSQ to coronene. Since the dummy molecules do not affect the electronic properties of SWCNTs, this method should be a good method to control carrier density precisely. As the next step, we will control the carrier density of thin semiconducting SWCNT film using this new method. We will show our recent results in the presentation.

This work was supported by JST CREST Grant Number JPMJCR16Q2, Japan.

[1] T. Takenobu et al. Nat. Mater. 2, 683 (2003).

Corresponding Author: H. Kataura
Tel: +81-29-861-2551, Fax: +81-29-861-2786,
E-mail: h-kataura@aist.go.jp

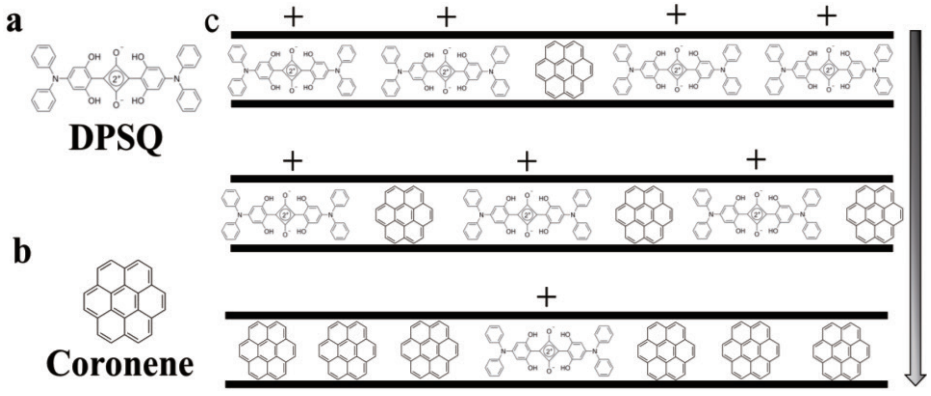

Fig. 1: The molecular structures of DPSQ (a) and coronene (b). Schematic of the carrier density control of SWCNTs (c).

1P-7

Surface chemical modification of defect-introduced graphite

○Y. Obata[1], H. Ishihara[2], G. K. Sunnardianto[3], T. Nishimura[4], K. Kusakabe[5], T. Kyotani[2], K. Takai [1,4]

[1]Dept. Applied Chemistry, Hosei University, Tokyo 184-8584, Japan, [2]Institute of Multidisciplinary Research for Advanced Materials, Tohoku Univ., [3]Faculty of Engineering and Technology, Sampoerna Universitity, [4]Research Center of Ion Beam Technology, [5]Dept. Materials Engineering Science, Osaka University, Osaka 560-8531, Japan

The presence of defects in graphene gives remarkable changes in chemical structure and electric properties due to its 2-dimensional nature [1]. In this study, defects are introduced into the surface by Ar-ion beam irradiation and the changes in chemical structure and carrier scattering by the surface adsorption of gaseous molecule are evaluated.

Defects were introduced into the surface of salvaged graphite as a model graphene by irradiation with Ar^+ ion beam at the acceleration voltage of 3 keV after pre-annealing under 10^{-5} Pa around 200℃ in an UHV chamber, followed by exposing to 100 kPa of hydrogen molecules or oxygen molecules or air exposure. Samples were analyzed by XPS, Elastic Recoil Detection Analysis ERDA, TPD [2], and Raman spectroscopy.

The atomic composition ratio of O to C obtained by XPS shows Oxygen content is much smaller for the graphite surface exposed to hydrogen molecules immediately after the defect introduction, compared with the air-exposure samples (Fig. 1). ERDA analysis shows the amount of hydrogen greatly increases for defects exposed to hydrogen molecules (Fig. 2). These suggest we can control the termination atoms of defects by atmosphere after defects introduction to graphite surface. Indeed, TPD shows H_2 deposition was clearly seen in hydrogenated graphite above 300℃ (Fig. 3a), which was hardly observed in the oxygen exposed sample (Fig. 3b) as similar as typical non-treated graphites in the temperature region less than 800℃ [2] . The presence of a large amount of meta-stable hydrogen is understood by hydrogen migration into the graphene plane through atomic vacancy [3], resulting in the formation of graphane [4]. The smaller Raman D-band for hydrogenated vacancies than that for oxygen terminated vacancies suggests the inter valley scattering depends on the chemical structure of defects in graphene. Exposing defects introduced into graphite by ion-beam irradiation to hydrogen molecule and air enables to control the terminating atoms of defects such as C-H and C-O termination of vacancies.

[1] Chen, et al., Nat. Phys. **7**, 535 (2011). [2] T. Ishii, et al, Carbon **125**, 146, (2017). [3] G. K. Sunnardianto,et al, Int. J. Hydrogen Energy, **43** (2017). [4] D. C. Elias, et al., Science **323**, 610 (2009).

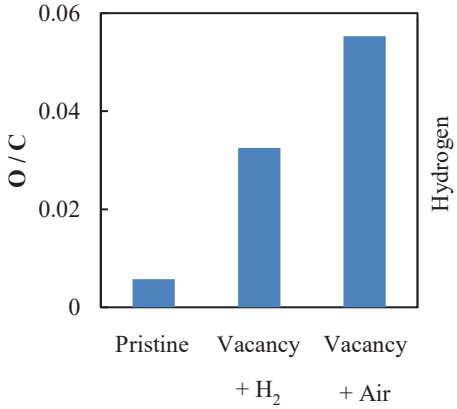

Fig. 1 XPS O / C composition ratio

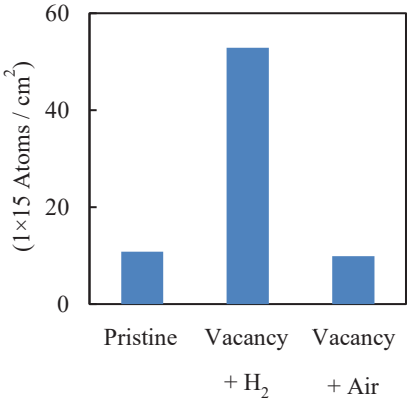

Fig. 2 Hydrogen amount in defects layers obtained by ERDA

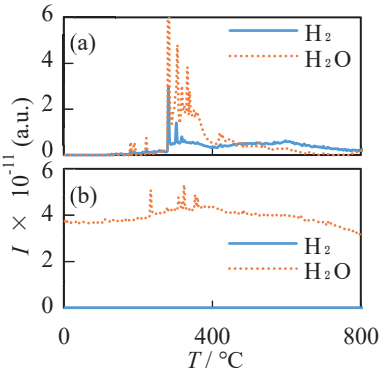

Fig. 3 TPD profiles for graphite (a) Vacancy + H_2 and (b) Vacancy + O_2

Electronic band modification of graphene by surface reconstruction of Au (001)

○Tomo-o Terasawa[1,2], Satoshi Yasuda[1], Naoki Hayashi[3], Wataru Norimatsu[3], Takahiro Ito[4], Shinichi Machida[1], Masahiro Yano[1], Koichiro Saiki[2], and Hidehito Asaoka[1]

[1] *Advanced Science Research Center, Japan Atomic Energy Agency, Ibaraki 319-1195, Japan*
[2] *Graduate School of Frontier Science, The University of Tokyo, Chiba, 277-8561, Japan*
[3] *School of Engineering, Nagoya University, Aichi 464-8603, Japan*
[4] *Nagoya University Synchrotron radiation Research center, Aichi 464-8603, Japan*

Graphene shows constant absorptance of 2.3% in the wide range of wavelengths [1]. The modification of the band structure of graphene is expected to tune such the optical properties of graphene, which will be useful for opto-electronic devices of graphene. Recently, quasi-one dimensional potential of hex-Au(001) reconstructed structure was reported to modify the electronic properties of graphene grown on this structure [2]. Scanning tunneling spectroscopy showed that the density of state of graphene from its Dirac point by 1-2 eV decreased when graphene was grown on hex-Au(001). However, the band structure of graphene on hex-Au(001) was not observed, nor the relation between the band structure of graphene and the structure of Au(001) and graphene has not been revealed.

Here, we report the band structure of graphene grown on hex-Au(001) using angle resolved photoemission spectroscopy (ARPES). We prepared graphene on hex-Au(001) by chemical vapor deposition [3]. Figure (a) shows the low energy electron diffraction (LEED) pattern of graphene grown on Au(001) single crystal. Four-folded and twelve-folded spots correspond to 90-degree rotated one-dimensional hex-Au(001) reconstructed structures and epitaxially grown graphenes on them, respectively. Figure (b) shows the ARPES image of this sample taken at AichiSR BL7U. The linear graphene band shows the intensity reduction at the binding energy of approximately 0.9 eV, indicating the modification of band structure of graphene by hex-Au(001). We will discuss the relation between the band structure of graphene and the structure of graphene and hex-Au(001) on the basis of the results of ARPES, LEED, and scanning tunneling microscopy in the poster presentation.

[1] R. R. Nair, *et al*. Science, **320**, 1308 (2008).
[2] X. Zhou, *et al*., ACS nano, **10**, 7550 (2016).
[3] T. Oznuluer, *et al*., Appl. Phys. Lett., **98**, 183101 (2011).

Corresponding Author: T. Terasawa
Tel: +81-29-284-3504,
Fax: +81-29-284-3504,
E-mail:
terasawa.tomoo@jaea.go.jp

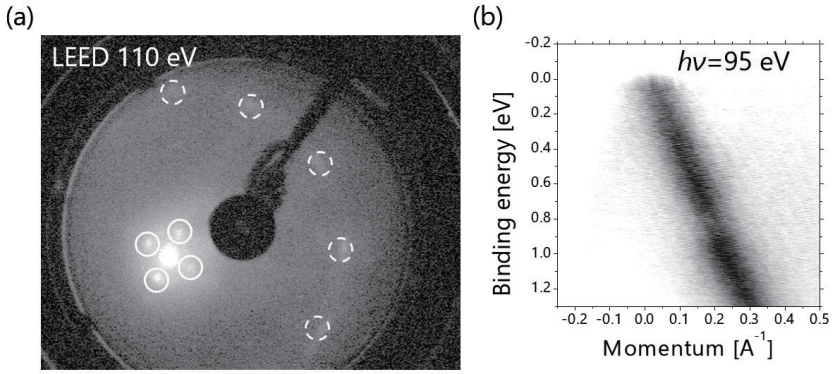

Figures (a) LEED pattern and (b) ARPES image of graphene grown on hex-Au(100) reconstructed surface. (a) White and white broken circles highlight diffraction spots from Au and graphene. The incident electron beam was tilted from the surface normal to show the diffraction spots from graphene. (b) Energy reduction at the binding energy of approximately 0.9 eV is observed.

Fabrication of transparent solar cell with directly grown WS_2 in large scale

○X. He[1], Y. Yamaguchi[1], T. Kaneko[1], and T. Kato[1,2]

[1]*Department of Electronic Engineering, Tohoku University, Sendai 980-8579, Japan*
[2] *JST-PRESTO*

Layered transition metal dichalcogenide (TMD) is known as a true 2D material with excellent semiconducting properties. TMD is one of the most attractive materials for future transparent and flexible optoelectrical devices due to their atomically thin structure, band gap in visible light range, and high optical transparency. Although the solar cell of TMD has been widely investigated by many groups, those are based on the pn junction type solar cell. Since complicated structures are required to form pn junction structures in TMD such as dual gate electrodes or position selective doping, the device size of pn junction solar cell with TMD is limited within very small region (few μm). In spite of the outstanding advantages of TMD, those merits of TMD have not been applied for transparent and flexible solar cell, which is attracted intense attention as a next-generation energy harvesting technology.

Recently, we have developed a new fabrication process of TMD-based solar cell [1]. In our process, Schottky type device configuration is utilized, which can be simply formed by asymmetrically contacting electrodes and TMD. The power conversion efficiency clearly depended on the work function difference between two electrodes (ΔWF), and a higher efficiency could be obtained with higher ΔWF (Pd-Ni), which is consistent with our concept, where Ni and Pd can form large and small Schottky barriers to operate as power-generation and carrier-collect regions, respectively. Based on the optimizations of electrodes and distance, the power conversion efficiency can be reached up to 0.7 %, which is the highest value for solar cell with similar TMD thickness [1].

In our previous study, we used conventional metals such as Ni and Pd to tune the Schottky barrier height between electrode and TMD, which suppress the transparency of whole device. Furthermore, the device size was limited within μm scale because of the size of exfoliated TMD.

To improve the transparency of whole device, we use indium tin oxide (ITO) as electrodes. The directly grown large area WS_2 film are also used to overcome the limited device size. After controlling the ΔWF of ITO electrodes and optimizing the synthesis method of WS_2, clear power generation can be observed with ITO/WS_2 based transparent solar cell in large scale(Fig.1). Since our simple fabrication process includes high potential for large scale fabrication, this achievement is very important for realizing the industrial application of TMD as a transparent and flexible solar cell.

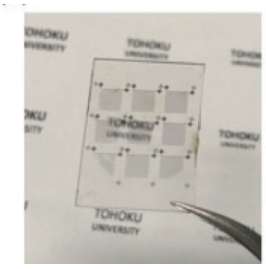

Fig. 1. Typical optical image of transparent solar cell fabricated with directly grown WS_2 crystal.

[1] T. Akama, W. Okita, R. Nagai, C. Li, T. Kaneko, and T. Kato, Sci. Reports **7**, 11967 (2017).

Corresponding Author: Xing He

Tel: +81-22-795-7046, Fax: +81-22-263-9225, E-mail: he.xing.q7@dc.tohoku.ac.jp

Installing Various Functional Groups on $Li^+@C_{60}$ Using Azide-containing 1,3-Cyclohexadienes

○Hiroshi Okada,[1,2] Takumi Takada,[3] Shota Nagasawa,[3] Yusuke Sasano,[3] Eunsang Kwon,[4] Yutaka Matsuo,[1,2,5] Yoshiharu Iwabuchi[3]

[1] *Department of Mechanical Engineering, School of Engineering, The University of Tokyo, Tokyo 113-8656, Japan*
[2] *Center for Fundamental and Applied Research of Novel Nanocarbon Derivatives, Center for Key Interdisciplinary Research, Tohoku University, Sendai 980-8578, Japan*
[3] *Department of Organic Chemistry, Graduate School of Pharmaceutical Sciences, Tohoku University, Sendai 980-8578, Japan*
[4] *Research and Analytical Center for Giant Molecules, Graduate School of Science, Tohoku University, Sendai 980-8578, Japan*
[5] *University of Science and Technology of China, Hefei 230026, China*

Functionalized fullerenes have served an important role in energy-related and biology-related research areas. Especially, appropriate functional groups introduced on a fullerene cages provide particular functions, *e.g.*, solubility improvement,[1] specific morphology,[2] and photoinduced electron transfer.[3]

To date, several chemical modifications of lithium-ion-containing fullerene ($Li^+@C_{60}$) have been achieved using diazo or diene compounds.[4] In general, introducing a functional group to $Li^+@C_{60}$ is often problematic due to several reasons. Facile and reliable methods to connect various functional groups with $Li^+@C_{60}$ is desired for further application researches.

In this work, we employed the previously reported selective oxidation reactions from cyclohexene to 1,3-cyclohexadiene,[5] in which high reactivity of $Li^+@C_{60}$ toward dienes has been already known.[4b] Azide-containing 1,3-cyclohexadiene (**1**) was linked with several acetylenes (**2a-h**) by Huisgen reactions to synthesize compounds **3a-h** which reacted with $[Li^+@C_{60}]TFSI^-$ to give functionalized lithium-ion-containing fullerenes (**4a-h**) in moderate yields. This methodology can offer a reliable method to link $Li^+@C_{60}$ with desired functional groups.

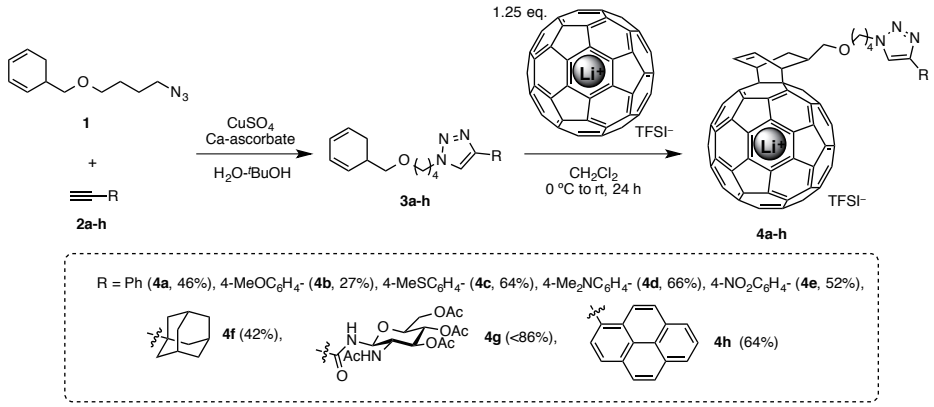

References

[1] K. Okuda *et al.*, *Fullerene. Sci. Technol.* **2000**, *8*, 89–104. [2] M. J. Hollamby *et al.*, *Nature Chem.*, **2014**, *6*, 690–696. [3] K. Ohkubo *et al.*, *Angew. Chem. Int . Ed.* **2004**, *43*, 853–856. [4] a) Y. Matsuo *et al.*, *Org. Lett.* **2012**, *14*, 3784–3787. b) H. Kawakami *et al.*, *Org. Lett.* **2013**, *15*, 4466–4469. c) H. Ueno *et al.*, *J. Am. Chem. Soc.* **2014**, *136*, 11162–11167. d) H. Okada *et al.*, *J. Org. Chem.* **2017**, *82*, 5868–5872. e) H. Ueno *et al.*, *J. Org. Chem.* **2017**, *82*, 11631–11635. [5] S. Nagasawa *et al.*, *Angew. Chem. Int. Ed.* **2016**, *55*, 13189–13194.

Corresponding Author: H. Okada, Tel: +81-3-5841-0978, E-mail: hokada@photon.t.u-tokyo.ac.jp

ESR study of Sc-dimetallofullerene anions: $(Sc_2C_n)^-$ (n=76, 78, 80)

○Shun Yoshida, Koichi Kikuchi, Yohji Achiba, Takeshi Kodama

Department of Chemistry, Tokyo Metropolitan University, Tokyo 192-0397, Japan

In the previous symposium [1], we reported the isolation of $(Sc_2C_{76})^-$, $(Sc_2C_{78})^-$, and $(Sc_2C_{80})^-$. For $(Sc_2C_{78})^-$ and $(Sc_2C_{80})^-$, two isomers, $(Sc_2C_{78}(1, 2))^-$ and $(Sc_2C_{80}(1, 2))^-$, were obtained respectively. For $(Sc_2C_{80}(1))^-$, the ESR spectrum was measured, and the simulation spectrum was well reproduced the observed one. On the other hand, for $(Sc_2C_{80}(2))^-$, the ESR signals could not be observed likely due to its small amount. In this study, we reinvestigated the ESR of $(Sc_2C_{80}(2))^-$. In addition, the ESR of $(Sc_2C_{76})^-$ and $(Sc_2C_{78}(1, 2))^-$ were measured.

Sc-dimetallofullerenes were produced and isolated by the same method reported previously, and the amount of sample was increased [1]. The X-band ESR spectra of the isolated Sc-dimetallofullerenes were measured at room temperature.

As shown in Fig. 1, both the ESR spectra of $(Sc_2C_{80}(1, 2))^-$ were obtained. ESR spectra of $(Sc_2C_{80}(1, 2))^-$ essentially consisted of 64 peaks respectively (some peaks were overlapped). It is consistent with an unpaired spin is located on the encaged Sc dimer because the nuclear spin of Sc is 7/2. The simulation spectrum for $(Sc_2C_{80}(2))^-$ was also well reproduced the observed one. On the simulation parameters for two isomers, the g-factors are almost equal (g(1)=1.9948, g(2)=1.9947), but the hyperfine coupling constants are about 7% different (A(1)=497.5 MHz, A(2)=464.8 MHz). The difference might come from the different cage structure of them.

For $(Sc_2C_{76})^-$ and $(Sc_2C_{78}(1, 2))^-$, the ESR signals could not be observed. The results suggested that $(Sc_2C_{76})^-$ and $(Sc_2C_{78})^-$ might be $(ScC_{80})^-$ and $(ScC_{82})^-$ because the difference of the mass number between Sc_2C_n and ScC_{n+4} is only about three. Therefore, we tried to neutralize $(Sc_2C_{76})^-$ and $(Sc_2C_{78})^-$ and to measure ESR spectra. The results will be presented in the symposium.

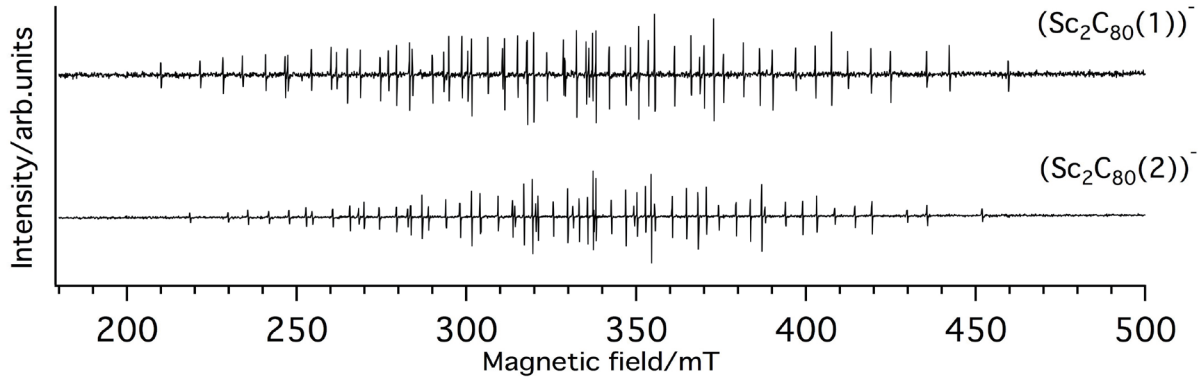

Fig. 1 ESR spectra of $(Sc_2C_{80}(1))^-$ and $(Sc_2C_{80}(2))^-$.

[1] S. Yoshida, *et al*. *The 55th Fullerenes-Nanotubes-Graphene General Symposium* 126 (2018).

Corresponding Author: Takeshi Kodama
Tel: +81-42-677-2530, Fax: +81-42-677-2525
E-mail: kodama-takeshi@tmu.ac.jp

Isolation and structure determination of trifluoromethylated gadolinium metallofullerenes

○Shinobu Aoyagi[1], Ayano Nakagawa[2], Haruka Omachi[2,3], Hisanori Shinohara[2]

[1]*Department of Information and Basic Science, Nagoya City University, Nagoya 467-8501, Japan*
[2]*Department of Chemistry and* [3]*Research Center for Materials Science, Nagoya University, Nagoya 464-8602, Japan*

Endohedral metallofullerenes have been extensively studied since the first experimental observation of La@C_{60} in a laser-vaporized supersonic beam in 1985. However, most of these studies have focused on metallofullerenes larger than C_{60} such as Ln@C_{82} (Ln: lanthanide). There are few examples for isolation of small-cage (C_{60}, C_{70}, C_{72}, and C_{74}) lanthanide metallofullerenes because of their extremely high chemical reactivity. Recently, we developed an in situ trifluoromethylation method for the extraction and purification of these missing metallofullerenes [1−3]. Here we report the isolation and structure determination of trifluoromethylated gadolinium metallofullerenes (Gd@$C_{60}(CF_3)_3$, Gd@$C_{60}(CF_3)_5$, Gd@$C_{70}(CF_3)_3$, Gd@$C_{74}(CF_3)$, and Gd@$C_{74}(CF_3)_3$). Gd-metallofullerenes are promising as magnetic resonance imaging (MRI) contrast agents. The fully enclosing carbon cage completely prevents leaching of the Gd atoms, resulting in lower toxicity than commercially available metal chelate reagents such as Gd-DTPA.

Trifluoromethylated Gd-metallofullerenes were synthesized by the modified arc-discharge method. PTFE rods are placed near the discharge area as CF_3 source. During arc discharge, PTFE was decomposed and evaporated to produce CF_3 radicals. Gd-metallofullerenes and empty fullerenes were extracted from the raw soot with *o*-xylene. Rapid separation of Gd-metallofullerenes from empty fullerenes was carried out by the $TiCl_4$ Lewis acid method. High-performance liquid chromatography (HPLC) purification was conducted for isolation of trifluoromethylated Gd-metallofullerenes. Single crystals of trifluoromethylated Gd-metallofullerenes were obtained from solution. The single-crystal X-ray diffraction data for structure determination were collected at SPring-8 large synchrotron radiation facility.

Figures show the molecular structures of Gd@$C_{74}(CF_3)$ (I), Gd@$C_{74}(CF_3)$ (II), and Gd@$C_{74}(CF_3)_3$ derived from the X-ray crystal structure analysis. The closed-shell molecular structures are theoretically stable and have wide HOMO-LUMO energy gaps.

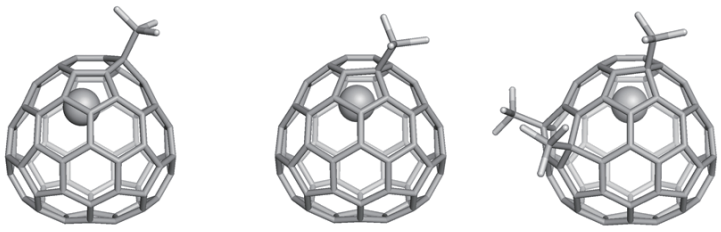

Gd@$C_{74}(CF_3)$ (I) Gd@$C_{74}(CF_3)$ (II) Gd@$C_{74}(CF_3)_3$

[1] Z. Wang *et al*. Angew. Chem. Int. Ed. **55**, 199 (2016).
[2] A. Nakagawa *et al*. Nature. Commun. **9**, 3073 (2018).
[3] A. Nakagawa *et al*. R. Soc. Open Sci. **5**, 181015 (2018).

Corresponding Author: S. Aoyagi
Tel: +81-52-872-5061
E-mail: aoyagi@nsc.nagoya-cu.ac.jp

Electron excitation of an atom encapsulated in C_{60} fullerene

○Haruki Torii[1], Masayuki Toyoda[1], Susumu Saito[1], Tomonari Wakabayashi[2], Yasuyuki Kanai[3], Noboru Sasao[4], Motohiko Yoshimura[4]

[1] *Department of Physics, Tokyo Institute of Technology, Tokyo 152-8551, Japan*
[2] *Department of Chemistry, Kindai University, Higashi-Osaka 577-8502, Japan*
[3] *Nishina Center for Accelerator-Based Science, RIKEN, Wako 351-0198, Japan*
[4] *Division of Quantum Universe, RIIS, Okayama University, Okayama 700-853, Japan*

C_{60} fullerene has a hollow structure, and it is possible to stably trap a heterogeneous (X) atom inside C_{60} fullerene. In fact, it has been confirmed experimentally that rare gas atoms [1], alkali metal atoms [2], 15 group atoms [3], H_2 molecule [4] and H_2O molecule [5] can be contained stably in C_{60} fullerenes. We use C_{60} fullerenes as a cage to enclose an X atom, and we can create a pseudo isolated atomic state inside C_{60} fullerene.

These X atoms endohedral C_{60} fullerene ($X@C_{60}$) can make isolated atomic groups by collecting in large quantities. It should be possible to create coherent quantum states with isolated atomic groups using $X@C_{60}$ and laser. We expect them to be available for experiments related to the emission of neutrinos by the process of releasing neutrino pair and photons with the transition of coherent atoms from the excited states to the grand state [6].

The aim of the present work is to theoretically predict the possibility of selective excitation that can excite only encapsulated X atoms without exciting C_{60} fullerenes. We use the density functional theory (DFT) and the time-dependent density functional theory (TDDFT).

We calculated the oscillator strength distribution of X atom, C_{60} fullerene, and $X@C_{60}$ (Fig.1). Following these results, we discuss the possibility of selective excitation of X atoms.

[1] M. Saunders *et al.*, R. J. Poreda, Science **259** 1428 (1993).
[2] R. Tellgmann *et al.*, Nature **382**, 407 (1996).
[3] P. Jakes *et al.*, Phys. Chem. Chem. Phys., **5**, 4080 (2003).
[4] K. Komatsu, M. Murata and Y. Murata, Science **307**, 238 (2005).
[5] K. Kurotobi and Y. Murata, Science **333**, 613 (2011).
[6] 植竹 智，吉村 太彦，吉村 浩司，笹尾 登，高エネルギー物理学研究者会議 高エネルギーニュース **33**, 99 (2014).

Corresponding Author: H. Torii
Tel: +81-3-5734-2703, Fax: +81-3-5734-2739
E-mail: torii@stat.phys.titech.ac.jp

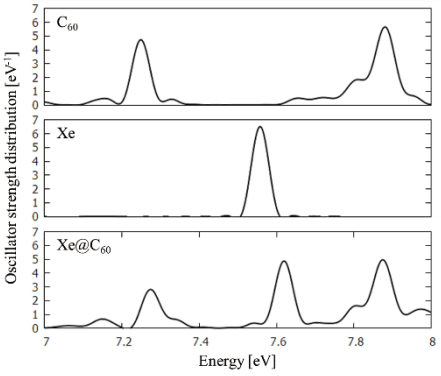

Fig.1 The oscillator strength distribution in the case of X = Xe.

Degradation of single-wall carbon nanotubes by lung macrophages of mouse *in vivo*

OYing Xu[1], Minfang Zhang[1]*, Mei Yang[1], Masako Yudasaka [1, 2], Toshiya Okazaki[1]

[1]*National Institute of Advanced Science and Technology (AIST)*
[2]*Meijo University*

Carbon nanotubes (CNTs) have been demonstrated as promising nanomaterials for a wide range of applications due to their unique properties. However, the toxicity of CNTs has not been fully understood especially the long-term toxicity and the degradation in vivo. Because CNTs are most possibly to enter into lung of living body when they were exposed into environment such as air, the investigations for the degradation in lung and pulmonary toxicity of CNTs were extremely important. In this study, we have investigated the degradation of single-wall CNTs (SWNTs) by lung macrophages as well as the pulmonary toxicity after single intravenous injection into mice for 2 months.

The SWNTs used in this study were produced by the super-growth method (SG-CNTs) [1] and dispersed in BSA solution by sonication as we reported previously [2]. After injection of SG-CNTs into mice at 5 time-points in the period of 60 days, the blood and all organs were taken out and analyzed. The degradation of CNTs in lung was estimated by observation of the color change and measurements of the quantities of CNTs in lung lysates, which were prepared by treatment of lungs with collagenases and surfactant such as SDS. The pulmonary toxicity was investigated by measurements of inflammatory cytokines in blood plasma and lung lysates.

Our results showed that the lungs were changed to grey-color after single CNT-injection for 24 h indicating the CNT-accumulation in lungs. This grey-color of lung was gradually faded and the quantities of SG-CNTs in lung lysates were decreased with increase of post-injection time. About 60% of SG-CNTs were cleared from lungs within 60 days. The measurement results of cytokines of TGF-β1, IL-6, INF-γ and TNF-α in blood plasma and lung lysates indicated there are no significant differences between the groups of control and SG-CNTs injected mice, suggesting the low pulmonary toxicity of SG-CNTs. To further confirm the degradation of SG-CNTs by lung macrophages, the study in vitro by using lung macrophage cell line of MH-S was performed. The results showed that about 20 % SG-CNTs inside of MH-S cells were degraded in one week. All results indicated that lung macrophages digested SG-CNTs.

[1] K. Hata, *et al.* Science, **306**, 1362 (2004).
[2] M. Zhang *et al*. Carbon, **127**, 93 (2018).

Corresponding Author: M. Zhang
E-mail: m-zhang@aist.go.jp

Revisiting transport mechanism in semiconducting carbon nanotube films with the aid of far-infrared plasmon response

○Kanae Oi[1], Tsuyoshi Kawai[1], Yoshiyuki Nonoguchi[1,2]

[1] *Division of Materials Science, Nara Institute of Science and Technology, NAIST, Takayama, Ikoma, Nara 8916-5, Japan*
[2] *JST PRESTO, 4-1-8 Honcho, Kawaguchi, Saitama 332-0012, Japan*

Single-walled carbon nanotubes (SWNTs) are known to exhibit unique ballistic carrier transport, while transport in their assembled films can be understood in terms of tube-to-tube tunneling.[1] In this context, the methods of the Fermi level characterization are required in order to understand the relationship between tunneling and doping level. The field effect application has mostly been used to tune and estimate the Fermi level. Here we use one-dimensional plasmon resonance in the far-infrared (FIR) region for the estimation of carrier concentration.[2] Using this technique, this study demonstrates relationship between doping level and electrical conductivity.

We used ~98% purity semiconducting SWNTs prepared using density gradient ultracentrifugation (DGU) with nonionic surfactant pluronic F108.[3] This technique enables the extraction of relatively low-doped SWNTs. Obtained SWNT dispersion was used to prepare semitransparent SWNT thin films on PET substrates. The doping level of SWNTs was modulated with a one-electron oxidant, silver bis-(trifluoromethanesulfonyl)imde (AgTFSI).

As-purified semiconducting SWNT films showed small FIR absorption whereas, in the same region, non-separated films provide strong plasmon resonance derived from the metallic SWNTs. This fact suggests the successful purification of high quality, semiconducting SWNTs up to ~98%. Upon chemical doping, the S_{11} absorption in the near infrared (NIR) region decreased and the broad extinction in the FIR gradually evolved, depending on the concentration of oxidants (Fig.1(a)). Within the Drude model, this evolution could be proportional to the carrier concentration (N) of each semiconducting SWNTs. The identical semiconducting SWNT films showed different electrical conductivity dependent on the oxidant concentration, that is, carrier concentration. The conductivity can be fitted with the exponential function of integrated plasmon resonance (0.02-0.084 eV) (Fig.1(b)). Assuming $E_F \propto N$ in the shallow doping region, this observation strongly suggests tunneling transport in the semiconducting SWNT films. [1]

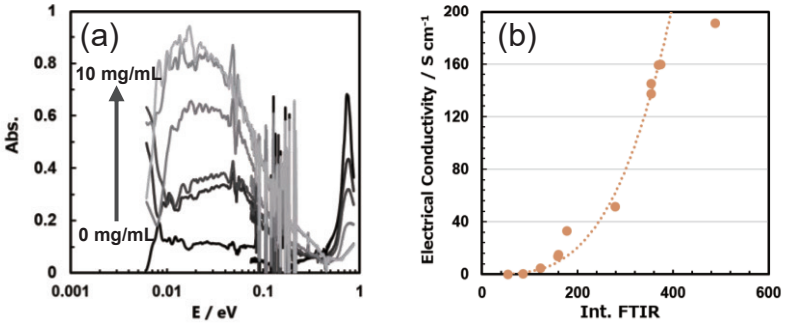

Fig.1 (a) NIR-to-FIR spectra of semiconducting SWNT films dependent on doping concentration. (b) Electrical conductivity of semiconducting SWNT films as a function of integrated plasmon resonance (0.02~0.084 eV). (A dotted curve shows an-exponential fitting line.)

[1] T. Yamamoto *et al.* J. Appl. Phys., **122**, 015308 (2017).
[2] A.Ugawa *et al.* PRB, **60**, R11305 (1999).
[3] C. M. Homenick *et al.* J. Phys. Chem. C., **118**, 16156−16164 (2014).

Corresponding Author: Yoshiyuki Nonoguchi
E-mail: nonoguchi@ms.naist.jp

Mechanical properties of carbon nanotubes with vacancy under the uniaxial strain

○Kazufumi Yoneyama and Susumu Okada

Graduate School of Pure and Applied Sciences, University of Tsukuba, Tsukuba 305-8571, Japan

Carbon nanotubes (CNTs) are known to exhibit remarkable mechanical properties: mechanical toughness and flexibility against tensile strain and bending, respectively, tubular covalent networks of sp^2 C atoms. Theoretical works elucidated that the mechanical properties of CNTs strongly depend on their diameter and, chirality. However, comprehensive knowledge about the mechanical properties with respect to both local and global geometries is not clearly elucidated to date. So, in this work, we aim to elucidated mechanical properties of CNTs with the diameter of about 0.95 nm in terms of their chirality and atomic vacancies under the uniaxial tensile strain, using the density functional theory with the generalized gradient approximation.

We consider (12,0), (10,4), and (7,7) CNTs as the representative zigzag, chiral, and armchair CNTs, respectively, with the diameters of about 0.95 nm. With the choice of the CNTs, we can make quantitate investigation on the energetics of CNTs with respect to the chirality and vacancies. Our calculations show that the Young's modulus of pristine CNTs is 0.741, 0.748, and 0.754 TPa for (12,0), (10,4), and (7,7) CNTs, respectively. Atomic vacancies decrease the Young's modulus irrespective of the CNT chirality: the calculated values are 0.670, 0.650, and 0.601 TPa for (12,0), (10,4), and (7,7) CNTs, respectively. As for the structural deformation, the armchair CNT is the tougher than the chiral and zigzag CNTs: The armchair CNT retains its tubular structure up to 40 % tensile strain with the critical tension of 200.84 nN. In contrast, the zigzag and chiral CNTs retains 22 % with the tension 170.82 nN and 24 % with 195.56 nN, respectively. With the defects, the critical tension substantial decreases down to 94.18, 96.02, and 85.40 nN for the zigzag, chiral, and armchair CNTs, respectively.

Corresponding Author: K. Yoneyama
E-mail: kyoneyama@comas.frsc.tsukuba.ac.jp

Fermi-level dependence of THz high-harmonic generation in single-wall carbon nanotubes

○Hiroyuki Nishidome [1], Kohei Nagai [2], Yota Ichinose [1], Kengo Fukuhara [1], Junji Nozaki [1], Junko Eda [1], Yohei Yomogida [1], Junichiro Kono[3], Koichiro Tanaka [2, 4], Kazuhiro Yanagi [1]

[1] *Department of Physics, Tokyo Metropolitan University, Tokyo 192-0397, Japan*
[2] *Department of Physics, Kyoto University, Kyoto 606-8502, Japan*
[3] *Department of Electrical and Computer Engineering, Rice University, Texas 77005, USA*
[4] *Institute for Integrated Cell-Material Sciences, Kyoto University, Kyoto 606-8501, Japan*

Recent advancement of high power laser source in mid-infrared and terahertz (THz) region enables us to investigate the extreme nonlinear optics in solids where the ground state of solid becomes unstable due to strong light-matter interactions [1]. One of the unique phenomena in the extreme nonlinear optics is high-harmonic generation (HHG). HHG has been intensively studied in atomic gases, but observation of HHG in solid has long been difficult because of unavoidable damage on samples by extremely strong laser light. But since observation of HHG from ZnO [2] using THz light, HHG by intense THz light has been observed in various kinds of materials such as semiconductor crystals and two-dimensional materials (graphene [3], MoS_2 [4], etc.). In solid, there are two mechanisms in HHG, the interband and intraband mechanisms, but contributions of the two mechanisms to HHG are still elusive because various physical parameters, such as crystal structure, band structures, and conduction electrons, affect nonlinear processes in solid.

Here in this study, we investigated the relationship between HHG intensity and carrier density in single wall carbon nanotubes. We used electric-double-layer (EDL) carrier injection with ionic liquid to tune carrier density.

We prepared a high-purity (6,5) thin film, and transferred it to a sapphire substrate, and fabricated EDL devices. Then we investigated HHG using 62.5 THz laser with changing Fermi level. The results are shown in Figure 1. We observed decrease of HHG intensities as the shift of gate voltage. This indicates, in this sample, the interband mechanism is more dominant than the intraband mechanism. Moreover Fermi-level dependence of different order harmonic intensities are plotted in Fig.2, which is normalized by the intensity at 0 V. This shows that higher-order harmonics decrease more rapidly. The shift of Fermi-level more strongly influences on the higher-order harmonic generations.

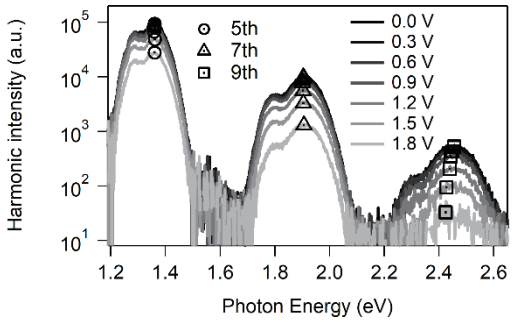

Fig.1 HHG spectra as a function of gate voltage

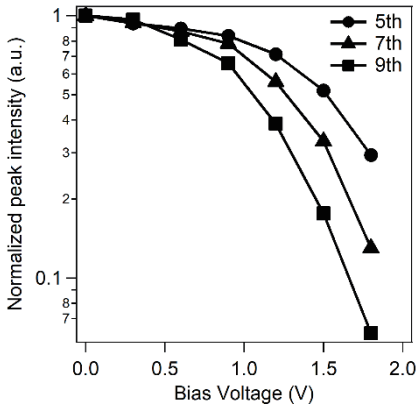

Fig.2 Fermi-level dependence of 5th, 7th and 9th order harmonic generation. Each intensity is normalized at 0 V

References:
[1] K. Tanaka, Hikaribussei kenkyukai tutorial (2017)
[2] S. Ghimire *et al.,* Nature Physics, 7, 138 (2010)
[3] N. Yoshikawa *et al.*, Science **356**, 736 (2017)
[4] H. Liu *et al.,* Nature Physics, 13, 262 (2016)

Corresponding Author: K. Yanagi, Tel: +81-42-677-2494, E-mail: ynagi-kazuhiro@tmu.ac.jp

Preparation of SWNT/PE Composites *via* Melt Blending

○Nao Otsuki, Ryota Yamada, Takumi Adachi, Yutaro Saito, Masaru Sekido

Department of Materials Science and Engineering, National Institute of Technology, Sendai College, Natori 981-1239, Japan

Due to their outstanding mechanical properties, Young modulus around 1 TPa, tensile strength about 100 times greater than steel, and low density CNTs are considered as the ideal reinforcement fillers for the nanocomposite materials. Previously we have reported the tensile strength of SWNT/Polyethylene (PE) composites prepared by Melt Blending and found that tensile strength of SWNT/PE was increased as the weight ratio of SWNT was increased. In this work we introduced carboxy group (COOH) and ocatadecylamine (ODA) on the surface of SWNT and studied the tensile strength of SWNT-COOH/PE and SWNT-ODA/PE composites.

Preparation of SWNT-COOH and SWNT-ODA was shown in scheme 1[1]. Briefly SWNT (3 g) was added into 60 mL of a mixture (v/v, 1/3) of nitric acid and sulfuric acid. Then the suspension was stirred for 24hours at room temperature to introduce the carboxy group (SWNT-COOH). Obtained SWNT-COOH (3 g) was added into the mixture of thionyl chloride (60 mL) and DMF (1.5 mL). Then the mixture was stirred for 24hours at 70 °C to obtain SWNT-COCl. The mixture of SWNT-COCl (3 g) and ODA (12 g) were stirred for 24hours at 100 °C to afford SWNT-ODA. SWNT-COOH/PE and SWNT-ODA/PE composites were prepared by Melt Blending at 220 °C, screw speed of 100 rpm and a recycle time of 10 minutes.

We will discuss the difference among SWNT, SWNT-COOH and SWNT-ODA as a reinforcement filler for PE matrix.

Scheme 1

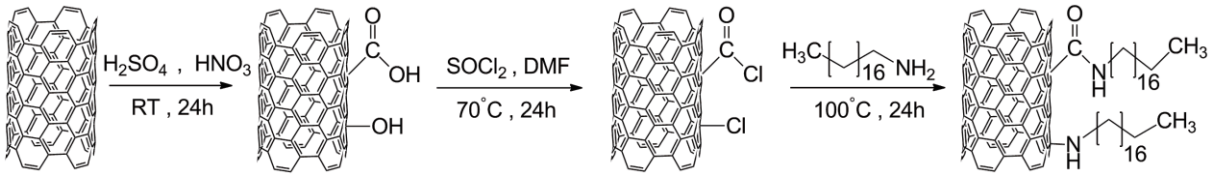

[1] Mohamed Abdel Salam, Robert Burk. *Arabian Journal of Chemistry*. **10**, 921-927(2017)

Corresponding Author: Nao Otsuki

Tel: +81-22-381-0329, Fax: +81-22-381-0329 , E-mail: s1400312@sendai-nct.jp

Electron emitters of textured carbon nanotube arrays for X-ray tubes via facile, rapid few-minute processes

Sae Kitagawa[1], Hisashi Sugime[2], Hayato Ochi[3], Daizo Takahashi[3], ○Suguru Noda[1,4]

[1] *Department of Applied Chemistry, Waseda University, Tokyo 169-8555, Japan*
[2] *Waseda Institute for Advanced Study, Waseda University, Tokyo 169-8050, Japan*
[3] *MEIDENSHA CORPORATION*
[4] *Research Institute for Science and Engineering, Waseda University, Tokyo 169-8555, Japan*

There are increasing demands for X-ray scanners for non-destructive inspections in industrial, medical, and security applications. X-ray tubes with electron field emitters (FEs) can make the whole devices compact/portable owing to the low power consumption. Carbon nanotubes (CNTs) have been extensively studied and excellent performances have been reported for morphology-controlled CNT-FEs via lithography-based processing for flat-panel display applications [1,2]. Low-cost production of CNT-FEs is essential for their wide use.

In this work, we propose facile fabrication of morphologically-controlled CNT-FEs. Si substrates with pyramid-shaped textures were formed by sandpaper-rubbing and alkaline-etching and used as the template substrates. Fe/Al catalyst was sputter-deposited, tens-μm-tall vertically-aligned CNTs were synthesized by chemical vapor deposition, Ag-Cu braze alloy was vapor-deposited on the CNTs, the CNTs were brazed to Cu holders, and the CNTs/Ag-Cu/Cu holders were peeled off from the substrates. Each step took a few minutes.

CNTs on the Ag-Cu braze alloy had pyramid-shaped morphology (Fig. 1a). The CNTs can be brazed and transferred to the multiple Cu holders at once (Fig. 1b,c). The four CNT-FEs showed good FE performances (Fig. 1d). An X-ray photograph of an electric drill taken using a CNT-FE is shown as an example (Fig. 1e). The CNT-FEs are processed at high temperature and free from organic compounds such as binders, thus will show little degassing, which is important for vacuum applications including X-ray tubes.

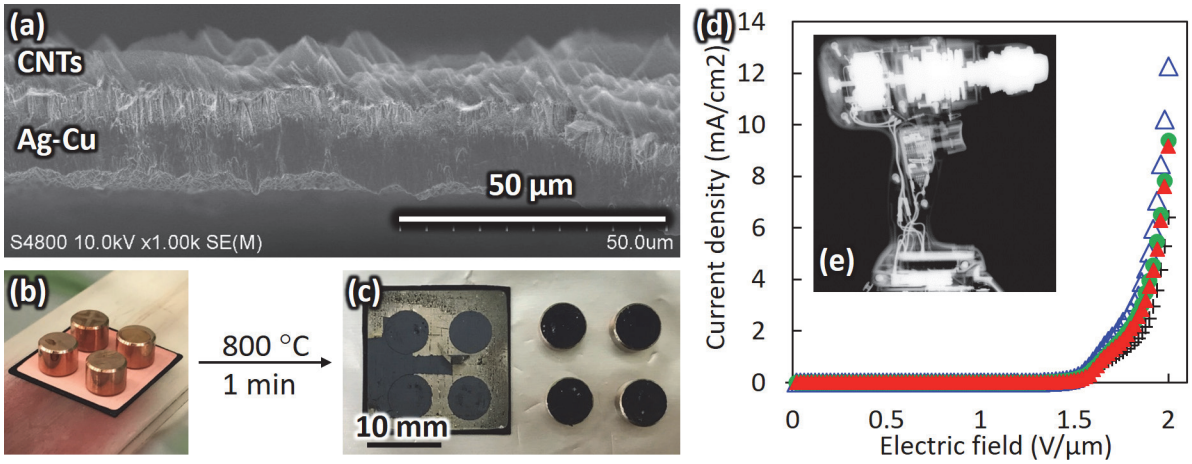

Fig. 1. CNT-FEs in this work. (a) Cross-sectional SEM image of CNTs held on Ag-Cu braze alloy. (b,c) Brazing CNT-FEs to Cu holders. (d) FE performance. (e) X-ray photograph.

[1] L. Gangloff, et al., Nano Lett. 4, 1575 (2004).
[2] Y. Shiratori, et al, Nanotechnology 20, 475707 (2009).

Corresponding Author: S. Noda Tel&Fax: +81-3-5286-2769, E-mail: noda@waseda.jp

1P-20

Atomic Scale In-Situ Study on Carbon Nanotube Growth from Co-Co_3C Catalysts

○Feng Yang, Yan Li
College of Chemistry and Molecular Engineering, Peking University, Beijing 100871, China

The metal catalysts play important roles in chemical vapor deposition (CVD) of single-walled carbon nanotubes (SWNTs). It was reported that solubility of carbon in transitional metal nanoparticles such as Fe, Co, and Ni is associated with the SWNT growth, which is generally believed to via a vapor–liquid–solid mechanism [1, 2]. Revealing the catalyst structure with atomic resolution under reactive environment is crucial for understanding the controlled growth mechanism.

Here, using Co as a model catalyst, we investigated the role of active species Co-Co_3C in catalyzing SWNT nucleation and growth by using aberration-corrected environmental transmission electron microscope (ETEM). We recorded the carbon atoms dissolving into Co nanoparticles and formation of inhomogeneous Co-Co_3C structure during CVD. The growth of SWNTs was realized only by the cooperation of Co and Co_3C in proper carbon feeding conditions. The evidences are *in situ* and real time with atomic scaled resolution. These findings are crucial for the rational design of catalysts for high efficiently catalyzing SWNTs.

[1] V. Jourdain and C. Bichara. Carbon, **58**, 2 (2013).
[2] M. Li, Y. Li *et al*. Top. Curr. Chem., **375**, 29 (2017).

Corresponding Author: Yan Li
Tel: +86-10-62756773, Fax: +86-10-62756773,
Web: http://old.chem.pku.edu.cn/page/liy/
E-mail: yanli@pku.edu.cn

Separation of metal/semiconductive SWNTs by ATP separation technique and Raman spectroscopy aimed for film-making

Hinano Yamada[1], Tsubasa Shiogai[1], ○Shinzo Suzuki[1]

[1]*Department of Physics, Kyoto Sangyo University, Kyoto 603-8555, Japan*

Aqueous two phase (ATP) separation technique, first developed by C.Y. Khripin et al. [1] have been applied to mono-dispersed sodium cholate (SC) solution (2 wt%) of SWNTs produced by arc-burning of Ni/Y-carbon composite rod in helium atmosphere [2, 3] and mono-dispersed solution of CoMoCAT SWNTs [4], in order to investigate the optimum condition for the separation of metal/semiconductive SWNTs, in combination with Raman spectroscopy and fluorescence spectroscopy.

In this presentation, this combination of ATP separation technique and Raman spectroscopy was further applied to mono-dispersed solution of SWNTs produced by arc-burning technique and others, aimed for getting enough amount of metal/semiconductive SWNTs for thin-film making on the membrane filter after filtration procedure.

Figure 1.

Figure 1 shows an example of thin-film made from PEG fraction after ATP separation from SWNTs generated by arc-burning technique. Its color is ocher, suggesting that the ratio of semiconductive SWNT in PEG solution is higher than that in raw dispersed solution.

[1] C.Y. Khripin et al., *J. Am. Chem. Soc.*, **135**, 6822-6825(2013).

[2] N. Kanazawa et al., The 46th fullerenes-nanotubes-graphene general symposium, 1P-27 (2014).

[3] K. Uratani, et al., The 52nd fullerenes-nanotubes-graphene general symposium, 3P-15 (2017).

[4] T. Watase et al., The 54th fullerenes-nanotubes-graphene general symposium, 1P-20 (2018).

Corresponding Author: S. Suzuki

Tel: +81-75-705-1631, Fax: +81-75-705-1640,

E-mail: suzukish@cc.kyoto-su.ac.jp

Growth of Boron Nitride Layers on Single-Walled Carbon Nanotubes and Graphite

○Hayato Arai[1], Satoshi Yotsumoto[1], Yongjia Zheng[1], Taiki Inoue[1], Rong Xiang[1], Shohei Chiashi[1], Shigeo Maruyama[1,2]

[1] *Department of Mechanical Engineering, The University of Tokyo, Tokyo 113-8656, Japan*
[2] *Energy Nanoengineering Lab, National Institute of Advanced Industrial Science and Technology (AIST), Ibaraki 305-8564, Japan*

Single-walled carbon nanotubes (SWCNTs) have been attracting attention since they were discovered. The excellent properties such as high carrier mobility [1] and high thermal conductivity [2] of SWCNTs make them promising material for nanoelectronics [3], optoelectronics [4], and so on. Hexagonal boron nitride (h-BN) and boron nitride nanotubes (BNNTs) also have been drawing interest as low-dimensional insulating materials. These materials can be used to screen the effects of impurities or substrates on the properties of graphene or SWCNTs [5, 6]. Therefore, synthesis of heterostructures of these materials are highly desired. We developed the facile CVD method to grow BN layers on SWCNT templates using ammonia borane as a precursor [7]. However, the detailed mechanism on nucleation and growth is still unclear.

In this work, we performed comparative study of BN-layer growth on SWCNTs and graphite for realizing higher quality SWCNT-BNNT heterostructures. Suspended SWCNTs and exfoliated graphite were prepared on Si substrates, and BN-layers were grown on them. The morphology of synthesized layers was investigated by SEM, TEM and AFM. As shown in Fig. 1(a), BN-layers were grown on SWCNTs. Figure 1(b) shows BN-layers grown on graphite surface. AFM observation reveals that BN-layers were grown to form pyramidal structures, which indicates the growth was non-self-limiting. Additionally, we compared BN-layers grown with and without hydrogen and found that hydrogen during CVD growth was effective for removal of the impurities which are derived from ammonia borane.

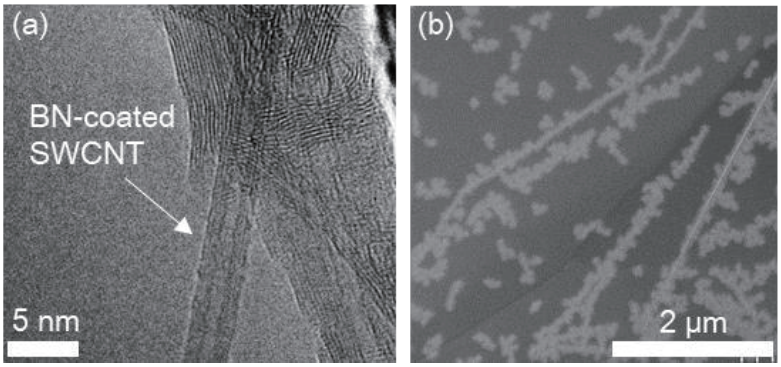

Fig. 1 (a) TEM image of BN-coated SWCNT. (b) SEM image of BN-layers grown on graphite surface.

[1] T. Durkop, *et al.*, *Nano Lett.*, **4**, 35 (2004). [2] M. Fujii, *et al.*, *Phys. Rev. B*, **95**, 65502 (2005). [3] S. J. Tans, *et al.*, *Nature*, **393**, 49 (1998). [4] J. A. Misewich, *et al.*, *Science*, **300**, 783 (2003). [5] C. R. Dean, *et al.*, *Nat. Nanotechnol.*, **5**, 722 (2010). [6] A. Baumgartner, *et al.*, *Appl. Phys. Lett.*, **105**, 23111 (2014). [7] R. Xiang, *et al.*, arXiv:1807.06154.

Corresponding Author: S. Maruyama
Tel: +81-3-5841-6421, Fax: +81-3-5800-6983, E-mail: maruyama@photon.t.u-tokyo.ac.jp

Analysis of oxidation effects on the reactions between cobalt clusters and ethanol by FT-ICR mass spectrometer

○Ryohei Yamada[1], Tomoyasu Inoue[1], Shohei Chiashi[1], Shigeo Maruyama[1,2]

[1] *Department of Mechanical Engineering, The University of Tokyo, Tokyo 113-8656, Japan*
[2] *Energy NanoEnginerring Lab. National Institute of Advanced Industrial Science and Technology (AIST), Ibaraki. 305-8564, Japan*

Single-walled carbon nanotubes (SWCNTs) are studied all over the world because they are expected to be useful materials of devices such as supercapacitor electrode and solar cells. Chemical vapor deposition (CVD) method is one of the most common methods to produce SWCNTs. Although there are a lot of studies about SWCNTs, their growth mechanism is not clear. It is important to understand how SWCNTs grow in order to improve quality of SWCNTs. Alcohol catalytic CVD (ACCVD) method is one of the CVD methods. In ACCVD method, cobalt and ethanol are often used as the catalyst and carbon source, respectively. Moreover, cobalt catalyst may be oxidized because of exposure to atmosphere before SWCNTs growth.

Fourier transform ion cyclotron resonance (FT-ICR) mass spectrometer makes it possible to analyze the chemical reactions between atom clusters and gas molecules. In the past research, reactions of cobalt non-oxide clusters and ethanol is studied and “simple chemisorption” and “dehydrogenated chemisorption” were observed [1]. In this study, reactions between cobalt oxide clusters and ethanol were observed by FT-ICR mass spectrometer.

It was found that cobalt oxide clusters ($Co_xO_y^+$) showed different reaction depending on both x and y. When $Co_{13}O_2^+$ cluster and ethanol reacted, “simple chemisorption” or “dehydrogenated chemisorption” occurred as shown in Fig. 1(a). This reaction is the same as the reaction of cobalt non-oxide clusters. On the other hand, H_2 adsorption and C_2H_4 adsorption mainly occurred in the reaction of $Co_{13}O_{16}^+$ cluster as shown in Fig. 1(b). In summary, ratio of oxygen affects reactivity of cobalt oxide clusters. When oxygen-rich clusters reacted with ethanol, H_2 adsorption is likely to occur. When oxygen-poor clusters reacted with ethanol, “simple chemisorption” and “dehydrogenated chemisorption” occurred. Moreover, C_2H_4 adsorption occurred in the reaction of most of cobalt oxide clusters.

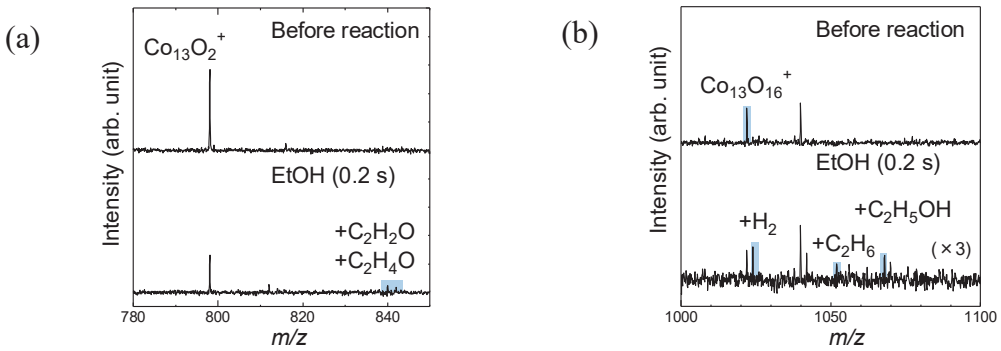

Fig. 1 Spectra of $Co_{13}O_2^+$ (a) and $Co_{13}O_{16}^+$ (b) cluster and products resulted from ethanol reaction.

[1] S. Inoue *et al*. *Jpn. J. Appl. Phys.*, **47-4**, 1931-1936 (2008).

Corresponding Author: S. Maruyama Tel: +81-3-5841-6421, Fax: +81-3-5841-6983,
Web: http://www.photon.t.u-tokyo.ac.jp/index-j.html E-mail: maruyama@photon.t.u-tokyo.ac.jp

The Enhancement of the Electric Field around the Metallic Cylindrical Tube

○Yuan Tian, Fenda Rizky Pratama, Muhammad Shoufie Ukhtary, Riichiro Saito

Department of Physics, Graduate School of Science, Tohoku University,

Sendai 980-8578, Japan

Electric field properties around nanotube and nanowire has become a point of interest in the field of plasmonic science and tip enhanced Raman spectroscopy(TERS), in which the tip can be modelled as a nanowire [1]. There are lots of researches on the near field excitation around different kinds of nanowire (NW) and nanotube (NT). However, most of the researches conducted about near-field excitation of NW and NT focus on the situation of a plasmon excited by an incoming light that was linearly polarized in parallel to NW&NT's axial direction, in which situation would excite plasmon that propagates in parallel to axial direction [2,3]. It is important to investigate the behavior of radial and tangential component of the electric field, which could excite a plasmonic resonance mode that propagates radically around the surface of NW/NT [4]. This kind of plasmonic resonance might play some role in electric field enhancement and enhanced Raman intensity.

In this work, we investigate the near field excitation around a metallic NW by solving the Maxwell equations. We are mainly interested in the radial component of the TM mode. We solve possible frequency of the radial TM mode, which was restricted by boundary conditions at surface of the nanowire. A relationship between the mode frequency and the diameter is plotted in Fig. 1. We then study the near field excitation when an incident light was introduced (Fig.2). By changing the diameter of the cylinder and the frequency of the incident light, we investigate the enhancement of the electric field surrounding the cylinder due to the excitation of the TM mode.

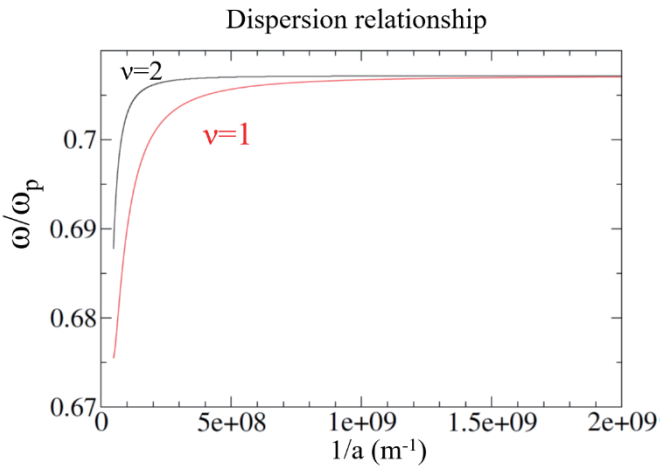

Figure.1 Dispersion relation of surface plamon frequency ω as the function of 1/a, where a is the radius of NW, ν is the frequency mode, and ω_p is plasma frequency.

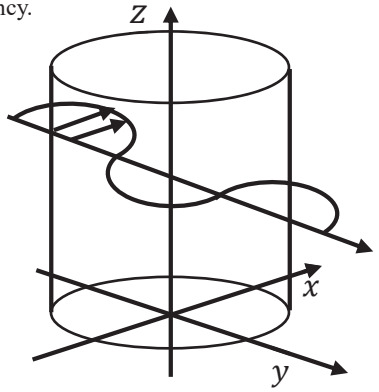

Figure.2 An incident light linearly polarized perpendicular to axial direction of NW.

Reference:
[1] Alexander S. McLeod *et.al.*, Phys. Rev. B 90, 085136 (2014).
[2] Daksh Agarwal *et.al.*, Nano Lett., 17 (3), pp 1839–1845 (2017).
[3] Pan Deng *et.al.*, Chinese Phys. B 22 097305 (2013).
[4] Ken-ichi Sasaki *et.al.*, Appl. Phys. Lett. 108, 163109 (2016).

1P-25

Effect of water on NO adsorption of ACFs

◯Y.Hikage[1], S.Nishijima[1], K.Takai[1,2]

[1]*Graduate school of Science and Engineering, Hosei University, Tokyo 184-8584, Japan*
[2]*Department of Chemical Science and Technology, Hosei University, Tokyo 184-8584, Japan*

NO_x are one of the harmful chemical species causing air pollution, where NO molecule is major species in the vicinity of the source of pollution. Elimination of NO_x diluted in huge volume of air, adsorption by activated carbon fibers (ACFs) is a promising strategy [1]. However, the details mechanism of NO_x adsorption has been not well known yet. One of the reason making the phenomena complexed is the presence of a lot of water vapor in the actual atmosphere. In microscopic view point, ACFs consists of 3D random network of nanographenes having localized spins. Thus, spin magnetism is good prove to investigate the adsorption phenomena of NO molecule having spin moment (S=1/2) into ACFs. In this study, adsorption properties and chemical reactivity of NO in ACFs is investigated in terms of spin magnetism.

Activated Carbon Fibers (FR-20, Kuraray) of 0.5 mg was vacuum-heated at 473 K for 30 min at 2.7×10^{-3} Pa, followed by introducing water vapor to ACFs at 2.5 kPa for 30 minutes. After that, NO gas introduction into water-introduced ACFs at a partial pressure of 2 kPa and evacuation down to 2.7×10^{-3} Pa was repeated each ca. 10 hrs. The spin magnetism in each step evaluated by a ESR spectrometer (JEOL FA-300) at room temperature.

Fig.1 shows the time evolution the ESR linewidth (ΔH_{pp}) and the peak-integrated area (I) NO-adsorbed ACFs without water introduction. Both the ΔH_{pp} and I decreases when evacuation of ACFs and are recovered by NO-introduction again. This is atributted to the dipolar field of NO and its chemical reactions with the edge of nanographen [2]. Fig.2 shows the changes in ΔH_{pp} and I after water adsorption (w) and NO introduction (w-NO) and evacuation (w-NO-VAC) from those for vacuum-heated for ACFs (HT). Irrespective to the presence of water, the ΔH_{pp} and I shows similar behavior after water / NO introduction and their evacuation. This is attributed that NO is hardly soluble in water in contrast to its oxidized form; NO_2. The nanographen edge is known to oxidize NO but it is prevented due covering with water.

[1] T. Shimohara et al, J. Jpn. Soc. Atmospheric Env., 2013, 48, 65-73.

[2] S. Nishijima etal FNTG (2016)

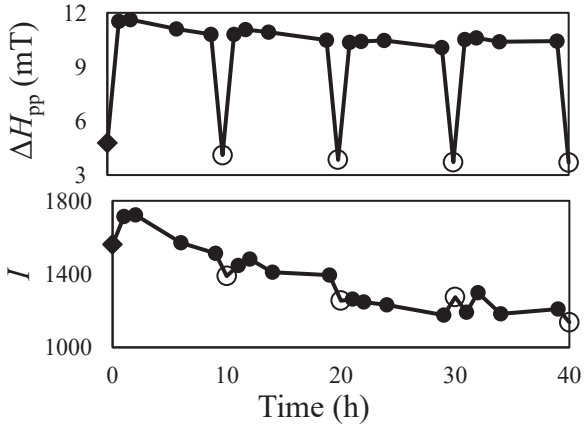

Fig.1 Time dependence of ΔH_{pp} and I for NO adsorbed (●) and desorbed (○) ACFs

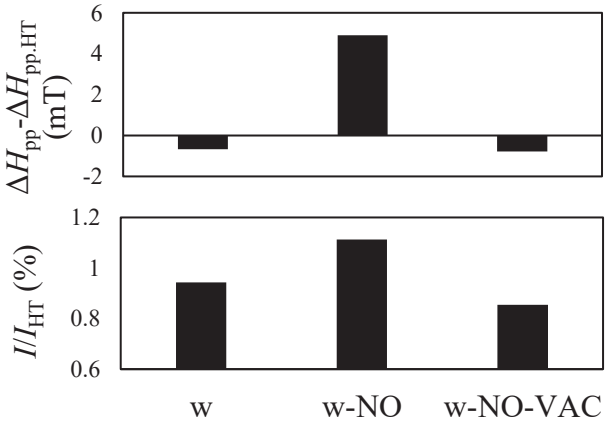

Fig.2 Changes in ΔH_{pp} and I for w, w-NO, w-NO-VAC from those of HT.

Corresponding Author: Kazuyuki Takai
Tel: +81-42-387-6138, Fax: +81-42-387-7002

Van der Waals Epitaxy of Gallium Nitride on Graphene

Ukyo Ooe, Shinichiro Mouri, Yasushi Nanishi, Tsutomu Araki

Department of Electrical and Electronic Engineering, Ritsumeikan University, Kusatsu, Shiga 525–8577, Japan

Atomically thin layered materials are promising materials for future electronic and optical and electronic devices [1]. On the other hand, gallium nitride (GaN) is known as a useful material as the component of light emitting device and one of the hopeful candidates of power conversion semiconductor device at high frequency region. Integration of these layered materials on GaN could further enlarge the functionality of these devices. To progress this issue, the challenge to grow high quality film of GaN on layered materials by van der Waals epitaxy [2] is required. Here, we demonstrated that metal covered van der Waals epitaxy, which is the repetition of Ga and nitrogen-rich supply, was effective to obtain GaN thin film on graphene.

Figure 1 (a) shows the SEM image of the GaN grown on the graphene supported on SiO_2/Si substrate by ordinal MBE growth procedure, the simultaneous supply of Ga and nitrogen plasma. The nanoscale small crystals of GaN with random orientation were obtained. The impact of nitrogen plasma introduced defects on graphene which might work as nucleation centers for these misoriented nanocrystals. Figure 1 (b) shows the SEM image of the GaN grown on the graphene supported on SiO_2/Si substrate by metal covered van der Waals epitaxy. It is obtained nearly continuous film of GaN but a lot of small grains were still remained on the surface. Initial coverage of gallium on graphene prevents the nitrogen plasma damage on graphene which could reduce the misoriented nucleation resulting in the film growth. The substrate under the graphene might be also important to improve the film quality. Figure 1 (c) shows the SEM image of the GaN grown on the graphene supported on GaN template by metal covered van der Waals epitaxy. The number of small grains were reduced, and relatively flat film were obtained. This could be caused by the remote homoepitaxy [3] which is the epitaxial growth using the potential of substrates under the graphene.

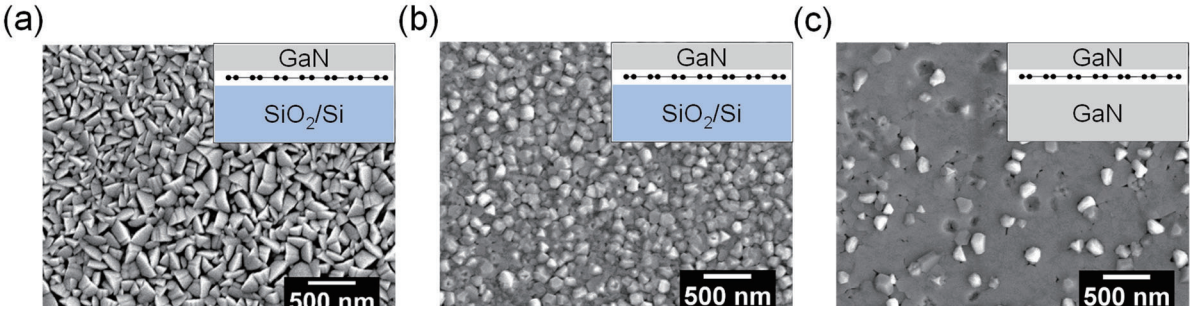

Fig. 1 (a) SEM image of GaN crystals grown on graphene/SiO_2/Si by ordinal MBE growth. (b) SEM image of GaN crystals grown on graphene/SiO_2/Si by metal covered van der Walls epitaxy. (c) SEM image of GaN crystals grown on graphene/GaN template by metal covered van der Walls epitaxy.

[1] Q. H. Wang *et al.*, *Nat. Nanotechnol.* **7**, 699 (2012).
[2] A. Koma, J. Cryst. Growth 201, 236 (1999).
[3] Y. Kim *et al.*, Nature **544**, 7650 (2017).
Corresponding Author: S. Mouri
Tel:+81-77-561-2884
E-mail; iguchan@fc.ritsumei.ac.jp

Tuning structure and electron transport properties of Graphene by chemical modification using Ion-beam irradiation

○Kosuke Nakamura[1], Hiroki Yoshimoto[2], Tomoaki Nishimura[3], Kazuyuki Takai [1, 2, 3]

[1] *Graduate School of Science and Engineering, Hosei University, Tokyo 184-8584, Japan*
[2] *Faculty of Bioscience and Applied Chemistry, Hosei University, Tokyo 184-8584, Japan*
[3] *Research Center of Ion Beam Technology, Hosei University, Tokyo 184-8584, Japan*

Irradiation of ion-beam is one of the interesting strategy for chemical modification of graphene to tune its structure and electronic properties. In this study, we attempted to modify graphene by irradiating Au^+ ion directly to graphene (200 keV, 10^{13} - 10^{14} / cm^2). Irradiated ion would penetrate through bare graphene on the substrate, so a NaCl thin-film sacrificial layer was fabricated in order to distribute ions around graphene position [1]. The ion-modified graphene after removing the sacrificial layer was evaluated by Raman spectroscopy (LabRAM HR), Rutherford Backscattering Spectrometry (RBS), and electric conductivity measurement.

Raman spectroscopy of Au^+ irradiated graphene with NaCl thin-film sacrificial layer, shows clear G band near 1580 cm^{-1}, indicating honeycomb lattice structure of graphene remained even after irradiation (**Fig. 1**). A significant Raman D band (1340 cm^{-1}) and D' band intensity (1620 cm^{-1}) suggests a successful introduction of defects causing intervalley scattering and intravalley scattering after irradiation, respectively.

Field effect transistor (FET) of graphene was fabricated after irradiation, and the mobility of irradiated graphene was measured by applying gate voltage sweep range (**Fig. 2**). Irradiated graphene showed hole-doped nature, and the mobility decreased down to 57 cm^2 / Vs from 87 cm^2 / Vs, being responsible for the larger scattering by introduced ions and defects by the irradiation. We will also present the effect of irradiation of I^-, which has opposite sign of the charge compared with Au^+ on graphene on our poster.

This project was supported by JSPS and RFBR under the Japan - Russia Research Cooperative Program.

[1] K. Nakamura, et al, FNTG symposium (2018)

Corresponding Author: Kazuyuki Takai
Tel: +81-42-387-6138, Fax: +81-42-387-7002, E-mail: takai@hosei.ac.jp

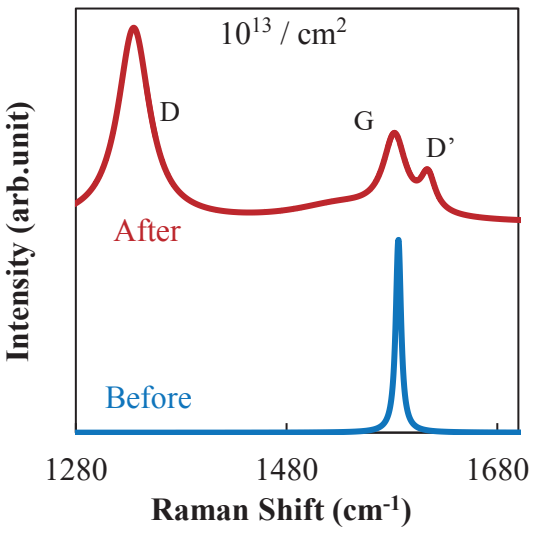

Fig. 1 Raman spectra of graphene before / after irradiation

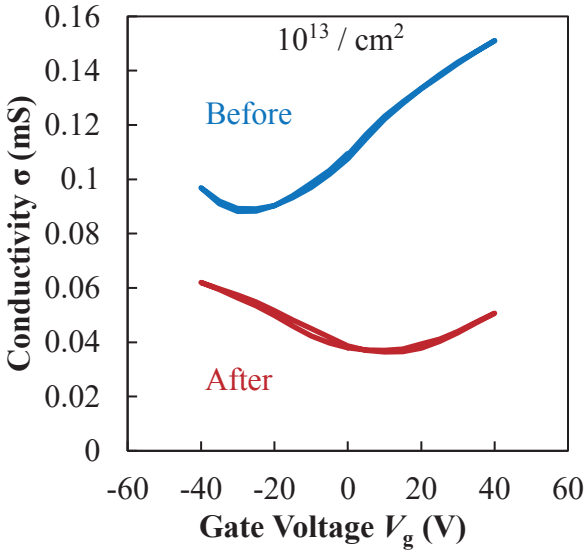

Fig. 2 Conductivity of graphene before / after irradiation

Probing phonon energy redistribution by MD dynamics of transient dispersion relation at graphene nanoribbon

○Tatiana Zolotoukhina[1], Yukie Noda [1]

[1] *Department of Mechanical Engineering, University of Toyama, Toyama 930-8555, Japan*

Study of plasmons in graphene, hexagonal BN, MoS_2 and another monolayer atomic crystal reveals the production of hybridized plasmon-phonon modes [1]. In graphene/h-BN metastructures, coherent oscillations of the electron density in graphene and the atomic vibrations in h-BN produce hybridized plasmon-phonon modes. Experimentally, acoustic phonons in monolayer and nanowire structures are probed by nanophotonic methods [2] that will be developed to distinguish modulated or hybridized modes.

On the time-scale of electron energy transfer to phonons within 500 fs, the propagation of phonons within a few ps can be considered as a guided by interaction process. However, phonon dispersion relation in thermal energy transfer is considered primarily as an equilibrium process. In plasmonic applications, such approach can't resolve coupling of electronic excitation with phonons in dynamics. In order to be able to distinguish dynamic changes in phonon dispersion relations, we test an approach where transient calculations in molecular dynamics (MD) method estimate dispersion relation matrix D(ω,k) variation. The sequence of transient values of consequent D(ω,k) matrices are collected with fixed delay during thermal pulse propagation in the graphene sample. To extract changes in phonon mode dispersion functions ω(k), we consider the distribution of each mode's maxima on the series of D(ω,k) matrix. The difference in the matrices due to maxima location and amplitude can be evaluated by differentiation in k-space that will produce an exact (ω,k) location of maxima in the dynamics of the phonons. Previous calculation of single D(ω,k) for different temperatures in graphene nanoribbon has shown energy redistribution between maxima inside a single mode dispersion function ω(k). The mode propagation changes energy distribution between phonon modes in the graphene sample. The MD method with REBO potential for graphene nanoribbon that was thermally excited in a small area at one end has been tested. The energy distribution between basic and transient phonon modes in the 1st Brillouin zone in Γ M direction is calculated, see Fig. 1. We expect to see in the ω(k) maxima changes related to mode propagation and the intensity-dependent mode cut-off on the transient dispersion matrix will serve to separate different amplitudes.

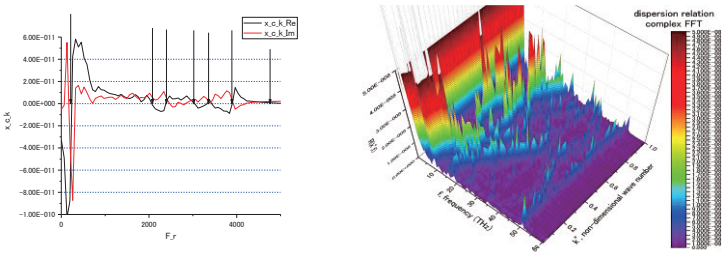

Fig.1 The k-space derivative (left) locales maxima (ω,k) with 0 values (across single k) for the transient dispersion matrix D(ω,k) in the Γ M direction (right),

[1] A. Politano and G. Chiarello, Nanoscale, 2014, DOI: 10.1039/c4nr03143a

[2] P.-A. Mante, L. Belliard and B. Perrin, Nanophotonics 2018; 7(11): 1759–1780

[3] T. Zolotoukhina, K. Kumaki, K. Tawara, Abstracts of the 54th FNTG General Symposium 2018.

Corresponding Author: T. Zolotoukhina

Tel: +81-76-445-6739, Fax: +81-76-445-6739,

E-mail: zolotu@eng.u-toyama.ac.jp

Asymmetric field screening of h-BN for carrier accumulation in graphene

Susumu Okada

Graduate School of Pure and Applied Sciences, University of Tsukuba, Tsukuba 305-8571, Japan

A single sheet or thin films of h-BN are regarded as the supporting substrate or the insulating layer for other two-dimensional materials, such as graphene and transitionmetal dichalcogenides, owing to their atomically flat surfaces and insulating electronic property. Indeed, graphene adsorbed on h-BN exhibits remarkable transport properties compared with that on surfaces of bulk insulating materials. In this work, we aim to explore the field screening ability of h-BN thin films for graphene in the field effect transistor (FET) structure to give the guiding principle for designing the FET using h-BN as an insulating layer for the gate electric field. Using the density functional theory combined with the effective screening medium method, we found that h-BN thin films act as insulating layers for carrier accumulation in graphene under the low carrier concentrations. In contrast, under high carrier concentrations, hole is spilled over the outermost h-BN layer while the most of the electron is still accommodated in graphene, indicating their asymmetric field screening ability for carrier injection in graphene.

Corresponding Author: S. Okada
Tel: +81-29-8535921
E-mail: sokada@comas.frsc.tsukuba.ac.jp

Preparation of Atomically Thin $NbSe_2$ Layers by Selenizing Nb Films

○Chisato Anndo, Yusuke Nakanishi, Hong En Lim, Yutaka Maniwa, and Yasumitsu Miyata

Department of Physics, Tokyo Metropolitan University, Hachioji, 192-0397, Japan

Atomically thin $NbSe_2$ can serve as the models for exploring superconductivity in the two-dimensional (2D) limit [1], as well as future ohmic electrodes [2]. To date, 2D $NbSe_2$ has been fabricated by exfoliation, molecular beam epitaxial [3], and chemical vapor deposition. On the other hand, selenization of Nb precursors is also a promising technique for the synthesis of thin-layer $NbSe_2$ films. This approach enables the controlled growth of $NbSe_2$ films at desired position, allowing for the design of functional devices [4]. However, the selenization strategy for atomically thin $NbSe_2$ films still remains unexplored.

In this work, we studied the growth of 2D $NbSe_2$ films by selenizing Nb films. Thin Nb films (<20 nm) were first prepared on Si wafers by electron beam deposition. Then, the Nb films were exposed to selenium vapor at high temperatures (~800 °C). Figure 1 shows Raman spectra of the samples obtained by selenizing the deposited Nb films with various thicknesses. Raman spectra of these samples show two prominent peaks around 230~250 cm^{-1}, which can be attributed to E^1_{2g} and A_{1g} peaks of $NbSe_2$. The peak separations increase as the thickness of precursor Nb films is reduced, suggesting that the layer numbers of $NbSe_2$ films can be controlled by the initial film thickness. Detailed discussion will be presented in the conference.

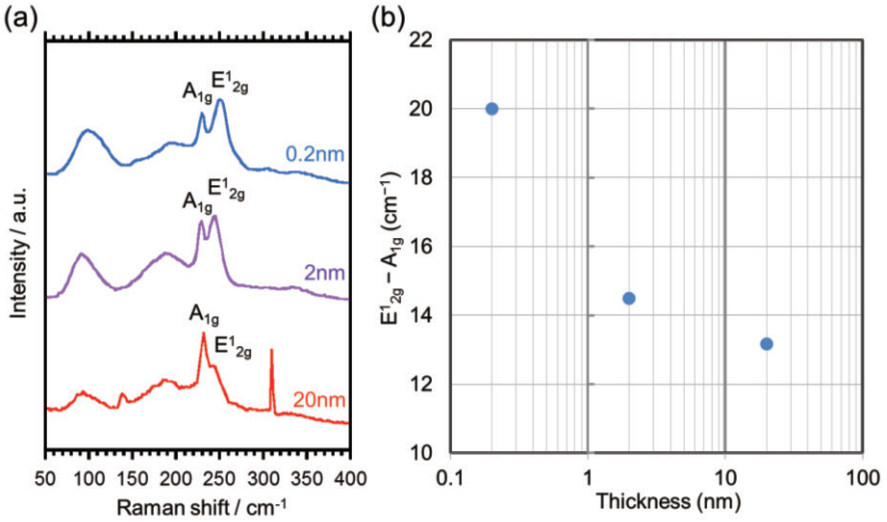

Fig. 1 (a) Raman spectra of thin-layer $NbSe_2$ fabricated by selenizing Nb films with various thicknesses. (b) The peak separation between E^1_{2g} and A_{1g} modes depending on the film thickness.

[1] N. E. Staley *et al. Phys. Rev. B.* **80**, 184505 (2009).
[2] A. R. Kim, *et al. Nano Lett.* **16**, 1890-1895 (2016)
[3] T. Hotta, *et al. Appl. Phys. Lett.* **109**, 133101 (2016)
[4] Y. Kim, *et al. Nano Lett.* **16**, 5928-5933 (2016)

Corresponding Author: Y. Nakanishi, Y. Miyata,
Tel: 042-677-2508, E-mail: naka24ysk@tmu.ac.jp, ymiyata@tmu.ac.jp

Analysis of plane antenna which radiates circular polarized light

○Masato Maruoka[1], Taisei Maeda[2], Riichiro Saito [1]

[1] *Department of Physics, Tohoku University, Sendai 980-8578, Japan*
[2] *National Institute of Technology, Sendai College 989-3128, Japan*

When linearly polarized light comes into the chiral shape antenna such as the capital S-shape, the induced current partially radiates left or right-handed circularly polarized light depending on the position of the antenna [1]. However, the physical origin of circularly polarized light is not clear even though some simulation was performed. Previously, our group showed that doped graphene absorbs almost 100% of the incident electromagnetic wave in GHz and THz frequency [2]. Combining both the stories, graphene could be used for an atomic layer antenna that strongly absorbs and radiates THz circularly polarized light.

In order to discuss the optical response of circularly polarized light, we use the so-called MEEP [3] which solve the Maxwell equation numerically within the finite-difference-time-domain (FDTD) method. We obtain the S-shaped antenna radiates circularly polarized light depending on the position of the antenna numerically. Moreover, not only S-shaped antenna but rectangular antenna can radiate circularly polarized light when the incident light is linearly polarized oblique to the antenna. In both case, rotating positive and negative charge can be seen where circularly polarized light comes out.

We will also discuss the physical interpretation why circularly polarized light is radiated. We expect the circularly polarized light originates from the current which the direction of flow is rotating. Regarding the antenna as RLC circuit, the resistance, inductance, and capacitance depend on the thickness, length, and width of the antenna [4]. The phase difference of current which flow at longitudinal direction and transverse direction appear when there is the anisotropy of resistance, inductance, and capacitance.

[1] T. Narushima and H. Okamoto, J. Phys. Chem. C **2013**, 117 (45).
[2] M. S. Ukhtary et al. APEX, **8**, 055102 (2015).
[3] https://meep.readthedocs.io/en/latest/
[4] C. P. Huang, X. G. Yin, H. Huang, and Y. Y. Zhu, Opt. Express **17**(8), 6407–6413 (2009).

Corresponding Author: Masato Maruoka
Tel: +81-22-795-6442, Fax: +81-22-795-6447,
E-mail: maru@flex.phys.tohoku.ac.jp

Exciton Diffusion in hBN-encapsulated Monolayer TMDs

○Takato Hotta [1], Shohei Higuchi[1], Yosuke Uchiyama[1], Keiji Ueno [2], Kenji Watanabe [3], Takashi Taniguchi [3], Hisanori Shinohara [1] and Ryo Kitaura [1]

[1] *Department of Chemistry, & Institute for Advanced Research, Nagoya University, Nagoya 464-8602, Japan*
[2] *Department of Chemistry, Saitama University, Saitama 338-8570, Japan*
[3] *National Institute of Materials Science, Tsukuba 305-0044, Japan*

Optical responses from low-dimensional systems, such as transition metal dichalcogenides (TMDs), are dominated by the excitonic effect even at room temperature due to the strong coulomb interaction between electrons and holes. In response to optical excitation of TMDs, a series of responses, including creation, diffusion and radiative recombination of excitons, occurs in the optical excitation of TMDs, and the exciton diffusion is one of the important processes for understanding optical properties of TMDs. However, to investigate intrinsic exciton diffusion in TMDs, extrinsic effects, such as substrate effects, need to be suppressed. In this work, we have conducted systematic investigations of exciton diffusion in hBN-encapsulated monolayer TMDs.

We have fabricated high-quality hBN-encapsulated TMDs with (1) the all-dry transfer method and (2) the dry-transfer combined with nano-squeeze method [1]. In the nano-squeeze method, contaminants between hBN layers and a TMD are removed through sweeping the surface of samples by AFM tip in the contact mode. Fig. 1 shows an optical microscope image of the fabricated hBN-encapsulated monolayer MoS_2. The monolayer MoS_2 was grown directly onto a hBN substrate, and a hBN flake was transferred on it to form the hBN-encapsulated structure. The Red flame in Fig.1 corresponds to the region treated with the nano-squeeze method, where no bubbles can be seen. Fig. 2 (a) and (b) show an image of excited laser spot and a PL image of excitonic emission of hBN/MoS_2/hBN, respectively. As clearly seen in the line profile shown in Fig. 2 (c), the PL image is larger than the image of laser, which clearly demonstrates the diffusion of excitons. The details of sample preparation and PL measurement will be discussed in this presentation.

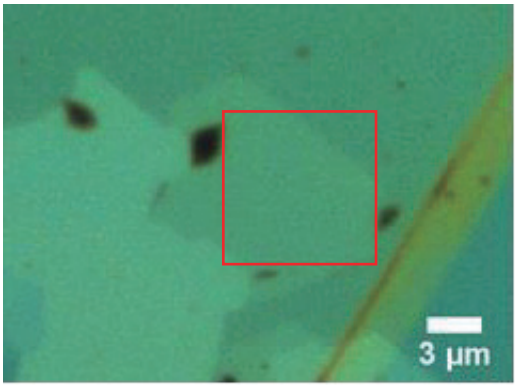

Fig. 1 An optical microscope image of the fabricated hBN/MoS_2/hBN structure. Red flame corresponds to a region cleaned with AFM.

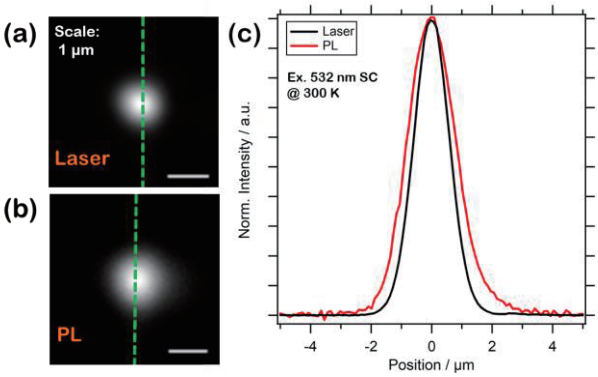

Fig. 2 (a) and (b) Images of excitation laser (532 nm) spot and PL of excitonic emission (1.88 eV) at 300 K. (c) line profiles of laser (black) and PL (red) intensity along green lines in Fig 2 (a) and (b)

[1] M. R. Rosenberger, et. al., ACS Appl. Mater. Interfaces 10, 10379-10387 (2018).

Corresponding Author: R. Kitaura Tel: +81-52-789-3660, Fax: +81-52-747-6442,
E-mail: r.kitaura@nagoya-u.jp

Growth of TMDs with Cold-walled Metal-Organic Chemical Vaper Deposition

○Satoshi Iida, Takato Hotta, Hisanori Shinohara, and Ryo Kitaura

Department of Chemistry, Nagoya University, Nagoya 464-8602, Japan

¥Since the discovery of graphene, two-dimensional (2D) materials have been attracting considerable attention. Recent research on 2D heterostructures, including heterostacks and heterojunctions, has clearly demonstrated the possibility on emergence of novel properties in these heterostructures[1]. To fully explore the possibility, development of a highly-controllable crystal growth method is indispensable. For this purpose, we have focused on Metal-Organic Chemical Vaper deposition (MOCVD), in particular, a cold-wall type MOCVD. In this presentation, in addition to development of a cold-wall MOCVD setup, results on MOCVD growth of a transition metal dichalcogenide, WS_2, is presented.

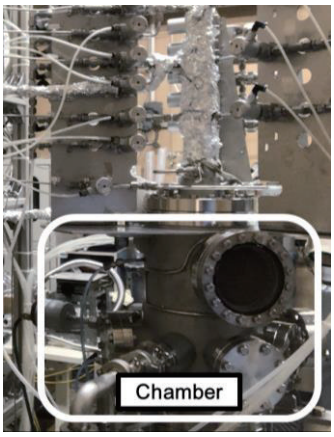

Figure 1 shows a photograph of the cold-wall MOCVD setup developed. This is a vertical type chamber, and metal organic sources are supplied from top to down through the shower head to a substrate placed on PBN heater. We used $(t\text{-Bu}=)_2W(NMe_2)_2$ and Et_2S as W and S precursors, respectively, and reaction temperature is typically 700 ~ 800 ℃. Figure. 2(a) and (b) show a typical optical image of WS_2 grown on SiO_2/Si substrate without NaCl-assist and with NaCl-assist, respectively. We have successfully reduced nucleation density to form triangular WS_2 crystals on SiO_2. We also found that it is possible to reduce nucleation density without NaCl assist through precise control of growth condition.

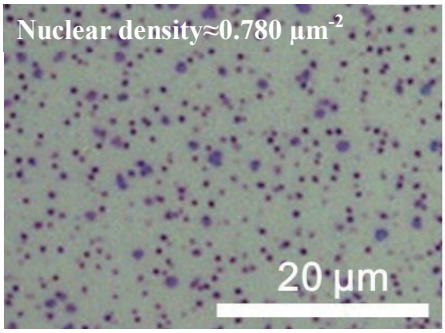

Fig. 2(a) Optical image of WS_2 grown on SiO_2/Si substrate.

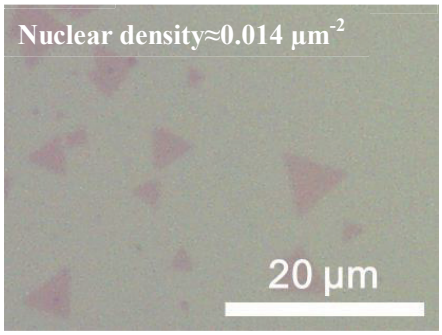

Fig. 2(b) Optical image of WS_2 grown on SiO_2/Si substrate using NaCl assist.

[1] A. K. Geim. *et al.,* Nature **499**, 419-425 (2013).

Corresponding Author: R.Kitaura Tel: +81-52-789-2477, Fax: +81-52-747-6442

E-mail: r.kitaura@nagoya-u.jp

In-Plane Heterostructures of Twisted Bilayer Transition Metal Dichalcogenides

○ Hong En Lim[1], Zheng Liu[2], Takahiko Endo[1], Kana Kojima[1], Yusuke Nakanishi[1], Yutaka Maniwa[1], Yasumitsu Miyata[1]

[1]Department of Physics, Tokyo Metropolitan University, Hachioji, Tokyo 192-0397, Japan
[2]Inorganic Functional Materials Research Institute, National Institute of Advanced Industrial Science and Technology (AIST), Nagoya, Aichi 463-8560, Japan

In-plane heterostructures of transition metal dichalcogenides (TMDCs) provide a novel platform for the study of one-dimensional confined electron system at an atomically thin interface [1]. Besides using the combination of different materials such as MoS_2 and WSe_2, in-plane heterostructures can also be formed with only a single component, giving the chemically homogenous electronic heterostructures [2, 3]. As the band structure of TMDCs is governed also by the layer thickness and/or the stacking configuration [4, 5], one could foresee the generation of such hybrid structures through the manipulation of these factors.

Herein, we report the synthesis of angle-modulated, in-plane bilayer TMDCs heterostructures. (Fig. 1). Monolayer crystals of WSe_2 was fabricated on top of its single-layer-thick, polycrystalline film, generating the bilayer domains with regions of different stacking configurations. Raman intensity map displays an inhomogenous coupling interactions within bilayer structure (Fig. 1b), which is due to the different interlayer distance present for each stacking orientations as they undergo dissimilar degree of steric effect [5]. Region of higher crystal symmetry, the AA' or AB stacking, exhibits stronger B^1_{2g} signals with lowered PL energy and weakened PL intensity (Fig. 1c, d). The unequal electronic structures created forms the heterojunction with chemically homogenous components, which would be useful to create a functional 1D interface.

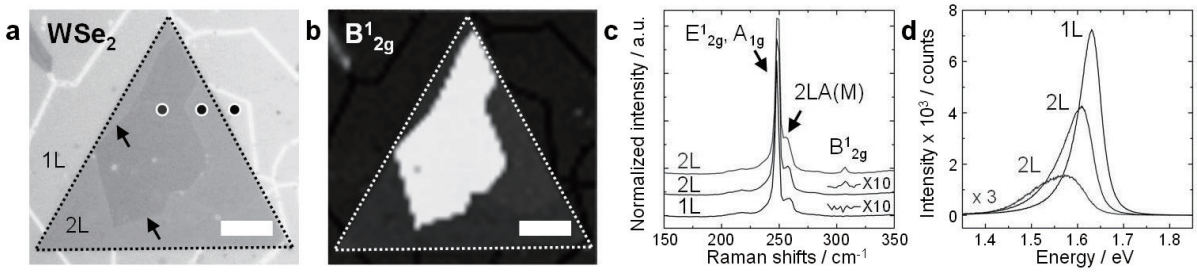

Fig.1 (a) Optical image of the bilayer WSe_2 heterostructure synthesized. Dotted line outlines the bilayer domain. Grain boundaries are marked with arrows. (b) Raman intensity map of the B^1_{2g} peak, which clearly indicates the presence of different coupling interactions within the bilayer domain. (c) Raman and (d) PL spectra taken at spots indicated in (a). Scale bars are 10 μm.

[1] K. Kobayashi *et al.* Sci. Rep **6**, 31223 (2016).
[2] G. Eda *et al.* ACS Nano **6**, 7311-17 (2012).
[3] S. Cho *et al.* Science **349**, 625-628 (2015).
[4] W. Zhao *et al.* ACS Nano **7**, 791-797 (2013).
[5] K. Liu *et al.* Nat. Commun. **5**, 4966 (2014).

Corresponding Authors: H. E. Lim, Y. Miyata
E-mail: lim@tmu.ac.jp, miyata-yasumitsu@tmu.ac.jp
Tel: +81-42-677-2508

UV-Polarizer Film of Aligned Polyyne Molecules

Ryoske Sata[1], Hal Suzuki[1], Y. Morisawa[1], M. Hatanaka[2], ○Tomonari Wakabayashi[1]

[1] *Department of Chemistry, Kindai University, Higashi-Osaka 577-8502, Japan*
[2] *Institute for Research Initiatives, Nara Institute of Science and Technology (NAIST), Ikoma 630-0192, Japan, and PRESTO, JST, Kawaguchi 332-0012, Japan*

Electronic absorption bands of conjugated linear carbon chain molecules, namely polyynes $H(C{\equiv}C)_nH$ (n = 5-7), are exploited to devise light-polarizing films applicable to the UV. Laser ablated polyynes are separated in size and dispersed in a film of polyvinyl alcohol (PVA), which is stretched to align the trapped linear polyyne molecules inside. As a nature of the structural anisotropy, transition dipole of the UV absorption for polyyne molecules is in parallel with the molecular axis and the absorption occurs only for the electromagnetic wave having the amplitude of its electric vector along the molecular axis. Aligned and fixed orientationally in the solid PVA film, polyyne molecules act as selective absorbers of one of the polarization components of incident light at particular wavelength. Using a light source of linearly polarized UV light, whose direction of polarization is rotatable, angular dependence of the absorption intensity is investigated for the stretched PVA film containing aligned polyyne molecules and analyzed in terms of an order parameter in the theory of linear dichroism.

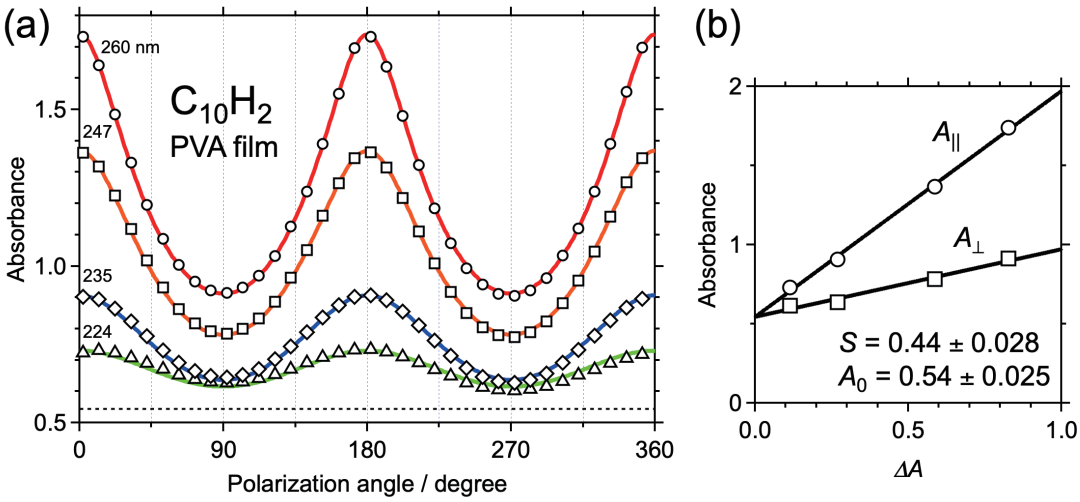

Figure. (a) Absorption intensity of linearly polarized light plotted as a function of the angle between the direction of polarization and the direction of stretching of the PVA film. Four curves correspond to absorption bands of $C_{10}H_2$ at λ = 260, 247, 235, and 224 nm, which are fitted by the equation, $A(\lambda,\theta) = \alpha - \log [1 - \{\beta / (1 + \beta)\}(1 + 3 \cos 2\theta)]$. (b) The line fitting of the maximum or minimum absorption intensity, namely $A_{\parallel}$ or $A_{\perp}$, for the four curves in (a) provides the common offset, A_0, and the order parameter, S.

Corresponding Author: T. Wakabayashi
Tel: +81-6-4307-3408, Fax: +81-6-6723-2721,
E-mail: wakaba@chem.kindai.ac.jp

Laser Ablated Octatetrayne Derivative $C_{12}H_8$

Nozomu Kitamura[1], Ayato Osawa[1], Ryoske Sata[1], Hal Suzuki[1], Yusuke Morisawa[1], Miho Hatanaka[2], ○Tomonari Wakabayashi[1]

[1] *Department of Chemistry, Kindai University, Higashi-Osaka 577-8502, Japan*
[2] *Institute for Research Initiatives, Nara Institute of Science and Technology (NAIST), Ikoma 630-0192, Japan, and PRESTO, JST, Kawaguchi 332-0012, Japan*

Laser ablation of carbon particles in liquid organic solvents produces stable linear carbon chain molecules in abundance [1]. Besides the series of major products, i.e. hydrogen-end-capped polyynes $H(C{\equiv}C)_nH$ (n = 4-8), other series of molecules, namely polyyne derivatives, are known to form efficiently [2]. For selective formation of molecules having a specific length or an end-capping group, it is crucial to understand the formation mechanism of polyyne chains under the experimental condition [3]. We have pursued a series of specific polyyne derivatives, which are identifiable by systematic wavelength shifts in their UV absorption spectra and classified by their appearance in the spectral band shape. In this work, we identified one of those derivatives as an octatetrayne derivative, $R(C{\equiv}C)_4R'$, having the molecular formula of $C_{12}H_8$. The UV-resonance Raman spectra were interpreted by molecular orbital calculations of sixteen structural isomers for the octatetrayne derivative.

The target molecule was formed by laser ablation of graphite particles in liquid hexane, followed by separation using HPLC [4,5]. Figure 1 shows UV absorption spectra of the isolated derivative in hexane. In addition to the strong UV absorption band at 234 nm, peaks are discernible at longer wavelengths with an increment of ~2000 cm^{-1} as finger prints for the polyynic skeleton. The phosphorescence spectrum in solid hexane at 20 K in Figure 2 is peaking at 532 nm in the proximity to the counterpart of $H(C{\equiv}C)_4H$, indicating a polyynic chain of C_8 present in the molecular framework. Knowing the molecular weight of m/z 152 by resonant two-photon ionization mass spectroscopy (R2PI-MS), there remains C_4H_8 having one degree of unsaturation for the rest part of the molecule, R and R'. We will discuss the molecular structure of the octatetrayne derivative in more detail.

[1] M. Tsuji *et al*. Chem. Phys. Lett. **355**, 101 (2002). [2] Y. Wada *et al*. Eur. Phys. J. D **66**, 322 (2012). [3] A. Ramadhan *et al*. Carbon **118**, 680 (2017). [4] T. Wakabayashi *et al*. Chem. Phys. Lett. **433**, 296 (2007). [5] T. Wakabayashi *et al*. Carbon **50**, 47 (2012).

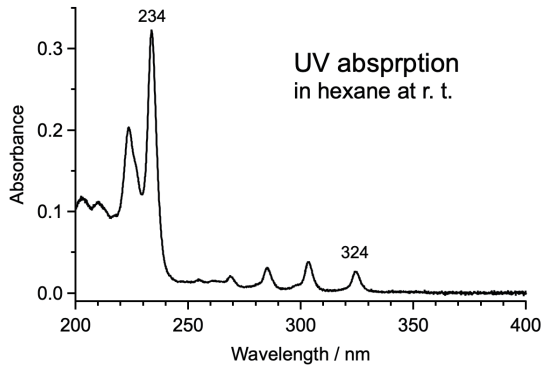

Fig. 1. UV absorption spectra.

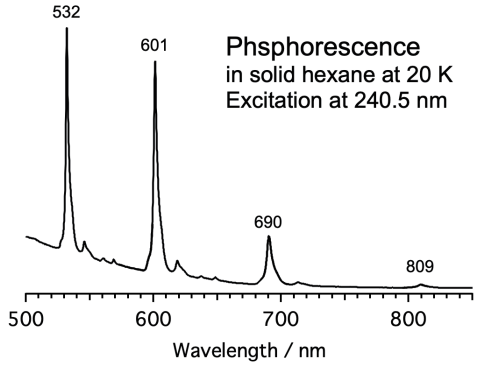

Fig. 2. Phosphorescence spectra.

Corresponding Author: T. Wakabayashi
Tel: +81-6-4307-3408, Fax: +81-6-6723-2721,
E-mail: wakaba@chem.kindai.ac.jp

First order resonant Raman spectra of TaP

○Pang Xiaoqi, Nguyen T. Hung, Ahmad R. T. Nugraha and Riichiro Saito

Department of Physics, Tohoku University, Sendai 980-8578, Japan

TaP is Weyl semimetal which has been inferred experimentally from its bulk electronic band structure determined from ARPES measurements [1]. As a Weyl semimetal, Tap has a great potential for applications, because of its topological nature of Weyl nodes. Thus it would be useful to product the resonant Raman spectra, one of the conventional method to verify the crystal and electronic structure of materials, of TaP. We also need it to understand the optical properties and optimize the crystal structure in the synthesis of TaP for practical applications.

In this work, we will obtain the resonant Raman spectra of Tap theoretically based on first-principles calculation. Raman intensity is proportional to square of the product of two electron-photon matrix elements and an electron-phonon matrix element. We obtain the electron-photon matrix element by Quantum Espresso package [2] and electron-phonon matrix element by modified EPW package [3]. Then, we use our own program to calculate the first order resonant Raman spectra [4]. In Fig 1, we show the refractive index obtained by electron-photon calculation. At last, we will compare the calculation result of resonant Raman spectra with the recent experimental result.

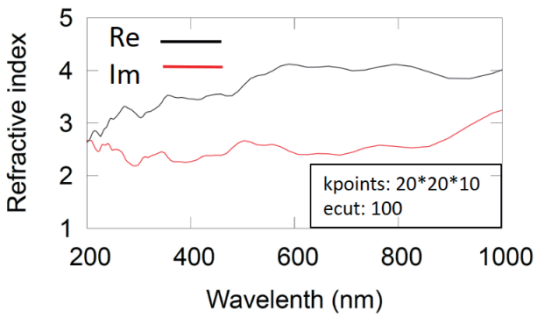

Figure 1: The real part and image part of refractive index of TaP.

[1] L. X. Yang, *et al*., arXiv:1507.00521
[2] P. Giannozzi, *et al*., J. Phys.: Condens. Matter 21, 395502 (2009)
[3] J. Noffsinger, *et al*., Compt. Phys. Commun. 181, 2140 (2010)
[4] Y.Tatsumi, *et al*., Phys. Rev. B 94, 235408 (2016)
Corresponding Author: Pang Xiaoqi
Tel: +81-22-795-6442, Fax: +81-22-795-6447,
E-mail: pang@flex.phys.tohoku.ac.jp

Angle-Dependent Resonant Raman Spectra of LaAlSi

○Tong Wang, Nguyen T. Hung, Ahmad R.T. Nugraha, Riichiro Saito

Department of Physics, Tohoku University, Sendai 980-8578, Japan

Recently, a class of topological materials, so called the Weyl semimetal such as LaAlSi (Fig. 1), have been attracted for the angle-resolved Raman spectroscopy due to their unique electron structure. Thus it would be useful to know resonant Raman spectra for understanding crystal structure and phonon properties.

In this study, we calculate the resonant Raman intensity for Weyl semimetal LaAlSi by considering both electron-photon and electron-phonon interactions. To obtain the Raman tensor, we use our own program [1] combined with the first-principle calculation, in which the electron-photon interaction matrix elements can get from the Quantum–Espresso package [2], and electron-phonon interaction matrix elements can get from EPW package [3]. Our results are consistent with the experimental data, in which we will show the angle- and laser energy-dependent of the Raman intensity.

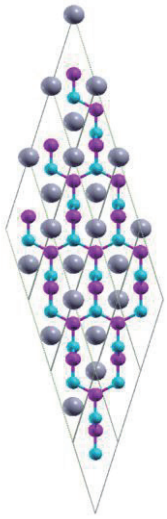

Fig.1 Structure of LaAlSi

[1] Y. Tatsumi, R. Saito, Phys. Rev. B 97, 115407 (2018).

[2] P. Giannozzi, *et al*., J. Phys.: Condens. Matter 21, 395502 (2009)

[3] J. Noffsinger, *et al*., Compt. Phys. Commun. 181, 2140 (2010)

Corresponding Author: Tong Wang
E-mail: wang@flex.phys.tohoku.ac.jp

Epoxide contamination in fullerenol production caused by ambient ozone

Sirikanya Chokaouychai[1,*] , Qi Zhang[1]

[1]*School of Aerospace, Transport and Manufacturing, Cranfield University, Cranfield, MK43 0AL, United Kingdom*

This work reports a pitfall in fullerenol (hydroxylated fullerene) production which should be taken into account when establishing research or production facilities. The work was an unforeseen part of the project on fullerenol production via phase-transfer catalysis [1]. Following laboratory relocation, some of the produced fullerenol showed unusual observation during production, unexpected infrared absorption in addition to fullerenol characteristic absorptions [1,2], and significant change in thermal decomposition behaviour. Analyses of infrared spectra and thermogravimetric data indicated presence of epoxide groups in the product [3], in addition to the desired hydroxyl groups. Empirical formulae derived from thermogravimetric and elemental analyses were also in agreement with the results from infrared and thermogravimetric techniques. Considering frequent uses of laser-based equipment (which generates ozone) in nearby laboratories in the same proximity, it was suggested that ambient ozone might have converted some fullerene (in toluene reservoir) to fullerene epoxide ($C_{60}O$) before the hydroxylation step [4]. Ideally, a $C_{60}O$ molecule should be easily converted to fullerenol with a diol structure, and a two-step reaction mechanism has been proposed for the conversion. Nevertheless, the presence of epoxide groups in the product indicated that some epoxides had not been converted. Explanation has been suggested that polarity of $C_{60}O$ molecules in toluene reservoir might have been key to preventing epoxide groups from being converted to diols. Hydroxylation took place only at accessible regions of the fullerene cages. Epoxide contamination affects fullerenol purity, properties and behaviours, which are critical to its applications. Therefore, it is strongly recommended for fullerenol to be produced under ozone-free environment in order to avoid epoxide contamination in the product.

[1] Li *et al*. J. Chem. Soc., Chem. Commun. **0**, 1784 (1993).
[2] Kokubo *et al*. Nano Res. **4**, 204 (2011).
[3] Goswami *et al*. Thermochim. Acta. **419**, 97 (2004).
[4] Dattani *et al*. J. Colloid Interface Sci. **446**, 24 (2015).

Corresponding Author: S. Chokaouychai*
Tel: +66-2-564-7000 Ext. 6695
E-mail: sirikanya.cho@nanotec.or.th

* Current Affiliation: National Nanotechnology Center, National Science and Technology Development Agency, 111 Innovation Cluster 2 (INC2), Thailand Science Park, Phahonyothin Road, Khlong Nueng, Khlong Luang, Pathum Thani, 12120, Thailand.

Energetics and electronic structure of single walled carbon nanotube encapsulated in boron nitride nanotube

○Kaoru Hisama[1], Susumu Okada[2], Shohei Chiashi[1] and Shigeo Maruyama[1,3]

[1] *Department of Mechanical Engineering, The University of Tokyo, Tokyo 113-8656, Japan*

[2]*Graduate School of Pure and Applied Sciences, University of Tsukuba, Tsukuba 305-8571, Japan*

[3] *Energy NanoEngineering Lab., National Institute of Advanced Industrial Science and Technology (AIST), Ibaraki 305-8564, Japan*

Tubular structures of C or BN allow them to form one-dimensional van der Waals (vdW) heterostructures by coaxially arranging them with appropriate diameter difference. Indeed, a recent experiment demonstrated that a carbon nanotube (CNT) is wrapped with BN nanotube (BNNT) [1] as an ultimate version of the surrounded gate transistor where CNT and BNNT are conducting channel and dielectric, respectively. Because the physical properties of CNT and BNNT are sensitive to their diameter, such one-dimensional vdW hybrids may exhibit interesting variation in their energetics and electronic structures, being different from the simple superpose of each constituent. Thus, in the present work, we aim to provide the energetics and electronic structures of CNT encapsulated in BNNT, using the density functional theory with the local density approximation.

Here, we consider double-walled NT consisting of inner (*n*,0) CNT and outer (*m*,0) BNNT, as the representative structure of the hybrids. The total energy calculation elucidated that the most stable combination of chirality index is *m*=*n*+9 where the interwall spacing is 0.35 nm. Under the optimum combinations, the calculated cohesive energies of the NTs are about 10 meV/atom weakly depending on the tube index and interwall atomic arrangements [Fig. 1(a)]. As for the electronic structure, band gaps of inner CNTs are modulated by forming the hybrid structures depending on the interwall stacking arrangements [Fig. 1(b)].

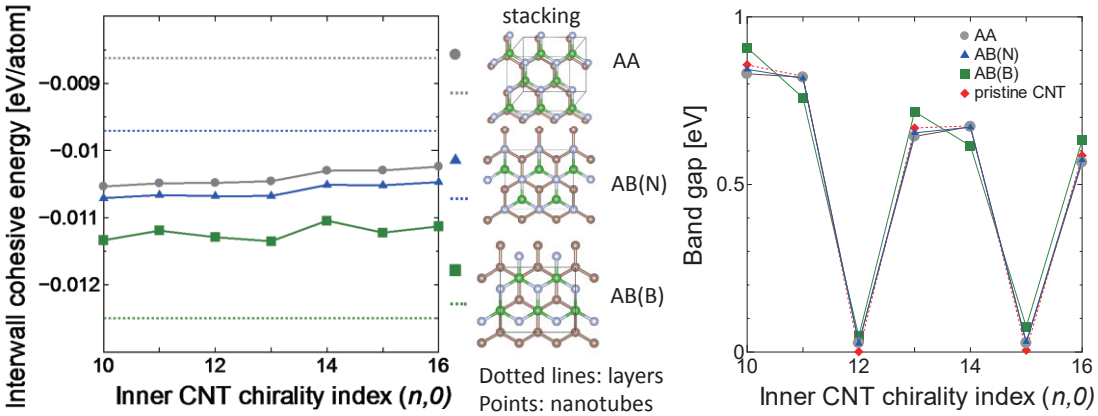

Figure 1 (a) Interwall cohesive energy and (b) band gap of CNT(*n*,0)@BNNT(*n*+9,0) as a function of the index *n*. Dotted lines in (a) indicate the cohesive energy of hBN and graphene with AB(B), AB(N) and AA stacking arrangements.

[1] R. Xiang, *et al*., arXiv preprint arXiv:1807.06154.

Corresponding Author: Shigeo Maruyama Tel: + 81-3-5841-6421, Fax: +81- 3-5800-6983,
E-mail: maruyama@photon.t.u-tokyo.ac.jp

Thermoelectric Simulation for Carbon Nanotube Film

○Kotaro Fujisaki, Masaaki Tsukuda, Takahiro Yamamoto

Department of Electrical Engineering, Tokyo University of Science, Tokyo 125-8585, Japan

Nano carbon materials are expected to be potential candidates for nontoxic, flexible and high power thermoelectric devices, which are suitable for wearable power generation application [1, 2]. Carbon nanotube (CNT) thin films consisted of CNT network are ones of such thermoelectric devices. However, the physical origin of their thermoelectric performance remains to be elucidated yet due to complexity of CNT thin films. In order to increase the conductance and the Seebeck coefficient of CNT films, it is essential to understand the relation between the CNT network structure and its electrical and thermal properties.

To understand the relation between the CNT network structures and its thermoelectric performance, we theoretically investigated the effect of several parameters such as CNT length and density on thermoelectric performance with the thermal circuit model and the electrical circuit theory. First, we generated two-dimensional random network (as shown in Fig. 1) by changing the CNT length and density. Second, for the generated CNT network, we calculated the temperature distribution by solving thermal circuit equations. Third, we calculated voltage of each CNT by temperature difference based on the temperature distribution. Forth, we calculated the Seebeck coefficient and electrical conductance by solving electrical circuit equations for the CNT networks. In this simulation, the CNT length was changed from 0.5 μm to 1.5 μm, keeping the density at 2 μg/cm^2. The obtained results in this study are summarized as follows.

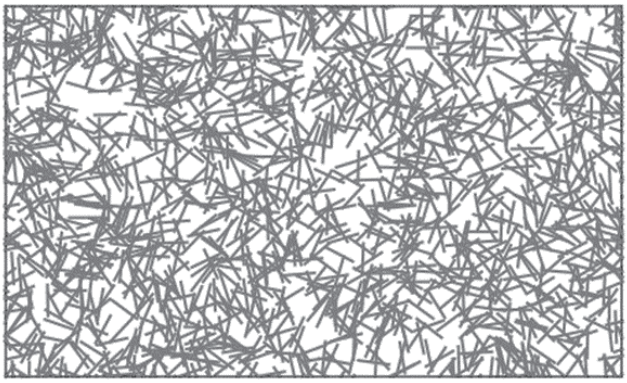

Fig. 1: Generated two-dimensional random CNT network

1. The electrical conductance of the films increases with the CNT length.
2. The Seebeck coefficient of the films is almost dependent on the Seebeck coeffient of the contact points between two CNTs in any CNT lengths.

[1] T. Izawa, K. Takashima, S. Konabe and T. Yamamoto, Synthetic Metals **225**, 98-102 (2017).

[2] J. Bahk, H. Fang, K. Yazawa and Ali Shakouri, Journal of Materials Chemistry C, **3**, 10362-10374 (2015).

Corresponding Author: T. Yamamoto

Tel: +81-3-5876-1492

E-mail: takahiro@rs.tus.ac.jp

Improvement of catalytic performance by adding single-walled carbon nanotubes aqueous dispersion

○Kazuki Kishida[1], Toru Harigai[1], Tsuyoshi Tanimoto[1], Hirofumi Takikawa[1], Takeshi Hashimoto[2], Takumi Yana[2], Yoshiyuki Suda[1]

[1] *Department of Electric and Electronic Information Engineering, Toyohashi University of Technology, Toyohashi, Aichi 441-8580, Japan*
[2] *Meijo Nano Carbon Co., Ltd., Nagoya, Aichi 463-0003, Japan*

Polymer electrolyte fuel cells (PEFC) have been attracting attention due to a variety of feature such as low environmental pollution, low operating temperatures, and high theoretical efficiency of energy conversion. However, reduction of platinum usage is one of major problems since utilization of platinum leads high expense. Therefore, carbon nanomaterials which have high conductivity, durability and high surface area are widely used as catalyst supports [1]. In this study, aqueous dispersion including single-walled carbon nanotubes (SWNT) with high crystallinity was added to commercial fuel cell catalyst and catalytic performance of prepared catalysts were evaluated based on electrochemical measurements.

Commercial fuel cell catalyst (Pt/Vulcan XC-72, TEC10V50E, 50 wt.%-Pt) and single-walled carbon naotubes aqueous dispersion (200 mg / 100 ml) were obtained from TANAKA KIKINZOKU KOGYO K.K. and Meijo Nano Carbon Co. Ltd., respectively. Following amounts of single-walled carbon naotubes were added to 200 mg of Pt/Vulcan XC-72 catalyst: 0, 5.0, 7.5, 10 and 20 mg. And then they were mixed physically by auto pestle for 5 minutes. Further appropriate amounts of nafion and methanol were added to slurry-like catalyst followed by ultrasonication for 30 minutes to prepare catalyst ink. Catalytic performance was evaluated based on cyclic voltammetry in water bath at 25 ℃. Herein, Ag/AgCl electrode, platinum electrode, glassy carbon electrode and 0.5 M of sulfuric acid (H_2SO_4) were used as reference electrode, counter electrode, working electrode and electrolyte, respectively.

The cyclic voltammogram at the 10th of each catalyst ink is shown in Fig.1. The catalytic performances were evaluated based on calculation of electrochemical active surface area (ECSA) with following equation.

$$\mathrm{ECSA}\ [\mathrm{m^2/g}] = \frac{Q_H\ [\mathrm{C}]}{Q_s\ [\mu\mathrm{C/cm^2}] \times \mathrm{Pt}\ [\mathrm{g}]} \qquad (1)$$

where, Q_H is the charge derived from the area surrounded with electric double layer capacity and the voltammetric peaks. And the charge associated with hydrogen desorption per unit surface area (Q_s) has been accepted as 210 μC/cm^2 in the case of polycrystalline platinum. According to calculated ECSA, Pt/Vulcan XC-72 catalyst added 10 mg of SWNT showed highest catalytic activity. Therefore, we found that addition of appropriate amount of SWNT leads catalytic performance to improvement.

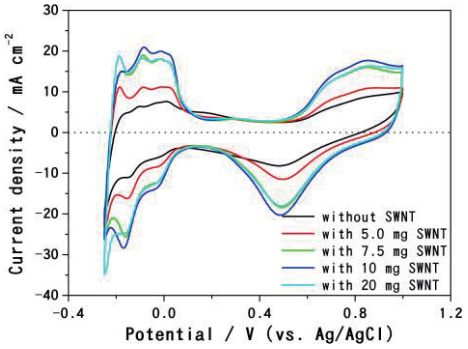

Fig.1 Cyclic voltammogram of different catalysts in 0.5 M H_2SO_4 at 25 ℃

[1] Y. Suda, et al., Materials Today Communications, **3**, 96 (2015)

Corresponding Author: Y. Suda
Tel: +81-532-44-1211
E-mail: kishida.kazuki@pes.ee.tut.ac.jp

Molecular Dynamics Simulations of the Influence of a Single Water Layer on the Electrical Conductivity of Graphene

○Yusei Kioka[1], Yuki Maekawa [2], Kenji Sasaoka [3], Takahiro Yamamoto [1,2,3]

[1] Department of Electrical Engineering, Tokyo University of Science, Tokyo, 125-8585, Japan
[2] Department of Liberal Arts, Tokyo University of Science, Tokyo, 125-8585, Japan
[3]Water Frontier Science & Technology Research Center, RIST, Tokyo University of Science, Tokyo, 125-8585

It had long been believed that a graphene cannot be adsorbed by water molecules because it is a hydrophobic material. However, the previous theoretical studies based on classical molecular dynamics (MD) simulations showed that single or double water layers are formed on a graphene surface, depending on number of water molecules [1,2]. Before the results obtained from these simulations, Homma et al. discovered the existence of the similar water molecular layers around a carbon nanotube by both photoluminescence measurements and classical MD simulations [3]. The microscopic structure of the surface water layer parallel to the graphene had been clarified by our research. According to this study, the two-dimensional (2D) hydrogen-bond network is formed on the water layers on graphene surface [4]. Following these previous studies, we investigated the influence of such a 2D network on the electrical properties of the graphene.

In this work, we constructed the microscopic structure of a single water layer between a graphene and a hexagonal boron nitride substrate using classical MD simulations. For the obtained structures, we calculated the electric dipole of water molecules when electric field applied in the direction perpendicular to the graphene. By using this result, we estimated the electrical conductivity of the graphene. We explain that the correlation between electric dipole of a single water layer and the electrical conductivity of graphene at poster session.

[1] T. A. Ho and A. Striolo, J. Chem. Phys. **138**, 054117 (2013).

[2] A. Akaishi, T. Yonemaru, and J. Nakamura, ACS Omega **2**, 2184 (2017).

[3] Y. Homma, *et al*., Phys. Rev. Lett. **110**, 157402 (2013).

[4] Y. Maekawa, K. Sasaoka and T. Yamamoto, Jpn. J. Appl. Phys. **57**, 035102 (2018).

Corresponding Author: Takahiro Yamamoto,
Tel&FAX: +81-3-5213-0990,
E-mail: takahiro@rs.tus.ac.jp

Charged exciton (trion) in anisotropic atomically thin 2D material ReS_2

○Xiaofan Wang, Keisuke Shinokita, Yuhei Miyauchi and Kazunari Matsuda

Institute of Advanced Energy, Kyoto University, Uji, Kyoto 611-0011, Japan

Atomically thin transition metal dichalcogenides MX_2 (M=Mo, W, X=S, Se, Te) have attracted much attentions in the fields of semiconductor physics and applications [1]. In monolayer MX_2 with isotropic crystal structure, the fundamental optical properties are governed by exciton (electron-hole pairs) and trion (charged exciton) due to their enhanced attractive Coulomb interactions [2]. Recently, the exciton and trion in anisotropic atomically thin materials such as unstable black phosphorus (BP) has also been experimentally observed [3].

Here we studied the optical properties of stable rhenium disulfide (ReS_2) with anisotropic crystal structure. The few layer ReS_2 with field effect transistor structure was fabricated by dry transfer process. Figure 1(a) shows photoluminescence (PL) spectra of three-layer (3L) ReS_2 by applying the gate voltage of -40 and +40 V. The PL spectrum at -40 V shows the strong emission peaks at 1.58 eV, and 1.62 eV, which are attributed to the recombination of bound electron-hole pair (neutral exciton) [4]. In contrast, the additional emission peak (hatched peak) in the spectra at +40 V appears at 1.56 eV due to negatively charged exciton (negative trion). This is the first experimental observation of charged exciton (trion) in ReS_2. Figure 1(b) shows the polar plot of detected PL intensity with linearly polarized components from trions. The strongly polarized anisotropic emission from the trions are experimentally observed. The detail natures of anisotropic trion in ReS_2 will be discussed.

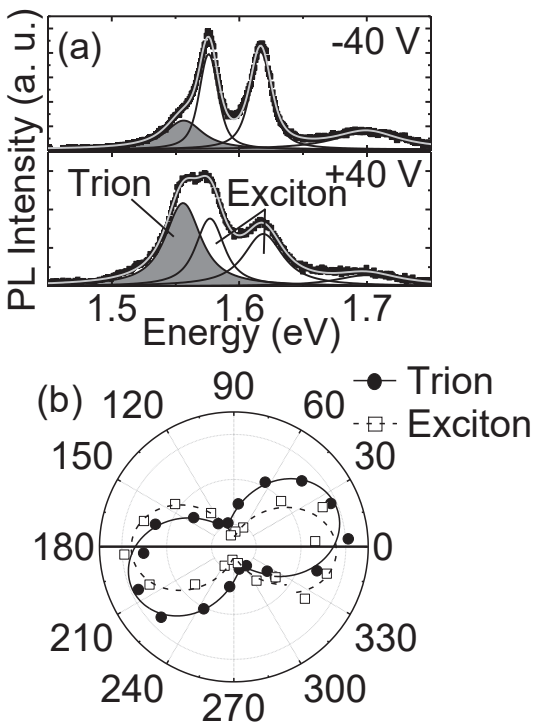

Figure 1 (a) PL spectra of 3L-ReS_2 at back gate voltage of -40 V and +40 V at 20 K. The spectra were fitted with multiple Voigt functions. Filled lines correspond to trion contributions. (b) Polarization dependence of the integrated PL intensity of trion and exciton (1.58 eV) components at +40 V.

[1] S. Z. Butler *et al.,* ACS Nano **7**, 2898 (2013).
[2] A. Chernikov *et al.,* Phys. Rev. Lett. **113**, 076802 (2014).
[3] R. Xu *et al.,* ACS Nano **10**, 2046 (2016).
[4] X. Wang *et al.,* Adv. Funct. Mater. 1806169 (2018).

Corresponding Author: Kazunari Matsuda
Tel: +81-774-38-3460
E-mail: matsuda@iae.kyoto-u.ac.jp

Interface electroluminescence from in-plane heterostructures based transition metal dichalcogenide monolayers

○Yuhei Takaguchi[1], Jiang Pu[2], Hirofumi Matsuoka[2], Yu Kobayashi[1], Yutaka Maniwa[1], Taishi Takenobu[2], Yasumitsu Miyata[1]

[1] *Department of Physics, Tokyo Metropolitan University, Hachioji 192-0397, Japan*
[2] *Department of Applied Physics, Nagoya University, Nagoya 464-8603, Japan*

Heterostructures of transition metal dichalcogenides (TMDCs) are an attractive system to realize high-performance devices such as light-emitting diodes and tunnel field-effect transistors. To investigate their electronic properties and device performance, we have developed growth processes of various in-plane heterostructures based on TMDC monolayers [1] and have demonstrated the electric double layer light emitting diodes (EDLEDs) of the heterostructures [2,3]. In our previous study, the WS_2/MoS_2 EDLED shows linear electroluminescence (EL) around the heterointerface and the two prominent EL peaks of MoS_2 and WS_2 as observed in photoluminescence (PL) spectra. In this study, we report anomalous interface EL from the heterointerface of $WSe_2/MoSe_2$ in-plane heterostructures. $WSe_2/MoSe_2$ in-plane heterostructures were grown on sapphire substrates by salt-assisted chemical vapor deposition (CVD). To observe EL, we have fabricated the EDLEDs with ion gel. The devices show linear light emission from the interface by applying voltage. Interestingly, the EL spectra show four different peaks, which is drastically different from PL spectra of the interface. Furthermore, the intensities of these EL peaks strongly depend on bias voltage. In the presentation, we will show the details of sample preparation and discuss possible origins of EL peaks in the present EDLEDs.

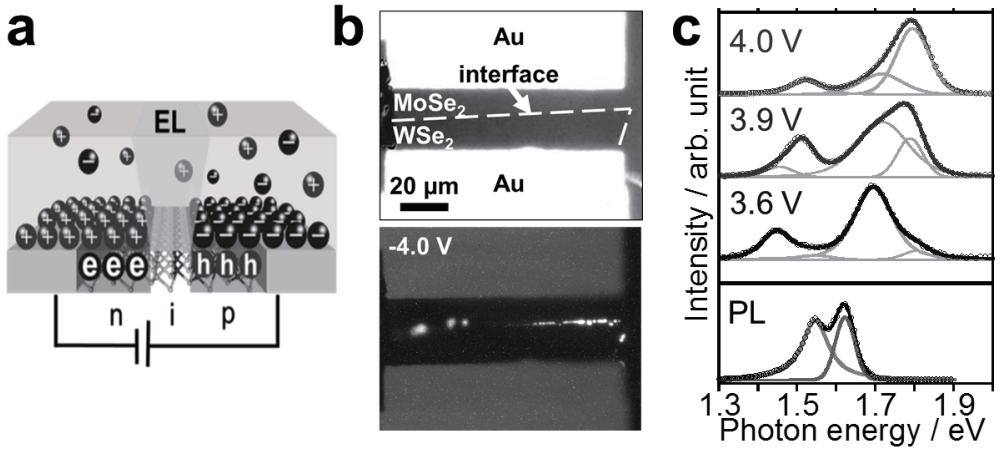

Fig.1 (a) Illustration and (b) optical and electroluminescence (EL) images of $WSe_2/MoSe_2$-based EDLED device. Arrows indicate the observed EL. (c) EL and photoluminescence (PL) spectra of the EDLED device.

[1] Y. Kobayashi *et al.,* ***Sci. Rep.***, 6, 31223 (2016). [2] J. Pu *et al.,* ***Adv. Mater.*** *,* 29, 1606918 (2017).

[3] Y. Takaguchi et al., 55th FNTG symposium.

Corresponding Author: Yasumitsu Miyata, Tel: 042-677-2508, E-mail: ymiyata@tmu.ac.jp

Analytic properties of topological states in 2D SSH model

Daichi Obana[1], Feng Liu[1], Katsunori Wakabayashi[1]

[1] *Department of Nanotechnology for Sustainable Energy, School of Science and Technology, Kwansei Gakuin University, Gakuen 2-1, Sanda 669-1337, Japan*

Topological edge states are robust to weak perturbations such as edge roughness and impurities and provide robust electronic transport channel. In zigzag edges of graphene, edge states appear at the energy near the Dirac point [1] and provide perfectly conducting channel [2]. The edge state can associated with topological phase called Zak phase [3].

Su-Schrieffer-Heeger (SSH) model, which has been originally proposed for studying the electronic states of polyacetylene, is a minimum theoretical model to demonstrate the properties of Zak phase. In this model, the topological phase transition is governed by tuning the ratio between intra-cell and inter-cell hopping γ'/γ. Particularly, transition of the topological phase associated with Zak phase corresponds to the emergence of edge states in finite systems.

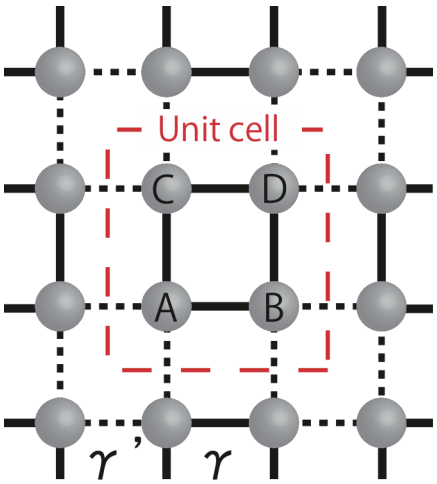

Fig. 1 Lattice structure of 2D SSH model

In this work we extend the concept of Zak phase to two-dimensional (2D) materials by employing 2D SSH model, where two types of hopping γ and γ' are periodically arranged on a square lattice as shown in Fig.1[4]. In our presentation, we analytically solve the equations of motion of electrons for the two topologically distinct phases of bulk and ribbon structures. We show the bulk-edge correspondence in 2D SSH model in terms of Zak phase by using a theoretical approach of Ref. [1]. Our results will serve to design new 2D materials which possess non-zero Zak phase and edge states which are necessary for robust electronic transport.

[1] K. Wakabayashi, and S. Dutta, Solid State Comm., **152**, 1420 (2012). K. Wakabayashi, K Sasaki, T Nakanishi, T Enoki, Sci. Technol. Adv. Mater. **11**, 054504 (2010).
[2] K. Wakabayashi, Y. Takane, M. Sigrist, Phys. Rev. Lett.**99**, 036601 (2007).
[3] P. Delplace, D. Ullmo and G. Montambaux , Phys. Rev. B, **84**, 13 (2011).
[4] F. Liu, and K. Wakabayashi , Phys. Rev. Lett.,**118**, 076308 (2017).

Corresponding Author: K. Wakabayashi (E-mail: waka@kwansei.ac.jp)

Synthesis of Single-Walled Carbon Nanotubes Coated with Thiol-Reactive Gel via Emulsion Polymerization for Cancer Active Targeting

○Yukiko Nagai[1], Minoru Kawaguchi[5], Jun Ohno[5], Tsuyohiko Fujigaya[1,2,3,4]

[1]Department of Applied Chemistry, Graduate School of Engineering, Kyushu University, 744 Motooka, Fukuoka 819-0395, Japan [2]WPI I²CNER, Kyushu University [3] Precursory Research for Embryonic Science and Technology (PRESTO), Japan Science and Technology Agency (JST) [4]Center for Molecular Systems, Kyushu University [5]Center for Regenerative Medicine, Fukuoka Dental College, Fukuoka, Japan.

Single-walled carbon nanotubes (SWNTs) have unique near-infrared absorption and photoemission properties that are attractive for *in vivo* biological applications such as photothermal cancer treatment and bioimaging. Therefore, a smart functionalization strategy to create biocompatible surfaces and to introduce various ligands for SWNTs to active target cancer cells without losing the unique optical properties of the SWNTs is strongly desired.

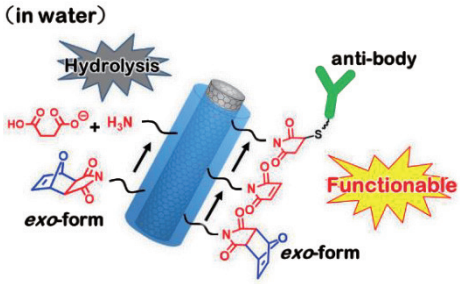

Fig. 1. Graphical abstract of this research.

In this study, we developed a SWNT/gel hybrid containing maleimide group, which reacts with various thiol compounds through thiol-ene reactions (***Fig. 1.***). [1] In this hybrid, the method called carbon nanotube micelle polymerization [2] was used to non-covalently modify the surface of SWNTs with a cross-linked polymer gel layer. Since this method can form an extremely stable gel layer on SWNTs; essential for *in vivo* biological applications.

The new vynyl monomer used to form the gel layer contained a maleimide group, which was protected with furan in *endo*-form. The resulting hybrid was treated in water to induce deprotection via retro Diels–Alder reaction and then functionalized with thiol compounds through click reaction. It was revealed that the *endo*-form underwent clear deprotection by heating and functionalization with thiol compounds in water at room temperature, while their *exo*-isomer resulted in the hydrolysis upon the deprotection. To synthesize the SWNT/gel hybrid, carbon nanotube micelle polymerization was carried out in the presence of PEG methacrylate as a co-monomer. After the deprotection of the hybrid and subsequent reaction with an antibody, the resulting hybrid enabled active cancer cell targeting *in vitro* (***Fig. 2.***), indicating the successful functionalization of the hybrid with thiol compounds via thiol-ene reaction. Based on the present results, we propose that the SWNT/gel hybrid can be used as a "platform" for various antibody functionalization.

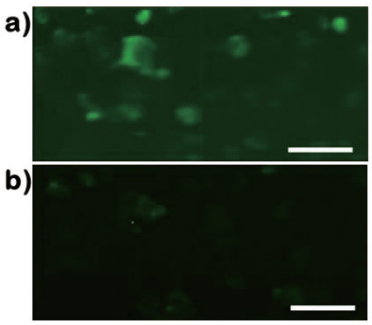

Fig. 2. G-band Raman imaging of cells conjugated the hybrid (a) with and (b) without antibody. The scale bar is 100 μm.

[1] Y. Nagai and T. Fujigaya et al., *J. Am. Chem. Soc.* **2018**, *140*, 8544.
[2] T. Fujigaya et al., *RSC. Adv.* **2014**, *4*, 6318.

Corresponding Author: T. Fujigaya
Tel: +81-92-802-2842, Fax: +81-92-802-2842, E-mail: fujigaya.tsuyohiko.948@m.kyushu-u.ac.jp

Synthesis of [C_{60}]fullerene nanowhisker-cadmium selenide nanoparticle composites and photocatalytic degradation of methylene blue

○Jeong Won Ko [1], Jeong Hoon Park [2],Weon Bae Ko [1,2,3]

[1]Nanomaterials Research Institute, [2]Department of Convergence Science, Graduate School, [3]Department of Chemistry, Sahmyook University, 815, Hwarang-ro, Nowon-gu, Seoul 01795, Republic of Korea

Cadmium oxide (CdO) solution was prepared by CdO, paraffin oil, oleic acid and heated at 160℃. Selenium (Se) solution was prepared by Se powder, paraffin oil and heated at 220℃. CdO solution was swiftly injected into the Se solution. The mixture solution was heated at 220℃ for 30 min. The precipitate was collected by centrifugation and was dried into the oven at 100 ℃ for 5 h to obtain solid state cadmium selenide (CdSe) nanoparticles. The CdSe nanoparticles solution was prepared by powdered CdSe nanoparticles dissolving into the mixture solution of distilled water and methanol. [C_{60}]Fullerene nanowhisker-CdSe nanoparticle composites were prepared by liquid-liquid interfacial precipitation(LLIP) method using C_{60}-saturated toluene, the CdSe nanoparticles solution and isopropyl alcohol. The product of [C_{60}]fullerene nanowhisker-CdSe nanoparticle composites was characterized by X-ray diffraction, scanning electron microscopy, Raman spectroscopy, and transmission electron microscopy. Photocatalytic activity of [C_{60}]fullerene nanowhisker-CdSe nanoparticle composites through degradation of methylene blue under UV light at 254 nm was confirmed by UV-vis spectroscopy.

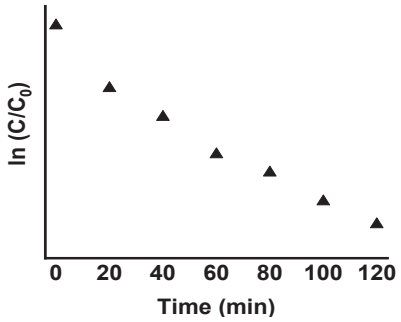

Fig.1 Kinetic Study for Photocatalytic Degradation of Methylene Blue with [C_{60}]Fullerene Nanowhisker- CdSe Nanoparticle Composites at 254 nm

[1] N. A. Hamizi *et al*. Mater. Chem. Phys. **124**, 395 (2010).
[2] K. Miyazawa *et al*. Surf. Eng. doi.org/10.1080/02670844.2017.1396779 (2017).

Corresponding Author: W. B. Ko
Tel: +82-2-3399-1700, Fax:, +82-2-979-5318,
E-mail: kowb@syu.ac.kr

Photoreactions of $Sc_3N@I_h$-C_{80} and $Lu_3N@I_h$-C_{80} with Disilirane: Characterization of Labile 1,2-Adducts

○Shinji Kanzawa[1], Fumiaki Ozeki[1], Shinpei Fukazawa[1], Masahiro Kako*[,1], Kumiko Sato[2], Michio Yamada[3], Yutaka Maeda[3], Makoto Furukawa[4], Takeshi Akasaka*[,2,3,4,5]

[1] *Department of Engineering Science, The University of Electro-Communications, Chofu 182-8585, Japan*
[2] *TARA Center, University of Tsukuba, Tsukuba, Ibaraki 305-8577, Japan*
[3] *Department of Chemistry, Tokyo Gakugei University, Tokyo 184-8501, Japan*
[4] *Foundation for Advancement of International Science, Tsukuba, Ibaraki 305-0821, Japan*
[5] *School of Materials Science and Engineering, Huazhong University of Science and Technology, Wuhan, Hubei 430074, P. R. China*

Endohedral metallofullerenes (EMFs) have acquired a lot of interest because of their fascinating structural and electronic properties. Exohedral functionalization has been extensively explored to broaden their range of potential applications in molecular electronics, nanomaterial science, and biochemistry [1]. In our ongoing study of fullerene chemistry,[1] disilicranes (1,2-disilacyclopropanes) have been employed as versatile silylating reagents for empty fullerenes and EMFs [1]. Previously, we reported that the photoreaction of $Sc_3N@I_h$-C_{80} with disilirane **1** afforded the corresponding 1,4- and 1,2-adduct (**2** and **3**, respectively) [2]. Although **2** was characterized using spectroscopic, electrochemical, and crystallographic studies, the properties of **3** have not been investigated because its isolation was not accomplished [2]. In addition, it was also reported that $Lu_3N@I_h$-C_{80} also reacted photochemically with disilicranes to produce the corresponding 1,4-adduct **4** and less stable intermediates during the photoreactions. Unfortunately, further structural analyses of the intermediates were unsuccessful due to their facile isomerization to **4** [3,4]. These results prompted us to characterize **3** derived from $Sc_3N@I_h$-C_{80} with disilicranes because the properties of fullerene derivatives depend on the regiochemistry of exohedral functionalization. We now report the details of the photoreactions of $M_3N@I_h$-C_{80} (M = Sc, Lu) describing the characterization of 1,2-adducts **3** and **5** [5]. The experimentally observed isomerization of the 1,2-adduct to the 1,4-adduct was rationalized based on the relative energies of the optimized structures by theoretical calculations. The electrochemical studies indicated the electron-donating effects of the silyl groups in these products in comparison with those of the related compounds.

Scheme 1.

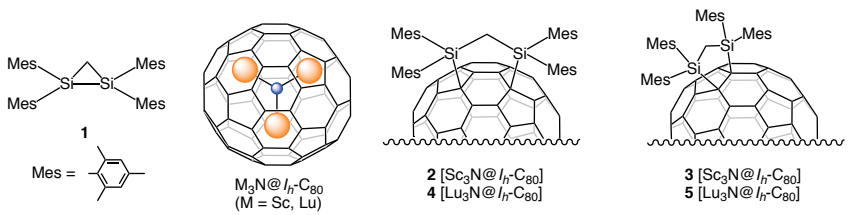

(Partial structures of **2**-**5**. The parent EMFs are shown in brackets, respectively.)

[1] M. Yamada *et al.* Bull. Chem. Soc. Jpn. **87**, 1289–1314 (2014). [2] Y. Iiduka *et al.* J. Am. Chem. Soc. **128**, 9919–9925 (2006). [3] K. Sato *et al.* Org. Lett. **14**, 5908–5911 (2012). [4] M. Kako, *et al.* Chem. Eur. J. **21**, 16411–16420 (2015). [5] M. Kako, *et al.* Heteroatom Chem. e21477 (2018).

Corresponding Author: Masahiro Kako Tel: +81-42-442-5570. E-mail: kako@e-one.uec.ac.jp

Near infrared emission of dimetallofullerene anions encapsulating Nd or Er

○Shinya Nishimoto[1], Takaaki Hirayama[1], Hiroyuki Nishidome[2], Yasumitsu Miyata[2], Kazuhiro Yanagi[2], Koichi Kikuchi[1], Yohji Achiba[1], Takeshi Kodama[1]

[1]*Department of Chemistry, Tokyo Metropolitan University, Tokyo 192-0397, Japan*
[2]*Department of Physics, Tokyo Metropolitan University, Tokyo 192-0397, Japan*

Er-metallofullerenes[1] and Tm-metallofullerenes[2] have long been the only ones that exhibit the emission from the encapsulated metal ion. In 2006, we reported the emission around 1 μm from the encapsulated Nd ion for Nd-metallofullerenes, but it was very weak[3]. Last year, we reported the synthesis, isolation, and emission of novel Nd-dimetallofullerenes, $(Nd_2@C_{78}(D_{3h}))^-$ and $(Nd_2@C_{80}(I_h))^-$, which are stable only as an anion form. In addition, the mixture of homo-, and hetero-dimetallofullerenes for $(MM'@C_{78}(D_{3h}))^-$ or $(MM'@C_{80}(I_h))^-$ (M, M'=Nd, La) were also investigated[4]. But, unfortunately, there is an uncertainty for the assignment of the emission spectra for Nd-dimetallofullerenes. Therefore, in this work, novel Er-dimetallofullerenes, $(Er_2@C_n)^-$ (n=78, 80), which are also stable only as anion form, were produced, isolated, and the emission spectra of them were measured. Then, the assignment of the emission spectra of Nd-dimetallofullerenes was reconsidered by taking into account of the emission spectra of Er-dimetallofullerenes. Moreover, hetero-dimetallofullerenes, $NdY@C_n$ and $ErY@C_n$, were also studied.

Soot containing metallofullerenes was produced by direct-current (60 A) arc discharge of M/C composite rods (M:C=2:98) under a 500 Torr He atmosphere. The raw soot was extracted with a mixed solvent of triethylamine and acetone. By multi-step ion pair chromatography, $(Er_2@C_n)^-$ (n=78, 80), $(NdYC_{80})^-$ were isolated and $(MM'C_{78})^-$ (M, M'= Nd, Y), $(MM'C_n)^-$ (M, M'= Er, Y; n=78, 80) were obtained as a mixture. The structures of these metallofullerenes were determined by UV-vis-NIR absorption spectra.

Emission spectra of $(M_2@C_{80}(I_h))^-$ (M=Nd, Er, Y) are shown in Fig.1. The broad peak around 900 nm with asterisk was observed for all the samples. Then, tentatively, the peak was assigned to contaminated impurities. For $(Nd_2@C_{80}(I_h))^-$, besides a broad peak around 900 nm, very weak shoulders indicated by arrows can be seen around 1100 nm and 1250 nm. For $(Er_2@C_{80}(I_h))^-$, emission around 1550 nm surrounded by a dotted line is clearly observed, which is characteristic for Er^{3+}. The emission spectra of hetero-dimetallofullerenes will be discussed in the presentation.

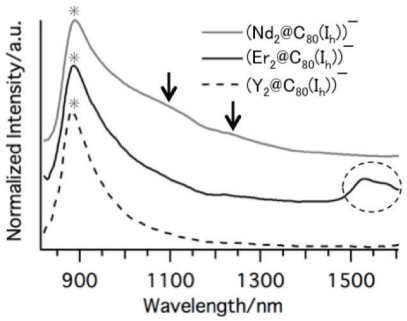

Fig.1 Emission spectra of $(M_2@C_{80}(I_h))^-$ (M=Nd, Er, Y).

[1] X. Ding, et al. *Chem. Phys. Lett.* **269**, 72 (1997).
[2] Z. Wang, et al. *ACS Nano* **10**, 4282 (2016).
[3] N. Murata, et al. *The 30th Commemorative Fullerenes-Nanotubes General Symposium* 106 (2006).
[4] S. Nishimoto, et al. *The 54th Fullerenes-Nanotubes-Graphene General Symposium* 47 (2018).
Corresponding Author: Takeshi Kodama
Tel: +81-42-677-2530, Fax: +81-42-677-2525
E-mail: kodama-takeshi@tmu.ac.jp

Analysis of Self-Absorption Effect on Resonance Raman Spectroscopy of Single-Chirality Single-Wall Carbon Nanotubes

○Xiaojun Wei[1,2], Shilong Li[1,2], Dehua Yang[1,2], Jiaming Cui[1,2], Huaping Liu[1,2], Weiya Zhou[1,2], Sishen Xie[1,2], Takeshi Tanaka[3], and Hiromichi Kataura[3]

[1] *Beijing National Laboratory for Condensed Matter Physics, Institute of Physics, Chinese Academy of Sciences, Beijing 100190, China*
[2] *Beijing Key Laboratory for Advanced Functional Materials and Structure Research, Beijing 100190, China*
[3] *Nanomaterials Research Institute, National Institute of Advanced Industrial Science and Technology (AIST), Tsukuba, Ibaraki 305-8565, Japan*

Raman spectroscopy is one of the most promising characterization techniques, which has been widely applied to assign the chiral indices (*n*,*m*) of single-wall carbon nanotubes (SWCNTs) and evaluate the relative abundance of each (*n*,*m*) species. However, the self-absorption effect cannot be ignored when the optical absorbance at the wavelength of the Raman scattering light is significantly large, which may lead to an unexpected underestimation in intrinsic spectral intensity because the experimentally observed intensity does not correspond to the intrinsic intensity [1]. In this study, we systematically analyzed the influence of the self-absorption effect for the resonance Raman spectra measurement of various chirality-sorted SWCNTs by modifying the focal depth in the confocal micro-Raman measurement and the sample concentration.

Figure 1a shows the observed G^+-band intensities of (8,3) solutions with different SWCNT concentrations measured at various focal depths lay inside the front surface. When the laser was focused at front surface (corresponding to 0 mm), the G^+-band intensity was observed to linearly increase with increasing the SWCNT concentration. By contrast, when the laser was focused inside the solution, the G^+-band intensity became to nonlinearly increase with increasing the SWCNT concentration. Furthermore, the G^+-band intensity even dropped as both of the focal depth and the SWCNT concentration were large enough (corresponding to 8 mm). This observed Raman intensity dependence on the focal depth and the SWCNT concentration could be explained by the self-absorption effect of Raman scattering light because all observed Raman intensities were well fitted by Lambert-Beer law. Based on the experimental measurement shown in Figure 1a, we can simulate the observed Raman intensity as a function of the focal depth and the SWCNT concentration (Figure 1b), which is very important for the quantitative evaluation of Raman intensity of each (*n*,*m*) species, even their abundances.

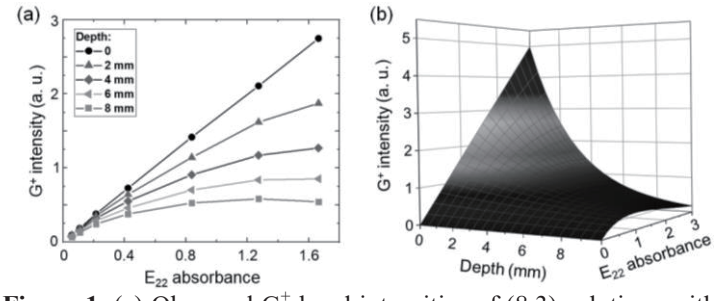

Figure 1. (a) Observed G^+-band intensities of (8,3) solutions with different SWCNT concentrations (denoted as their E_{22} absorbance) measured at various focal depths at an excitation wavelength of 633 nm. (b) Simulation of the observed G^+-band intensity as a function of the focal depth and the SWCNT concentration.

This work was supported by National Key R&D program of China (Grant No. 2018YFA0208402), NSFC (Grant No. 51472264, 11634014, 51820105002, 51872320, 51561022), and KAKENHI No. 25220602.

Corresponding Author: X. Wei; H. Kataura
E-mail: weixiaojun@iphy.ac.cn; h-kataura@aist.go.jp

Subdiffraction imaging of carbon nanotubes using nonlinear excitonic processes

○Keigo Otsuka [1,2], Akihiro Ishii [1,2], Yuichiro K. Kato [1,2]

[1] *Quantum Optoelectronics Research Team, RIKEN Center for Advanced Photonics, Saitama 351-0198, Japan*
[2] *Nanoscale Quantum Photonics Laboratory, RIKEN Cluster for Pioneering Research, Saitama 351-0198, Japan*

Single-walled carbon nanotubes can be promising bioimaging probes owing to their near-infrared fluorescence, which show deep penetration and low scattering in living bodies [1]. Fluorescence intensity of carbon nanotubes nonlinearly depends on excitation power because either one of two excitons go through an annihilation process upon collision. In one-dimensional system of nanotubes, the annihilation process shows particularly strong dependence on exciton density [2] in comparison to two- or three-dimensional materials, leaving a chance for improving the spatial resolution in far-field imaging.

Here we demonstrate subdiffraction imaging of air-suspended carbon nanotubess by extracting exciton-exciton annihilation rates from two fluorescence images which are obtained with different excitation powers. As shown in Fig. 1(a), full width at half maximum of annihilation rate profiles (circles) is smaller than that of raw fluorescence (open squares). This is because the frequency of exciton interactions in nanotubes shows a superlinear dependence on its generation rate (Fig. 1(b)). Figure 1(c) shows a fluorescence image of two adjacent nanotubes, and these can be more clearly distinguished in an image of the extracted annihilation rates (Fig. 1(d)).

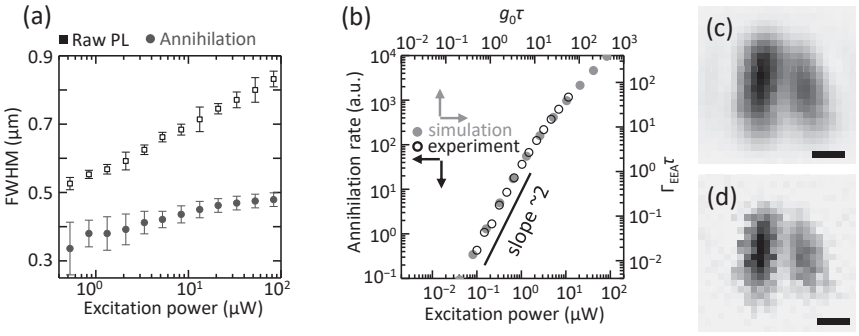

Figure 1 (a) Width of fluorescence intensity profiles and extracted annihilation rate profiles of a nanotube. Reference power for the extraction is fixed at 0.05 μW. (b) Excitation power dependence of exciton-exciton annihilation rates from experiments and Monte Carlo simulations. (c,d) 2D images of two nanotubes for fluorescence intensity (c) and the extracted annihilation rate (d). Scale bars: 500 nm.

Work supported by JSPS (KAKENHI JP16H05962) and MEXT (Nanotechnology Platform). We thank the Advanced Manufacturing Support Team at RIKEN for technical assistance.

[1] G. Hong, S. Diao, A.L. Antaris, and H. Dai, *Chem. Rev*. **115**, 10816 (2015).
[2] A. Ishii, M. Yoshida, and Y.K. Kato, *Phys. Rev. B* **91**, 125427 (2015).

Corresponding Author: Yuichiro K. Kato
Tel: +81-48-462-1449, Web: http://katogroup.riken.jp/, E-mail: yuichiro.kato@riken.jp

Enhanced in-plane thermal conductivity of single-walled carbon nanotube/boron nitride nanotube composite films

○Pengyingkai Wang[1], Yongjia Zheng[1], Taiki Inoue[1], Rong Xiang[1], Makoto Watanabe[1], Shohei Chiashi[1], Shigeo Maruyama[1, 2]

1 Department of Mechanical Engineering, The University of Tokyo, Tokyo 113-8656, Japan
2 Energy Nanoengineering Lab, National Institute of Advanced Industrial Science and Technology (AIST), Ibaraki 305-8564, Japan

Single-walled carbon nanotube (SWCNT) films exhibit promising potential as thermal interface material due to the superior thermal conductivity [1] and the outstanding mechanical property. However, it is still not yet successful for the SWCNT films to inherit the excellent thermal conductivity of ideal SWCNTs due to the limited thermal transport channels and relatively low oxidation temperature (450–500 ℃) [2,3]. Meanwhile, boron nitride nanotubes (BNNTs) possess high thermal conductivity comparable to SWCNTs and higher thermal stability in air than SWCNTs. A study has realized a 90% increase in thermal conductivity by encapsulating multi-walled CNT array with BNNTs [4].

In this work, we synthesized coaxial SWCNT-BNNT composite films by CVD method [5] and investigated thermal conductivity of them. SWCNT films were prepared by the aerosol chemical vapor deposition synthesis method. With the SWCNT films as templates, we synthesized BN layers for 3 hours using ammonia borane as precursors. FTIR spectra of the SWCNT films before and after coating with BNNTs are shown in Figure 1. In-plane thermal conductivity of this composite was studied by a contact free steady-state IR method [6] as schematically shown in Figure 2. We observed a thermal conductivity enhancement of SWCNT films (from ~68.1 W/m K to ~ 91.3 W/m K, ~ 30% increase) by further growing outer BNNTs (~3 walls). The characterization of the sample with SEM and TEM and the detailed experiment process will be presented.

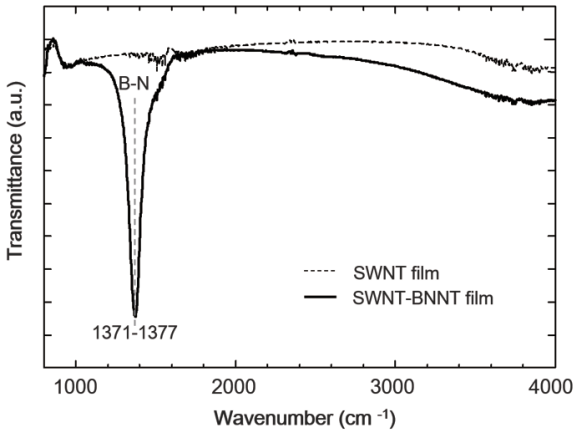

Fig. 1. Transmittance measured by FTIR of the SWCNT film and SWCNT-BNNT film.

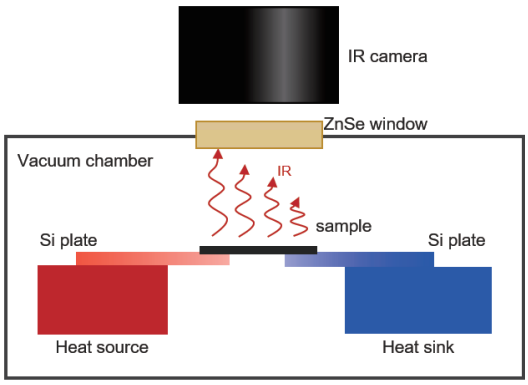

Fig. 2. A schematic of the thermal conductivity measurement setup.

[1] J. Hone *et al.*, Appl. Phys. Lett, **77**, 666 (2000). [2] A. M. Marconnet *et al.*, Rev. Mod. Phys., **85**, 3 (2013).
[3] Y Chen *et al.*, Appl. Phys. Lett., **85**, 2430 (2004) [4] J. Lin *et al.*, ACS Appl. Mater. Interfaces, **9**, 14555 (2017).
[5] R. Xiang *et al.*, arXiv :1807.06154 . [6] Y. Feng *et al.*, Jpn. J. Appl. Phys. **57** , 075101 (2018).
Corresponding Author: S. Maruyama, Tel: +81-3-5841-6421, Fax: +81-3-5841-6421,
E-mail: maruyama@photon.t.u-tokyo.ac.jp

Structure dependence of electron-acoustic-like-phonon interaction in individually suspended single-walled carbon nanotubes

○Takumi Inaba, Yoshikazu Homma

Department of Physics, Tokyo University of Science, Tokyo162-8601, Japan

Evaluations of electron-phonon coupling in well-defined nanostructure is necessary when applications based on the vibration of materials move into the quantum regime. Raman scattering, where changes in polarization caused by lattice oscillation are probed by light, is an excellent means to analyze electron-phonon interaction. In this study, the Raman intensities of individually suspended single-walled carbon nanotubes (SWCNTs) were analyzed in order to evaluate variations in electron-phonon coupling in response to changes in the arrangement of carbon atoms (i.e., chirality).

We evaluated intensities of four Raman peaks generated from individually suspended SWCNTs, the radial breathing mode (RBM), the intermediate frequency mode (IFM), the D-mode, and the G-mode. The chirality of SWCNTs were determined from photoluminescence spectroscopy. Here, the IFM is the Raman peak found in the range of 400-600 cm^{-1}. Recent reports showed that the origin of the IFM is the phonon modes which was acoustic in graphene but turns to optical in tubular structure of SWCNTs [1]. Furthermore, the IFM has non zero momentum. Thus, the IFM has similar property as the RBM and the D-mode. As results, we found the relation between intensities of four Raman peak as

$$\frac{I_{RBM}}{I_G}=\frac{I_{IFM}}{I_D}.$$

Although (12,5) nanotubes is unlikely satisfy the equation as shown in Fig. 1, the equation holds for most SWCNTs we assessed. The qualitative explanation of the relation was given with referencing the prior theoretical study [2]. From the qualitative analysis, we proposed that the D-mode belongs to the longitudinal optical branch in semiconducting SWCNTs.

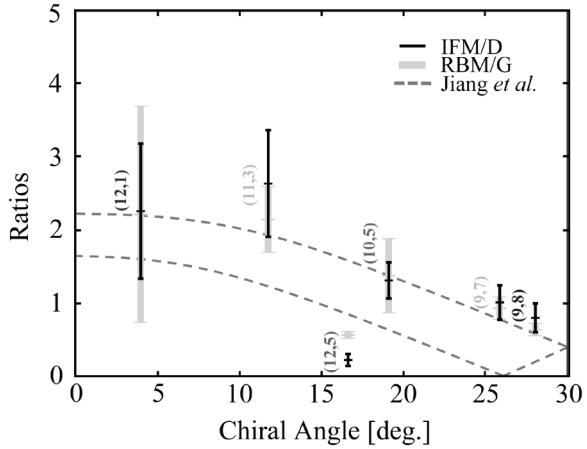

Figure 1 Chiral angle dependence of Raman intensity ratios IIFM/ID and IRBM/IG.

[1] A. Vierck, *et al.*, *Carbon* **117**, 360 (2017).
[2] J. Jiang, *et al.*, *Phys. Rev.* **B 72**, 235408 (2005).
Corresponding Author: T. Inaba
E-mail: takumi.inaba.63@rs.tus.ac.jp

Free-standing mode triboelectric generators with carbon nanotube thin film

○Masahiro Matsunaga[1], Jun Hirotani[2], Shigeru Kishimoto[2], Yutaka Ohno[2,3]

[1]*Venture Business Laboratory, Nagoya University, Nagoya 464-8603, Japan*
[2]*Department of Electronics, Nagoya University, Nagoya 464-8603, Japan*
[3]*Institute of Materials and Systems for Sustainability, Nagoya University, Nagoya 464-8603, Japan*

With rapid growth of the field of the internet of things, energy harvesting devices have been attracting attention for an alternative way of battery to drive electronics. Recently, triboelectric generator (TEG), which is a kind of mechanical energy harvesters, is attracting interests for highly-efficient energy harvester [1]. The working mechanism of the TEG is a combination of contact electrification and electrostatic induction. The TEG has a potential for wearable electronics using stretchable materials such as carbon nanotube (CNT) thin film [2]. In previous study, we reported transparent and stretchable TEGs toward wearable energy harvester, using a CNT thin film as an electrode [3]. However, an external ground electrode was required to configure a closed circuit loop, and restricted the stretchability of the TEG. In this study, to remove the external ground electrode, we fabricated the TEG which was consisted of two electrodes with different surface modification of triboelectric layers.

The TEG was composed of a carbon nanotube thin film sandwiched with polydimethylsiloxane (PDMS) layers. After spin-coating PDMS onto a plastic substrate, the CNT transparent electrodes were patterned on the PDMS surface by the spray coating of CNT ink (Meijo Nano Carbon, eDIPS ink) with a shadow mask as shown in Fig. 1. The top PDMS was spin-coated to cover the CNT electrode. To form the different triboelectric surface, we then applied CF_4 plasma to modify the PDMS surface on one of the electrodes. The TEG was able to drive a blue light-emitting diode embedded between the electrodes by tapping with a nitrile-glove worn hand.

Acknowledgment: This work was supported by JST/CREST (JPMJCR16Q2).

[1] Z. L. Wang, Mater. Today **20**, 74 (2017).

[2] N. Fukaya *et al*., ACS Nano **8**, 3285 (2014).

[3] M. Matsunaga *et al*., The 55th Fullerenes-Nanotubes-Graphene General Symposium, 1P-8 (2018).

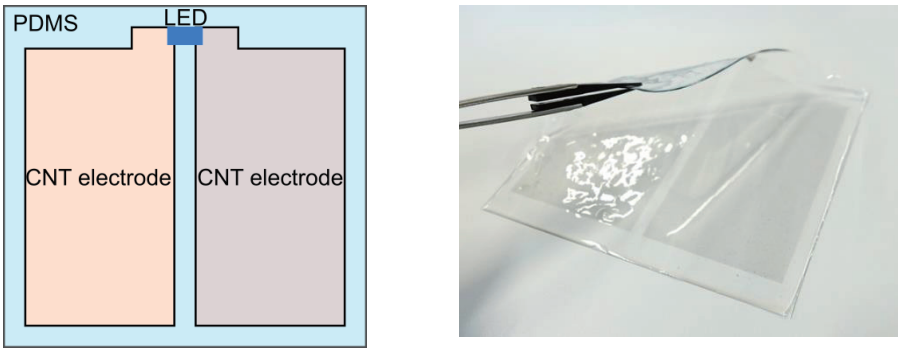

Fig. 1 Schematic and fabricated triboelectric generator.

Corresponding Author: Y. Ohno
Tel & Fax: +81-52-789-5387,
E-mail: yohno@nagoya-u.jp

Polyaromatic Anthracene Clencher on Single-Walled Carbon Nanotubes as Cathodes in Perovskite Solar Cells

○Shuhei Okawa[1], Il Jeon[1], Esko I. Kauppinen[2], Yutaka Matsuo[1], Shigeo Maruyama[1,3]

[1]*Department of Mechanical Engineering, The University of Tokyo, Tokyo 113-8656, Japan*
[2]*Department of Applied Physics, Aalto University School of Science, FI-00076 Aalto, Finland*
[3]*Energy Nano Engineering Laboratory, National Institute of Advanced Industrial Science and Technology (AIST), Tsukuba 305-8564, Japan*

Single-walled carbon nanotubes (SWNTs) possess excellent electrical conductivity and optical transparency, qualifying them for an alternative to transparent conductors in optoelectronic devices. SWNTs have been frequently used as an anode (hole-conductor) in perovskite solar cells (PSCs) [1] since SWNTs are naturally a p-type conductor in air. On the other hand, due to the low power conversion efficiency (PCE) arising from the challenging nature of its energy alignment, SWNT cathode has not been explored extensively. Previously, Jeon et al. reported a PCE of 10.5% from an inverted-type PSC in which a SWNT cathode drenched in $PC_{61}BM$ was used as the top electrode [2]. This demonstrated that the SWNT films can be used as a cathode and produce a PCE comparable to the anode counterpart.

In this work, we explored different materials to $PC_{61}BM$ to improve the SWNT cathode properties in PSCs from the optoelectronic perspective. After a through interface engineering of SWNTs cathodes, we achieved a PCE of 11.1% with SWNT film top electrode-based PSCs by incorporating polyaromatic anthracene ammonium (AA) molecules [3] which clenched onto SWNTs film [4] to enhance its charge selectivity. In order to protect perovskite layer from AA and ethanol, perovskite crystal was fully covered with $PC_{61}BM$ (Fig. 1 and 2). The resulting PSCs exhibited much higher PCE while being semi-transparent owing to AA firmly clenching onto the SWNTs and possessing a better energy alignment than $PC_{61}BM$.

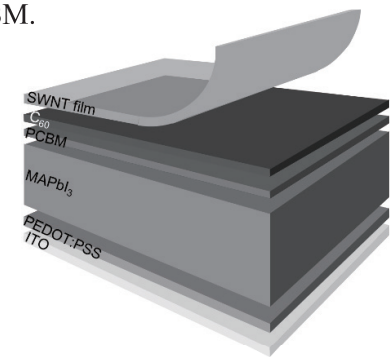

Fig. 1 Structure of the device.

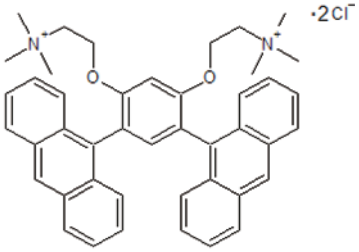

Fig. 2 Molecular structure of AA.

[1] Z. Li *et al*., *ACS Nano* **2014**, *8*, 6797.
[2] I. Jeon *et al*., *J. Phys. Chem. C* **2017**, *121*, 25743.
[3] I. Jeon *et al*., *ACS Appl. Mater. Interfaces* **2016**, 8, 29866.
[4] A. Kaskela *et al*., *Nano Lett.* **2010**, *10*, 4349.

Corresponding Author: S. Maruyama
Tel: +81-3-5841-6421,
Fax: +81-3-5800-6983,
E-mail: maruyama@photon.t.u-tokyo.ac.jp

Research of Fracture Behavior CNT/HDPE Composites *via* Melt Blending

○Koichi Utsugi, Mitsuhiro Takeda, Manami Mori, Riku Ota, Shu Kozaki, Masaru Sekido

Department of Materials and Environmental Engineering, National Institute of Technology, Sendai College, Natori 981-1239, Japan

CNTs are considered as the ideal reinforcement fillers for the nanocomposite materials due to their outstanding mechanical properties, tensile strength about 100 times that than steel, light weight, and low density. Previously we have prepared CNT/high density polyethylene (HDPE) composites by Melt Blending and measured tensile strength. As a result, the tensile strength increased as the weight ratio of CNTs was increased while the fracture strain decreased with addition of CNTs [1]. In this work we investigated the reason why the fracture strain of CNT/HDPE composites was decreased by observing the crystal state of HDPE and the dispersion of CNT.

The crystal state of HDPE was studied using a polarized optical microscope and the dispersion of CNTs was studied by a scanning electron microscope (SEM).

The difference of fracture surfaces depending on the different weight ratio of CNT/HDPE was observed by SEM (Fig. 1). Aggregation of CNTs was not observed from the composite with a weight ratio of 5/100. It is suggested that the cause of the decrease in fracture strain is not due to peeling of the interface between the CNT and the base material.

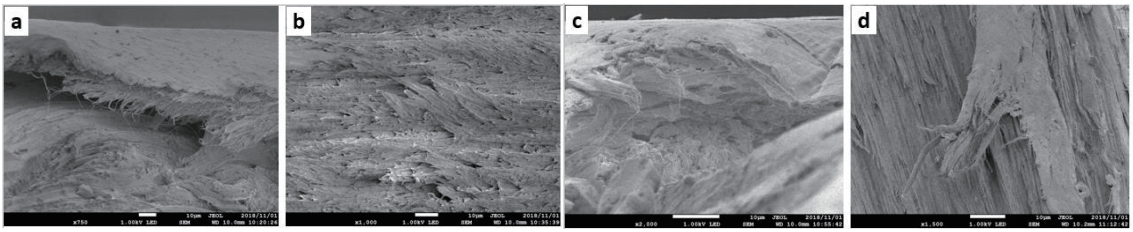

Fig. 1 SEM images of Fracture surface for CNT/HDPE composites. (a, b) are SWNT/HDPE composites. (a) weight ratio is 3/100. (b) weight ratio is 5/100. (c, d) are MWNT/HDPE composites. (c) weight ratio is 3:100. (d) weight ratio is 5:100.

[1] Atsushi Onodera *et al.,* The 54th Fullerenes-Nanotubes-Graphene General Symposium, 1P-11(2018)

Corresponding Author: Koichi Utsugi

Tel: +81-22-381-0329, Fax: +81-22-381-0329

E-mail: s1400309@sendai-nct.jp

Growth Mechanism of (6,5) Carbon Nanotube: Edge Structures and their Regioselectivities

○ Tomohiro Nishikawa[1,2], Tohru Sato[1,2,3], Naoki Haruta[2], Takeshi Kodama[4], Yohji Achiba[4]

[1]*Fukui Institute for Fundamental Chemistry, Kyoto University,*
[2]*Department of Molecular Engineering, Graduate School of Engineering,Kyoto University,*
[3]*Unit of Elements Strategy Initiative for Catalysts & Batteries, Kyoto University,*
[4]*Department of Chemistry, Graduate School of Science, Tokyo Metropolitan University,*

The growth mechanism of single-walled carbon nanotubes by the laser ablation method has been proposed[1]. The proposed mechanism is the followings: (1) precursor caps are produced in a gas phase; (2) the caps adsorb on metal catalyst; (3) nanotubes grow by C_2 addition to the edges of the caps. Various structures are possible in the precursor caps. However, the regioselectivities of C_2 addition to the precursor caps have not been discussed in detail.

Vibronic Coupling Density (VCD) analysis is effective as a reactivity index for regioselectivities of fullerene and graphene, which are difficult to be predicted based on the conventional frontier orbital theory [2-4]. In this work, we discuss the growth mechanism of (6,5) tube by investigating all the possible edge structures in (6,5) tube and their regioselectivities of C_2 addition to the edges based on the VCD analysis.

On the basis of the proposed mechanism, we made the following assumptions: (a) nanotubes grow by cycloaddition of C_2; (b) nanotubes are in anionic states generated by a charge transfer from the catalyst; (c) $C_{109}H_{11}$ isomers can be regarded as a precursor nanotube with an enough length for the electronic structures of the precursors not to depend on. The extended Hückel and DFT calculations were performed for the $C_{109}H_{11}$ isomers which are the capped (6,5) precursor tube with all the possible edge structures. As a result, there exist recurrent paths when the precursor tube is an acceptor in the growth reaction. On the other hand, if the precursor tube is a donor, such a path does not exist.

Based on the obtained paths, the reactive regions of the C_2 cycloaddition from $C_{109}H_{11}$ to $C_{129}H_{11}$ are identified using the VCD analysis. All the analyses indicate reactive regions of (6,5) tubes for C_2 cycloadditions to elucidate the one-layer growth path of (6,5) tube.

[1] Y.Achiba , *Mol. Sci.* **6**, A0055 (2012). [2] T. Sato *et al.*, *J. Phys. Chem. A* **112**, 758 (2008). [3] T. Sato *et al.*, *Chem. Phys. Lett.* **531**, 257 (2012). [4] N. Haruta *et al.*, *Tetrahedron Lett.* **56**, 590 (2015).

Corresponding Author: Tohru Sato
Fukui Institute for Fundamental Chemistry, Kyoto University,
Nishihiraki-cho 34-4, Sakyo-ku, Kyoto 606-8103, Japan
Tel: +81-75-711-7849
E-mail: tsato@scl.kyoto-u.ac.jp

Growth of vertically-aligned single-walled carbon nanotubes having small diameters from Ir catalysts: Effect of catalyst amount

○Takuya Okada[1], Kamal P Sharma[1,2], Tomoko Suzuki[2], Takahiro Saida[1,2], Shigeya Naritsuka[3]
Takahiro Maruyama[1,2]

[1]*Department of Applied Chemistry, Meijo University, Japan*
[2] *Nanomaterials Research Center, Meijo University, Japan*
[3]*Department of Materials Science and Engineering, Meijo University, Japan*

Single-walled carbon nanotubes (SWCNTs) have been anticipated for application in a lot of future nanodevices. To fabricate SWCNT devices, it is important to grow high-density semiconducting SWCNTs having small diameters, because the band gap of an SWCNT is in inversely proportional to its diameter. Previously, we reported that small-diameter SWCNTs were grown from Ir catalysts [1]. However, the effect of the amount of Ir catalysts for SWCNT growth has not been investigated. In this study, we carried out SWCNT growth using Ir catalysts by alcohol catalytic chemical vapor deposition (ACCVD) method to clarify the relationship between the amount of catalysts and the property of grown SWCNTs.

Using Ir catalysts, SWCNTs were grown on SiO_2/Si substrates by ACCVD in an ultra-high vacuum (UHV) chamber, a type of cold-wall CVD equipment. Ir catalysts were deposited using arc plasma deposition and the amount of deposition was controlled by the number of applied pulses required for discharge. The growth temperature was 800°C. The grown SWCNTs were characterized by FE-SEM, Raman spectroscopy, PL, and TEM.

Fig. 1 shows Raman spectra of SWCNTs grown for 60 min from various amount of Ir catalysts under ethanol pressure of 1×10^{-1} Pa. Irrespective of the amount of Ir catalysts, both G band and radial breathing mode (RBM) peaks were observed, indicating that SWCNTs were grown. By increasing the deposition amount of Ir catalysts, RBM peaks shifted to the lower wavenumbers, indicating that the SWCNT diameters increased. Fig. 2 shows SEM images of the samples in Fig. 1. High-density vertically-aligned SWCNTs were observed for all the samples, whose lengths were about 2 μm. This indicates that control of the amount of Ir catalysts is important to obtain small-diameter SWCNTs. We will discuss the electronic type of grown SWCNTs.

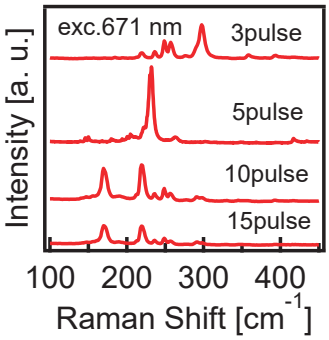

Fig.1 Raman spectra

This work was supported in part by Private University Research Branding Project from the Ministry of Education, Culture, Sports, Science and Technology (MEXT), Japan. Part of this work was conducted at the Institute for Molecular Science (IMS), supported by the "Nanotechnology Platform" of the MEXT, Japan.

[1] T. Okada et al. 55th FNTG Symposium 3P-22.

Corresponding Author: T. Maruyama
Phone: +81-52-838-2386, Fax: +81-52-832-1179
E-mail: takamaru@meijo-u.ac.jp

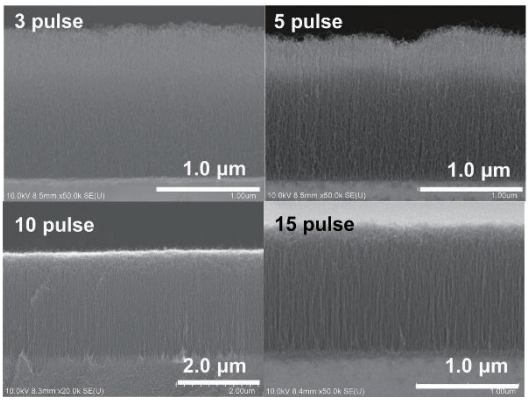

Fig.2 SEM image

The effect of noble metals addition into iron catalyst on the synthesis of vertically aligned single-walled carbon nanotube without reducing gas

○Shunsuke Sakurai, Jinping He, Kenji Hata, Don N. Futaba

CNT Application Center, National Institute of Advanced Industrial Science and Technology (AIST), 1-1-1 Higashi, Tsukuba, Ibaraki, 305-8565, Japan

In an efficient synthesis of single-walled carbon nanotube (SWNT) possessing vertically-aligned structure (forest) by chemical vapor deposition (CVD) method, both the oxidizing (such as water) and the reducing gases (such as hydrogen (H_2)) are well recognized to play important roles [1-3]. Especially, importance of H_2 during pre-annealing process of thin metal film (such as iron) to prepare catalyst nanoparticle has been frequently addressed [2]. Thus, the impact of oxidation status of metal catalyst has also attracted the attention of the researcher in this field [3].

Here, we report an unexpected effect of the addition of noble metals (NM = iridium, rhodium, and platinum) into iron catalyst even with a small fraction (<0.5 at%) on the SWNT synthesis efficiency during the process without any reducing gases. Specifically, composite film containing iron with/without NM were deposited by spin-coating, and then pre-annealed in helium atmosphere, and finally followed by an exposure into carbon source and water. As a result, a highly-efficient synthesis of tall (>600 μm) SWNT forests was achieved by NM addition though only poor growth was obtained in the case without NM. X-ray photoelectron spectroscopy (XPS) analyses on the catalyst films after annealing helium ambient suggested that the existence of NM assisted the formation of metallic status of iron even without any reducing gas. This work was supported by JSPS KAKENHI Grant Number JP17K14090.

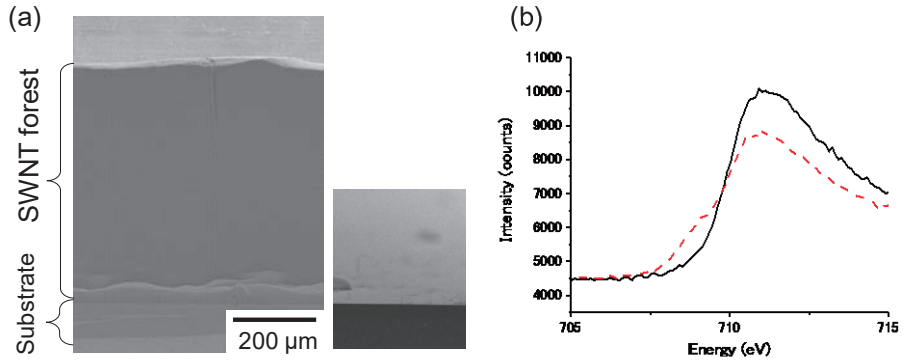

Fig. 1 (a) SEM images of CNT forest from iron/rhodium catalyst (left) and iron catalyst. (b) XPS spectra (Fe 2p region) of iron/iridium (continuous line) and iron (dotted line) catalyst.

[1] K. Hata, D. N. Futaba, K. Mizuno, T. Namai, M. Yumura, and S. Iijima, Science **306**, 1362 (2004).

[2] S. Sakurai, H. Nishino, D. N. Futaba, S. Yasuda, T. Yamada, A. Maigne, Y. Matsuo, E. Nakamura, M. Yumura, and K. Hata, J. Am. Chem. Soc. **134**, 2148 (2012).

[3] Y. Qian, H. An, T. Inoue, S. Chiashi, R. Xiang, and S. Maruyama, Phys. Status Solidi B **255**, 1800187 (2018).

Corresponding Author: S. Sakurai

Tel: +81-29-861-6205, Fax: +81-29-861-4851,

E-mail: shunsuke-sakurai@aist.go.jp

2P-23

Relationship between Catalysts and Diameter of Single-Walled Carbon Nanotubes

○Akio Nakano[1]

[1] *Yokohama Science Frontier High School,6 Ono-cho, Tsurumi-ku, Yokohama 230-0046, Japan*

Single-walled carbon nanotubes (SWCNTs) are expected to be applied to various industrial fields. The SWCNTs can be produced by arc discharge using carbon electrodes containing Ni or Y_2O_3 as a catalyst under low-pressure helium circumstance. In this study, the effect of molar ratio of Ni : Y_2O_3 (Table 1) contained in a carbon cathode on a diameter of SWCNTs was considered. The diameters (nm) of SWCNTs were calculated with the wavenumbers of Radial Breathing Mode (RBM, peaks at 160-300cm^{-1}) on Raman spectra, by formula [1] as below,

$$Dt = 248 / \omega$$ (Dt: diameter of tubes, ω : wavenumbers of RBM)

Table 1. The ratio of catalysts

	ratio I	ratio II	ratio III	ratio IV
Molar ratio (Ni : Y_2O_3)	2:1	1:1	1:2	4:1
Ni (g / 2.00g Carbon)	0.0587	0.0294	0.0294	0.0587
Y_2O_3 (g / 2.00g Carbon)	0.1129	0.1129	0.2258	0.0565

Peaks of RBM at around 165cm^{-1} were mainly observed with small peaks on the larger side of wavenumbers. These peaks appeared at five positions on the Raman spectra, which were calculated in approximately 1.50, 1.45, 1.36, 1.32 and 1.09 nm, as given on Table 2. With ratio I, only a single RBM peak was appeared, and Dt was in the largest region, 1.50nm. The double peaks were obtained with ratio II or III. The triple peaks were observed only with ratio III. However, no RBM peak were observed with ratioⅣ

Table 2. Diameter (nm) of SWCNTs produced under ratio I-III of catalysts

Dt 1.50 nm		Dt 1.45 nm		Dt 1.36 nm		Dt 1.32 nm		Dt 1.09 nm	
I(s)	1.486								
II(s)	1.519								
II(d)	1.502			II(d)	1.362				
III(s)	1.501	III(s)	1.445						
		III(d)	1.467			III(d)	1.323		
		III(t)	1.448			III(t)	1.317	III(t)	1.090

(s):RBM with single peak (d):with double peaks (t):with triple peaks

Double or triple peaks of RBM indicate the formations of SWCNTs with small diameters. The decrease in the diameter of the SWCNTs is related to the increase in the ratio of Y_2O_3. As a result, it is obvious that the diameter of the SWCNTs is related to the ratio of the catalysts of Ni : Y_2O_3 and that SWCNTs are not produced when the ratio of catalysts is too biased.

[1] R.Saito, *et al*., Phys.Rev.B, **61**, 2981 (2000).

Corresponding Author: A. Nakano
Tel: +81-45-511-3654, Fax: +81-45-511-3644

Structural Analysis of Carbon Nanobrushes and Carbon Nanohorn Aggregates using Small-Angle X-Ray Scattering Method

○Ryota Yuge, Kimiyoshi Fukatsu, Takashi Miyazaki

System Platform Research Laboratories, NEC Corporation, Tsukuba 305-8501, Japan

Fibrous aggregates of single-walled carbon nanohorns (CNHs), named as carbon nanobrushes (CNBs), were recently discovered [1-2]. Each carbon nanohorn radially gathered and were one-dimensionally connected in the range of several micrometers. The CNBs are drawing attention as electrode materials for various devices such as nanocarbon-polymer actuators, electric double layer capacitors, and fuel cells since they show high electrical conductivity, high dispersibility in solutions, and large specific surface areas [3]. So for, the morphology of the CNBs and CNHs in dispersion solutions has been well evaluated although local structural analysis such as TEM and SEM was demonstrated. In this study, we tried the structural analysis of CNBs and CNHs using small-angle X-ray scattering (SAXS) and ultra SAXS (USAXS) method.

CNBs was prepared by CO_2 laser ablation on catalyst-containing carbon targets at room temperature under ambient pressure. The CO_2 laser was operated at the power of 3.2 kW in the continuous-wave mode. The target of 30 mm in diameter and 50 mm in length was rotated at 1 rpm for 30 second during the laser ablation. The gas pressure in the growth chamber was kept at 700-800 Torr by controlling the evacuation rate while the buffer gas of nitrogen was kept at a flow rate of 10 L/min. The carbon target and iron-containing carbon target were used in our experiments. The SAXS and USAXS measurements for CNBs and CNHs mixture and CNHs in ethanol solutions were performed at the beam line BL08B2 and BL24XU-A1 of the synchrotron radiation facility SPring-8 (Hyogo, Japan). Their energies were 8 and 10 keV, respectively. The measurements were carried out in the range of 10^{-3} - 10 nm^{-1} of wave vectors Q.

From SAXS and USAXS results of CNHs, there were secondary aggregates of CNHs with several micro meters in ethanol solution. Therefore, we found that CNHs is not completely mono-dispersed. The particle size of aggregate structure was estimated as 160 nm, which is similar with results of SEM and TEM. The shape of CNHs was ellipsoid rather than spherical structure. Mean diameter of the individual CNH is estimated by 3.7 nm, which is approximately equal to observation results of TEM. The morphology of CNBs will be discussed in the presentation.

[1] R. Yuge *et al*. *Adv. Mater*. **28**, 7174 (2016).

[2] R. Yuge *et al*. *Carbon*, **122**, 665 (2017).

[3] R. Yuge *et al*. *Carbon*, **138**, 379 (2018).

Corresponding Author: R. Yuge, Tel: +81-29-850-1566, Fax: +81-29-856-6137, E-mail: r-yuge@bk.jp.nec.com

Simulation of Defect Generation by Irradiation of Platinum Particles on Graphite

○Toshiki Sonoda [1], Takahiro Yamamoto [1,2]

[1] *Department of Electrical Engineering, Tokyo University of Science, Tokyo 125-8585, Japan*
[2] *RIST, Tokyo University of Science, Tokyo 125-8585, Japan*

A fuel cell is expected to apply to battery of vehicles because of high efficiency and environmentally friendly fuel. However, since a platinum nanoparticle used as catalyst of the fuel cell is a valuable and costly resource, it is desired to reduce the amount of platinum. As a solution to this problem, an Arc Plasma Deposition (APD) method has been proposed.

In the previous study, it was reported that the platinum nanoparticles deposited on graphite by the APD method improves catalytic activity. As a reason of such an enhancing, it is considered that grain boundaries of graphite deform structures of the nanoparticles [1,2]. Furthermore, in another previous study, the adsorption energy of a platinum atom to graphene with a point defect was calculated by the first principle calculation, showing the highest adsorption energy when the platinum atom is located at the point defect [3]. From these results, defects formed on the graphite surface are considered to improve the catalytic performance because such the defects may cause deformation of lattice constant and strengthen the adsorption force between platinum nanoparticles and graphite surface. However, it is not clear how and what defects are generated by the APD method.

In this study, we simulate the situation of the APD method by a molecular dynamics method for investigating how and what defects are generated on the graphite surface. We perform two kinds of simulations for investigating the shapes and the number of defects:

1. Irradiating a platinum atom to graphite with varying the velocity and the position (Fig. 1).
2. Irradiating multiple platinum atoms to graphite for the random positions with varying the velocities and the incident angles (Fig. 2).

Our calculations show that shape and size of the defects are affected by the irradiation the position, the velocity and the angle of a platinum atom.

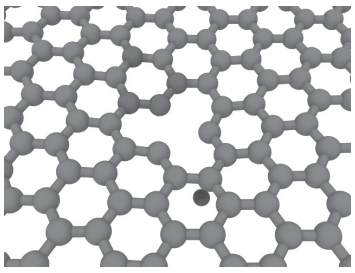

Fig.1 Schematic illustration of simulation 1

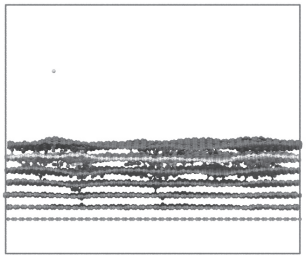

Fig.2 Schematic illustration of simulation 2

[1] K. Miyazawa, M. Yoshitake, Y. Tanaka, Journal of Nanoparticle Research **19**, 6 (2017).
[2] S. Kattel, G. Wang, *et al*., J Chem Phys **141** (2014).
[3] K. Okazaki-Maeda, Y. Morikawa, S. Tanaka, M. Kohyama, Surface Science **604** (2018).

Corresponding Author: Takahiro Yamamoto
Tel&Fax +81-3-5876-1486,
E-mail: takahiro@rs.tus.ac.jp

2P-26

Transport properties of armchair graphene nanoribbons

○ M. S. Islam, N. T. Hung, A. R. T. Nugraha, R. Saito
Department of Physics, Tohoku University, Sendai 980-8578, Japan

Graphene nanoribbons (GNRs) are one-dimensional materials, which have promising applications in nanoelectronic and optoelectronic devices [1]. The energy bandgaps (E_g) of armchair graphene nanoribbons (AGNRs) are inversely proportional to their ribbon widths [2]. The experiment showed the same E_g for both undoped and boron-doped 7-AGNR, around 2.3 eV [3, 4]. Recently, Y. Wu et al. reported that the GNRs with larger E_g family are more suitable for nanoscale device application [5]. Moreover, Z. Chen et al., found that the resistivity of GNRs increase with decreasing ribbon width in the graphene nanoribbon field-effect transistor (GNRFET) [6]. However, we expect that the electronic band structures and carrier concentration not only depend on ribbons width but also depend on doping. For making advanced electronic devices, the key factor is the ability to modulate the energy band structure and carrier concentration of AGNRs, by doping with p-type or n-type dopant heteroatoms at a specificed position in the nanoribbon [7]. In this study, we investigate the energy band structure of the AGNRs with position selectively doped boron and nitrogen atoms. We also simulate the current-voltage relationship for both undoped and boron and nitrogen doped AGNRs with changing ribbon width.

In order to confirm the doping effect, we theoretically calculate the energy band structures of AGNRs, with doping boron and nitrogen atoms, by using the density functional theory (DFT). The calculated result shows that the energy band structure of the AGNRs is affected by doping. The nanoribbons become metallic for doping odd number of boron or nitrogen atom and become semiconductor if we dope both boron and nitrogen atom together. For computing the transport properties of the AGNRs, we use non-equilibrium Green's function approach [8]. Our calculated results will explain the doping dependence I-V characteristics of the device as shown in Fig. 1.

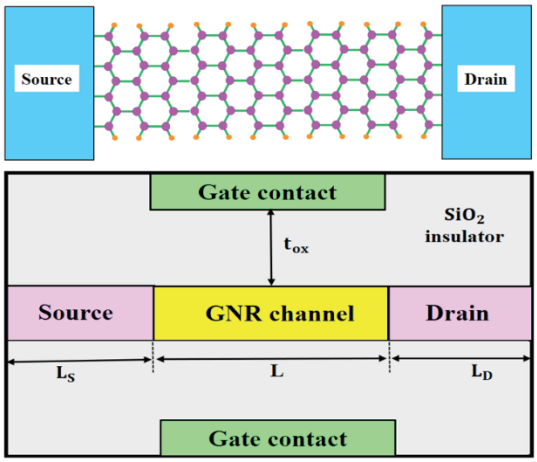

Fig. 1: Structure of simulated GNRFET

[1] A. Kimouche *et al*., Nat. Commun. **6,** 10177 (2015)
[2] Y. W. Son *et al*., Phys Rev. Lett. **97,** 216803 (2006)
[3] P. Ruffieux *et al*., ACS Nano. **6** (8), 6930 (2012)
[4] S. Kawai *et al.,* Nat. Commun. **6**, 8098 (2015)
[5] Y. Wu et al. 2014 International Conference on Anti-Counterfeiting, Security and Identification (ASID), Macao, 2014, pp. 1-4
[6] Z. Chen et al., Physica E **40** 228 (2007)
[7] R. R. Cloke *et al.,* J. Am. Chem. Soc. **137**, 8872 (2015)
[8] S. Bruzzone *et al,* IEEE Transaction on Electron Devices **61**(1), 48 (2014)

Corresponding Author: Md Shafiqul Islam
E-mail: islam@flex.phys.tohoku.ac.jp

Electronic structures of porphyrin graphene nanoribbons

○Hideyuki Jippo[1], Manabu Ohtomo[1], Shintaro Sato[1], Hironobu Hayashi[2], Hiroko Yamada[2], Mari Ohfuchi[1]

[1]AI Platform Business Unit, Fujitsu Limited, 10-1 Morinosato-Wakamiya, Atsugi, Kanagawa 243-0197, Japan
[2] Graduate School of Materials Science, Nara Institute of Science and Technology (NAIST), 8916-5, Takayama-cho, Ikoma, Nara 630-0192, Japan

We propose novel graphene nanoribbons (GNRs) with metal porphyrin complexes (Porphyrin-GNRs), which can be obtained by the bottom-up GNR synthesis [1]. In this study, we investigate the electronic structures of the Porphyrin-GNRs using the first-principles calculations.

Figure 1 shows the most stable geometries for the Porphyrin-GNRs without a metal center (M) and with M = Fe. The porphyrin rings are embedded in the armchair GNR with n = 7 width (7-AGNR). The densities of states by the GGA-PBE are partially shown in Fig. 2. The band gap for the Porphyrin-GNR without M is 0.54 eV, which is quite smaller than that of 1.6 eV for the 7-AGNR. We have found that the magnetic moment is 2.07 μB and 0.00 μB for M = Fe and Ni, respectively. The band gaps also differ depending on the M. These results suggest that we can control the electronic and magnetic properties of the Porphyrin-GNRs by changing the metal center. We also discuss the electronic properties of the Porphyrin-GNRs with another periodic models of the porphyrin rings.

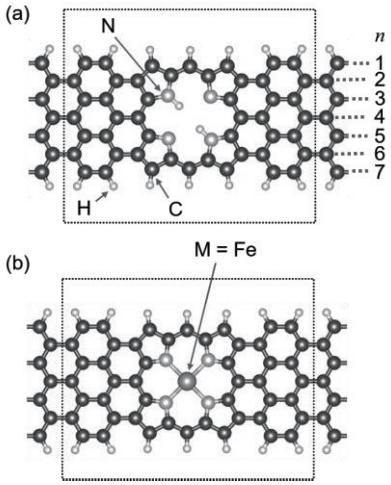

Fig. 1: Optimized geometries of Porphyrin-GNRs (a) without and (b) with a metal center. The dotted square indicates the unit cell.

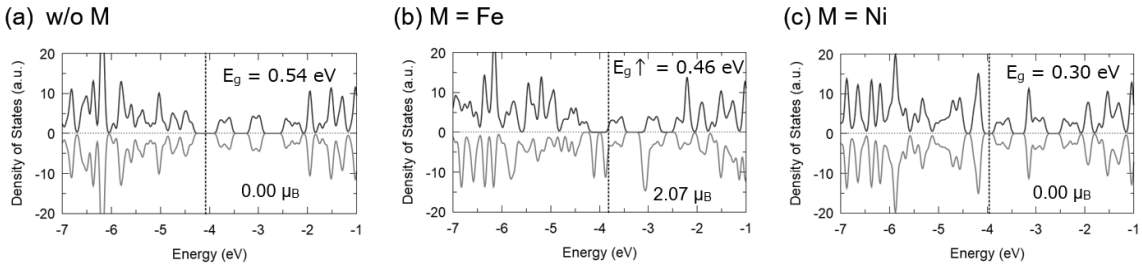

Fig. 2: Density of states (DOS) for Porphyrin-GNRs (a) without and (b)(c) with metal centers (M). The DOS for the up and down spins are shown in positive and negative values, respectively.

This work was partly supported by JST, CREST (No. JPMJCR15F1).
[1] J. Cai *et al*., Nature 466, 470 (2010).
Corresponding Author: H. Jippo, Tel: +81-46-250-8843, E-mail: jippo.hideyuki@jp.fujitsu.com

Electrostatic properties of graphene nanoribbons under an external electric field

Yoshimasa Omata, Susumu Okada

Graduate School of Pure and Applied Sciences, University of Tsukuba, Tsukuba 305-8571, Japan

Graphene and its derivatives have been attracting much attention as emerging materials for various functional devices because of their unique geometric and electronic structures. Graphene nanoribbons (GNRs) are one of representative examples of such materials for electronic and spintronic devices, because of their tunable electronic structure by controlling its width and edge shapes. For the electronics application, it is mandatory to corroborate electronic properties of GNRs under the electric field in terms of the carrier accumulations. Thus, in this work, we aim to investigate the electronic structure of GNRs under the external electric filed in terms of their width, edge shapes, and stacking arrangements, using the density functional theory with the effective screening medium method.

Figure 1 shows the contour plots of the electrostatic potential of bilayer armchair GNRs with AB-stacking arrangement. The electrostatic potential exhibits asymmetric feature with respect to the carrier species. For the hole injection, electric filed concentrate at the interlayer region, indicating that the carriers are accommodated in π electron states. In contrast, for the electron doping, the field is concentrated at the edge atomic site, indicating that the electrons are injected into σ electron states, even though the edge atomic sites do not possesses dangling bond states.

(a) (b)

Fig. 1 Contour plots of the electrostatic potential of the bilayer a GNRs with AB stacking arrangement under the electric filed injecting excess (a) 0.1h and (b) 0.1e. The gray circles denote C atoms.

Corresponding Author: S. Okada
Tel: +81-29-8535921
E-mail: sokada@comas.frsc.tsukuba.ac.jp

Kinetics of hydrazine molecular adsorption with Ethanol solution on mono-layer MoS_2

◯N.Kodama[1], Y.Ishiguro[2], K.Takai[1,2]

[1]*Graduate school of Science and Engineering, Hosei University, Tokyo 184-8584, Japan*
[2]*Department of Chemical Science and Technology, Hosei University, Tokyo 184-8584, Japan*

Electronic properties of 2D-materials is easily controlled by using solution-based dopant. A tunable electron doping by hydrazine aqueous is known for graphene thorough the precise controlling of the hydrazine concentration and the adsorption time [1, 2]. On mono-layer MoS_2, hydrazine aqueous also injects electron carrier but the presence of water causes hole doping [3]. In this study, mono-layer MoS_2 adsorbed with hydrazine solved in ethanol without water is investigated in terms of the comparison with the doping by aqueous solution.

Hydrazine solution was dropped on MoS_2 mono layer prepared by mechanical exfoliation on 90 nm SiO_2/Si substrate, followed by drying by air blow and immediate Raman and PL measurements with an excitation wavelength of 532 nm at room temperature. The same operation was repeated while varying the adsorption time or concentration of hydrazine.

On mono-layer MoS_2, the A_{1g} mode of Raman spectrum is sensitive to carrier doping. As shown in Fig.1, that peak position of A_{1g} mode red-shifts and the kinetics of doping is shorter with 10 % water-solution than 1 % one, indicating good tunability of kinetics by the hydrazine aqueous concentration. However the hydrazine aqueous adsorption is accompanied with the competition between electron doping by hydrazine and hole doping by oxygen in ambient atmosphere [3]. With ethanol-solution, hydrazine causes similar behavior to hydrazine in water solution and the kinetics of doping is shorter than water solution as shown in Fig.2. Moreover, PL results prove that hydrazine causes electron doping. Although the quantity of shift is different, no significant differences are observed in the kinetics of doping between 1 % hydrazine/ethanol-solution and 1 % water with 1% hydrazine/ethanol-solution. So using ethanol solution makes clear the behavior of hydrazine molecular adsorption on mono-layer MoS_2 that is unsure with aqueous solution.

This project was supported by JSPS and RFBR under the Japan - Russia Research Cooperative Program.

[1] Z.Chen *et al.*, *APPLIED PHYSICS LETTERS* 106, 091602 (2015), [2] T.Umehara *et al.*, FNTG (2015), [3] N.Kodama *et al.*, FNTG (2018)

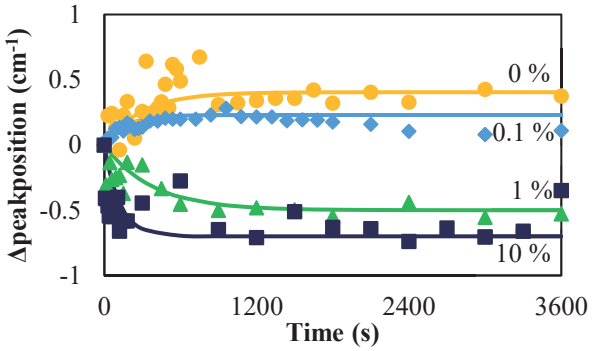

Fig.1 Kinetics of the quantity of peak position changing for A_{1g} peak on mono-layer MoS_2 adsorbed with water solution of hydrazine

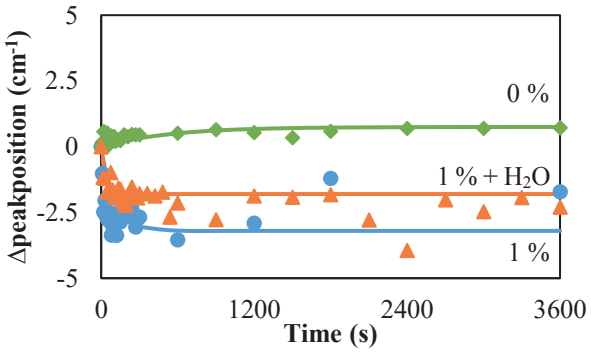

Fig.2 Kinetics of the quantity of peak position changing for A_{1g} peak on mono-layer MoS_2 adsorbed with ethanol solution of hydrazine

Corresponding Author: Kazuyuki Takai
Tel: +81-42-387-6138, Fax: +81-42-387-7002
E-mail: takai@hosei.ac.jp

Exciton polarizability and renormalization effects for optical modulation in monolayer semiconductors

○Jiang Pu[1], Keichiro Matsuki[2], Leiqiang Chu[3], Yu Kobayashi[4], Shogo Sasaki[4]
Yasumitsu Miyata[4], Goki Eda[3], and Taishi Takenobu[1,2]

[1]*Department of Applied Physics, Nagoya Univ., Nagoya 464-8603, Japan*
[2]*Department of Advanced Science and Engineering, Waseda Univ., Tokyo 169-8555, Japan*
[3]*Physics Department, National Univ. of Singapore, Singapore 117542, Singapore*
[4]*Department of Physics, Tokyo Metropolitan Univ., Tokyo 192-0397, Japan*

The strong quantum confinement in monolayer transition metal dichalcogenides (TMDCs) offers prominent optical modulation capability mediated by enhanced many-body interactions [1]. For example, the quantum-confined Stark effect (QCSE) has been demonstrated [2]. However, the excitons are typically insensitive to out-of-plane electric field because of tight confinement in vertical direction, so that inducing intense electric field is indispensable for yielding large QCSE. Another key approach is carrier doping effects, which is mainly derived from the interplay between the decrease of binding energy of excitons (blue-shifts) and bandgap renormalization effects (red-shifts) [3]. Thereby, the co-existence of these tunable many-body effects dominates optical transitions under carrier accumulations. In particular, bandgap renormalizations should be dominant to induce pronounced red-shifts of optical transitions at high carrier density regimes. This means the wide-range and continuous control of material carrier density is necessary to reveal the doping effects in optical modulations. Here, we combine electrolyte-gating method with high-quality CVD-grown monolayers to investigate the electric-field- and carrier-density-dependent luminescence properties.

The monolayer WS_2 and MoS_2 were grown on graphite *via* CVD process, followed by spin-coating ion-gel films, gelation of ionic liquids, to build electric double layer capacitors. (Fig 1a) [4]. As increasing voltage applications, the photoluminescence of WS_2 initially shows slight a quadratic red-shift of exciton resonance (~ 1 meV) without carrier accumulations, which is dominantly caused by the QCSE. Interestingly, a larger red-shift up to 10 meV is obtained followed by carrier density accumulation above 10^{13} cm^{-2}, arising from primal contributions of the doping-induced bandgap renormalizations (Fig. 1b). The observation of crossover from QCSE to many-body effects mediated optical tuning provides a comprehensive scheme in the use of TMDCs for light modulations. To further inspire our approach, we also introduce electrolyte-based TMDC light-emitting devices. Just biasing to electrolyte-induced p-i-n junctions, we can achieve red-shifts up to 40 meV for exciton and trion electroluminescence. Our results reveal the doping effects in high carrier density regimes provide significant optical modulation ability in monolayer semiconductors.

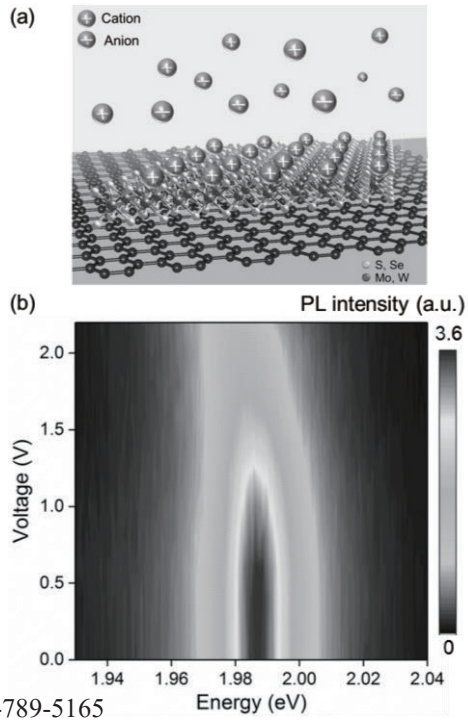

[1] Z. Sun, *et al*. *Nat. Photon.* **10**, 227 (2016)
[2] J. G. Roch, *et al*. *Nano Lett.* **18**, 1070 (2018)
[3] L. Meckbach, *et al*. *Appl. Phys. Lett.* **112**, 061104 (2018)
[4] Y. Kobayashi, *et al*. *ACS Nano* **9**, 4056 (2015)

Corresponding Author: J. Pu, T. Takenobu
E-mail: jiang.pu@ngoya-u.jp, takenobu@nagoya-u.jp, Tel/Fax: +81-52-789-5165

Development of molecular beam epitaxy for preparation of transition metal dichalcogenide atomic layers and their heterostructures

○Koki Terashima[1], Yuya Murai[1], Takato Hotta[1], Kenji Watanabe[2], Takashi Taniguchi[2], Hisanori Shinohara[1] and Ryo Kitaura[1]

[1] Department of Chemistry, Nagoya University & Institute for Advanced Research, Nagoya 464-8602, Japan, [2] National Institute for Materials Science, Tsukuba 305-0044, Japan

Two-dimensional (2D) materials, in particular, 2D-materials-based heterostructures have been attracting a great deal of attention. Recent research on superconductivity in bilayer graphene have clearly demonstrated that interlayer interactions in heterostructures can lead to properties that are drastically different from those of isolated monolayers[1]. To explore the emergence of novel properties in heterostructures, the important is to develop highly-controllable crystal growth method for 2D materials. For this purpose, we have focused on molecular beam epitaxy (MBE) method[2]. In MBE, you can supply sources as molecular beams, which can abruptly be on/off by the simple shutter operation. The supply of sources can be slow down to sub-monolayer per hour, which enables us to control, in principle, growth of 2D materials at atomic-level. In this work, we have focused on development of a MBE setup with a stable low-intensity, ~ 1 monolayer/hour, metal beam for the possible various heterostructures.

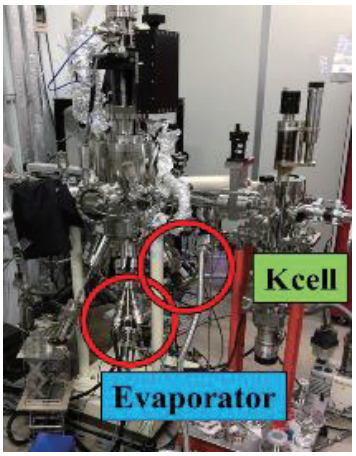

Fig.1 a photograph of our MBE setup.

Figure 1 shows a photograph of our MBE setup. Using the evaporator shown in the figure, we have successfully supply Mo with supply rate of ~ monolayer/hour. Figure 2(a), (b) shows a photograph and AFM image of $MoSe_2$ grown on a sapphire substrate and a hBN flake. As shown clearly, a large-area film and triangular crystals of $MoSe_2$ can be grown on a sapphire and hBN substrate, respectively. In the presentation, we will also address our recent work on growth of heterostructures.

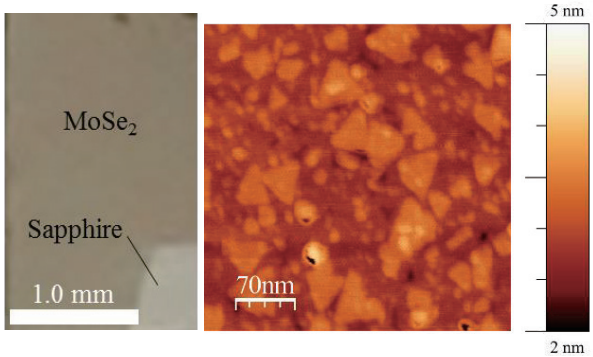

Fig.2(a) a photograph of $MoSe_2$ grown on a sapphire (b) an AFM image of $MoSe_2$ grown on a hBN flake.

Corresponding Author: R.Kitaura and H.Shinohara Tel: +81-52-789-2477, Fax: +81-52-747-6442

E-mail: r.kitaura@nagoya-u.jp and noris@nagoya-u.jp

[1] Y. Cao, *et al*, ***Nature***, 556, (2018).

[2] A. Y. Cho and J. R. Arthur, Prog. ***Solid State Chem***., 10, 157 (1975).

Single-layer MoS_2 as large voltage generator driven by liquid motion

○Adha Sukma Aji[1], Ryohei Nishi[1], Hiroki Ago[2], Yutaka Ohno[1]

[1] *Institute of Materials and Systems for Sustainability (IMaSS), Nagoya University, Nagoya 464-8601, Japan*
[2] *Global Innovation Center (GIC), Kyushu University, Fukuoka 816-8580, Japan*

Nowadays, large demand for clean energy drives researchers to find a new sophisticated way to extract the energy from clean source. In particular, the direct energy extraction from water is preferable due to its abundant availability. Recently, several examples of energy generation from liquid motion on top of two-dimensional (2D) materials (e.g., graphene) have been demonstrated.[1,2] However, due to small generated voltage resulted by using graphene, another approach is needed to gain a larger voltage. Here, we present an innovative method to increase the generation voltage by using single-layer MoS_2. The results show that single-layer MoS_2 could generate a large voltage over 5 V which is larger than the reported graphene-based generators mentioned above.

First, the large-area single-layer MoS_2 was synthesized by chemical vapor deposition method (CVD) using MoO_3 powder and sulfur powder on a c-plane sapphire substrate. Then, the as-synthesized MoS_2 was transferred onto a flexible polyethylene naphthalate (PEN) substrate. Next, 50 μL of 1 M NaCl droplets were dropped onto the MoS_2 sample that was inclined at 45º as shown in Fig. 1a. The generated voltage over 5 V, shown in the shaded area in Fig. 1b, was obtained as the water glided on hydrophobic MoS_2 surface. Furthermore, the generated power was also measured by connecting the system with load resistance. As shown in Fig. 1c, we found out that single-layer MoS_2 could generate power up to 1.75 nW from a small volume of a liquid droplet. Some improvements are required in the future to increase the generated power, such as by doping the materials or optimizing the liquid ion concentration.

In conclusion, we have demonstrated that single-layer MoS_2 film is a promising material for harvesting energy from the dynamics of water as renewable energy source.

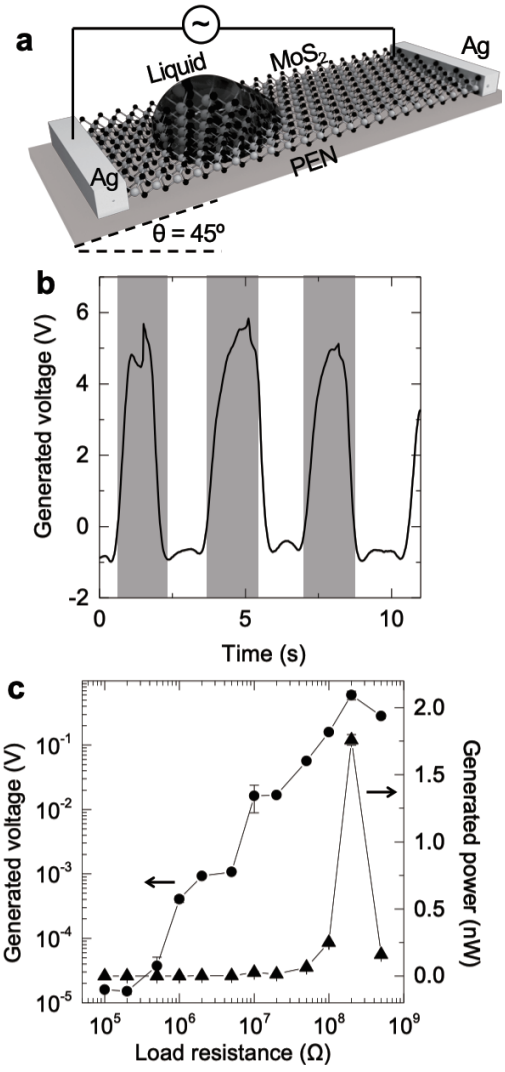

Fig. 1. (a) Schematic view of the device. (b) Generated voltage induced by liquid movement on MoS_2. (c) Generated voltage and power induced by liquid movement under different value of load resistance.

[1] J. Yin *et al*., *Nat. Nanotechnol*. **9**, 378 (2014).
[2] S. Kwak *et al.*, *ACS Nano* **10**, 7297 (2016)

Corresponding Author: Y. Ohno
Tel & Fax: +81-52-789-5387
E-mail: yohno@nagoya-u.jp

Acknowledgment: JST/CREST (JPMJCR16Q2)

2P-33

The spin angular momentum of surface plasmon in 2D material

M. Shoufie Ukhtary, Riichiro Saito
Department of Physics, Tohoku University, Sendai 980-8578, Japan

Surface plasmon (SP) is electromagnetic (EM) wave propagating on the surface of a material with carrying "spin angular momentum (SAM)", which gives torque and force to nano particle placed near the surface. SP is interesting due to the potential applications, such as optical switching devices, biosensors and wave guide based on the excitation of SP. The strength of EM field decays in the perpendicular direction to the surface, making the SP confined. The decaying of EM field gives the phase difference between in plane and perpendicular components of electric field, which is responsible for the emergence of unique spin angular momentum (SAM) of the SP due to the rotation of electric field [1,2]. This SAM is unique since it is transverse to the direction of propagation of the SP, in contrast to the SAM of the freely propagating circular polarized wave whose SAM is parallel to the direction of propagation [1]. Interestingly, the SAM of SP exerts torque, which spins the nanoparticle close to the surface of material [Fig. (a)]. The SAM can be observed experimentally by measuring this torque [1,2].

It is reported that the magnitude of SAM of SP on the surface of bulk metal depends on the frequency. However, it is not tunable for fixed frequency of SP. In this work, we investigate how to tune the magnitude of SAM of SP in 2D material, such as graphene, by controlling the properties of 2D material, such as the Fermi energy. The tuning of the Fermi energy can be done by using gate voltage. We show that the total magnitude of SAM decreases as a function of frequency and increases with the increasing Fermi energy [Fig. (b)], however, the magnitude of SAM per a plasmon is relatively constant. The torque exerted on the nanoparticle close to the surface of 2D material is also tunable by the Fermi energy. In this work, we also investigate how the SP obtains the SAM during the excitation by light, which is important to understand the physical origin of SAM of the SP.

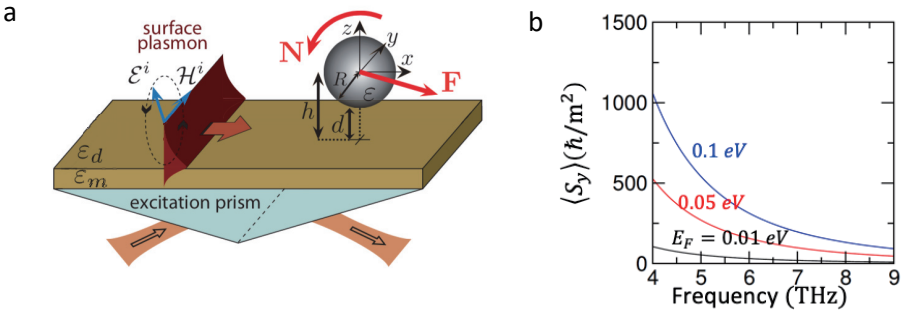

(a) The SAM of SP "spins" the nanoparticle, in which "N" and "F" denote, respectively, torque and force due to the SP [2] (b) The total SAM as a function of frequency for some values of the Fermi energy.

References:
[1] Bliokh et al. Nat. Comm. 5(1), 1825. (2014)
[2] Durand et al, PRA 89, 033841, (2014)

Corresponding Author: M. Shoufie Ukhtary,
Email:shoufie@flex.phys.tohoku.ac.jp

Growth dynamics of hexagonal boron nitride on Ni-Fe alloy catalysts

○Yuki Uchida[1], Kenji Kawahara[2], Masato Akiyama[1], Shigeto Yamasaki[1], Masatoshi Mitsuhara[1], Hiroki Ago[1,2,3]

[1] IGSES, Kyushu University, Fukuoka 816-8580, Japan, [2] Global Innovation Center (GIC). Kyushu University, Fukuoka 816-8580, Japan, [3] JST-CREST

Hexagonal boron nitride (h-BN) has been widely used as an insulating layer to obtain intrinsic properties of various 2D materials due to its atomically smooth and dangling bond-free surface with low polarizable surface optical phonons [1-3]. Recently, we have achieved uniform growth of multilayer h-BN on a Ni-Fe alloy film deposited on a spinel ($MgAl_2O_4$) (100) substrate using borazine ($B_3N_3H_6$) feedstock [4]. However, the growth mechanism of multilayer h-BN was not clearly understood, and expensive and small spinel substrates limited practical applications of the CVD-grown multilayer h-BN.

In this study, we investigate the growth mechanism of multilayer h-BN using Ni-Fe films supported on single-crystalline sapphire (α-Al_2O_3) substrates, because sapphire is cost-effective substrate with large available size. We studied different sapphire substrates with r-, a-, and c-planes. As shown in Figure 1a-c, the growth of uniform and continuous multilayer h-BN was observed on the Ni-Fe/r-plane sapphire, while the Ni-Fe/c-plane sapphire gave low-density, isolated h-BN grains. Figure 1d,e shows crystal plane maps of the Ni-Fe films measured before and after the borazine supply. The Ni-Fe film on c-plane sapphire, which did not give uniform h-BN film, showed a fcc(111) plane throughout the process (Fig. 1e). In contrast, the Ni-Fe film deposited on r-plane sapphire showed the drastic change from polycrystalline to fcc(111) by the introduction of borazine (Fig. 1d). It is interesting that such structural change occurred in 1 min. We speculate that the polycrystalline Ni-Fe film stimulates the dissolution of B and N atoms and the structural conversion to fcc(111) is accompanied with the segregation of uniform h-BN. Our engineered catalyst will allow to produce large-area h-BN with relatively low cost for stimulating various practical applications.

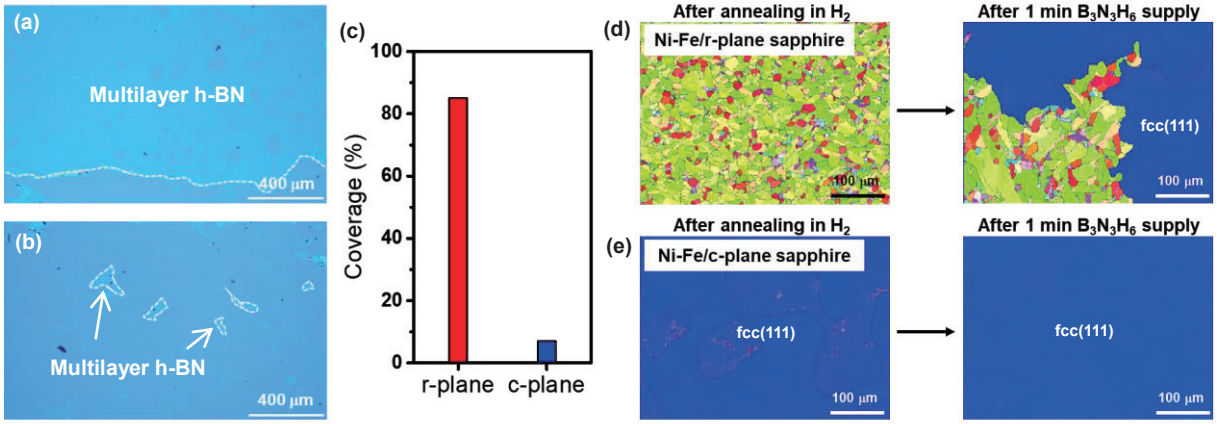

Fig. 1 Optical micrographs of h-BN grown on Ni-Fe/r-plane (a) and c-plane (b) sapphire measured after the transfer on SiO_2/Si. (c) h-BN coverages on each catalyst determined by optical micrographs. EBSD images of Ni-Fe/ sapphire r-plane (d) and c-plane (e) measured before and after the 1-minute borazine supply.

[1] C. R. Dean *et al., Nat. Nanotechnol.*, **5**, 722 (2010). [2] M. Okada *et al., ACS Nano*, **8**, 8273 (2014). [3] X. Cui *et al., Nat. Nanotechnol.,* **10**, 534 (2015). [4] Y. Uchida *et al., ACS Nano,* **12**, 6236 (2018).

Corresponding Author: H. Ago, Tel&Fax: 092-583-8852, E-mail: h-ago@gic.kyushu-u.ac.jp

Growth of monolayer chalcogenide nanoribbons and their heterostructures

○Yu Kobayashi[1], Zheng Liu[2], Toshifumi Irisawa[3], Yutaka Maniwa[1], Yasumitsu Miyata[1]

[1] *Department of Physics, Tokyo Metropolitan University, Hachioji, Tokyo 192-0397, Japan*
[2] *Inorganic Functional Materials Research Institute, National Institute of Advanced Industrial Science and Technology (AIST), Nagoya, Aichi 463-8560, Japan*
[3] *Nanoelectronics Research Institute, National Institute of Advanced Industrial Science and Technology (AIST), Tsukuba, Ibaraki 305-8568, Japan*

Transition metal dichalcogenides (TMDCs) have attracted much attention owning to their unique physical properties and potential applications. To take advantage of these potentials, it is important to develop a controlled growth process of various TMDC-based nanostructures such as nanoribbons (NRs) and superlattices. Here, we report the direct growth of monolayer $MoSe_2$ NRs and ribbon-templated heterostructures by using metal-organic chemical vapor deposition. As shown in Fig. 1a and b, the $MoSe_2$ NR with width of approximately 40 nm was successfully synthesized by controlling selenium-metal flux ratio. Electron microscope observations reveal that the $MoSe_2$ NRs correspond to twinned crystals with metal zigzag edges. This structure is completely different from the single-crystal $MoSe_2$ NRs reported previously [1]. Furthermore, we have demonstrated the fabrications of ribbon-based in-plane heterostructures of $WSe_2/MoSe_2$ and $MoS_2/MoSe_2$ by using $MoSe_2$ NRs as a template (Fig. 1c). Our findings would provide a useful way to create novel one-dimensional TMDC nanostructures and their hybrid systems.

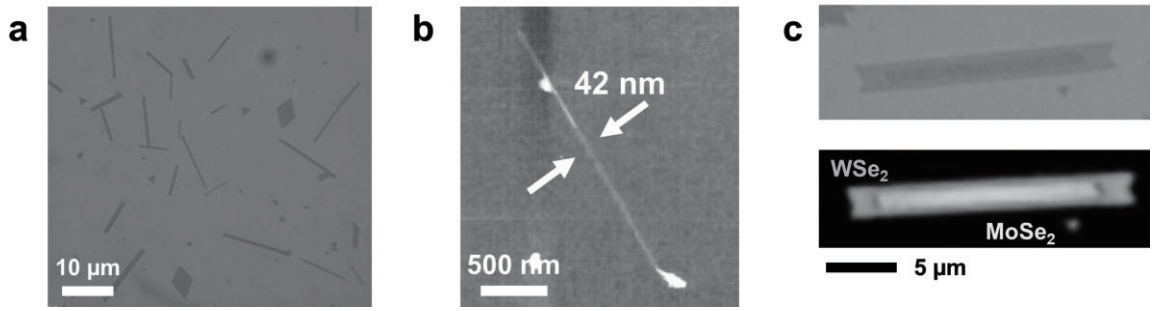

Fig.1 (a) Optical microscope and (b) atomic force microscope images of monolayer $MoSe_2$ nanoribbons grown on a SiO_2/Si substrate. (c) Optical microscope image (top) and photoluminescence (PL) intensity map (bottom) of $WSe_2/MoSe_2$ ribbon-shaped in-plane heterostructures. In the PL intensity map, blight and dark gray correspond to the PL intensities of monolayer $MoSe_2$ and WSe_2, respectively.

[1] Y. Chen *et al*. Nat. Commun. **8**, 15135 (2017).

Corresponding Author: Y. Miyata
Tel: +81-42-677-2508
Fax: +81-42-677-2483
E-mail : ymiyata@tmu.ac.jp

Phosphorescence Spectra of Cyanopolyyne $HC_{11}N$

Urszula Szczepaniak[1], Tsukumi Higashiyama[2], Ryoske Sata[2], Hal Suzuki[2],
Yusuke Morisawa[1], ○Tomonari Wakabayashi[2]

[1]*IRsweep AG, Laubisrütistrasse 44, Stäfa 8712, Switzerland*
[2]*Department of Chemistry, Kindai University, Higashi-Osaka, Osaka 577-8502, Japan*

Cyanopolyynes are known for their radio-frequency detection in the interstellar space in the late 70's. Molecules up to HC_9N have been identified, while the observation of $HC_{11}N$ in the molecular cloud TMC-1 [1] was recently negated [2]. Very recently, phosphorescence spectra were observed for cyanopolyynes, HC_5N, HC_7N, and HC_9N, in cryogenic matrices [3-5]. In this work, phosphorescence spectra were detected for the longer cyanopolyyne molecule of $HC_{11}N$ in solid matrices of acetonitrile at 20 K.

The sample molecule, $H(C{\equiv}C)_5C{\equiv}N$, was produced by laser ablation of graphite in liquid acetonitrile, and isolated by using HPLC techniques [6]. The solution containing $HC_{11}N$ in acetonitrile was co-condensed on a copper slab cooled at 20 K in vacuum. The solid matrix sample was irradiated with the second harmonics of OPO laser (GWU VersaScan, 215−300 nm) to record optical emission spectra on a polychromator with a CCD array detector (Acton SP308i, SPEC10).

Dispersed phosphorescence spectra of $HC_{11}N$ in solid acetonitrile at 20 K show vibrational progression, $0-\nu$ (ν = 0−2), at 644, 745, and 886 nm for the stretching mode, which is characteristic of the *sp*-carbon chain (Fig. 1). The phosphorescence lifetime was ~7.5 ms for the $a^3\Sigma^+ \rightarrow X^1\Sigma^+$ transition. The excitation spectra of $HC_{11}N$ in the UV region (Fig. 2 top) is comparable to the UV absorption spectra of the molecule in solution at ambient temperature.

[1] M. B. Bell *et al.* Astrophys. J. **483**, L61 (1997). [2] R. A. Loomis *et al.* Mon. Not. Roy. Astron. Soc. **463**, 4175 (2016). [3] M. Turowski *et al.* J. Chem. Phys. **133**, 074310 (2010). [4] I. Couturier-Tamburelli *et al.* J. Chem. Phys. **140**, 044329 (2014). [5] U. Szczepaniak *et al.* J. Phys. Chem. A **121**, 7374 (2017). [6] T. Wakabayashi *et al.* Carbon **50**, 47 (2012).

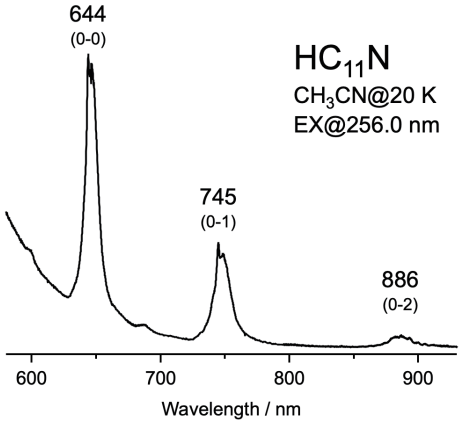

Fig. 1. Phosphorescence spectra of $HC_{11}N$.

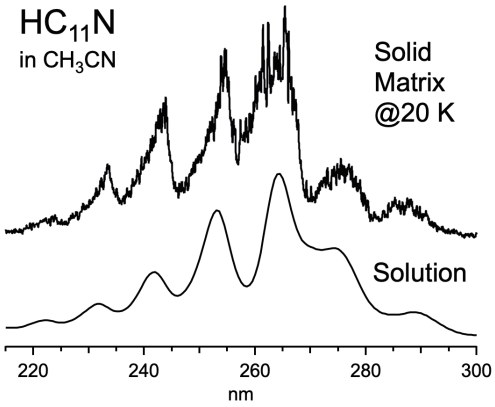

Fig. 2. Phosphorescence excitation spectra at 20 K (top) and absorption spectra in solution (bottom) of cyanopolyyne $HC_{11}N$ in acetonitrile.

Corresponding Author: T. Wakabayashi
Tel: +81-4307-3408, Fax: +81-6723-2721,
E-mail: wakaba@chem.kindai.ac.jp

Electrochemical characterization of CVD-grown graphene films for glucose biofuel cells

○Keishu Miki, Akihiro Kato, Takeshi Watanabe, and Shinji Koh

Department of Electrical Engineering and Electronics,
Aoyama Gakuin University, Sagamihara 252-5258, Japan

Enzyme-based biofuel cells are an attractive alternative to conventional fuel cell technology for portable power sources and in medical implantable device applications. In a development of biofuel cells, designing electrode/biomolecules interface is extremely important to achieve the efficient electron transfer. Graphene can be expected as electrode materials for biofuel cells due to high conductivity, large surface area, biocompatibility, and its ability to interact with molecules. These excellent properties can be utilized to facilitate direct electrical contact between the redox site of the enzyme and electrode surfaces, and to immobilize the enzymes onto the electrode surfaces. In particular, we focus on chemical vapor deposition (CVD)-grown graphene sheets because their high uniformity and controllability can facilitate the evaluation of biomolecule-modified electrodes. In this study, we evaluated electrochemical properties of CVD-grown monolayer and multi-layer graphene electrodes utilizing enzymes and mediators towards biofuel cells application.

Monolayer and multi-layer graphene sheets were prepared by CVD on copper foils and transferred onto SiO_2/Si substrates via a poly-methyl methacrylate (PMMA) assisted transfer method. The transferred graphene sheets were confirmed to be monolayer and multi-layer by Raman spectroscopy. The electrochemical properties of the graphene sheets were evaluated by cyclic voltammetry (CV) measurements in 0.2 M phosphate buffer solution (PBS) containing 10 μM glucose oxidase (GOx) and 10 mM ferrocenedicarboxylic acid (FcDA) as a mediator while changing the glucose concentrations.

Figure 1 presents the cyclic voltammograms of the monolayer graphene electrode in the absence and presence of 11 mM glucose. A vivid increase in the biocatalytic current is observed at E > 0.2 V (vs. Ag/AgCl) when glucose was added. The inset of Fig. 1 shows the plots of the biocatalytic current versus glucose concentration of monolayer and multi-layer graphene electrodes at a potential of 0.7 V, in which the biocatalytic current reached a plateau at glucose concentrations higher than 50 mM, indicating the Michaelis–Menten kinetics. It should be noted that the enzyme electrode reaction could be observed even with monolayer graphene having a thickness of only one atomic layer. From these results, it is considered that monolayer graphene electrodes will be useful platform to investigate direct electron transfer (DET) mechanism at a biomolecule/electrode interface for development of efficient DET-based enzymatic fuel cells.

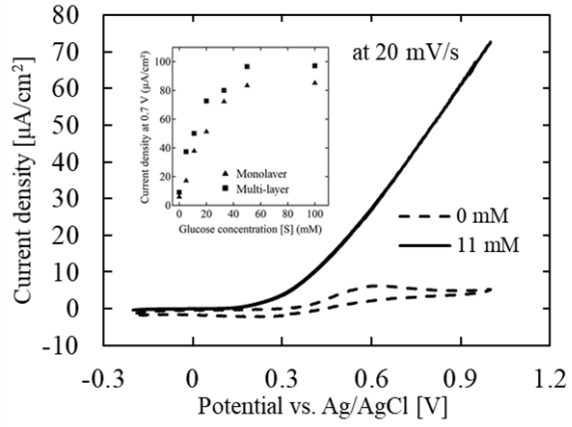

Fig.1 Cyclic voltammograms of monolayer graphene electrode. Inset: plots of the catalytic current vs. glucose concentration at E = 0.7 V.

Corresponding Author: Shinji Koh
Tel: +81-42-759-6251, Fax: +81-42-759-6251,
E-mail: koh@ee.aoyama.ac.jp

Quantification of Single-Walled Carbon Nanotubes in Mouse Feces

Mayumi Erata[1], Yuko Okamatsu-Ogura[2], Takeshi Tanaka[1], Hiromichi Kataura[1], ○Masako Yudasaka[1, 3]

[1]*Nanomaterials Research Institute, National Institute of Advanced Industrial Science and Technology (AIST), Tsukuba, 305-8565, Japan*
[2] *Department of Biomedical Sciences, Graduate School of Veterinary Medicine, Hokkaido University, Sapporo 060-0818, Japan*
[3]*Graduate School of Science and Technology, Meijo University, Nagoya 468-8502, Japan*

Single-walled carbon nanotubes (CNTs) administered in mice are reportedly shown to be excreted in feces and urines. We have been developing methods of quantifying CNTs in feces and urine by measuring optical absorption bands of CNTs extracted from feces and urine. The method proposed previously includes preparation of lysates of feces or urines and separation of CNTs by the phase transfer technique. The method has been improved to be applicable to a large amount of feces as is shown in this presentation.

The feces and urine were collected from mice after intravenous injection of PLPEG-CNTs. In the collection of feces and urines separately, metabolic cages were used. The collection time points were every 1 or 2 hours until 6 hours of post injection time (PIT), and 1-2 days, because CNTs are excreted in feces in 4-24 hours and in urines in a couple of hours of PIT.

The collected feces were immersed in an alkaline detergent (non-phosphoric acid type for removal of oil, fat, protein, hydrocarbon) for 2-3 hours and sonicated with horn-type tips for 1-2 min, obtaining feces lysates. For the separation of CNTs from the lysate, 30% KOH solution (1 mL) were added and vigorously mixed and centrifuged. As a result, cotton like floating objects were obtained at the upper area of the supernatant. Non-dissolving components from feces were fallen at the bottom via centrifuge, and the cotton like objects were sucked and put in another tube with the same amount of aq. KOH solution. After mixing, the tube was centrifuged and the liquid part was removed leaving 0.5 mL. The obtained cotton-like objects with 0.5 mL liquid was mixed with 30% KOH solution (0.5 mL), after that, isopropanol (1 mL) was poured and well mixed. After the centrifugation, the dispersion solution separated in two layers of KOH rich and isopropanol rich ones, and CNTs were precipitated at the interface of the two layers. The precipitated CNTs were taken out and its optical absorption spectra were measured. Here, when the KOH-rich lower layers were turbid, isopropanol/KOH phase transfer separation was repeated until the lower layer became clear, which was effective to lower the spectrum BG. Since the impurity peak appeared in 1000-1300 nm, the appropriate peaks for the CNT Quantification was those in 600-900 nm. The spectra were similar to that of the original one. The effect of improvements was confirmed by the CNT recovery rate of 80% in phantom experiments.

Corresponding Author: M. Yudasaka, E-mail: m-yudasaka@aist.go.jp

Platinum-catalyzed reaction of [60]fullerene with 9-Ethynyl-9*H*-fluoren-9-yl carboxylates

○Mayu Takizawa[1], Yoko Nukatani[1], Mitsuaki Suzuki[2], Yutaka Maeda [1], Michio Yamada[1]

[1] *Department of Chemistry, Tokyo Gakugei University, Koganei, Tokyo 184-8501, Japan*
[2] *Department of Chemistry, Josai University, Sakado, Saitama 350-0295, Japan*

Allenes have been recognized as valuable precursors in modern synthetic chemistry owing to the ability to undergo a variety of skeletal transformations [1]. Notably, allenes are applicable for fullerene functionalization [2], which has been a fascinating research topic in materials chemistry. It was reported that fluorenylideneallenes (Fig.1) are highly reactive and tend to dimerize easily to form isomeric mixtures of cyclobutanes even at low temperature [3]. Therefore, exploration of the applicability of fluorenylideneallenes for synthetic chemistry remains rather rare [4]. Recently, we have demonstrated that transition-metal-catalyzed reactions between [60]fullerene (C_{60}) and propargylic esters yielded formal [2+2] and [4+2] cycloadducts in reasonable yields [2d]. In that case, the formal [2+2] cycloaddition is likely to involve formation of allene intermediates via 6-*endo-dig* cyclization. This achievement motivated us to explore the reactivity of fluorenylideneallenes with fullerenes by examining the reactions of C_{60} with 9-ethynyl-9*H*-fluoren-9-yl carboxylates (**2a**–**2c**) in the presence of transition metals. In this presentation, we show that platinum-catalyzed reactions of C_{60} with carboxylates **2a**–**2c** yield the corresponding [2+2] cycloadducts **3** in reasonable yields (Scheme 1).

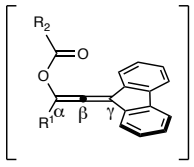

Fluorenylideneallene

Fig.1 Structure of fluorenylideneallene.

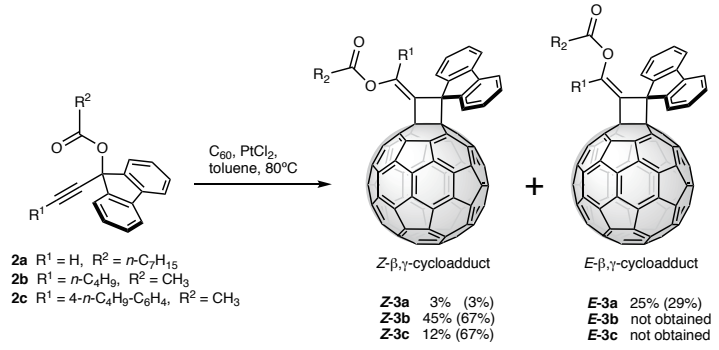

Scheme 1. Pt-Catalyzed reaction of C_{60} with **2a–2c**.

[1] *Modern Allene Chemistry, Volumes 1–2*; N. Krause, S. K. Hashmi, Eds.; Wiley-VCH: Weinheim, 2004.
[2] (a) V. Nair *et al*. Synthesis 1655 (2002). (b) B. Bildstein *et al*. Organometallics **18**, 4286 (1999). (c) M. Ueda *et al*. Chem. Commun. **52**, 13175 (2016). (d) M. Yamada *et al*. Org. Biomol. Chem. **15**, 8499 (2017).
[3] (a) Buchmeiser, M.; Schotenberger, H. Organometallics **12**, 2472 (1993). (b) Banide, E. V. *et al*. Chem. Eur. J. **12**, 32750 (2006). (c) Banide, E. V. *et al*. Eur. J. Org. Chem. 2611 (2007). Alcaide, B. *et al*. Chem. Soc. Rev. **39**, 783 (2010).
[4] (a) D. Palomas *et al*. Dalton Trans. **41,** 9073 (2012). (b) S. Qiu *et al*. Org. Lett. **18**, 6018 (2016).

Corresponding Author: M. Yamada
Tel: +81-42-329-7493, Fax: +81-42-329-7493
E-mail: myamada@u-gakugei.ac.jp

Observation of Single-Molecule Reactions Inside Individual Carbon Nanotubes

Chenmaya Xia, Juan Yang*, Henan Li, Daqi Zhang, Sheng Li,
Haoming Liu, Ruoming Li, Yan Li*

College of Chemistry and Molecular Engineering, Peking University, Beijing 100871, China

Monitoring the chemical reaction of an isolated single molecule (SM) is a long-standing challenge to understand the molecular reactivity at the most fundamental limit. The present methods of direct observation of a definite SM reaction [1,2] will inevitably interfere the target reaction. We here propose a strategy to encapsulate and isolate single molecules inside individual single-walled carbon nanotubes (SWNTs), the interior of which serves as a nanoscale confined space of inert environment to facilitate the study of SM reaction [3]. We utilize surface-enhanced Raman spectroscopy (SERS) to achieve the ultrasensitivity that can monitor the Raman fingerprints of the encapsulated single molecules as they undergo a chemical reaction. In this system, the unique 1D structure of SWNT plays important roles in facilitating SM study: The nanoscale interior (1-2 nm in diameter) allows SM encapsulation whereas the macroscale length (over 100 μm) and the excellent mechanical properties allow gold nanocrystals (AuNCs, typically 100-200 nm in edge) to deposit on the outer walls for SM detection by SERS. Our approach offers a robust and reliable method and opens new possibilities toward SM science by providing an excellent system facilitating the studies of chemistry and physics at the SM level.

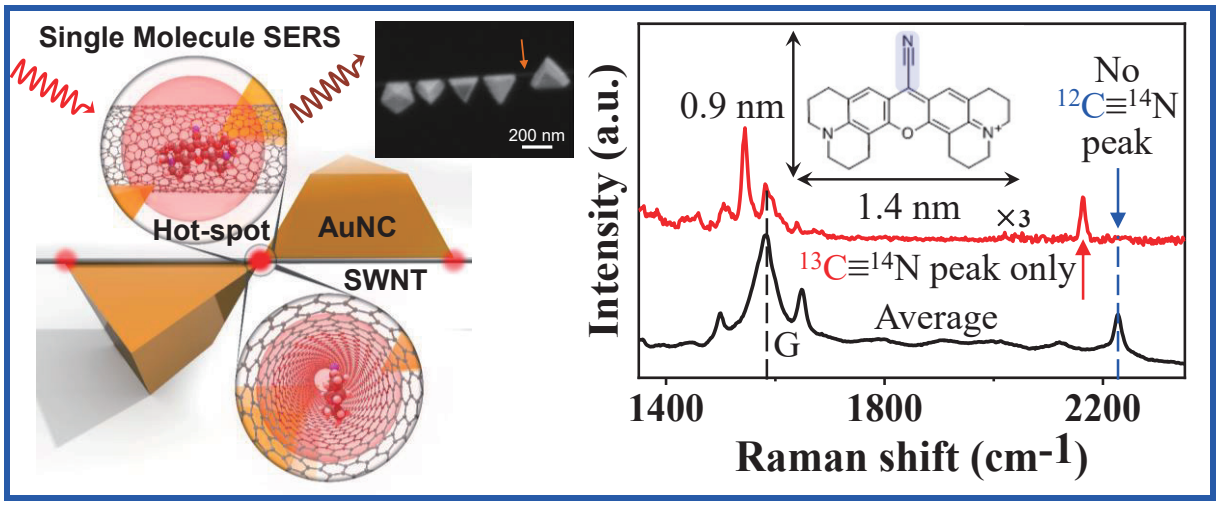

Fig.1 Schematics, SEM image and SERS spectra of the AuNCs-SWNT nanocomposite with a single rhodamine 800 molecule encapsulated inside the SWNT and located at the hot spot.

[1] K. C. Neuman, A. Nagy, Nat. Methods **5**, 491 (2008).

[2] D. G. de Oteyza, P. Gorman, Y. C. Chen *et al.* Science **340**, 1434 (2013).

[3] J. Yang, C. Xia, H. Li *et al.*submitted.

Corresponding Author: J. Yang

Tel: +86-10-62755357

E-mail: yang_juan@pku.edu.cn

Solvent dependence of photoluminescence energy shifts at locally functionalized sites of single-walled carbon nanotubes

○Yoshiaki Niidome[1], Tomohiro Shiraki[1,2], Tsuyohiko Fujigaya[1,2,3,4]

[1] *Department of Applied Chemistry, Kyushu University, Fukuoka 819-0395, Japan*
[2] *WPI-I²CNER, Kyushu University, Fukuoka 819-0395, Japan*
[3] *Center for Molecular Systems, Kyushu University, Fukuoka 819-0395, Japan*
[4] *JST-PRESTO, Saitama 332-0012, Japan*

Single-walled carbon nanotubes (SWNTs) show near infrared photoluminescence (PL) that is sensitively changed by microenvironments composed of surfactants and solvent molecules [1]. Recently, the SWNTs doped with defects such as oxygen atoms and sp^3 carbon are reported, in which local functionalization is utilized [2]. The resultant locally functionalized SWNTs (lf-SWNTs) emit E_{11}* PL that has narrower band-gap energy with higher quantum yields compared to E_{11} PL of pristine SWNTs. As a characteristic of lf-SWNTs, E_{11}* PL wavelengths are modulated depending on the chemical structures of the functionalized aryl groups having different substituents [2] and proximal modification [3].

In this study, we examined microenvironment effects on the E_{11}* PL of lf-SWNTs with aryl groups having different substituents. Here, lf-SWNTs having methoxyaryl (lf-SWNT-OCH_3) and nitroaryl (lf-SWNT-NO_2) were synthesized and solubilized in D_2O containing sodium dodecylbenzenesulfonate (SDBS). To create an organic solvent microenvironment, *o*-dichlorobenzene (*o*DCB) was added and mixed. By this procedure, the *o*DCB molecules are injected into the hydrophobic domains between the tubes and the coating SDBS micelles [4].

Fig.1 shows PL spectra of synthesized lf-SWNTs-OCH_3 and lf-SWNT-NO_2, in which E_{11}* PL was observed and their wavelengths were depending on the chemical structures of the functional aryl groups, as reported [2]. After injecting *o*DCB, the PL peaks of E_{11}* were red-shifted. We found that (1) the observed energy shifts for E_{11}* PL were different from those of E_{11} PL and (2) the shifts of E_{11}* PL for lf-SWNTs-OCH_3 and lf-SWNTs-NO_2 were almost same regardless of chemical structure difference. The mechanism of these findings will be discussed based on the interactions between the functionalized sites and solvent molecules.

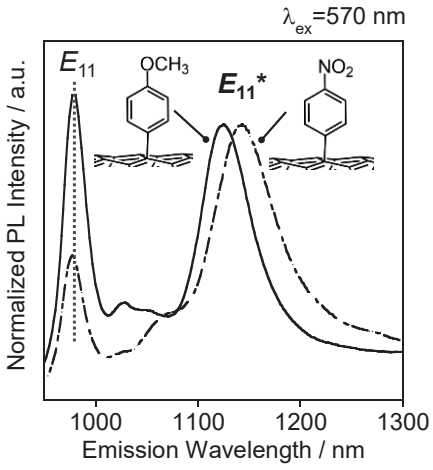

Fig. 1 PL spectra of lf-SWNT-OCH_3 (solid line) and lf-SWNT-NO_2 (dashed line) in D_2O containing SDBS.

[1] Y. Miyauchi *et al*. Chem. Phys. Lett. **442**, 394 (2007).
[2] Y. Wang *et al*. Nat. Chem. **5**, 840 (2013).
[3] T. Shiraki *et al*. Sci. Rep. **6**, 28393 (2016).
[4] K. J. Ziegler *et al*. Phys. Chem. Chem. Phys. **12**. 6990 (2010).

Corresponding Author: T. Fujigaya
Tel/Fax: +81-92-802-2842,
E-mail: fujigaya.tsuyohiko.948@m.kyushu-u.ac.jp

Low-voltage operable and stretchable carbon nanotube integrated circuits

○Yuya Nishio[1], Taiga Kashima[1], Jun Hirotani[1], Shigeru Kishimoto[1], and Yutaka Ohno[1,2]

[1]*Department of Electronics, Nagoya University, Nagoya 464-8603, Japan*
[2]*Institute of Materials and Systems for Sustainability, Nagoya University, Nagoya 464-8601, Japan*

Stretchable devices can closely contact with dynamic and free-form surfaces such as human skin, internal organs, and clothes, and they are considered to be useful for wearable biomedical applications or artificial electronic skins. Recently, formable carbon nanotube thin-film transistors (CNT TFTs) which utilize CNT thin films for the electrodes and channel have been reported. [1] However, they still have challenges such as robust electrical performance against externally applied tensile strain and the reduction of operation voltage. Moreover, stretchable integrated circuits are necessary to realize functionalities for precise and reliable wearable applications. In this work, we realized stretchable CNT integrated circuits (ICs) by introducing a local strain suppression layer.

We fabricated CNT ICs with a channel of a semiconducting CNT thin film, CNT transparent electrodes, and a 50 nm-thick Al_2O_3 gate dielectric layer on a stretchable poly (dimethylsiloxane) (PDMS) film. In order to suppress the influence of applied strain, local strain suppression layer composed of a rigid polymer with a high Young's modulus was introduced on top of the channel region.

We fabricated inverters composed of a driver transistor which controls current and a load transistor which functions as a resistor. Figure 1 shows transfer curves of a fabricated inverter drived at various supply voltages (V_{DD}'s) from -2.5 to -1 V. The inverter operated at low V_{DD} as -1 V with a gain of 5.5 dB. Moreover, negligible hysteresis was observed when $|V_{DD}|$ was less than 1.5 V. These results show that the present stretchable CNT ICs with a strain suppression layer are promising for realizing low power wearable devices.

Acknowledgments: The semiconducting CNTs used in this work was provided by TACS. This work was partially supported by JST/CREST (JPMJCR16Q2).

[1] D.-M. Sun *et al.*, *Nat. Comm.* **4**, 2302 (2013).

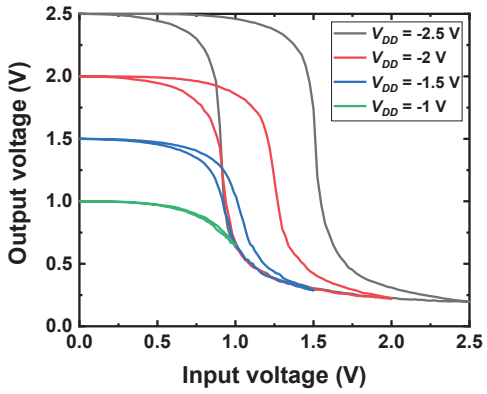

Fig. 1 Voltage transfer curves of a fabricated inverter.

Corresponding Author: Y. Ohno
Phone & Fax: +81-52-789-5387, E-mail: yohno@nagoya-u.jp

Photo-thermoelectric detection of cyclotron resonance in graphene

○Kei Kinoshita[1], Rai Moriya[1], Miho Arai[1], Satoru Masubuchi[1],
Kenji Watanabe[2], Takashi Taniguchi[2], and Tomoki Machida[1,3]

[1] *IIS, The University of Tokyo, Tokyo 153-8505, Japan*
[2] *NIMS, Ibaraki 305-0044, Japan* [3]*CREST-JST*

We demonstrate the detection of a cyclotron resonance in Landau-quantized graphene under infrared light irradiation by utilizing photo-thermoelectric effect, which is significant in graphene because of its small electron heat capacity and large thermoelectric coefficient. Since photo-thermoelectric effect contains photo-Seebeck and photo-Nernst components and their symmetry are different, we achieved the selective detection of each component by carefully tuning the symmetry of device.[1] (1) Photo-Seebeck effect generates voltage along thermal gradient created under light irradiation. To detect this, we fabricated double back-gated *h*-BN/Gr/*h*-BN device as shown in Figs. (a)(b). This creates asymmetric carrier density profile between left and right region of graphene. With the help of this asymmetric structure, we demonstrate infrared photodetection at zero-field [Fig. (c)]. (2) To detect photo-Nernst effect, a part of graphene is covered with metal mask to generate photo-induced thermal gradient perpendicular to the voltage probe as shown in Figs. (a)(b). Unlike photo-Seebeck effect, Photo-Nernst voltage was noticeable only under application of magnetic fields and its sign reversed upon a reversal of the magnetic field direction [Fig. (c)]. Importantly, both photo-Seebeck and photo-Nernst effect signal strongly enhanced at cyclotron resonance [Fig. (d)]. These results highlight possibility of high-sensitive infrared detection using photo-thermoelectric effect in graphene.

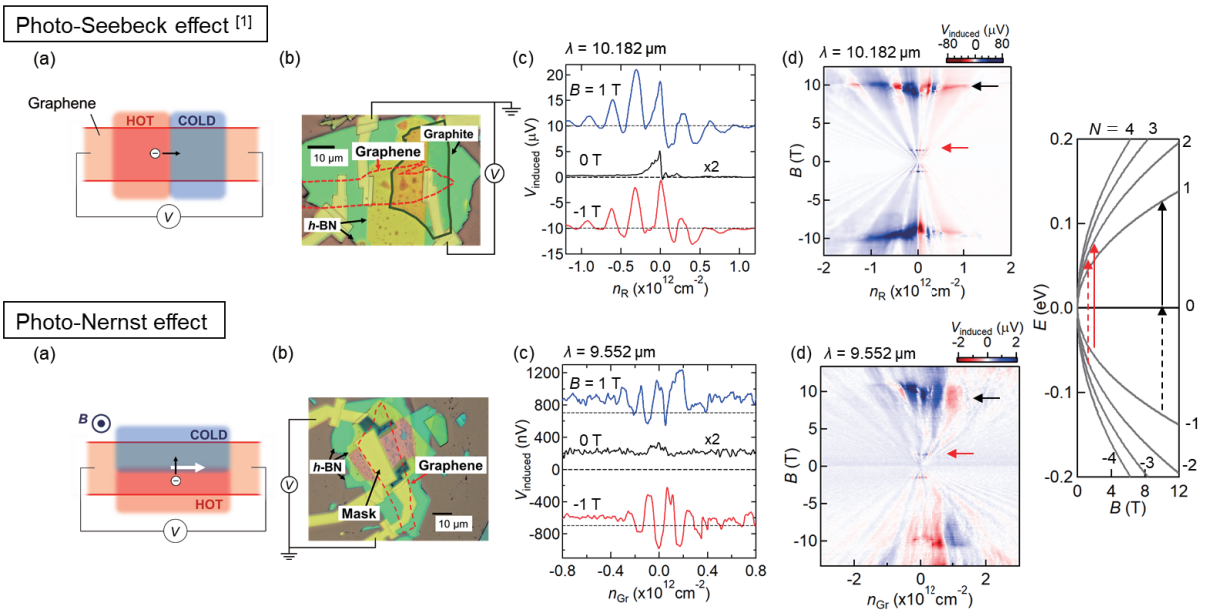

(Upper) Photo-Seebeck effect, (Lower) Photo-Nernst effect. (a) Experimental concept. (b) Optical micrograph of the device. (c) The photovoltage signal at low magnetic field. (d) Cyclotron resonance and Landau levels of graphene.

[1] K. Kinoshita *et al*. Appl. Phys. Lett. **113**, 103102 (2018). (**Selected as Editor's pick**)

Corresponding Author: K. Kinoshita
Tel: +81-3-5452-6158, Fax: +81-3-5452-6157,
E-mail: kkino@iis.u-tokyo.ac.jp

Theoretical Analysis on Thermoelectric Effects of Monolayer and Bilayer Graphene

○Hikaru Horii[1], Kenji Sasaoka[2], Takahiro Yamamoto[1,2], Hidetoshi Fukuyama[3]

[1] *Faculty of Engineering, Tokyo University of Science, Tokyo 125-8585, Japan*
[2] *RIST, Tokyo University of Science, Tokyo 125-8585, Japan*
[3] *Tokyo University of Science, Tokyo 162-8601, Japan*

Thermoelectric (TE) generation is a potential key technology for recovering energy from waste heat. Among the various potential candidates for TE materials, nanocarbon materials have attracted attention as flexible and high-performance TE materials. Most recently, Yamamoto and Fukuyama reported that the semiconducting carbon nanotubes (CNTs) exhibit high TE performance when the chemical potential μ locates near a band edge with sharp density of states (DOS) originating from its one dimensionality [1,2]. On the other hand, the monolayer graphene (MLG) cannot be expected to be high-TE performance because it has no band gap at the charge neutral point.

In this study, we focus on the bilayer graphene (BLG) since the band gap can be opened by applying the electric field perpendicular to the BLG, as shown in Fig. 1 [3]. We have calculated the Seebeck coefficient S and the power factor PF of the MLG and the BLG in the presence of vertical electric field $\boldsymbol{E}_\perp$ using the Kubo's linear response theory combined with thermal Green's function method which was recently developed [1,2]. We adopt the constant-τ approximation for self-energy due to carrier scattering [2].

We found that the values of S and PF can be controlled by changing the magnitude of $\boldsymbol{E}_\perp$. For example, we obtained $S \sim 200$ μV/K and $PF \sim 40$ mW/mK^2 when μ lies close to a band edge and the vertical electric field is $E_\perp = 4.7$ MV/cm. This is because the DOS of BLG under $E_\perp$ has a sharp peak near the band edge, which is similar to carbon nanotubes. On the other hand, in the high-energy regimes where μ is much larger than the band gap, S is inversely proportional to the chemical potential, *i.e.*, $S \propto \mu^{-1}$. The μ^{-1} behavior of BLG is similar to the case of CNTs. In contrast to S, the thermoelectric conductivity L_{12}, which is defined as the electric current density in response to the temperature gradient, shows the different μ dependence between the two-dimensional graphene and one-dimensional CNTs.

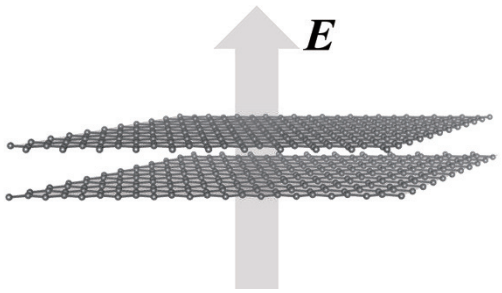

Fig. 1 Bilayer Graphene in Vertical Electric Field

[1] T. Yamamoto and H. Fukuyama, J. Phys. Soc. Jpn. **82**, 024707 (2018).
[2] T. Yamamoto and H. Fukuyama, J. Phys. Soc. Jpn. **87**, 114710 (2018).
[3] T. Ohta *et al.* , *Science* **313**, 951 (2006).

Corresponding Author: T. Yamamoto
Tel: +81-3-5876-1492
E-mail: takahiro@rs.tus.ac.jp

Topological Edge States Induced by Zak's Phase in A_3B Monolayers

Tomoaki Kameda, Feng Liu, and Katsunori Wakabayashi

Department of Nanotechnology for Sustainable Energy, School of Science and Technology, Kwansei Gakuin University, Sanda, Hyogo 669-1337, Japan

Tel: +82 79 565 9751, Fax: +81 79 565 9729 E-mail: waka@kwansei.ac.jp

Honeycomb lattice network provides a unique platform of various novel functional materials. One representation example is graphene, one atomic-thickness carbon sheet, where carbon atoms are placed on a honeycomb lattice with equal electron hopping. Here we show that in a A_3B honeycomb monolayer possessing alternating electron hopping can induce edge states in zigzag edge. These edge states have a topological origin similar to graphene, which corresponds to finite bulk charge polarization described by the Zak's phase [1,2].

A_3B is a monolayer which has eight atoms in a unit cell as displayed in Fig.1(a). There are two atomic species A and B. We calculate energy bands of A_3B zigzag nanoribbon system in Figs.1(b), using the tight-binding model and show that it has topologically protected edge states (TES). In further, we employ first-principles calculations based on the density functional theory (DFT) to search the possible materials to realize the electronic states of A_3B system. On the basis of DFT calculation, C_3N monolayer is a one of possible candidate materials possessing TES (Fig.1(c)-(e)). In addition, we confirm that the appearance of TES is owing to the Zak's phase.

We have discussed the realistic materials which can have TES originated from Zak's phase in a honeycomb lattice based on DFT. We have found that C_3N honeycomb monolayer is a possible candidate material which have TES. Our results will serve to design a new class of topological materials, especially in atomic-layer-materials.

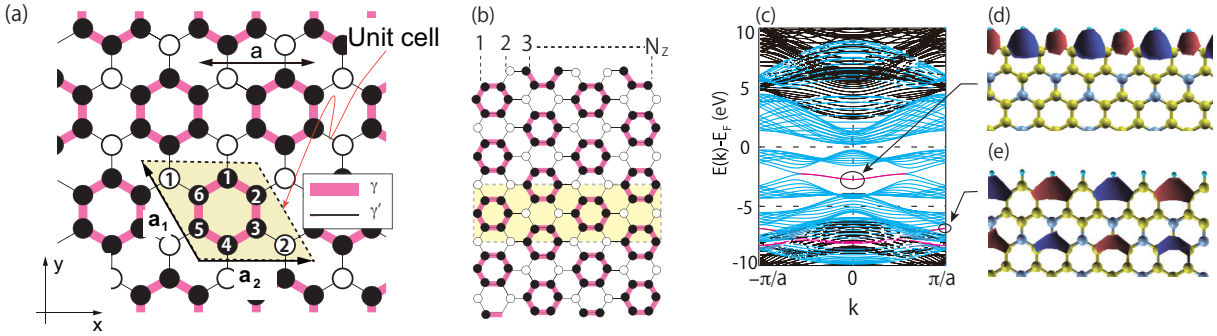

FIG. 1. (a) A_3B lattice structure. There are two atomic species A and B in a unit cell. Yellow shaded areas indicate unit cell. (b) Structure of A_3B zigzag ribbon. Thick and thin bonds represent the intracellular γ and inter-cellular γ' hopping, respectively. (c) C_3N zigzag nanoribbon energy band structure. Red and blue lines are energy dispersion for π electrons. Topological states are indicated by black circle, where two energy dispersions are degenerate. (d)(e) Wave function of TES, where electrons are localized at C_3N zigzag edge.

REFERENCES

[1] F. Liu, M. Yamamoto, and K. Wakabayashi, J. Phys. Soc. Jpn. **86**, 4 (2017).

[2] J. Zak. Phys. Rev. Lett. **62**, 2747 (1989).

High-resolution Measurement on Graphene Quantum Dots by Ion Trap Ion Mobility Measurement System

○Yudai Hoshino, Suzuka Tachi, Syota Kuwahara, and Toshiki Sugai

Department of Chemistry, Toho University, Miyama 2-2-1 Funabashi, 274-8510, Japan

Ion mobility spectrometry (IMS) has revealed novel information on nano materials[1]. However, its resolution is low so that the method has been utilized as a subsystem or a filter of the main measurement system such mass spectrometer to eliminate unnecessary samples. To improve the resolution, IMS systems with trap functions have been developed[2]. We also have been developing the ion trap ion mobility measurement system, achieving very long-term successive measurement up to seven hours and observation of quantized charges. However, the resolution is still too low to derive precise information of nano-materials. Here we present high-resolution measurement on graphene quantum dots (GQD) by an improved ion trap ion mobility system.

The system consists of several electrodes with a hole at the center, where an alternative currents with high and low frequency were applied. Ionized GQD by laser desorption ionization by a YAG laser were trapped for around an hour and were moved reciprocally by 15 mm in nitrogen gas at ambient pressure. The distance was increased by 5 times compared with the previous system of 3 mm. The movement was observed by a digital camera and the velocity and mobility were analyzed by video analyses.

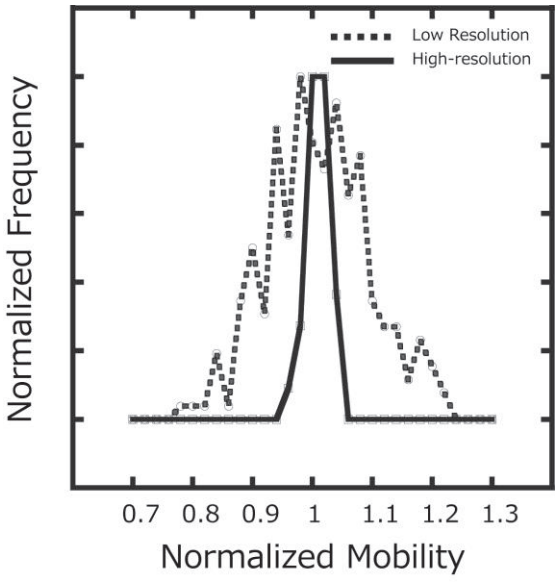

The Fig. 1 shows observed normalized mobility distribution of one particle of ionized GQD by the previous low-resolution and the present high-resolution systems. The standard deviations are 0.085 and 0.0196 showing that the resolution is enhanced by 4.3 times, which can help us to have more information on various nano materials. There still exist numbers of ways to improve its resolution. Details are going to be shown in the conference.

[1] T. Sugai *et al.*, *J. Am. Chem. Soc.* ***123***, 6427 (2001).

[2] F. Fernandez-Lima *et al.*, *J. Ion Mobil. Spec.* ***14***, 93 (2011)

TEL: +81-47-472-4406, E-mail: sugai@chem.sci.toho-u.ac.jp

Polyyne Formation from Ethylene and Acetylene by Laser Induced Breakdown

○Nobuyuki Takizawa[1], Sahr Al-Tuairqi[2], Qi Wang[2], Joseph H. Sanderson[2], Tomonari Wakabayashi[3], and Haruo Shiromaru[1]

[1]*Department of Chemistry, Tokyo Metropolitan University, Tokyo 192-0397, Japan*
[2]*Department of Physics and Astronomy, University of Waterloo, N2L 3G1 ON, Canada*
[3]*Department of Chemistry, Kindai University, Osaka, 577-8502, Japan*

In our previous study of Laser Induced Breakdown (LIB) [1], we have shown that there is a wide variation in polyyne production depending on the target molecules. In LIB, a strong electric field of tightly focused laser in gaseous media leads to a plasma formation. From the emission spectrum of the plasma and UV spectrum of the products dissolved in hexane, we found a correlation between C_2 swan band intensity and polyyne yield. Two different types of lasers were used in that study; one was a few nanosecond-pulsed Nd:YAG laser (@ TMU), and the other is an amplified Ti:Sapphire laser which generates 35 femtoseconds pulses (@ UW). They also differ in other parameters (Nd:YAG , Ti:Sapphire) , wavelength (532 nm , 800 nm), repetition rate (30 Hz, 1 kHz), pulse energy (150 mJ/pulse, 2.0 mJ/pulse), and focal length of the lens (70 mm, 80 mm), respectively.

Recently, Sun et al. revealed in their study of the crossed molecular beam experiment that the reaction of $C_{2n}H$ radicals and acetylene leads to the formation of longer polyynes [2]. In the present study, we targeted two small molecules, ethylene and acetylene, which are expected to be efficient sources of C_2 and C_2H. The experimental setup is the same as our previous study [1].

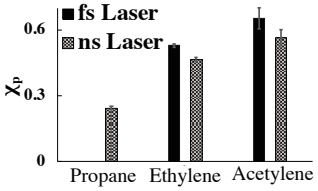

Fig. 1 χ_p value of ethylene and acetylene obtained in the present study. Propane is shown for the comparison

Figure 1 shows the efficiency of polyyne production, where χ_p is an index obtained by comparing the spectrum of the irradiated sample and ones from the size separated polyynes. It should be noted that χ_p does not have a quantitative physical meaning except being 0 and 1, but it is a measure of the preference in polyyne production. The value reached the highest in LIB with acetylene for both of ns and fs lasers. Between two lasers, fs laser gives higher values. In other words, fs laser irradiation to acetylene results in the highest selectivity of hydrogen-capped polyynes. Figure 2 (a) shows UV spectrum of the samples from ns laser (dashed line) and fs laser (solid line). As can be seen in the figure, longer polyynes are more prominent in fs laser. Figure 2 (b) shows closer look of (a) around 260 nm. It is noticeable that methyl-capped polyyne CH_3C_8H (247 nm) is produced in ns laser whereas hydrogen-capped polyyne (252 nm) is dominant in fs laser. It is considered that this contrast comes from the difference in fragmentation of molecules during LIB in two lasers. Emission spectrum of the plasma shows strong C_2 swan band in both of lasers, indicating that the efficient C_2, and most likely C_2H, formation results in the higher polyyne production.

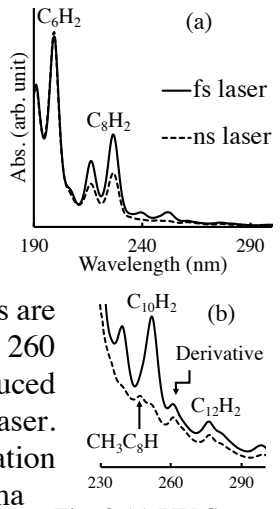

Fig. 2 (a) UV Spectra of irradiated samples and (b) the same data expanded around 260 nm. The absorbance is normalized at 199 nm (C_6H_2).

[1]. Taguchi, Y. *et al.,* Carbon, **115**, 169 (2017).
[2]. Sun, Y. L. *et al.,* J. Phys. Chem. Lett., **6**, 4117 (2015).
Corresponding Author: N. Takizawa Tel: +81-42-677-1111, Fax: +81-42-677-2525, E-mail: takizawa-nobuyuki@ed.tmu.ac.jp

Preparation of few-layered graphene using Graphite Intercalation Compounds (GICs)

○Yoshihisa Nanri[1], Hiroshi Yoshitani[2], Hiroji Fukui[2], Akira Nakasuga[2], Taro Kinumoto[1], Tomoki Tsumura[1], Masahiro Toyoda[1]

[1]Department of Applied Chemistry, Graduate School of Engineering, Oita University, 700 Dannoharu, Oita 870-1124, Japan

[2]Sekisui Chemical Co, LTD. 2-1 Hyakuyama, Shimamoto-cho, Mishima-gun, Osaka 530-8565, Japan

Introduction

Graphene exhibiting excellent conductivity and visible light transmission can be prepared using the Scotch tape method [1] or using the CVD method [2]; however, it is difficult to achieve large-scale production of graphene using these approaches. Hummers method [3] is based on the exfoliation of graphene oxide; however, it results in oxidation, which alters the characteristics of graphene oxide. In this study, few-layered graphene was prepared by adding water to the graphite intercalation compounds (GICs), which contained several planar layers of carbon-based hexagonal networks with negative charges as the reaction field. Further, GICs were exfoliated by the addition of aldehyde, which contains an electron-withdrawing substituent, thereby yielding few-layered graphene. The proposed technique facilitates the large-scale preparation of large area graphene with only a few defects. Here, we have demonstrated the fabrication of graphene by the addition of an aldehyde solution to K-tetrahydrofuran-GICs (K-THF-GICs) that were synthesized using the solution methods.

Materials and methods

A K-THF solution was prepared by dissolving naphthalene in THF and by further addition of potassium and stirring. Subsequently, K-THF-GICs were prepared by soaking the as-obtained graphite having a grain size of 100 μm in the prepared solution. Further, few-layered graphene was prepared by the addition of an aldehyde solvent (having an aromatic ring and alkyl chain of different lengths) to the K-THF-GICs and stirring. The obtained graphene was further characterized using TEM and Raman spectroscopy.

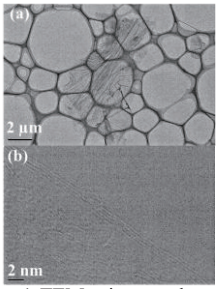

Fig. 1 TEM micrographs of graphene obtained by the exfoliation of K-THF-GICs in decanal solution.

Result and discussion

Figs. 1 (a) and (b) denote the TEM micrographs of the graphene layers of the products that have been obtained using the proposed approach with decanal. These images indicate that few-layered graphene was obtained in areas that have dozens of micrometers of thickness and that have approximately three layers of lamination. Figs. 2(a) and (b) denote the Raman spectra of the as-obtained graphite and the graphene layer products obtained using the proposed technique with decanal (i.e., the precipitate in a decanal supernatant), respectively. The graphite spectrum exhibited a two-dimensional (2D) band at around 2726 cm^{-1} while that of the product exhibited a 2D band at approximately 2693 cm^{-1}, representing a red shift of the 2D band. This observation indicates that the graphene contained five or less lamination layers. Such a red shift of the 2D band could not be confirmed in case of low wavenumbers in precipitates formed using an aldehyde solvent. Therefore, it can be concluded that it is possible to prepare few-layered graphene using decanal having long alkyl chains instead of the usage of an aldehyde solvent having aromatic rings and short alkyl chains.

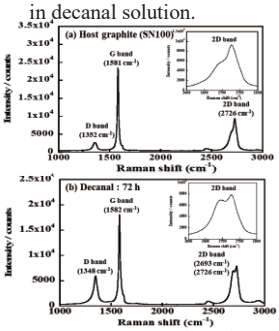

Fig. 2 Raman spectra of (a) the graphite used to prepare graphene and (b) the graphene product obtained using the proposed approach.

References

[1] K. S. Novoselov et al. “Electric field effect in atomically thin carbon films.”, Science, 306 (2004) 666-674

[2] C. M. Orofeo et al. “Influence of Cu metal on the domain structure and carrier mobility in single-layer graphene”, Carbon, 50 (2012) 2189-2196.

[3] W. S. Hummers and R. E. Offeman, “Preparation of Graphitic Oxide”, J. Am. Chem. Soc., 80 (1958) 1339.

Corresponding Author: M. Toyoda Tel/Fax: +81-97-554-7094, E-mail: toyoda22@oita-u.ac.jp

Attempt to produce dimetallofullerenes containing Yb with Ta

○Yamashita Yusuke, Kazuhiro Kobayashi, Koichi Kikuchi, Yohji Achiba, Takeshi Kodama

Department of Chemistry, Tokyo Metropolitan University, Tokyo 192-0397, Japan

Yb-containing dimetallofullerenes, $[Yb_2@C_n]^-$ and $[MYb@C_n]^-$ (M=Y,Sc), have never been obtained [1]. The reason was considered that Yb can not take a trivalent state in a fullerene cage because of its rather high ionization energy, which prevented the cage from being closed shell. Therefore, we tried to synthesize $[HfYb@C_n]^-$, because Hf can take the larger valence, +4. However, the formation of $[HfYb@C_n]^-$ could not be observed [2]. In this work, on the basis of these results, Ta was tried to be used instead of Hf, because Ta can take a possibility of the higher valence than Hf, such as +5.

The soot containing metallofullerenes was obtained by a direct-current arc discharge (60 A) of Ta/Yb/C composite rods (Ta:Yb:C=1:1:98) under a 500 Torr He atmosphere. The raw soot was extracted for 8h with a mixed solvent of triethylamine and acetone. The extract was separated by HPLC using a Buckyprep column and acetone with an ion-pair reagent, tetrabutylammonium bromide, as an eluent.

Fig. 1 shows the HPLC chromatogram of the extract. For all the fractions, LD-TOF-MS spectra were measured, and no peaks assigned to Yb_2C_n or $TaYbC_n$ were observed. (In addition, peaks assigned to TaC_n or Ta_2C_n could not be observed.) As a result, it was found that Ta can not play a role for controlling the charge in Yb-containing dimetallofullerenes.

To investigate an influence of ionization energy of encapsulated metal, we changed the metal from Yb to Sm which is known to take +2 oxidation state in Sm-monometallofullerenes and has rather high ionization energy but lower than Yb. The results will be reported in the presentation.

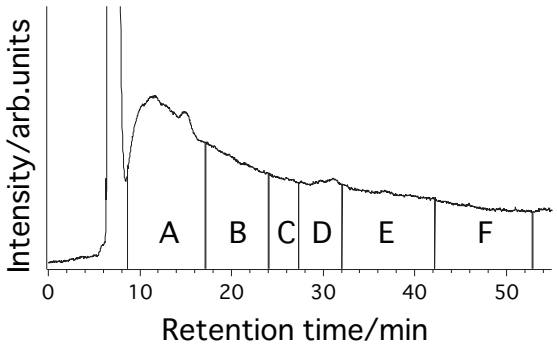

Fig. 1 HPLC chromatogram of the extract

[1] K. Kobayashi, et al. *The 52nd Fullerenes-Nanotubes-Graphene General Symposium*128 (2017).
[2] K. Kobayashi, et al. *The 11th Annual Meeting of Japan Society for Molecular Science* 2P055 (2017).
Corresponding Author: Takeshi Kodama
Tel: +81-42-677-2530, Fax: +81-42-677-2525,
E-mail: kodama-takeshi@tmu.ac.jp

Attempt to produce dimetallofullerenes containing Eu

○Yusuke Furiya, Koichi Kikuchi, Yohji Achiba, Takeshi Kodama

Department of Chemistry, Tokyo Metropolitan University, Tokyo 192-0397, Japan

So far, using the method combining the ion-pair chromatography with the mixed solvent extraction, we succeeded in the isolation of $Y_2@C_{80}(I_h)$[1], $Gd_2@C_{80}(I_h)$[2], etc. as an anion form, which are unstable in neutral form and have been known as "hidden" or "missing" metallofullerenes. Recently, Kobayashi, et al. tried to produce Yb-dimetallofullerenes using the same method, but Yb-dimetallofullerenes could not be obtained. The reason was thought to come from the rather high ionization energy of Yb because the encapsulated metals usually take +3 oxidation state in dimetallofullerenes but it is hard to take +3 state for Yb. In this study, we focused on Eu that has the ionization energy lower than Yb, and tried to produce Eu-dimetallofullerenes. For Eu-metallofullerenes, the isolation of monometallofullerene, $Eu@C_n$, has been reported[3], but there is no report on the dimetallofullerenes, $Eu_2@C_n$.

First, we carried out the experiment for the system of only Eu and carbon, but no evidence of the presence of Eu-metallofullerenes was obtained. Then, we move to the hetero metal system. First, we carried out direct-current arc discharge of Eu/Y/C composite rods (Eu:Y: C=1:1:98) under 500 Torr He atmosphere. The raw soot was extracted for 8h with a mixed solvent of triethylamine and acetone. The extract was separated by HPLC using Buckyprep column and acetone with an ion-pair reagent, tetrabutylammonium bromide, as an eluent.

Fig. 1 and 2 show HPLC chromatogram and LD-TOF-MS spectra of the fraction A, B, and C, respectively. In the fraction A, the peak of Y_2C_{80}, which should be $Y_2@C_{80}(I_h)$, was observed, but no peak of $EuYC_{80}$ and Eu_2C_{80}. Similarly, in the fraction B and C, the peak of YC_n (n=80, 82) and Y_2C_n (n=78, 80) was obtained, but no peak of $EuYC_n$ and Eu_2C_n. Therefore, it was suggested that dimetallofullerenes containing Eu, $EuY@C_n$ and $Eu_2@C_n$, were not produced in the raw soot or could not be extracted as an anion form by the present method. In the symposium, we will report on the result for Eu and La hetero metal system.

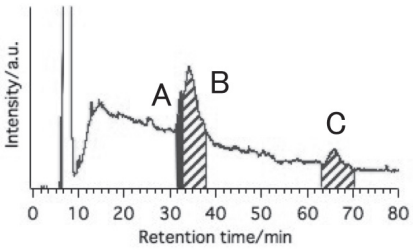

Fig.1 HPLC chromatogram for the extract

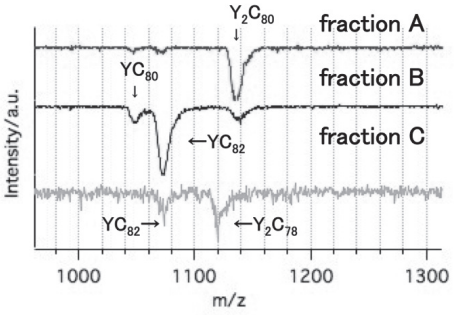

Fig.2 LD-TOF-MS spectra of the fraction A, B and C

[1] N. Nakatori, et al. *The 49th Fullerenes-Nanotubes-Graphene General Symposium* 46 (2015).
[2] T. Mitani, et al. *The 50th Fullerenes-Nanotubes-Graphene General Symposium*. 95(2016).
[3] Sun, B.Y. et al. *J. Phys. Chem. B* **108**, 9011(2004).

Corresponding Author: Takeshi Kodama
Tel: +81-42-677-2530
Fax: +81-42-677-2525
E-mail: kodama-takeshi@tmu.ac.jp

Temperature dependence of thermal conductivity of in-plane and out-of-plane directions in single-wall carbon nanotube thin film by periodic heating method

○Hiroyuki Matsuo [1], Yohei Yomogida [1], Takashi Yagi[2], Kazuhiro Yanagi [1]

[1] *Department of Physics, Tokyo Metropolitan University, Hachioji, Tokyo 192-0397, Japan*
[2] *Department of Physics, National Institute of Advanced Industrial Science and Technology, Tsukuba, Ibaraki,305-8563, Japan*

In recent years, organic conductive polymers and carbon nanotubes have attracted a lot of interest as thermoelectric materials. It is important to evaluate their thermal conductivity in their thin film form. We are evaluating of thermal conductivities of the in-plane and out-of-plane directions in the single-wall carbon nanotube(SWCNTs) thin films by using periodic heating method. This study investigated temperature dependence of thermal conductivities of the in-plane and out-of-plane direction in the film to understand the characteristics of heat transport of anisotropic materials such as carbon nanotubes.

SWCNT films (MEIJO nano carbon ARCSO, Unpurified: metal / semiconductor mixed sample) were dispersed into methanol and its free standing film was formed (thickness 54μm). The thermal diffusivity was measured by spot-heating the sample surface with a laser (wavelength: 808 nm) and detecting the phase delay of radiation from the back surface while controlling the temperature with the heater of the sample stage used by a vacuum chamber capable of liquid nitrogen cooling. Fig.1 shows the temperature dependence of the thermal diffusivity and thermal conductivities in the in-plane and out-of-plane directions. The thermal diffusivity in the both directions decreased as the increasing of temperature, but the slight difference is observed in the curvature around 200 K. The thermal conductivities of in-plane direction, 8.7 $Wm^{-1}K^{-1}$, was about 30 times larger than that of the out-of-plane, 0.29 $Wm^{-1}K^{-1}$, at room temperature. This result also coincides with the values obtained by the TDTR method. Difference in the behavior of temperature dependence in the in-plane and out-of-plane directions may reflect the heat flow anisotropy of the SWCNT thin film, and we are currently investigating in detail.

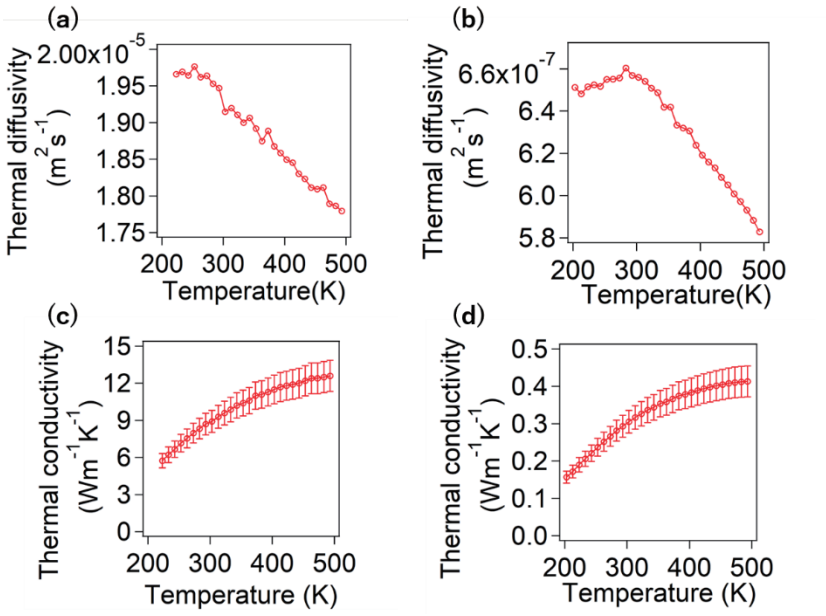

Figure1：Temperature dependence of Thermal diffusivities in the (a) in-plane and (b) out-of-plane directions of SWCNT thin film, and thermal conductivity in the (c) in-plane and (d) out-of-plane directions

Corresponding Author: K. Yanagi,
Tel: ＋81-42-677-2494,
E-mail: yanagi-kazuhiro@tmu.ac.jp

Simulation of Thermoelectric Properties of Carbon Nanotube with Mechanical Deformation

○Keiichiro Matsumoto [1], Takahiro Yamamoto [1,2]

[1] *Department of Electrical Engineering, Tokyo University of Science, Tokyo 125-8585, Japan*
[2] *RIST, Tokyo University of Science, Tokyo 125-8585, Japan*

Development of self-sustaining power sources is required to realize IoT (Internet of Things) society. As one of these sources, thermoelectric generation is expected to be a key technology for its realization. Hence, many studies have explored materials appropriate for the thermoelectric generation devices. Among these materials, a carbon nanotube (CNT) has attracted attention for flexible thermoelectric generation devices. In the CNT film, some of the CNTs are considered to be dented and/or bent, and the previous study experimentally confirmed the existence of bent CNTs [1]. Moreover, other experimental studies have reported that the thermoelectric properties vary when the CNT film is deformed by external forces [2,3]. However, the detailed influence of such mechanical deformations on thermoelectric properties has not yet been clarified.

In the present study, we investigate thermoelectric properties of a dented (10,0)-CNT as shown in Fig.1, using the non-equilibrium Green's function method coupled with the tight-binding method. We calculate electrical conductance, Seebeck coefficient and thermoelectric power factor of the CNT. Our calculation shows that the Seebeck coefficient is almost not affected by the dent while the electrical conductance and the thermoelectric power factor are reduced. In addition, we reveal that the larger the dent of CNT is, the more the electrical conductance and the thermoelectric power factor tends to decrease.

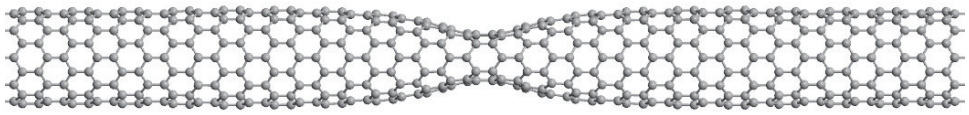

Fig.1 Schematic illustration of a dented (10,0) CNT

[1] J. Bernholc *et al*. Annu. Rev. Mater. Res. **32**, 347 (2002).
[2] H. E. Romeo *et al*. Phys. Rev. B. **65**, 205410 (2002)
[3] C. H. Hu *et al*. Appl. Phys. Lett. **93**, 033108 (2008)

Corresponding Author: Takahiro Yamamoto
Tel&Fax: +81-3-5876-1486,
E-mail: takahiro@rs.tus.ac.jp

Numerical study of disappearance of localization phenomena at finite temperature on electronic transport in a nitrogen-doped carbon nanotube

○Keisuke Ishizeki[1], Kenji Sasaoka[2], Kengo Takashima[1], Takahiro Yamamoto[1,2]

[1] *Department of Electrical Engineering, Tokyo University of Science, Tokyo 125-8585, Japan*
[2] *Research Institute for Science and technology (RIST), Tokyo University of Science, Tokyo 162-8601, Japan*

Impurity-doped semiconducting carbon nanotubes (CNTs) are expected to be used as materials of next-generation field effect transistors or thermoelectric devices owing to their remarkable electrical properties. As electronic transport properties of a doped CNT are characterized mainly by impurity and phonon scatterings, previous theoretical studies individually investigated their effects on electrical resistance. For example, in the previous theoretical study, it is shown that conduction electrons localize in CNT and resistance increases exponentially with tube length (non-ohmic transport) when a CNT has impurities at 0K [1]. On the other hand, as temperature increases, it is expected that phonon suppresses such localization phenomena, and that the transport property becomes ohmic transport because phase coherency disappears. However, the effects of phonon scattering on suppression of localization phenomena have not been clarified.

In the present study, we investigated electronic transport properties in a nitrogen-doped (8,0)-single-walled CNT (SWCNT) at finite temperatures using the Open-TDSE with MD simulation method developed in a previous study [2], which can simultaneously treat both localization effects due to impurity scattering and quantum decoherence due to phonon scattering. We confirmed that tube length dependence of electrical resistance shows exponential behavior in long length regime at 0 K (solid curve in Fig.1), while it shows linear behavior in short length regime (dotted line in Fig.1). On the other hand, resistance at 300 K decreases compared to the one at 0 K and tube length dependence of resistance shows linear behavior even in long length regime (solid line in Fig.1). This means that phonon scattering reduces phase coherence of conduction electrons. This work is the first theoretical report to investigate reduction of resistance of a nitrogen-doped CNT at finite temperature originated from disappearance of localization phenomena due to phonon scattering.

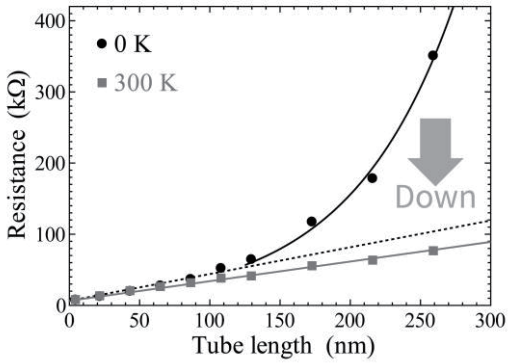

Fig.1. Tube length dependence of resistance of a nitrogen doped (8,0)-SWCNT with chemical potential 0.75 eV at nitrogen concentration 0.625 %.

[1] R. Avriller, S. Latil, F. Triozon, X. Blase, S. Roche, Phys. Rev. B **74**, 121406 (2006).
[2] K. Ishizeki, K. Sasaoka, S. Konabe, S. Satofumi, and T. Yamamoto., Phys. Rev. B **96**, 035428 (2017).

Corresponding Author: T. Yamamoto
Tel: +81-3-5876-1486
E-mail: takahiro@rs.tus.ac.jp

Synthesis and structural analysis of cellulose nanofiber/CNT composites

○Shiho Honda, Hsin-Hui Huang, Masamichi Yoshimura

Toyota Technological Institute, Nagoya 468-8511, Japan

1. Introduction

Recently, developing functional nanocomposites with the utilization of the sustainable natural resources has been attracted attention in the field of composite materials.[1] Cellulose nanofibers (CNF) are widely used as dispersants and strength additives. It is reported that properties such as electrical conductivity can be provided by combining with nanocarbons such as carbon nanotubes (CNT).[2] In this study, we prepare a uniform and flexible conductive film by adding CNT to CNF, and investigate the microstructure of the CNT-CNF nanocomposite films.

2. Experimental

2 wt% CNF gel (Rheocrysta, DKS Co. Ltd.), functionalized (carboxylic acid) or non-functionalized multiwalled CNT (f-MWCNT or MWCNT, Sigma-Aldrich) were suspended in de-ionized water and sonicated for 150 min. Nanocomposite films were formed by vacuum-filtering the dispersion using various membrane filters, such as cellulose acetate (CA, 0.2 μm), polytetrafluoroethylene (PTFE, 0.2 μm), and polyvinylidene difluoride (PVDF, 0.1 μm). The films were prepared after freeze-drying or natural drying. The nanocomposite films were finally fabricated by hot-pressing at a pressure of 10 MPa at 60 ℃ for 3 h.[3] These films are characterized by scanning electron microscopy (SEM), transmission electron microscopy (TEM), atomic force microscopy (AFM), and Raman spectroscopy. The conductivity is measured by four probe method.

3. Results and discussion

TEM images of the CNT-CNF composites showed CNT mixed with CNF dispersed well, whereas CNT were aggregated and its dispersibility was low in the solution without CNF. Films prepared by freeze-drying method showed non-uniform sheet resistance (70.8 ± 0.8 ~ 715.8 ± 25.7 Ωsq^{-1}). On the other hand, we obtained reproducible sheet resistance on the films prepared by natural drying (47.6 ± 0.7 ~ 84.0 ± 3.0 Ωsq^{-1}). Non-uniform sheet resistance is due to the voids remained in the nanocomposite film in the freeze-dried film. After drying, the nanocomposite film could be peeled off only from PVDF membrane filter. Fig.1 shows the change in sheet resistance with and without hot-pressing after natural drying. The sheet resistance decreased by hot-pressing (f-MWCNT: 7~26%, MWCNT: ~20%). The present results suggest that the voids decreased and the connection between the fibers increased after hot-pressing.

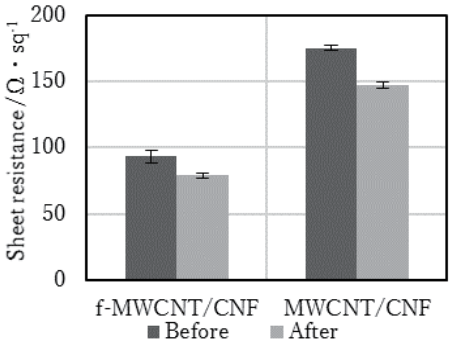

Fig.1 The sheet resistance before/after hot-pressing of nanocomposite films.

[1] C. Chen, M. Mo, W. Chen, M. Pan, Z. Xu, H. Wang, D. Li, Comp. Sci. Tech. 156 (2018) 103-108.

[2] Y. Wang, Z. Shao, F. Wang, W. Wang, R. Yang, European Polymer Journal 86 (2017) 85-93.

[3] H. Zhang, X. Sun, Z. Heng, Y. Chen, H. Zou, M. Liang, Ind. Eng. Chem. Res. 57, 50 (2018) 17152-17160.

Corresponding Author: M. Yoshimura

Tel: +81-52-809-1852, Fax: +81-52-809-1851, E-mail: sd18431@toyota-ti.ac.jp

Current response of DNN crystals/CNT thin film to hard X-ray

○Satoshi Ishii [1], Satoru Suzuki [1], Takahiro Ishikawa [2], Teruaki Konishi [2], Tsuyoshi Hamano [2], Jun Hirotani [3], Yutaka Ohno [3,4], Toshio Hirao [2]

[1] Department of Physics, Tokyo Denki University, Saitama 350-0394, Japan
[2] National Institute for Radiological Sciences, National Institutes for Quantum and Radiological Science and Technology, Chiba 263-8555, Japan
[3] Department of Electronics, Nagoya University, Nagoya 464-8602, Japan
[4] Institute of Materials and Systems for Sustainability, Nagoya University, Nagoya 464-8601, Japan

Real-time dosimetry has been attracting much attention for the precise control of the irradiation dose on the radiotherapy for cancer. An organic semiconducting single crystal of 1,5-dinitronaphthalene (DNN) has been reported to show the direct detection of X-ray stably at room temperature in air, together with the smaller X-ray attenuation than inorganic semiconductor [1]. CNT is also known to have high radiation tolerance [2], and therefore DNN crystals combined with the CNT thin film is expected to be applied for the wearable, large-area and transparent real-time dosimeter of the radiotherapy. In this study, we have fabricated the DNN crystals supported on the carbon nanotube thin film (DNN crystals/CNT thin film) and investigated its current response to hard X-ray.

Figure 1 shows the surface of the fabricated DNN crystals/CNT thin film. In the fabrication process, an aqueous dispersion of DNN crystals was firstly prepared by dropping a DNN/chloroform solution gently into deionized water using microsyringe with stirring. Then, the aqueous dispersion was dropped onto the surface of CNT thin film previously formed on the PEN substrate by dip coating, followed by drying. In the irradiation experiment, a hard X-ray (effective energy: 83 keV) was irradiated to the thin film, which was loaded in the exposure vessel filled with N_2 gas (50 kPa), from outside of the vessel at the dose rate of 36.1 mGy/sec. The current response of the thin film to X-ray was monitored under constant voltage conditions.

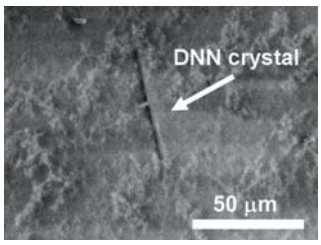

Fig.1 SEM image of DNN crystals supported on the CNT thin film.

Figure 2 shows the current responses of the DNN crystals/CNT thin film and the only CNT thin film to the X-ray irradiation at an applied voltage of 6 V. For the irradiation, the current of the DNN crystals/CNT thin film was increased, although that of only CNT thin film was decreased. When the irradiation was turned off, the current of both films began to recover. The current increase of the DNN crystals/CNT thin film seems to originate from the electrical response of DNN crystals to X-ray.

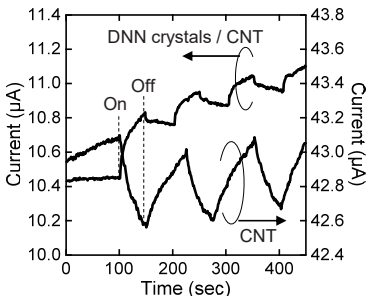

Fig.2 Current responses to the hard X-ray irradiation.

This work was supported partially by the joint usage/research program of the Institute of Materials and Systems for Sustainability (IMaSS), Nagoya University.

[1] B. Fraboni *et al*., Faraday Discuss. **174,** 219 (2014).
[2] C. D. Cress *et al*., IEEE Trans. Nucl. Sci. **57,** 3040 (2010).

Corresponding Author: S. Ishii
Tel: +81-49-296-1926, Fax: +81-49-296-2915,
E-mail: s.ishii@mail.dendai.ac.jp

The collective effects of iron amount and annealing temperature of a magnesia underlayer for the highly efficient growth of single-wall carbon nanotube forests

○Takashi Tsuji, Guohai Chen, Kenji Hata, Don N. Futaba, Shunsuke Sakurai

CNT-Application Research Center, National Institute of Advanced Industrial Science and Technology (AIST), Tsukuba, Ibaraki 305-8565, Japan

Recently, we reported that magnesia (MgO) could be used as a catalyst underlayer for the efficient growth of millimeter-scale single-wall carbon nanotube (SWCNT) forests with the appropriate thermal annealing to reduce the severe subsurface diffusion of iron (Fe) catalyst into the underlayer [1]. In addition, excessive underlayer annealing led to excessive crystallinity increasing which further suppressed catalyst subsurface diffusion and facilitate Ostwald ripening. As a result, loss in single-wall selectivity (formation of multiwall CNTs (MWCNTs)) occurred because of the formation of the larger particles from the excessive surface-bound Fe [2]. These results suggest that high yield SWCNT forest growth using such porous MgO underlayer requires a balance of surface-bound Fe as governed by the MgO crystallinity/porosity and the initial amount of deposited Fe.

Here, we demonstrate the existence of a well-defined region for high yield SWCNT forest growth in the domain of deposited Fe amount and MgO annealing temperature. Our results show that the collective effects of these two factors govern the amount of surface-bound Fe thus modulating both the CNT type (SWCNT, MWCNT) as well as the CNT yield [3]. Our study for a range of deposited Fe thicknesses (1–2 nm) and MgO annealing temperatures (no annealing–950 °C) showed three distinctly defined regions: low yield SWCNT growth, high yield SWCNT growth and high yield MWCNT growth regions. Furthermore, characterization by transmission electron microscope (TEM) revealed that the region for high yield SWCNT growth was bound on one side by a low yield SWCNT border and on the other side by a MWCNT border. Finally, we found that these two borders converged indicating that the allowable region for SWCNT growth for low MgO annealing temperature and high initial Fe becomes narrow. Topographic examination by atomic force microscopy (AFM) revealed that the origin of this high efficiency and SWCNT selectivity results from the stable formation of high density and small size of catalyst nanoparticles. This occurs due to the balance between the deposited Fe amount and the reduction in Fe subsurface diffusion into underlayer caused by the annealing of MgO underlayers. We believe that this work provides a general understanding for all catalyst/underlayer systems to achieve high yield single-wall carbon nanotube synthesis.

[1] T. Tsuji *et al*. J. Am. Chem. Soc. **138**, 16608 (2016).
[2] T. Tsuji *et al*. Nanoscale **9**, 17617 (2017).
[3] T. Tsuji *et al*. MRS Adv. accepted.

Corresponding Author: S. Sakurai
Tel: +81-29-861-4654, Fax: +81-29-861-4851,
E-mail: takashi.tsuji@aist.go.jp

Molecular Dynamics Simulation of SWCNT Growth from Seed Tube-Walls with Various Chiralities

○Kanau Mukai[1], Ryo Yoshikawa[1], Kaoru Hisama[1], Kakeru Hashimoto[1], Shohei Chiashi[1] and Shigeo Maruyama[1,2]

[1] *Department of Mechanical Engineering, The University of Tokyo, Tokyo 113-8656, Japan*

[2] *National Institute of Advanced Industrial Science and Technology, Ibaraki 305-8564, Japan*

It is highly important to understand the growth mechanism for structural control of single-walled carbon nanotubes (SWCNTs). Numerical simulation is suitable for observation in atomic scale, so we performed molecular dynamics (MD) simulations and analyzed SWCNT growth. We applied bond order potentials [1] and Lennard-Jones potential to represent the interaction among atoms, and observed defect-free growth of SWCNT from pure catalyst [2]. To study differences in growth of SWCNT with different chiralities or diameters, we prepared metal clusters connected with SWCNT sidewalls (seed tube-walls) as the initial structure. Then, we supplied them with carbon atoms with constant number (n) in the fully periodic cell ($10\times10\times10$ nm^3), and the growth of SWCNT from seed tube-wall was observed.

We used two types of metal catalysts, Co_{60} and Fe_{80}. We connected four types of seed tube-walls ((9, 8), (12, 4), (14, 1), and (15, 0)) to the Co catalyst and three types of seed tube-walls ((9, 1), (11, 1), and (15, 1)) to the Fe catalyst, and observed their elongation. On the Co catalyst, the interface between the near-armchair SWCNT and the catalyst became oblique to the axial direction of the SWCNT, and the edges changed to zigzag edges. Besides, defect structures were formed and the chirality of SWCNT changed toward zigzag. SWCNT with (9, 8) and (12, 4) suffered from a lot of defects and bent. On the other hand, we observed the defect-free side walls in the growth of SWCNT with (14, 1) and (15, 0). On the Fe catalyst, the kink growth of near-zigzag SWCNT was observed. Moreover, we found that (11, 1) was the structure with the least defect. The diameter of the SWCNT with (11, 1) was close to the diameter of the catalyst.

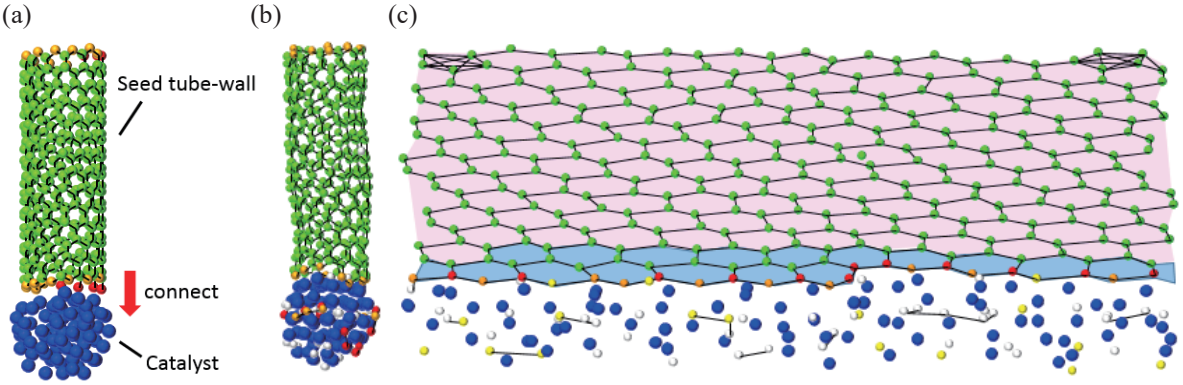

Fig. 1. (a) Connection of seed tube-wall and metal catalyst. The blue atoms are Fe, and the others are C. (b) SWCNT growth from (11, 1) seed tube-wall on Fe_{80} at 1100 K. (c) Developed view of (b). The pink area is seed tube-wall with (11, 1) which we prepared. The blue area grew newly by our MD simulation.

[1] K. Hisama et al., J. Phys. Chem. C, 2018, 122, pp 9648. [2] R.Yoshikawa et al., submitted.

Corresponding Author: S. Maruyama

Tel: +81-3-5841-6421 Fax: +81-3-5800-6983 E-mail: maruyama@photon.t.u-tokyo.ac.jp

Influence of alumina buffer layer on production of carbon nanotube black coating film

○Taishi Yamashita [1,2] , Hiromichi Watanabe [2], Takaya Akashi [3]

[1]*Graduate School of Science and Engineering, Hosei University, Koganei 184-8584, Japan*
[2]*Research Institute for Material and Chemical Measurement, National Institute of Advanced Industrial Science and Technology (AIST), AIST Tsukuba Central 3, 1-1-1*
[3]*Faculty of Bioscience and Applied Chemistry, Hosei University, Koganei 184-8584, Japan*

Carbon nanotubes (CNTs) can be applied as an optical / thermal absorption media for black-body radiation source and optical baffle, because of their extremely high emissivity. In the CNT growth process based on a chemical vapor deposition (CVD) method, carbon nanotubes are grown on a substrate by thermally decomposing a hydrocarbon gas with the assistance of metal fine particles used as the CNT catalyst. Generally, the carrier layer is formed by electron beam vacuum evaporation, but it is an obstacle to applying CNT as a blackbody radiation light source or light shielding material to costly and time-consuming to form a film on the surface of a three-dimensional object by this type of physical vapor deposition (PVD) method. We have proposed a method of depositing such a support layer by shot-blast (SB) processing that can be easily performed in the atmosphere[1].This method merely blows alumina fine particles at high speed onto the surface of the substrate with compressed air, and also has the advantage of enabling film formation on the entire surface of three-dimensional object against the PVD methods that require high-vacuum conditions. In this study, we compare the structures and characteristics of the alumina layers formed by electron beam evaporation and SB processing to evaluate the features and superiorities of catalyst-support layer formation methods.

In this work, W and Si coupons were used as the substrates for the deposition of alumina buffer layer and then CNT array. On a face of each of substrates, three kinds of alumina layer sections were established by the SB processing with alumina fine particles and by electron beam vacuum evaporation using Al and α-Al_2O_3 as the evaporation sources, respectively. Figure 1 shows the measurement results of the spectral reflectance in the visible region at room temperature of CNT grown by CVD method in which ferrocene and acetylene are used as the catalyst precursor and carbon source, respectively on both the alumina layers. The CNTs on the alumina buffer layers by electron beam vacuum evaporation using α-Al_2O_3 as the evaporation source and by the SB processing have exhibited the lowest reflectance, which indicates that the alumina layer produced by the SB processing is functioning sufficiently as the catalyst-support one, as well as that produced by the standard method is.

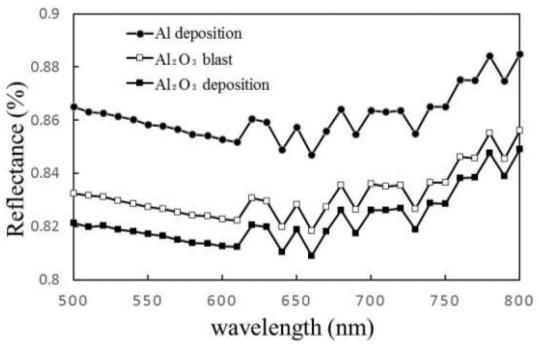

Fig.1. The reflectance spectra of CNT arrays formed on the three kinds of alumina buffer layers.

[1] H. Watanabe, J. Ishii, and K. Ota: Nanotechnology 27 (2016) 335605.

Corresponding Author: H. Watanabe
Tel: 042-387-6257, Fax: 042-387-7002,
E-mail: taishi.yamashita.8i@stu.hosei.ac.jp

Relation between growth conditions and growth profiles of individual SWNTs studied by digital isotope labeling

○Shun Yamamoto[1], Bunsho Koyano[1], Shota Hiraoka[1], Kaoru Hisama[1], Keigo Otsuka[2,3], Taiki Inoue[1], Rong Xiang[1], Shohei Chiashi[1], Shigeo Maruyama[1,4]

[1] *Department of Mechanical Engineering, The University of Tokyo, Tokyo, 113-8656, Japan*
[2] *Quantum Optoelectronics Research Team, Riken Center for Advanced Photonics, Wako, 351-0198, Japan*
[3] *Nanoscale Quantum Photonics Laboratory, Riken Cluster for Pioneering Research, Wako, 351-0198, Japan*
[4] *Energy NanoEngineering Lab, National Institute of Advanced Industrial Science and Technology (AIST), Tsukuba, 305-8564, Japan*

Single-walled carbon nanotubes (SWNTs) are highly expected toward the applications of electronic devices. Time-dependent growth of SWNTs has been investigated extensively for understanding the growth mechanism. However, most of the studies focused on growth curves of SWNT ensembles and did not discuss individual differences of SWNTs. Growth curves of individual SWNTs were obtained only for small numbers of short SWNTs [1]. Recently, we developed a new method for tracing time-resolved growth profiles of individual, long SWNTs by embedding digitally-coded isotope labels [2].

In this report, we investigated growth profiles of individual SWNTs in a wide range of temperature using iron or cobalt as catalyst on quartz substrates. We synthesized SWNTs from ethanol with addition of ^{13}C ethanol as labels and obtained growth curves by detecting the labels along each SWNT with Raman mapping (Fig. 1(a)). Comparison of growth curves and Raman RBM peaks reveals that the smaller the SWNT diameter is, the faster the growth rate is (Fig. 1(b)), and the growth rate does not depend on chiral angle (Fig. 1(c)). We changed temperature during synthesis (Fig. 1(d)) and examined activation energies using the Arrhenius plot. We also calculated thermal decomposition of ethanol under the growth conditions by COMSOL (Fig. 1(e)) and discussed the relation between the growth profiles and the feedstock composition.

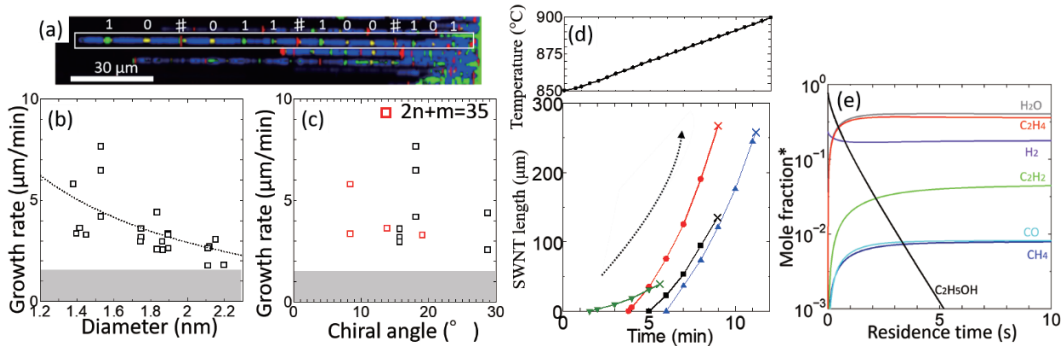

Fig. 1 (a) Raman mapping image colored by the shifts of G-band peaks. Growth rates plotted against (b) diameter and (c) chiral angle. (d) Growth curves of SWNTs grown at rising temperature (bottom) and temperature profile of this experiment (top). (e) Decomposition of ethanol with Ar/H_2 calculated with a zero-dimensional model. (* Mole fraction is determined without Ar).

[1] R. Rao *et al., Nat. Mater.* **11**, 213 (2012). [2] K. Otsuka, S. Yamamoto *et al., ACS Nano* **12**, 3994 (2018).
Corresponding Author: S. Maruyama Tel: +81-3-5841-6421, Fax: +81-3-5800-6983,
E-mail: maruyama@photon.t.u-tokyo.ac.jp

Growth and transfer of one-dimensional heterostructures

○Yongjia Zheng[1], Rong Xiang[1], Taiki Inoue[1], Yang Qian[1], Ming Liu[1], Shohei Chiashi[1], Esko I. Kauppinen[2], Shigeo Maruyama[1,3]

[1] *Department of Mechanical Engineering, The University of Tokyo, Tokyo 113-8656, Japan*
[2] *Department of Applied Physics, Aalto University School of Science, PO Box 15100, FI-00076 Aalto, Finland*
[3] *Energy NanoEngineering Lab., National Institute of Advanced Industrial Science and Technology (AIST), Tsukuba. 305-8564, Japan*

In recent years researchers have focused on two-dimensional van der Waals heterostructures (vdWH), which have generated great interests recently due to the possibility of combining diverse atomic layers to create novel materials and devices [1-2]. In this work, we demonstrate a new one-dimensional vdWH nanotube structure with similar heterostructure interfaces that combines the single-walled carbon nanotubes (SWCNTs), boron nitride nanotubes (BNNTs) and molybdenum disulfide nanotubes (MSNTs) in the radial direction (Fig. 1a-b) [3]. Techniques involving direct growth of 1D vdWH by chemical vapor deposition (CVD) will be presented in detail. In addition, we developed a method to transfer the suspended 1D vdWH nanotubes (Fig. 1c-e) to other substrate, making the characterization and application more achievable.

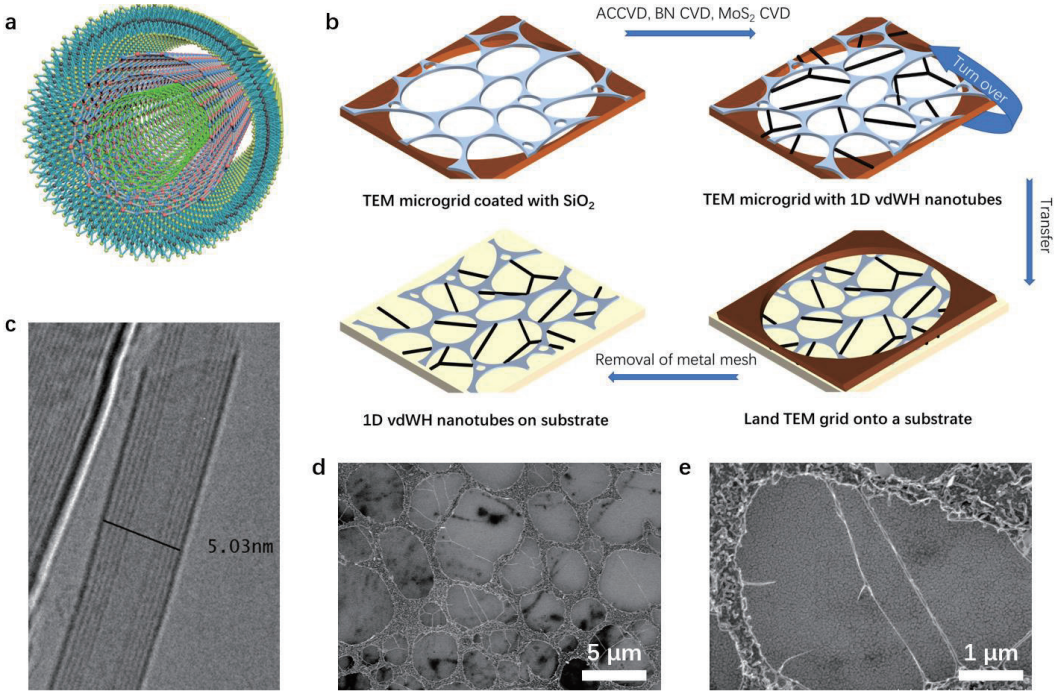

Fig. 1: (a) 3D model of the coaxial structure that combines the SWCNTs, BNNTs and MSNTs in the radial direction. (b) Diagram of transfer of suspended nanotubes onto another substrates. (c) TEM image of a 5 nm diameter ternary nanotubes consisting 1 SWNT, 3 layers of BN and 1 layer MoS_2 nanotube. (d) & (e) SEM images of 1D vdWH nanotubes transferred onto a gold surface for Tip-enhanced Raman spectroscopy (TERS).

[1] A. K. Geim *et al., Nature,* **499,** 7459 (2013).
[2] K. S. Novoselov *et al., Science,* **353,** 6298 (2016).
[3] R. Xiang *et al.,* arXiv:1807.06154

Corresponding Author: S. Maruyama
Tel: +81-3-5841-6421,
Fax: +81-3-5841-6983,
E-mail: maruyama@photon.t.u-tokyo.ac.jp

Study on one-dimensional stacking structure of polycyclic aromatic hydrocarbon molecules encapsulated in single-walled carbon nanotubes by molecular dynamics simulations

○Ryo Nagai[1], Yosuke Kataoka[3] and Hironori Ogata [1,2]
[1]*Graduate School of Sci. and Engin., Hosei University, Koganei, 184-8584, Japan*
[2]*Research Center for Micro-Nano Technology, Hosei University, Koganei, 184-0003, Japan*
[3]*Research Center for Computing and Multimedia Studies, Hosei University, Koganei, 184-8584, Japan*

Carbon nanotubes (CNTs) are one of the most promising materials due to their superior electronic, thermal and mechanical properties. Single-walled carbon nanotubes (SWNTs) have hollow spaces of about several nm in diameter. Various functional molecules such as fullerenes can be encapsulated in the hollow space, and it is expected that new functions will be developed by capsulation. It has been reported that columnar layered polycyclic aromatic hydrocarbon (PAH) molecules such as coronene encapsulated in SWNTs can exhibit unique luminescence properties depending on their molecular orientations. We have been investigat -ed the local structures and properties of various kinds of PAH molecules encapsulated in SWNTs systematically. In this study, molecular dynamics simulations were performed to clarify the condition (molecular structure and symmetry of molecule, chiral vector of SWNT, etc.) under which the PAH molecules(perylene, corannulene or coronene) encapsulated in SWNTs take a one-dimensional stacking structure. From the calculation results, it was found that coronene has the widest in the chiral vector region having a one-dimensional stacking structure. Detailed results will be discussed at the conference.

References:

[1] Miho Fujihara, *et al*., *J. Phys. Chem.* C **116**(2012)15141−15145.

[2] Alexander I. Chernov *et al., Phys. Status Solidi* B **251**(2014)2372–2377.

[3] Y. Sakane, *et al., AIP ADVANCES* **5** (2015)117113.

[4] Y.Joko, *et al., Phys. Chem. Chem. Phys*.**19**(2017)27704-27715.

[5] T.Koyama, *et al., J.Phys. Chem. C* **122**(2018)5805-5812.

Corresponding Author: H. Ogata
Tel: +81-42-387−6229, Fax: +81-42−387−6229, E-mail: hogata@hosei.ac.jp

Strain Effect of Single-Walled Carbon Nanotubes Encapsulated in BN Nanotubes

○Tatsurou Ogamoto[1], Satoshi Yotsumoto[1], Rong Xiang[1], Taiki Inoue[1], Shohei Chiashi[1], Shigeo Maruyama[1,2]

[1] *Department of Mechanical Engineering, The University of Tokyo, Hongo 7-3-1, Bunkyo-ku, Tokyo, Japan*

[2] *Energy NanoEngineering Laboratory, National Institute of Advanced Industrial Science and Technology (AIST), Tsukuba*

Single-walled carbon nanotube (SWCNT) attracts much attention owing to its electrical and mechanical properties. In order to make the best of SWCNTs, it is important to optimize the surrounding conditions around SWCNTs because their electrical properties easily change depending on the environment. Hexagonal boron nitride (h-BN) has been regarded as an ideal substrate because it has flatter surface and less charge traps than SiO_2 [1]. Additionally, from application viewpoints, SWCNTs coaxially coated with boron nitride nanotubes (BNNTs) are thought to be more versatile. However, the properties of SWCNTs encapsulated in BNNTs are veiled and the effects of BNNTs on SWCNTs are unknown, so we study the influence of BNNTs on the encapsulated SWCNTs by using optical measurement.

Suspended SWCNTs were grown by CVD method and then BNNTs were synthesized around SWCNTs by CVD method at high temperature (1100℃) [2]. SEM image in Fig. 1(a) shows that the BN-coating is not uniform along the tube axis. The some parts of SWCNT are coated with BN layer (position 1) and they exhibit the G-band downshift, as shown in Fig. 1(b). The downshift means that BN-coated parts of SWCNT are extended. Assuming that the both ends of SWCNT are fixed, the extension of the BN-coated SWCNT parts explains the bending in the uncoated part, as shown in Fig. 2.

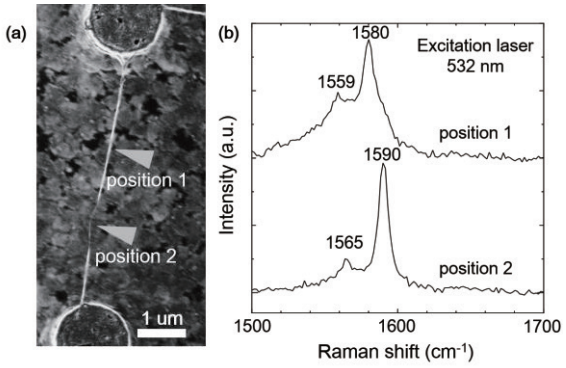

Fig. 1 (a) SEM image of suspended SWCNT after h-BN coating. (b) Raman spectrum of position 1 and position 2.

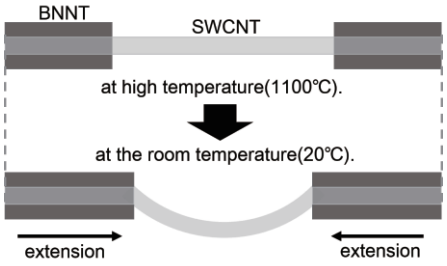

Fig. 2 Schematic drawing of mechanism of generation of strain.

[1] C. R. Dean et al., *Nat. Nanotechnol.* **5**, 722 (2010).
[2] R. Xiang et al., arXiv :1807.06154.

Corresponding Author: S. Maruyama.
Tel: +81-3-5841-6421
E-mail: maruyama@photon.t.u-tokyo.ac.jp

Thickness-selective exfoliation and extraction of graphene using pyrene-based nanocalipers

○Alejandro López-Moreno, and Naoki Komatsu

Graduate School of Human and Environmental Studies, Kyoto University, 606-8501 Kyoto

A number of physical and chemical methods have been developed to obtain high quality graphene. On the other hand, we have developed host-guest methodology to separate carbon nanotubes according to the diameter, handedness and even metallicity [1]. In this paper, we synthesized two kind of pyrene-based nanocalipers with pyrene (**1**) and anthracene (**2**) as spacer (**Figure 1**) and applied them to the exfoliation and extraction of graphene.

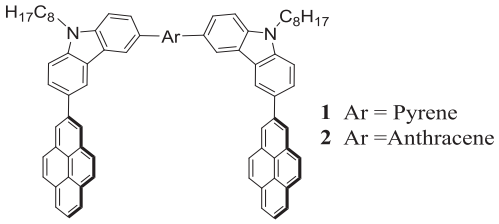

Figure 1 Structure of pyrene-based nanocalipers with pyrene (**1**) and anthracene (**2**) as spacer.

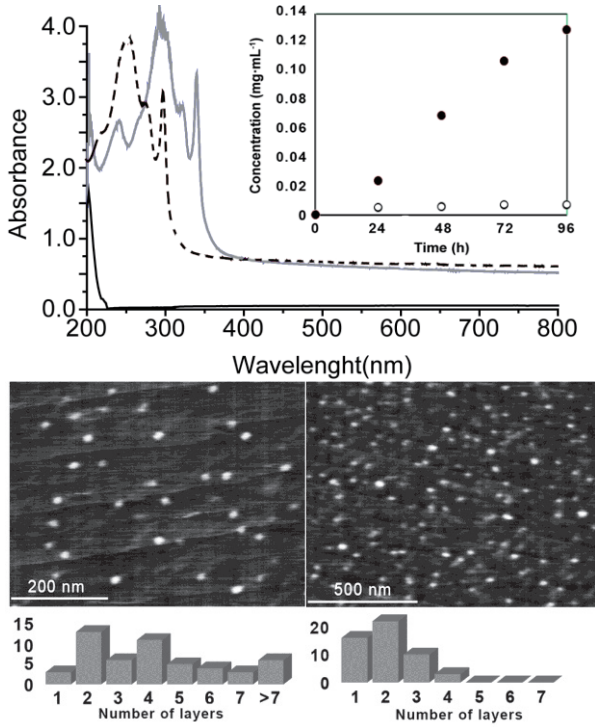

Figure 2 a) UV-vis spectra of the supernatants after 96 h sonication followed by centrifugation without nanocalipers (black), and with **1** (grey) and **2** (dashed black). Inset: Graphene concentration vs sonication time with **1** (black dot) and without nanocaliper (white dot). b) AFM micrographs of graphene and histogram exfoliated with **1** (left) and **2** (right).

In the extraction, graphite and the nanocalipers were sonicated in methanol for 96 hours. After centrifugation, the resultant black supernatant was analyzed by UV-vis and Raman spectroscopies, and AFM. The upward shifts of the baseline in UV-vis spectra (**Figure 2a**) imply the exfoliation and extraction of graphene with both **1** and **2**. The AFM shown in **Figure 2b** reveals the existence of graphene with different thickness with **1** and **2**. While thicker graphenes with an average thickness of 1.6 ± 0.7 nm corresponding to 4 layers are extracted with **1**, nanocalipers **2** having narrower cavity gave graphenes with less thickness of 0.9 ± 0.3 nm corresponding to 2 layers. With respect to the sizes, larger flakes were obtained using **1**, obtaining flakes of 51 ± 14 nm and 32 ± 7 nm for **1** and **2** respectively. Based on the extinction coefficient of graphene at 600 nm, the concentration was monitored according to the sonication time as shown in **Figure 2b**. Increase of the graphene concentration up to 0.13 $mg \cdot ml^{-1}$ and 0.14 $mg \cdot ml^{-1}$ for **1** and **2** respectively was observed, but no exfoliation was occurred in the absence of host molecules.

[1] G. Liu, A. F. M. M. Rahman, S. Chaunchaiyakul, T. Kimura, Y. Kuwahara, N. Komatsu, *Chem. Eur. J.* **19**, 16221 (2013); G. Liu, Y. Miyake, N. Komatsu, *Org. Chem. Front.*, **4**, 911 (2017).

Corresponding Author: A. López-Moreno Tel: +75-753-7871, E-mail: lopez.alejandro.74a@st.kyoto-u.ac.jp

Electrostatic actuation of mechanically coupled graphene mechanical resonators

○Keisuke Akazawa, Yuta Mochizuki, Taichi Inoue, Daiki Yoshikawa, Kuniharu Takei, Takayuki Arie, Seiji Akita

Department of Physics and Electronics, Osaka Prefecture University, Sakai 599-8531, Japan

Graphene is suitable for high performance mechanical resonator (MR) because of extremely low mass and high Young's modulus. Coupled mechanical resonators are one of emerging components for ultralow power information processing mimicking the superposition of states. Here, we demonstrate the coupled MRs consisting of two drum-type graphene MRs (G-MRs) connected with a graphene bridge.

Figure 2 shows the G-MRs coupled with a graphene bridge with a width of 2 μm, where the radii of the fabricated G-MRs was 3 μm. Both G-MR A and G-MR B were driven by the electrostatic actuation. The resonance properties of each G-MRs were individually measured using laser with a wavelength of 521 nm as indicated by green arrows in Fig. 2. When both of G-MRs were actuated, we irradiate another laser with a wavelength of 660 nm as indicated by a pink arrow in Fig. 2.

The resonances of both of G-MRs were successfully observed by electrostatic actuation. The resonance frequencies of G-MR A and B are 11.15 and 8.08 MHz, respectively, where the quality factors for both G-MRs are ~ 200. Figures 3 shows the change in amplitude of G-MR A when G-MR B is irradiated the laser with a wavelength of 660nm when the frequency is fixed at 11.15 MHz which is the resonance frequency of G-MR A. The amplitude of the G-MR A decreased by irradiating the laser to the G-MR B while driving the G-MR A. These indicate that the two G-MRs are mechanically coupled through the graphene bridge.

Acknowledgements This work was partially supported by KAKENHI Grant Numbers 15H05869, 16H00920, 16K14259, 16H06504, and 17H01040.

Corresponding Author: K. Akazawa, Tel: +81-72-254- 9261, E-mail: akazawa-4@pe.osakafu-u.ac.jp

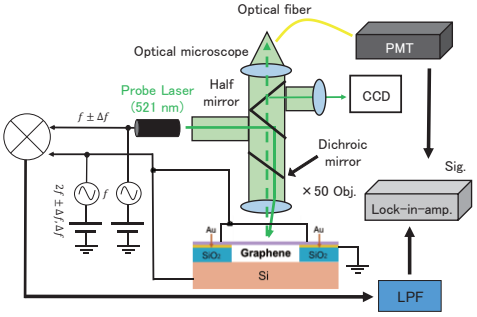

Fig. 1 Measurement setup

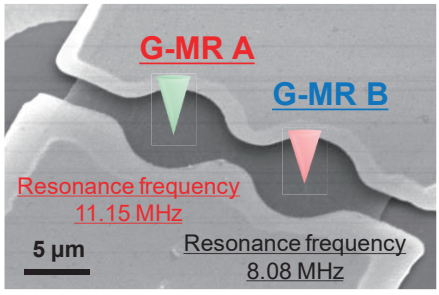

Fig. 2 SEM image of the graphene resonator and the laser position

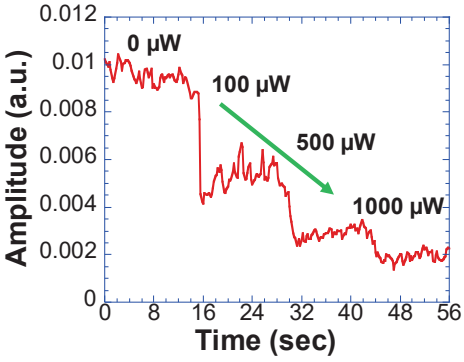

Fig. 3 Change in amplitude of G-MR A when G-MR B is irradiated the laser with a wavelength of 660 nm when the frequency is fixed at 11.15 MHz.

Mass sensing of Q-dots using graphene mechanical resonator

○Masashi Hori, Yuta Mochizuki, Kuniharu Takei, Takayuki Arie, Seiji Akita

Department of Physics and Electronics, Osaka Prefecture University, Sakai 599-8531, Japan

Graphene is widely applied to highly sensitive mass sensor based on nano-mechanical resonator (MR) because of its excellent electrical and mechanical properties. In order to append additional functionality, decoration of graphene with functional nanoparticle such as quantum dot (Q-dot) as shown in Fig. 1 is one of promising routes. In this case, number of Q-dots on the graphene is very curial information for the analysis. Here, we estimate the number of Q-dots on the graphene-MR (G-MR) from the resonance frequency shift.

Figure 2 shows a fluorescence image of a drum G-MR decorated with Q-dots. Several aggregated Q-dots are observed on the G-MR region, where the number of Q-dots on G-MR can be roughly controlled by the time for attachment process.

Figure 3 shows a resonance curve of the G-MR before and after the decoration of Q-dots. The resonance frequency downshifts from 11.2 to 7.8 MHz. This frequency shift corresponds to the mass of ~830 Q-dots. Thus, we have successfully confirmed that the resonance frequency was lowered due to adhesion of nanoparticles. In addition, we believe that G-MR is effective as nanoparticles detection and mass sensor.

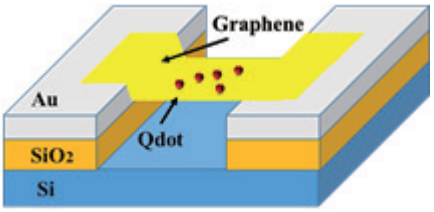

Fig. 1 Graphene resonator decorated with Q-dot.

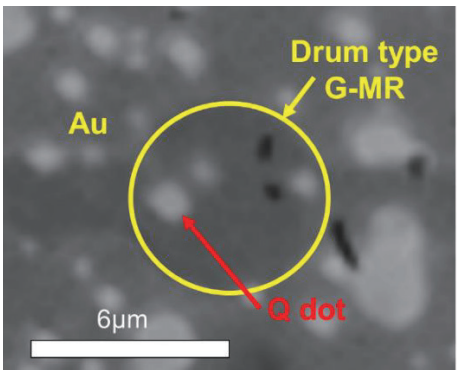

Fig. 2 Fluorescence microscope image of Q-dot on the G-MR

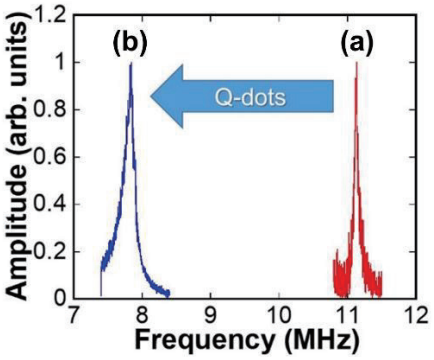

Fig. 3 Resonance curve of the (b) G-MR decorated with Q-dot measured and (a) normal G-MR in vacuum.

Acknowledgements This work was partially supported by KAKENHI Grant Numbers 16H00920, 16K14259, 16H06504, and 17H01040.
Corresponding Author: M. Hori, Tel: +81-72-254-9261, E-mail: hori-4@pe.osakafu-u.ac.jp

Ultra-fast and on-chip graphene blackbody emitters

○Kenta Nakagawa[1,2], Yusuke Fukazawa[2], Yusuke Miyoshi[2], Yuya Amasaka[2], Robin Reckmann[2,3], Tomoya Yokoi[2], Kenji Kawahara[4], Hiroki Ago[4] and Hideyuki Maki[2,5]

[1]*Kanagawa Institute of Industrial Science and Technology (KISTEC), Kanagawa 243-0435, Japan*
[2]*Department of Applied Physics and Physico-Informatics, Keio University, Kanagawa 223-8522, Japan*
[3]*Faculty of Electrical Engineering and Information Technology, RWTH Aachen University, Aachen 52074, Germany*
[4]*Global Innovation Center (GIC), Kyushu University, Fukuoka 816-8580, Japan*
[5]*PRESTO JST, Saitama 332-0012, Japan*

Nanocarbon-based optoelectronic devices are promising candidates for the high-speed and on-chip optical communication devices such as light sources [1-4]. In this study, we developed a blackbody emitter based on graphene in near-infrared region including telecommunication wavelength (Fig. (a)). An ultra-fast response time of ~100 ps, corresponds to ~10 GHz modulation under a rectangular voltage has been experimentally demonstrated (Fig. (b)). Theoretically calculation of the heat conduction equations considering the thermal model of the emitters including graphene and a substrate revealed that the fast modulation can be understood by remote quantum thermal transport via surface polar phonons of the substrates. Moreover, the optical communications, integrated two-dimensional array emitters with a chemical vapor deposition grown graphene, capped emitters operable in air, and the direct coupling of optical fibers to the emitters are also demonstrated. Recently, we found the visible light emission from the graphene emitters by increasing the number of graphene layers and the applied voltage (Fig. (c)).

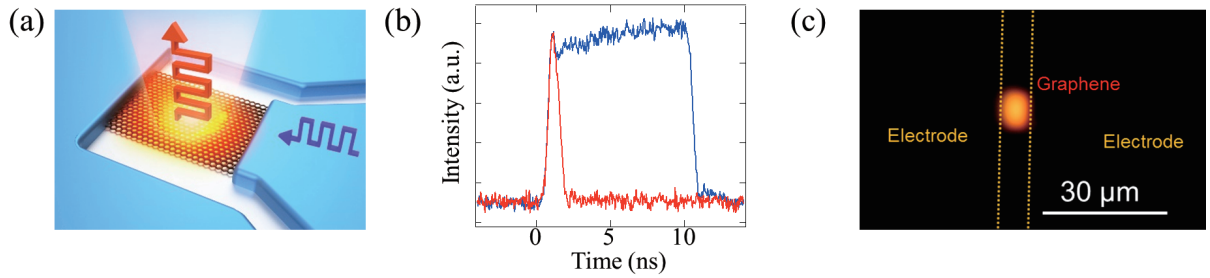

Fig. (a) Schematic image of the graphene light emitter. (b) Time-resolved emission from the graphene under 1 and 10 ns rectangular bias voltages. (c) Visible camera image of an emission from the graphene light emitter.

[1] N. Hibino, S. Suzuki, H. Wakahara, Y. Kobayashi, T. Sato & H. Maki, ACS Nano, **5**, 1215 (2011).
[2] M. Fujiwara, D. Tsuya & H. Maki, Appl. Phys. Lett., **103**, 143122 (2013).
[3] T. Mori, Y. Yamauchi, S. Honda & H. Maki, Nano Lett., **14**, 3277 (2014).
[4] Y. Miyoshi, Y. Fukazawa, Y. Amasaka, R. Reckmann, T. Yokoi, K. Ishida, K. Kawahara, H. Ago & H. Maki, Nat. Commun., **9**, 1279 (2018).

Corresponding Author: Prof. Dr. H. Maki
Tel: +81-45-566-1643, Fax: +81-45-566-1587,
E-mail: maki@appi.keio.ac.jp

Fabrication of high quality graphene nanoribbons using silver nanowires for energy gap opening

○Kensuke Aoki [1], Nobuyuki Aoki [1]

[1] *Department of Materials Science,Chiba University , Chiba 263-8522, Japan*

In order to apply graphene as a field effect transistor (FET), an energy gap must be introduced. To convert graphene into nanoribbons is one method of introducing energy gap opening. [1]

However, when graphene nanoribbons (GNR) samples are fabricated by the top-down method, generally advanced techniques such as electron beam lithography are required, which is unsuitable for industrial application. In addition, the edge property of the GNR becomes nonuniform when using a resist for electron beam lithography as an etching mask, and we expect that a uniform energy gap is not introduced throughout the GNR.

Therefore, we fabricated GNR FET samples by using silver nanowires (AgNW) as an etching mask. The diameter of AgNW is 30 [nm]. We expect that the edge property of GNR is nearly uniform because AgNW used as an etching mask is a single crystal whose surface is smooth. Fig.1 shows the result of observation with atomic force microscope (AFM). Although AgNW still remained on the obtained GNR, it was observed that GNR having a uniform width of about 30 [nm] was formed.

Next, the gate voltage dependence of the electric resistance at each temperature is shown in Fig.2. As shown in Fig. 2, a semiconductor behavior that the resistance value increases as the temperature decreases was observed. Also, Arrhenius plot was taken against the resistance and the energy gap was calculated to be 2.7 [meV]. This value was in good agreement with other papers [2]. Details of the fabrication method and observation results using Raman scattering spectroscopy will be discussed on that day.

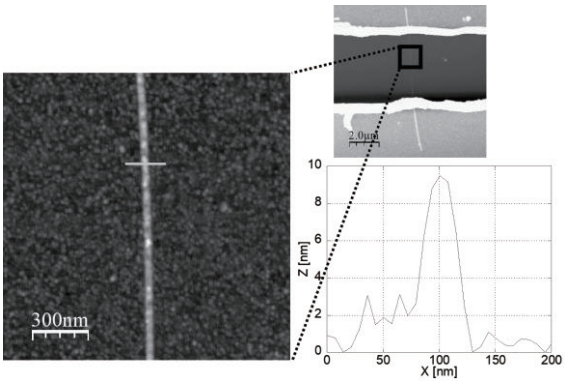

Fig.1 Topographic AFM image and line profile of GNR on SiO_2/Si substrate

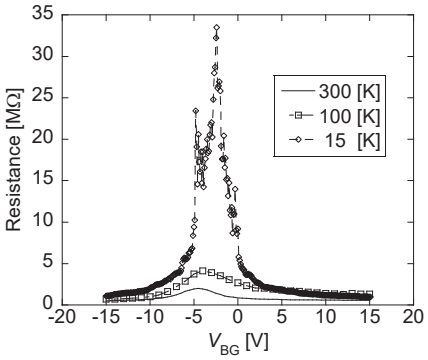

Fig.2 Resistance curves as a function of gate voltage at different temperatures

[1] X. Wang et al., PRL 100, 206803 (2008)

[2] M. Y. Han et al., PRL 98, 206805 (2007)

Corresponding Author: N. Aoki

Tel: +81-4-3290-3430, Fax: +81-4-3290-3427,

E-mail: n-aoki@faculty.chiba-u.jp

Ab initio study on magnetism in double-layered graphene with acetylenic crosslinks

Hiroyuki Yokoi

Department of Materials Science and Engineering, Faculty of Advanced Science and Technology, Kumamoto University, Kumamoto 860-8555, Japan

Emergence of magnetism in graphene has been investigated intensively through both theoretical and experimental approaches. It has been reported that structural modifications to the honeycomb lattice, including the formation of pores and the adsorption of hydrogen atoms, could generate half-filled localized states and induce magnetic moments. In these cases, it is essential to apply the modification to carbon atoms at the same type of sites (so called A-site or B-site) as the magnetic moment induced by modifications at A-site are canceled by that at B-site.

In the previous study [1], we have proposed a new class of structural modification of graphene, where two layers of graphene are cross-linked with ethylene groups. This modification does not induce magnetic moments basically as each ethylenic crosslink modifies carbon atoms at both A –site and B-site inevitably. However, we have found through ab initio calculations in 6x6 hexagonal supercell models that the magnetic moment of $2\mu_B$ is induced in a structure where six ethylenic crosslinks align circularly to surround twelve atoms of carbon on each sheet. In this configuration, the differential spin density is distributed over thus surrounded twenty four carbon atoms on both graphene sheets and the twelve carbon atoms on the six ethylenic crosslinks. If just one of the six crosslinks was missing, the magnetic moment disappeared. Therefore, we expected that quantum confinement of a π network with ethylenic crosslinks might favor the emergence of the localized magnetic moments.

In this study, we investigated the electronic states in double-layered graphene linked with acetylenic bridges through ab initio calculations. The supercell was set to a 6x6 hexagonal lattice. We have found that acetylenic crosslinks at the same type of sites induce the magnetic moment of about $2\mu_B$ a crosslink and the magnetic moment induced by a crosslink at A-site is canceled by that at B-site, which is similar to the case of the conventional modifications. In a structure where six acetylenic crosslinks align circularly to surround six carbon atoms on each sheet, the numbers of modified carbon atoms at A-sites and B-sites became equal and no magnetic moment was induced. The quantum confinement of a π network seemed ineffective to induce a magnetic moment in this configuration. We calculated the energy band structure for this structural model and found that the local state generated by the confinement situates away from the Fermi level. This result suggests that tuning of the energy of the local state induced by the confinement to the Fermi level could be essential to the emergence of magnetism in double-layered graphene with crosslinks.

[1] H. Yokoi, 54th Fullerenes-Nanotubes-Graphene General Symposium (Tokyo, March, 2018)

Corresponding Author: H. Yokoi
Tel: +81-96-342-3727, Fax: +81-96-342-3710,
E-mail: yokoihr@kumamoto-u.ac.jp

Gold-Mediated Growth of Few-Layer Molybdenum Disulfide

○ Hong En Lim[1], Toshifumi Irisawa[2], Naoya Okada[2], Takahiko Endo[1], Yutaka Maniwa[1], Yasumitsu Miyata[1]

[1]Department of Physics, Tokyo Metropolitan University, Hachioji, Tokyo 192-0397, Japan
[2]Nanoelectronics Research Institute (NeRI), National Institute of Advanced Industrial Science and Technology (AIST), Tsukuba, Ibaraki 305-8568, Japan

Atomically thin layers of transition metal dichalcogenides (TMDCs) are attractive for their sizeable bandgap and strong light matter interaction features, making them popular for future nano-optoelectronic devices [1, 2]. Present growth of these ultrathin layers frequently uses chemical vapor deposition (CVD). However, this process inevitably results in a random growth all over the substrate, which complicates device fabrication. A controlled growth of the TMDCs at desired position is thus important in aiding the design of functional devices.

Herein, we report a position-specific synthesis of few-layer molybdenum disulfides (MoS_2) with pre-patterned gold (Au) blocks. The Au patterns were first deposited onto SiO_2/Si substrates with resistive heating, and the MoS_2 was subsequently grown by alkali metal halide-assisted CVD growth [3]. In this way, few-layer MoS_2 is found to grow underneath the gold patterns, as observed from the cross-section transmission electron microscope image shown in Fig. 1a. Dissolving the Au on top leaves the bottom MoS_2 behind (Fig. 1b), which gives the characteristic E^1_{2g} and A_{1g} Raman vibration peaks at 384 and 407 cm^{-1}, respectively (Fig. 1c) [4]. The PL spectrum obtained is presented in Fig. 1d. This provides a simple and yet useful means for the potential assembly of these ultrathin sheets into sophisticated nanodevices such as monolithic 3D integrated digital circuits [5].

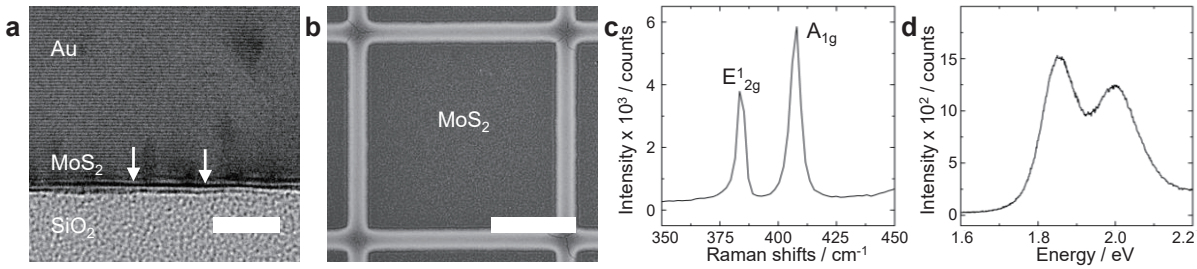

Fig.1 (a) Cross-section transmission electron miscroscope (TEM) image of the MoS_2 grown with Au-patterned SiO_2/Si substrate. Arrows indicate the MoS_2 layers. (b) Optical image of the MoS_2 obtained after Au removal (square area). (c) Raman and (d) PL spectra taken at region after Au removal. Scale bars are (a) 5 nm and (b) 50 μm.

[1] Q. H. Wang *et al.* Nat. Nano **7**, 699-712 (2012).
[2] X. Xu *et al.* Nat. Phys. **10**, 343-350 (2014).
[3] S. Li *et al.* Appl. Mater. Today **1**, 60-66 (2015).
[4] H. Li *et al.* Adv. Func. Mat. **22**, 1385-90 (2012).
[5] A. B. Sachid *et al.* Adv. Mater. **28**, 2547-54 (2016).

Corresponding Authors: H. E. Lim, Y. Miyata
E-mail: lim@tmu.ac.jp, miyata-yasumitsu@tmu.ac.jp
Tel: +81-42-677-2508

Controlling temperature and sulfur addition for synthesis of thin WS_2 nanotubes

○Yohei Yomogida and Kazuhiro Yanagi

Department of Physics, Tokyo Metropolitan University, Tokyo 192-0397, Japan

Tungsten disulfide (WS_2) nanotubes are cylindrical multiwall nanotubes of WS_2 sheets. WS_2 nanotubes exhibit only semiconducting characteristics regardless how they are rolled and have advantages for semiconductor applications compared to carbon nanotubes. Their properties are dependent on diameter and wall number and thin WS_2 nanotubes with small diameter and few walls are interesting because of their band gap tunability and superior flexibility. Previously, we have developed device applications [1,2] and sorting techniques [3] of WS_2 nanotubes using CVD-grown commercial sample. Then, for further researchs using thinner nanotubes, we have synthesized thin WS_2 nanotubes by sulfurization of solution-synthesized tundsten oxide nanowires. However, the synthesized sample show inhomogenity of structure and more controlled synthesis is necessary. In this study, we optimized synthesis of thin WS_2 nanotubes by controlling temperature and sulfur addition in the sulfurization process, which are known as impotant parameters for synthesis of two-dimensional WS_2 materials.

Tungsten oxide nanowire precursors were synthesized via solvothermal reaction of WCl_6 in ethanol, carried out in a teflon-lined stainless-steel autoclave at 180°C for 24 h. Then, the obtained nanowires were reacted with sulfur precursor at various temperatures ranging from 650 to 850°C for 2 h in Ar flow to allow formation of WS_2 nanotubes.

Fig. 1 shows a typical TEM image of WS_2 nanotubes sulfurized at 750°C. Mean diameter of the WS_2 nanotubes is about 20 nm and smaller than that of the sorted CVD-grown sample (32 nm) [3]. We found that 700-750°C is suitable for sulfurization. In the temperature range, the oxide nanowires can be converted to WS_2 nanotubes with their structure maintained. On the other hand, lower and higher temperature leads to insufficient sulfurization and collapse of nanowire structure, respectively. Since sulfurization is strongly depending on the temperature, homogeneous temperature distribution is important for homogeneous sulfurization, which can be achieved by introducing sulfur precursor after temperature is stabilized. Moreover, we investigated their transistor performances by ionic-liquid gating approaches (Fig. 2).

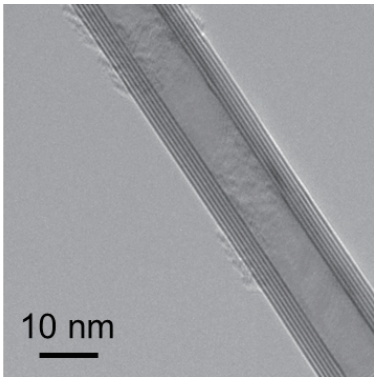

Fig. 1 TEM image of synthesized WS_2 nanotubes

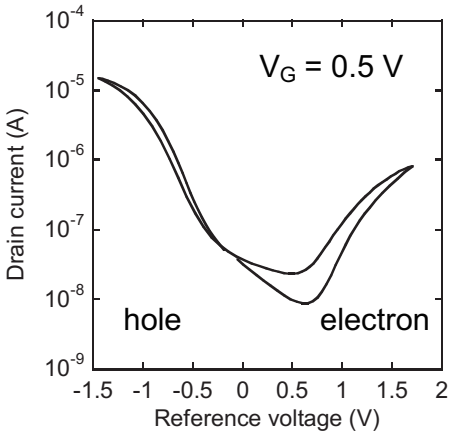

Fig. 2 Transfer characteristics of ionic-liquid gated transistors based on WS_2 nanotube networks

[1] M. Sugahara et al, Appl. Phys. Express 9, 075001 (2016).
[2] H. Kawai et al, Appl. Phys. Express 10, 015001 (2017).
[3] Y. Yomogida et al, ACS Omega 3, 8932-8936 (2018).

Optical conductivity of the Haldane model on honeycomb lattice

○ F.R. Pratama[1], M. Shoufie Ukhtary[1], R. Saito[1]

[1]Department of Physics, Graduate School of Science, Tohoku University,
Sendai 980-8578, Japan

In the Haldane model on honeycomb lattice (see Fig. 1), the complex-valued hopping parameters are introduced between second-nearest neighbor atoms in order to break the time-reversal symmetry, which enables the occurrence of quantum Hall effect without the external magnetic field [1, 2]. Recently, it is theoretically demonstrated within the dipole approximation by Ghalamkari *et al*. that the material with the honeycomb Haldane Hamiltonian also exhibits an interesting phenomenon of perfect circular dichroism (PCD) in K and K' points, where the material only absorbs the right- or left- hand side circularly polarized light [3]. However, they did not calculate the absorption spectra as a function of the laser excitation energy. In this study, we numerically calculate the transversal and longitudinal optical conductivities of the honeycomb Haldane material with the Kubo formula, from which we can predict the optical and plasmonic properties of the material over broad range of frequency. The result shows that our calculations are consistent with the optical absorption with the dipole approximation, in which PCD occurs for circularly-polarized light with energy close to the energy gap in the Haldane energy dispersion. We also discuss the plasmon spectra as the function of Fermi energy.

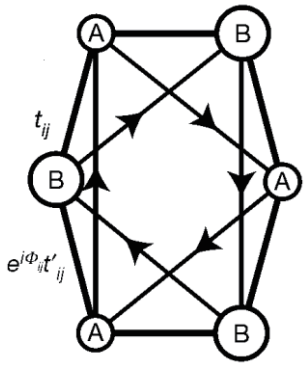

Fig. 1. Haldane model on honeycomb lattice. The hopping parameters between first-nearest neighbor atoms t_{ij} is real-valued, whereas the complex second-nearest neighbor hopping $e^{i\Phi ij}t'_{ij}$ carries tunable phases indicated by arrows [2].

References:

[1] F.D.M. Haldane, Phys. Rev. Lett. **61**, 2015 (1988).

[2] G. Jotzu *et al*., Nature **515**, 237 (2014).

[3] K. Ghalamkari *et al*., J. Phys. Soc. Jpn. **87**, 063708 (2018).

Corresponding author: F.R. Pratama

Email: pratama@flex.phys.tohoku.ac.jp

Softening effect on resonance frequency of MoS_2 mechanical resonator induced by persistent photoconductivity

○Taichi Inoue[1], Takahiko Endo[2], Kuniharu Takei[1], Takayuki Arie[1], Yasumitsu Miyata[2], Seiji Akita[1]

[1] *Department of Physics and Electronics, Osaka Pref. University, Sakai 599-8531, Japan*
[2] *Department of Physics, Tokyo Metropolitan University, Hachiohji 192-0397, Japan*

MoS_2 is expected as elements for sensor using FET or mechanical resonator (MR) [1, 2] because of its unique electrical, mechanical, and optical properties. In FET, persistent photoconductivity (PPC) [3] is often observed and the realization of the PPC contributes to high performance photosensor or memory. In MR, however, the effect of the PPC is hardly revealed although it is one of challenges toward high performance in optically tuned nano-electro-mechanical systems. Here, we investigate the PPC effect on MoS_2 MR.

We performed resonance measurement of MoS_2 MR under the vacuum of ~ 10^{-3} Pa (Fig. 1). The MoS_2 was synthesized by chemical vapor deposition [4]. The actuation was induced by applying AC drain source voltage V_{ds}. The vibration was detected by amplitude modulation mixed current I_{mix} with frequency f_{mod} = 1 kHz. The resonance frequency can be controlled by electrostatic force of gate voltage V_{gs}. The laser was irradiated on MR through microscope. The laser wavelength is 660 nm and the radius is ~ 11.5 μm.

Firstly, we investigated PPC effect on the suspended MoS_2 FET. Fig. 2 shows temporal variation of drain source current ΔI_{ds} after laser pulse with 1 W/cm^2 for 10 s. The current did not return to initial state over 20 min, which indicates typical behavior of PPC [3]. The origin of PPC in suspended MoS_2 FET is most likely due to trapped photogenerated holes in defects or contaminations of MoS_2. Next, we investigated PPC effect on MoS_2 MR with the same laser conditions. Fig. 3 shows time response of resonance frequency shift of MoS_2 MR after laser pulse. The down shift was appeared by laser pulse and the shift was kept over 20 min. This down shift is induced by not photothermal effect but softening effect of electrostatic force by trapped holes.

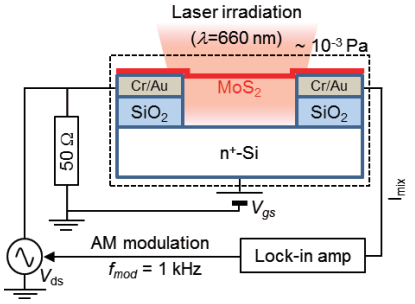

Fig. 1 Measurement setup.

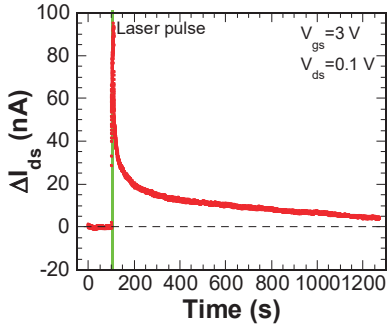

Fig. 2 Temporal variation of drain source current ΔI_{ds} after laser pulse.

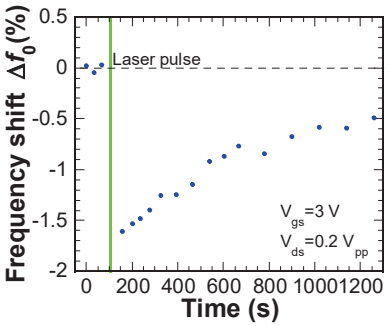

Fig. 3 Time response of resonance frequency shift after laser pulse.

Acknowledgements: This work was partially supported by KAKENHI Grant Number JP15H05869, J16H00920, 16K14259, 16H06504, and 17H01040.

Reference: [1] T. Inoue *et al.*, *ACS omega,* **2**, 5792 (2017) [2] T. Inoue *et al.*, *2D Materials*, **5**, 045022 (2018) [3] Y. Miyamoto *et al.*, *Jpn. J. Appl. Phys.,* **57**, 06HN01 (2018) [4] Y. Kobayashi *et al.*, *Nano Res.*, **8**, 3261 (2015)

Corresponding Author: T. Inoue, Tel: +81-72-254- 9261, E-mail: t_inoue-4@pe.osakafu-u.ac.jp

Layer-number dependence of NCCDW-ICCDW phase transition in TaS_2

○Yasushi Ishiguro[1], Naoko Kodama[2], Kirill Bogdanov[3], Alexander Baranov[3], Kazuyuki Takai[1,2]

[1] Dept. of Chemical Science and Technology, Hosei University, Tokyo 184-8584, Japan
[2] Graduate School of Science and Engineering, Hosei University, Tokyo 184-8584, Japan
[3] St. Petersburg National Research University of Information Technologies, Mechanics and Optics, Saint Petersburg 197101, Russia

The electronic properties of two dimensional (2D) nanomaterials depend on how degree they are "two dimensional". TaS_2 is known a 2D material having charge density wave (CDW) phase transitions, where several groups have reported the change in the conductivity between commensurate- and nearly-commensurate- (NC) CDW phases around 150 K modulated by controlling dimensionality [1,2]. In our study, the change in electronic properties is investigated for the NCCDW-incommensurate (IC) CDW phase transition around 350 K.

The TaS_2 thin flakes were prepared by mechanical exfoliation of bulk crystals of TaS_2 grown by the chemical transport synthesis on a SiO_2 (285 nm) /Si substrate. A FET device for the conductivity measurement were fabricated by EB-lithography process. Raman spectroscopy was performed with an excitation wavelength of 532 nm on a temperature controllable stage.

The resistivity abruptly decreases on entering the ICCDW phase from the NCCDW phase as shown in Fig. 1. Most notably, the transition temperature depends on the sample thickness. The transition temperature increases as decreasing layer number of TaS_2. This is explained by the metastable nature of NCCDW states, which is a short range order of CCDW state. As the dimensionality of TaS_2 becomes lower with decreasing in the number of layers, the temperature region of NCCDW states becomes wider due to more quantum fluctuation. Thus, the transition temperature between NCCDW-ICCDW increases as the number of layers decreases. Raman spectra are also changed in accordance with NCCDW-ICCDW phase transition as shown in Fig. 2. As increasing temperature, the peaks at 75 cm^{-1} broaden and the peaks at 105, 245, 307 and 382 cm^{-1} disappear. The temperature dependence of the position and half width of the peaks also indicate the transition temperature increases as the layer number decreases.

This project was supported by JSPS and RFBR under the Japan - Russia Research Cooperative Program.

[1] M. Yoshida et al., Sci. Adv. 1, 9, (2015). [2] M. J. Hollander et al., Nano Lett. 15, 3, (2015).

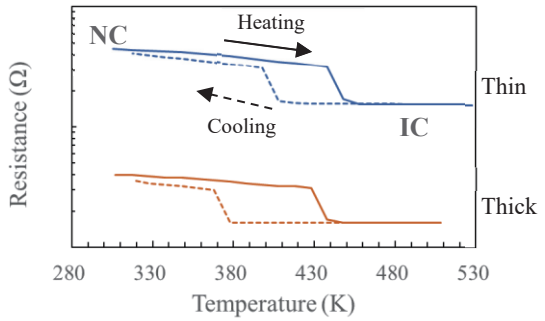

Fig. 1. Temperature dependence of resistivity around NC-IC phase transition for TaS_2 thin film (～19 layers) and thick film (～24 layers)

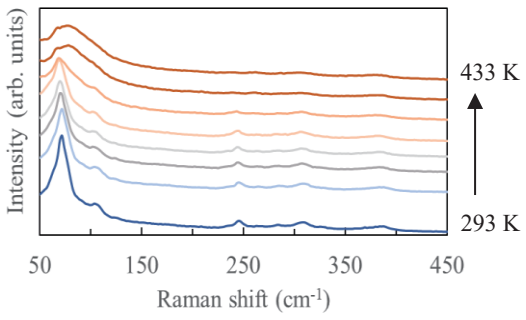

Fig. 2. Temperature dependence of Raman spectra around NC-IC phase transition for TaS_2 thick film

Corresponding Author: Kazuyuki Takai
Tel: +81-42-387-6138, Fax: +81-42-387-7002, E-mail: takai@hosei.ac.jp

Does Lateral Size of MoS_2 Nanosheets Influence Photoelectrochemical Performance?

Ahmad Tayyebi[1], Tomokazu Umeyama[2], Meysam Tayebi[3], Naoki Komatsu[1]

[1]Graduate School of Human and Environmental Studies, Kyoto University, Kyoto 606-8501
[2]Department of Molecular Engineering, Graduate School of Engineering, Kyoto University
[3]Department of Civil and Environmental Engineering, University of Ulsan, Republic of Korea

Designing visible-light active semiconductors for water splitting requires a suitable bandgap and band alignment, effective charge separation, fast charge transfer, and long-term durability in aqueous environments. Two-dimensional (2D) transition-metal dichalcogenides (TMDs) with 5 - 10% of light absorption in visible range and valence band maximum more positive than the water oxidation potential have shown a great promise for the production of H_2 or further, to reduce CO_2 to hydrocarbon. Combining TMD nanosheets having different dimensions with appropriate semiconductors seems an interesting design strategy for meeting such requirements. The active catalytic sites located at the edge of TMDs nanosheets play a crucial role in hydrogen production and catalytic reactions [1]. This report aims to investigate the effect of active sites of MoS_2 on photoelectrochemical performance by controlling the lateral size of MoS_2 nanosheets. To make photoelectrodes of MoS_2 with different sizes, two fluorinated tin oxide (FTO) electrodes and FTO/SnO_2 were inserted into the cuvette and a dc voltage (200 V) was applied for 2 min across these two electrodes [2]. Furthermore, to prepare semiconductor/MoS_2 photoelectrodes, nanosheets with different lateral size in-situ hybridized with zinc oxide (ZnO) and bismuth vanadate ($BiVO_4$) as wide and narrow band gap metal oxides semiconductors. Then, a 0.1 mg/mL ethanol suspension of ZnO/MoS_2 and $BiVO_4$/MoS_2 deposited on the surface of clean FTO surface by drop-casting method. The IPCE values at 400 nm for pure MoS_2 nanosheets with lateral size of 130 nm become 3-fold higher than that of MoS_2 with size of 270 nm. The UV-vis absorption spectra showed that the bandgap energy of ZnO nanoparticles decreased from 3.1 to 2.9 eV after hybridization with MoS_2 nanosheets. X-ray diffraction measurements indicated that monoclinic and Wurtzite structures were formed for $BiVO_4$ and ZnO, respectively. The photocurrent density-potential (J-V) and photo responses plots for bare ZnO, ZnO/MoS_2 (270nm) and ZnO/MoS_2 (130 nm) are shown in Figure 1. Addition of MoS_2 nanosheets enhanced the photocurrent density for ZnO/MoS_2 compared to bare ZnO. Furthermore, hybridization of ZnO with smaller MoS_2 nanosheets extract higher photocurrent density probably due to the higher density of active sites at the edges of smaller nanosheets.

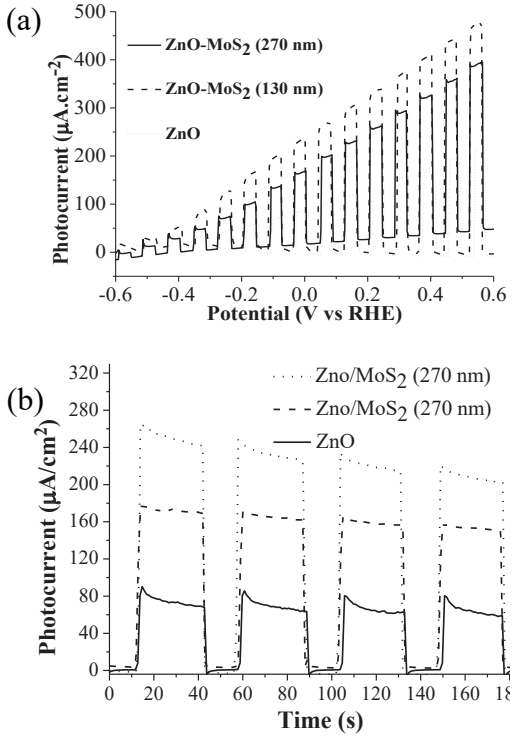

Figure 1: (a) Chopped photocurrent density vs. applied potential curves. (b) Photocurrent responses under visible-light (λ > 420 nm) illumination.

[1] M. Faraji et al. Energy Environ. Sci. 2019.
[2] T. Umeyama, et al. Chem. A Eur. J. 24, 1561 (2018).

Corresponding Author: A. Tayyebi
Tel, Fax: +81-75-753-7871, E-mail: atayebi162@gmail.com

Enhancing the Stability of Perovskite Solar Cells via Lithium-ion Endohedral Fullerenes on Top of Laminated Carbon Nanotube Electrodes

○ Ahmed Shawky [1], Il Jeon [1], Hiroshi Ueno [2], Hiroshi Okada [1], Esko I. Kauppinen [3], Shigeo Maruyama,[1,4,*] and Yutaka Matsuo[1,2,*]

[1] Department of Mechanical Engineering, The Univ. of Tokyo, Tokyo 113-8656, Japan, [2] School of Chemistry, Northeast Normal Univ., Changchun, Jilin 130024, P. R. China, [3] School of Science, Aalto Univ. Aalto, FI-00076, Finland, [4] Energy Nano Engineering Lab., AIST, Ibaraki 305-8564, Japan

Replacing the metal electrode by carbon electrode has been reported to be one of the most effective ways in perovskite solar cell (PSC) technology toward commercialization. This aims to enhance the device stability of PSCs due to no ion migration and outstanding encapsulation effect. Among the carbon electrodes, the application of freestanding carbon nanotubes (CNTs) has given the highest PCEs with the use of 2,2′,7,7′-tetrakis(*N,N*-di-*p*-methoxyphenylamine)-9,9′-spirobi-fluorene (spiro-MeOTAD) hole transporting layer (HTL). However, it is reported that the use of Spiro-MeOTAD with hygroscopic lithium bis(trifluoromethanesulfonyl)imide (Li^+TFSI^-) limits the full potential of the CNT-PSCs in terms of long-term stability due to moisture-driven degradation. Recently, we reported lithium-ion-containing C_{60} fullerene trifluoromethanesulfonylimide salt ($[Li^+@C_{60}]TFSI^-$) that induced an instant oxidation of spiro-MeOTAD producing spiro-MeOTAD$^{\bullet+}TFSI^-$ and neutral $[Li^+@C_{60}]^{\bullet-}$ (= $Li@C_{60}$), which functioned as an antioxidant, protecting PSCs from intruding oxygen [1]. The stability of PSCs improved by 10-fold compared with the reference devices. Thus, combining the two technologies described above can provide a synergic and ultimate solution to the PSC stability.

Therefore, we incorporated the mixture of spiro-MeOTAD and $[Li^+@C_{60}]TFSI^-$ into the CNT top electrode in PSCs. The HTL solution is typically drop-casted onto the CNT network in CNT-PSCs. A saturated solution seeped through the CNT network while any undissolved $[Li^+@C_{60}]TFSI^-$ and $Li@C_{60}$ suspensions stayed on the top. This led to more effective hole extraction by avoiding $[Li^+@C_{60}]TFSI^-$ in the pathway and more effective anti-oxidation activity by placing $Li@C_{60}$ next to air. Since the drop-casting on CNTs separated the dissolved species from the undissolved species, the oxidation reaction of spiro-MeOTAD came to a stop. From various analyses and investigation, we found that 2 h stirring for the HTL solution gave the highest Photoconversion efficiency (PCE) of 17% and the longest operating stability of unencapsulated devices. The obtained PCE are close to the gold electrode-based PSCs (18.5%) while the device stability is approximately 100 times greater. Such excellent stability is attributed to no ion-migration and antioxidant activity of $Li@C_{60}$ that uniformly covering the CNT electrode. Not only did we demonstrate highly stable and efficiency CNT-PSCs but also discovered a new reaction mechanism within the spiro-MeOTAD and $[Li^+@C_{60}]TFSI^-$ HTL solution.

References:

[1] Jeon, I. *et al. Angew. Chemie Int. Ed.* **57,** 4607–4611 (2018).

Corresponding authors: maruyama@photon.t.u-tokyo.ac.jp, matsuo@photon.t.u-tokyo.ac.jp

発表索引
Author Index

Author Index

< Z >

2019 年 3 月 2 日発行

第 56 回フラーレン・ナノチューブ・グラフェン総合シンポジウム
講演要旨集

≪フラーレン・ナノチューブ・グラフェン学会≫
〒113-8656 東京都文京区本郷 7-3-1
東京大学大学院工学系研究科　機械工学専攻
丸山研究室内
Phone/Fax：03-3830-4848
E-mail：fntg@photon.t.u-tokyo.ac.jp
URL：http://fullerene-jp.org
印刷　/　製本　（株）創志企画

チューナブル OPO レーザー
C-WAVE

HÜBNER

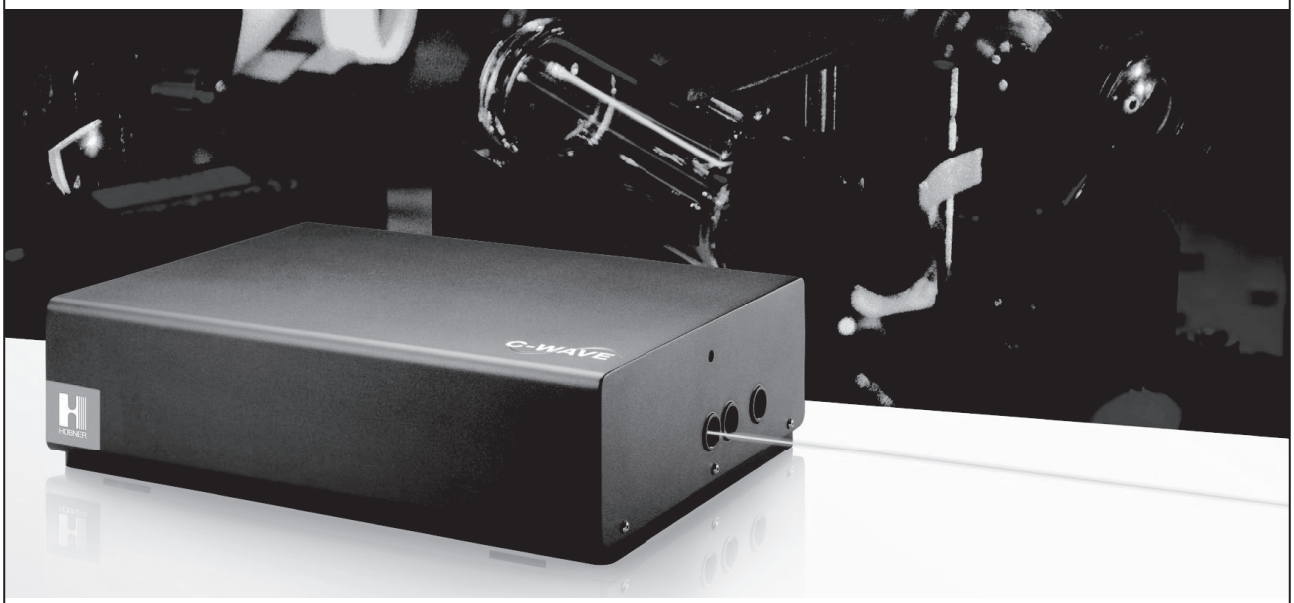

広いスペクトル可変幅と簡単な波長選択機能

- ✓ **可視域から近赤外までを完全コンピュータ制御波長チューニング**
- ✓ **パワーレベル選択可：1.5W（ポンプレーザ内蔵）、5W（外部レーザ）**
- ✓ **高精度：外部リファレンスによる周波数安定化機能**

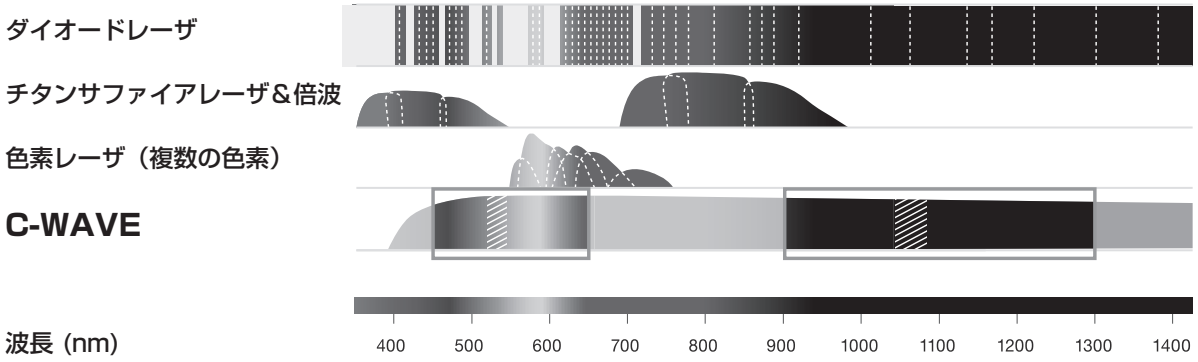

https://www.japanlaser.co.jp/ E-mail: jlc@japanlaser.co.jp

JLC JAPAN LASER 株式会社日本レーザー

東京本社 東京都新宿区西早稲田2-14-1 TEL 03-5285-0863(直)
大阪支店 大阪市東淀川区東中島1-20-12 TEL 06-6323-7286
名古屋支店 名古屋市中区錦3-1-30 TEL 052-205-9711

書籍のご案内

◆定価は本体価格＋税です。
◆各QRコードから小社ホームページにアクセスできます。

カーボンナノチューブ・グラフェンハンドブック

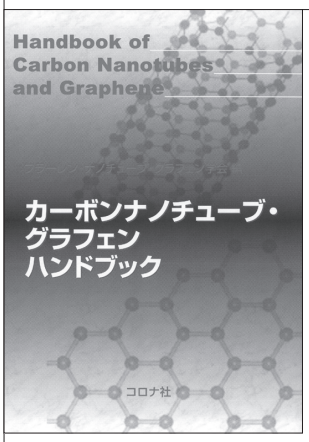

フラーレン・ナノチューブ・グラフェン学会 編
B5判／368頁
本体10,000円

本ハンドブックでは，カーボンナノチューブの基本的事項を解説しながら，エレクトロニクスへの応用，近赤外発光と吸収によるナノチューブの評価と光通信への応用の可能性を概観。最近嘱目のグラフェンやナノリスクについても触れた。

真空科学ハンドブック

日本真空学会 編
B5判／590頁
本体20,000円

真空の基礎科学から作成・計測・保持する技術に関わる科学的基礎を解説。また，成膜，プラズマプロセスなどの応用分野で真空環境の役割を説き，極高真空などのこれまでにない真空環境が要求される研究・応用への取組みなどを紹介。

カーボンナノチューブの材料科学入門
齋藤弥八 編著／A5判／250頁／本体3,400円

カーボンナノチューブの基礎
齋藤弥八・坂東俊治 共著／A5判／220頁／本体2,800円

ドライプロセスによる表面処理・薄膜形成の基礎
表面技術協会 編／A5判／208頁／本体2,800円

ドライプロセスによる表面処理・薄膜形成の応用
表面技術協会 編／A5判／318頁／本体4,600円

材料の熱力学 入門
正木匡彦 著／A5判／240頁／本体3,200円

例題で学ぶ化学プロセスシミュレータ
―フリーシミュレータCOCO/ChemSepとExcelによる解法―
化学工学会 編　伊東　章 著／A5判／234頁／本体3,500円

温度計測―基礎と応用―
計測自動制御学会 温度計測部会 編／
A5判／452頁／本体6,500円

研究室では「ご安全に！」
―危険の把握，安全巡視とヒヤリハット―
片桐利真 著／A5判／224頁／本体2,800円

理工系の技術文書作成ガイド
白井　宏 著／A5判／136頁／本体1,700円

ネイティブスピーカーも納得する技術英語表現
福岡俊道・Matthew Rooks 共著／A5判／240頁／本体3,100円

科学技術と共に歩む
株式会社 コロナ社
〒112-0011　東京都文京区千石4-46-10　振替00140-8-14844
TEL (03)3941-3131（代），-3132，-3133（営業部直通）
http://www.coronasha.co.jp　　FAX (03)3941-3137
E-mail eigyo@coronasha.co.jp

モデルチェンジ　～スマートなデザインに簡単操作～

BRANSON 超音波ホモジナイザー

長くご愛顧いただいておりますBRANSON超音波ホモジナイザーで新たなモデルが誕生しました。

主な特長

1.電気エネルギーから超音波振動への変換効率が95%以上
→ 無駄なエネルギーロスが小さく、安定した振幅が得られる。

2.通常では、液体の種類によって振幅が安定し難い。
→ 条件を変えても一定の振幅を保つ機能がついている。

3.ジュール（watt×sec）による発振制御が可能
→ Total何ジュールでこの処理が完了するという情報が論文に掲載できる。

20kHz超音波ホモジナイザー
BRANSON SONIFIER SFX250,550

40kHz超音波ホモジナイザー
BRANSON SONIFIER SFX150HH

主なアプリケーション

分散

カーボンナノチューブ　有機顔料　無機顔料　セラミック　セメント　感光体　記録材料
磁性粉　粉末冶金　酸化鉄　金属酸化物　シリカ　アルミナ　カーボンブラック
ポリマー　ラテックス　製紙　ファンデーション
研磨剤　電池　フィラー　光触媒　触媒　ワクチン　体外診断薬　歯磨き粉　シャンプー
半導体　電子基盤　液晶　貴金属　金属　宝石　タイヤ　発酵菌類　その他

乳化

エマルジョン製剤　農薬　トナー　ラテックス　界面活性剤　クリーム　乳液　その他

日本国内販売総代理店　株式会社 セントラル科学貿易

東京本社: 〒136-0071 東京都江東区亀戸1-28-6 タニビル3F TEL 03-5627-8150 FAX 03-5627-8151
技術物流センター: 〒272-0146 千葉県市川市広尾2-1-9 TEL 047-701-6100 FAX 047-701-6116
大阪支店: 〒533-0031 大阪府大阪市東淀川区西淡路1-1-36 新大阪ビル TEL 06-6325-3171 FAX 03-6325-5180
福岡営業所: 〒812-0016 福岡県福岡市博多区博多駅南1-2-15 事務機ビル TEL 092-482-4000 FAX 092-482-3797
札幌出張所: 〒001-0911 北海道札幌市北区新琴似11条13-7-13-2 TEL 011-764-3611 FAX 011-764-3612
https://www.cscjp.co.jp

当日出荷対象製品が大幅に増加しました。

倉庫面積を大幅拡張。国内在庫がさらに充実し、
ますます多くの製品が当日出荷可能となりました。*1, 2

お急ぎの製品は、是非一度当社ウェブサイトで
納期をご確認ください。
お客様の急なニーズにも迅速に対応いたします

当日出荷が可能な製品の一例です。

出荷予定日はウェブサイトでご確認いただけます。

■ パワー＆エネルギーメータ

PM400
タッチパネル式パワー＆
エネルギーメーターコンソール

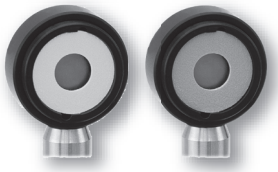

S120シリーズ
フォトダイオードパワーセンサ

サーマルセンサ、顕微鏡用スライド型センサ
なども当日出荷対象製品を取り揃えています。

「Today」の表示は
当日出荷の対象製品

+1	数量	資料	型番 - ユニバーサル規格		定価(税抜)	出荷予定日
+1			PM400	タッチパネル式パワー＆エネルギーメーターコンソール、マルチタッチ対応	¥ 180,283	Today

+1	数量	資料	型番 - ユニバーサル規格		定価(税抜)	出荷予定日
+1			S120VC	標準フォトダイオードパワーセンサ、Si 、200～1100 nm、50 mW	¥ 56,817	Today
+1			S120C	標準フォトダイオードパワーセンサ、Si、400～1100 nm、50 mW	¥ 40,973	Today
+1			S121C	標準フォトダイオードパワーセンサ、Si、400～1100 nm、500 mW	¥ 44,525	Today
+1			S122C	標準フォトダイオードパワーセンサ、Ge、700～1800 nm、40 mW	¥ 81,810	Today

■ レーザ保護メガネ

LG11

LG11A

+1	数量	資料	型番 - ユニバーサル規格		定価(税抜)	出荷予定日
+1			LG11	レーザ保護メガネ、クリアレンズ、可視光透過率：75%	¥ 47,133	Today
+1			LG11A	レーザ保護メガネ、クリアレンズ、可視光透過率：75%、コンフォートタイプ	¥ 47,133	Today

＊1. ご注文の時間帯によっては、翌営業日の出荷となる場合がございます。
2. 弊社に直接ご注文いただいた場合の出荷予定日です。出荷予定日は在庫状況に応じて変わる可能性がありますので
ご了承ください (上記の出荷予定日、価格などは2019年1月現在のウェブサイト上の製品情報です)。

www.thorlabs.co.jp E-mail: sales@thorlabs.jp

THORLABS ソーラボジャパン株式会社 2018年 7月17日より下記住所へ移転しました
〒179-0081 東京都練馬区北町3-6-3 TEL：03-6915-7701 FAX：03-6915-7716

POWERED BY Neo Engine

JEM-ARM200F NEOARM

原子分解能分析電子顕微鏡

"NEOARM"は、当社独自の技術で開発された
冷陰極電界放出形電子銃(Cold-FEG)と
高次の収差まで補正可能な
新型球面収差補正装置(ASCOR)を標準搭載し、
200 kVの高加速電圧だけでなく
30 kVの低加速電圧においても
原子分解能での観察を実現しました。

JEOL 日本電子株式会社

本社・昭島製作所 〒196-8558 東京都昭島市武蔵野3-1-2 TEL:(042)543-1111(大代表) FAX:(042)546-3353
www.jeol.co.jp ISO 9001・ISO 14001 認証取得

JEOLグループは、「理科学・計測機器」「産業機器」「医用機器」の3つの事業ドメインにより事業を行っております。
「理科学・計測機器事業」電子光学機器・分析機器・計測検査機器 **「産業機器事業」**半導体関連機器・産業機器 **「医用機器事業」**医用機器

Princeton Instruments

高感度
高ダイナミックレンジ
高繰り返し

高感度近赤外線2次元InGaAsカメラ

NIRvana™:640

- 低暗電流ノイズ（電子冷却：-80℃、液体窒素：-190℃）
- 110fps（ビデオレート以上）
- 標準GigEインターフェースで50mまで延長可
- 空冷ファンと水冷を切替可能

アプリケーション例

・フォトニック結晶PLイメージング及びスペクトル
・一重項酸素イメージング及びスペクトル
・太陽電池PLイメージング及びスペクトル
・天体観測微弱光イメージング
・食品断面イメージング
・In-Vivoイメージング　など

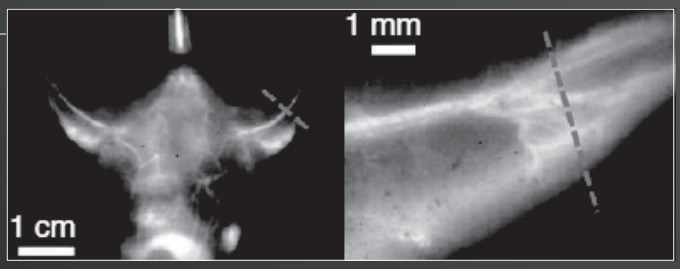

仕様

モデル	NIRvana:640ST	NIRvana:640	NIRvana:640LN
センサー	640 x 512 x InGaAs		
素子サイズ	20μm x 20μm		
波長範囲	0.9 ～ 1.7 μm		
冷却温度	-60℃	-80℃	-190℃
ダークチャージ	1500 e-/p/sec	300 e-/p/sec	<8 e-/p/sec
読み出しノイズ	<120 e-rms		15 e-rms
ダイナミックレンジ	16 Bit (>15Bit@1 素子)		
フレームレート	110 fps@10MHz		2.77 fps@250KHz
インターフェース	Gig E		
ソフトウェア	LightField, SITK-LabVIEW, WinX32		

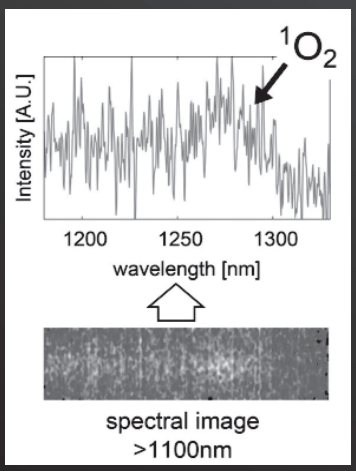

www.pi-j.jp

株式会社 日本ローパー　P I 事業部

〒135-0033 東京都江東区深川2 - 8 - 19 サクライビル3F
電話 03-5639-2741　FAX 03-5639-2775

NIPPON ROPER